Autoregulation of the Human Cerebrovasculature by Neurovascular Coupling

Hannah Farr

A thesis presented for the degree of
Doctor of Philosophy
in
Bioengineering
at the
University of Canterbury,
Christchurch, New Zealand.

29 July 2013

Preface

Many of the model equations and results included in Chapters 6 and 7 have been previously published in Farr and David [54]. Authors publishing in the Journal of Theoretical Biology and other Elsevier Journals retain the rights to publish their work in a thesis[1]. As this journal article was written in conjunction with my supervisor, Prof Tim David, I have included a co-authorship form with this thesis.

Verification of the model described in Chapters 6 and 7 was performed by Kristina Raba, a summer scholarship student in the BlueFern High Performance Computing Research Group at the University of Canterbury. She has kindly given permission for her work to be discussed in Chapter 7 of this thesis.

[1] See [2] for further information.

Acknowledgements

> I not only use all the brains that I have, but all that I can borrow.
>
> – Woodrow Wilson

I would like to thank all of you who have allowed me to borrow from your brains and minds. Although this includes everyone I know, I will attempt to give the abridged version. And here it is:

I would like to thank my supervisor, Tim David, for his patient guidance, wisdom, and friendship. Thank you for reminding me that research is all about making mistakes.

Thanks to Richard Watts for helping unravel the mystery of MRI for me. Thanks also to the dozens of people who participated in my ill-fated MRI project – it is a shame that I could not include here all that I learnt from you.

Thanks to all the other crazy, wonderful people that decided to research brains for a living (bet you're kicking yourself that you didn't study something less complex). Special thanks to the researchers whose work is so intertwined with mine (Steve Moore, Samara Alzaidi, Navid Safaeian, Mohsin Shaikh and Kristina Raba). Extra special thanks to all my colleagues, friends and unofficial editors at the Van der Veer Institute for Parkinson's and Brain Research (now the New Zealand Brain Research Institute). Thanks for the cake and the encouragement.

Thanks to the Swedish contingent; namely, Erik and Edvard. We shall meet again someday for tea and some general bilingual frivolity.

Thanks to Ralph Waldo Emerson, Carl Jung, Lyall Watson, Lewis Carroll, Gerard Manley Hopkins, Thomas Willis, Rainer Maria Rilke, Leonardo Bianchi, Emily Dickinson, Arnold Bennett, Virginia Woolf, Plato, William F. Allman, François de la Rochefoucald, Santiago Ramón y Cajal, Oliver Wendell Holmes, Walt Whitman, Don Marquis, Friedrich Nietzsche, Alexander Pope, Colin Blakemore, William Shakespeare, Primo Levi, Albert Einstein, Daryl Hine, Rudyard Kipling, The White Stripes, Iain McGilchrist, Margaret Atwood, Carl Zimmer, Charles Dickens, Ken Robinson, Leonardo Da Vinci, Peter Medawar, Richard Feynmann, Martin Schwartz, Anne Lamott, E.L. Doctorow, John Milton, William Butler Yeats, Elizabeth Connor and a few others.

Thank you to my whānau, extended whānau, and extended extended whānau. Aroha nui.

Thank you to Leonie, Kelsangs Luma, Shewang and Drolchog, and the Kalpa Bhadra Sangha.

Thanks to my father for encouraging me to “sell science.” Om Namah Shivaya.

Thanks to all my kind mothers – especially my mother, grandmother, and my sisters. There are too many things you’ve taught me to count, so I won’t even try.

And last, but certainly not least, thank you to my partner, Jarred Arthur. Thank you very much for putting up with all my crazy. Love love xo

Contents

List of Figures

List of Tables

Glossary

β-amyloid see amyloid-β.

IP_3 inositol triphosphate.

PIP_2 phosphatidylinositol 4,5-bisphosphate.

a priori "formed or conceived beforehand [112]".

in vivo "in the living body of a plant or animal [112]".

20-HETE 20-hydroxy-eicosatetraenoic acid.

20-hydroxy-eicosatetraenoic acid 20-HETE; arachidonic acid derivative which acts as a vasoconstrictor.

AA arachidonic acid.

actin protein involved in muscle contraction; contraction occurs due to the interdigitation of myosin "heads" with actin filaments.

action potential "a momentary reversal in the potential difference across a plasma membrane that occurs when a cell has been activated by a stimulus [112]".

AD Alzheimer's disease.

adaptive methods numerical methods of solving differential equations which adapt the step size at each iteration to maintain accuracy of the solution.

adenosine plays an important role in energy transfer (as adenosine triphosphate (ATP) and adenosine diphosphate (ADP)), as well as in signal transduction (as cyclic adenosine monophosphate (cAMP)); it is also an inhibitory neurotransmitter.

adenosine triphosphate ATP; "a phosphorylated molecule composed of adenosine and three phosphate groups that supplies energy for many biochemical cellular processes by undergoing enzymatic hydrolysis to ADP [112]".

afferent "bearing or conducting inward; specifically : conveying impulses toward the central nervous system [112]".

agonist "a chemical substance (as a drug) capable of combining with a receptor on a cell and initiating the same reaction or activity typically produced by the binding of an endogenous substance [112]".

Alzheimer's disease AD; a degenerative brain disease that results in progressive memory loss and impaired thinking; it is marked by neuronal damage and death and by the presence of neurofibrillary tangles and plaques containing amyloid-β.

amyloid-β the main constituent of the plaques characteristic of Alzheimer's disease.

analytical solution exact solution found using analytical mathematical methods.

anterior "situated before or toward the front [112]".

APP amyloid precursor protein.

aquaporins proteins embedded in the cell membrane that regulate the flow of water.

arachidonic acid AA; second messenger molecule; precursor to prostaglandins and other molecules that can act as vasomodulators.

arteriole "any of the small terminal twigs of an artery that ends in capillaries [112]".

artery any of the tubular branching muscular- and elastic-walled vessels that carry blood from the heart through the body [112].

astrocyte star-shaped glial cell involved in the control of vascular tone and the maintenance of the neuronal environment.

atherosclerosis inflammation or "hardening" of the walls of the arteries.

ATP adenosine triphosphate.

atrophy "decrease in size or wasting away of a body part or tissue [112]".

autocrine "of, relating to, promoted by, or being a substance secreted by a cell and acting on surface receptors of the *same* cell – compare **paracrine** [112]".

autoregulation the process by which blood vessels in the brain adjust their calibre to maintain adequate blood supply to brain tissue.

axon structure that extends from the neuron cell body and transmits signals to other neurons.

basal tone the degree of tension or constriction the smooth muscle of a blood vessel has *at rest*.

BBB blood-brain barrier.

BK "big" or "large" conductance voltage- and calcium- gated potassium channel.

blood-brain barrier tightly packed endothelial cell lining of the blood vessels that keeps unwanted chemical substances from reaching the neuronal environment.

CAA cerebral amyloid angiopathy.

calculus the study of change; a branch of mathematics focused on derivatives and integrals.

calmodulin "an abbreviation for CALcium-MODULated proteIN; also CaM; a calcium-binding protein that mediates cellular metabolic processes (as muscle-fiber contraction) by regulating the activity of specific calcium-dependent enzymes [112]".

CaM calmodulin.

capacitance the ability of an object to store electrical charge.

capillary smallest vessels in the vasculature (about 7–9μm in diameter); their purpose is to deliver nutrients to, and remove wastes from, the tissue.

CBF cerebral blood flow.

CBV cerebral blood volume.

CCE capacitative calcium entry.

cell membrane a fatty, semipermeable membrane that surrounds the content that resides within cells.

cerebral "of, relating to, affecting, or being the cerebrum [112]".

cerebral amyloid angiopathy deposition of amyloid-β-peptide found in the blood vessels of a brain affected by Alzheimer's disease.

cerebral cortex outer part of the cerebrum.

cerebrovascular "of or involving the cerebrum and the blood vessels supplying it [112]".

cerebrovascular autoregulation mechanisms which counteract normal fluctuations in arterial pressure and shear stress by adjusting the calibre of cerebral arterioles.

cerebrovasculature blood vessels of the brain.

cerebrum "an enlarged anterior or upper part of the brain; especially: the expanded anterior portion of the brain that in higher mammals overlies the rest of the brain, consists of cerebral hemispheres and connecting structures, and is considered to be the seat of conscious mental processes [112]".

cGMP cyclic guanosine monophosphate.

CICR calcium-induced calcium release.

Circle of Willis CoW; "a complete ring of arteries at the base of the brain that is formed by the cerebral and communicating arteries and is a site of aneurysms [112]".

coagulability "ability of a fluid to become viscous or thickened into a coherent mass [112]".

cognitive "of, relating to, or being conscious intellectual activity (as thinking, reasoning, remembering, imagining, or learning words) [112]".

compressive stress acts to compress a deformable body.

conceptual models models based on mathematical descriptions of underlying physical processes.

conductance "the power, readiness, or capacity to conduct something; the readiness with which a conductor transmits an electric current expressed as the reciprocal of electrical resistance [112]".

coronary "of, relating to, or being the coronary arteries or veins of the heart; broadly: of or relating to the heart [112]".

cortical spreading depression CSD; spreading depression occurring in the cortex – see **spreading depression**.

cotransporter a protein residing in the cell membrane that helps to transport molecules or ions into the cell.

CoW Circle of Willis.

CSD cortical spreading depression.

current "a flow of electric charge [112]".

cyclic guanosine monophosphate cGMP; second messenger molecule important for NO-mediated vasodilation mechanism.

cytoplasm "the organized complex of inorganic and organic substances external to the nuclear membrane of a cell and including the cytosol and membrane-bound organelles [112]".

cytosol "the fluid portion of the cytoplasm exclusive of organelles and membranes [112]".

dementia "a usually progressive condition marked by the development of multiple cognitive deficits [112]".

dendrite structure that extends from the neuron cell body and receives signals from other neurons.

dendritic spine protrusion from a dendrite that receives input from an axon.

depolarization "loss of polarization; especially: loss of the difference in charge between the inside and outside of the plasma membrane of a muscle or nerve cell due to a change in permeability and migration of ions [112]"; change in cell membrane potential to a less negative value.

derivative a mathematical expression that describes a rate of change; for example, the rate of change of quantity a with respect to quantity t as the quantity t approaches zero.

DHET dihydroxyeicosatrienoic acid.

diabetes mellitus "a variable disorder of carbohydrate metabolism caused by a combination of hereditary and environmental factors and usually characterized by inadequate secretion or utilization of insulin, by excessive urine production, by excessive amounts of sugar in the blood and urine, and by thirst, hunger, and loss of weight [112]".

differential equation "an equation containing differentials or derivatives of functions [112]".

diffusion the movement of particles from an area of higher concentration to that of a lower one.

dihydroxyeicosatrienoic acid DHET; derivative of EET (which is a derivative of AA); acts as a vasodilator.

dissociation constant "a constant that depends upon the equilibrium between the dissociated and undissociated forms of a chemical combination [112]".

distal "situated away from the point of attachment or origin or a central point – compare **proximal** [112]".

distensible "capable of being distended, extended, or dilated [112]".

E. coli "an enterobacterium (*Escherichia coli*) that is used in medicine and genetics as a research organism [112]".

EC endothelial cell.

ECS extracellular space.

EET epoxyeicosatrienoic acid.

elastic modulus "the ratio of the stress in a body to the corresponding strain [112]".

electrochemical "pertaining to electrochemistry, a science that deals with the relation of electricity to chemical changes and with the interconversion of chemical and electrical energy [112]".

endfoot the end of an astrocyte branch that surrounds neighbouring neurons or blood vessels.

endogenous "growing from or on the inside [112]".

endoplasmic reticulum "a system of interconnected vesicular and lamellar cytoplasmic membranes that functions especially in the transport of materials within the cell and that is studded with ribosomes in some places [112]"; cell "stores".

endothelial cells thin, flat cells that line the lumen of blood vessels.

endothelial nitric oxide synthase enzyme found in endothelial cells that is capable of producing vasodilatory nitric oxide.

eNOS endothelial nitric oxide synthase.

epoxyeicosatrienoic acid EET; arachidonic acid derivative which acts as a vasodilator.

ER endoplasmic reticulum.

erythrocytes see **red blood cells**.

expression as in *gene expression*; the process by which information from a gene is used to produce a cellular structure, such as an ion channel.

fibrous astrocyte astrocytes with long, thin, unbranched processes [114].

fMRI functional magnetic resonance imaging.

forepaw stimulation experimental method where neuronal activation is initiated in the cortex by first stimulating the forepaw of the experimental animal.

functional hyperaemia the mechanism by which increased neuronal activity is matched by a rapid and regional increase in blood supply [54].

functional magnetic resonance imaging fMRI; an MRI procedure that estimates the amount of brain activity by detecting changes in blood oxygen.

G-protein "any of a class of cell membrane proteins that are coupled to cell surface receptors and upon stimulation of the receptor by an extracellular molecule (a hormone or neurotransmitter) bind to GTP to form an active complex which mediates an intracellular event [112]".

gap junction "an area of contact between adjacent cells characterized by modification of the plasma membranes for intercellular communication or transfer of low molecular-weight substances [112]".

gK(Ca) voltage- and calcium- gated potassium channel.

glia "supporting tissue intermingled with the essential elements of nervous tissue especially in the brain, spinal cord, and ganglia [112]".

glial "of, relating to, or constituting glia [112]".

glutamate neurotransmitter released by active neurons.

gray matter "neural tissue especially of the brain and spinal cord that contains cell bodies as well as nerve fibres, has a brownish-gray colour, and forms most of the cortex and nuclei of the brain, the columns of the spinal cord, and the bodies of ganglia called also *gray substance* [112]".

GTP guanosine-5'-triphosphate.

guanosine-5'-triphosphate "an energy-rich nucleotide analogous to ATP that is composed of guanine linked to ribose and three phosphate groups and is necessary for peptide bond formation during protein synthesis [112]".

haemorrhage "copious discharge of blood from the blood vessels [112]".

heterocellular coupling gap junction coupling between different cell types.

Hill equation mathematical expression that describes the binding of a ligand to a receptor.

histology "a branch of anatomy that deals with the minute structure of animal and plant tissues as discernible with the microscope [112]".

homocellular coupling gap junction coupling between the same cell type.

hyperaemia see **functional hyperaemia**.

hypercholesterolaemia "the presence of excess cholesterol in the blood [112]".

hyperglycaemia high blood sugar.

hyperpolarization "to produce an increase in potential difference across (a biological membrane) [112]"; change in cell membrane potential to a more negative value.

hypertension abnormally high blood pressure.

hypotension abnormally low blood pressure.

infinitesimal "taking on values arbitrarily close to but greater than zero; immeasurably or incalculably small [112]".

innervated supplied by nerve fibres.

inositol triphosphate molecule important for cell signalling.

integration anti-differentiation.

interstitial clefts the space that surrounds the cells of a given tissue.

intima "the innermost coat of an organ (as a blood vessel) consisting usually of an endothelial layer backed by connective tissue and elastic tissue – called also *tunica intima* [112]".

inwardly rectifying potassium channel KIR channel; despite their name, "inwardly rectifying" potassium channels can actually pass potassium ions both in and out of the cell; they are just able to pass ions into the cell *more readily* (i.e., with less resistance).

ion channel "a cell membrane channel that is selectively permeable to certain ions [112]".

ion pump a cell membrane protein that uses ATP to provide energy to move ions across the membrane against their concentration gradient.

ionotropic type of neurotransmitter receptor that forms a ion channel pore; when activated, a ionotropic receptor allows ions to flow through it.

ischaemia "deficient supply of blood to a body part (as the heart or brain) that is due to obstruction of the inflow of arterial blood (as by the narrowing of arteries by spasm or disease) [112]".

Kelvin-Voigt type of viscoelastic model formed by a dashpot and a spring connected in parallel.

kinetics "the mechanism by which a physical or chemical change is effected [112]".

KIR inwardly rectifying potassium channel.

knockout "having all or part of a gene eliminated or inactivated by genetic engineering; for example, knockout mice predisposed to diabetes mellitus serve as animal models in the study of human diabetes [112]".

L-Arginine basic amino acid.

Laplace's Law if you have a larger vessel radius, you will need a larger wall tension to withstand a given internal fluid pressure.

ligand small molecule that can form complexes with cellular proteins.

lumen "the cavity of a tubular organ or part [112]".

mathematical model a physical system described using mathematical language.

mechanism "a piece of machinery; a bodily process or function; the fundamental physical or chemical processes involved in or responsible for an action, reaction, or other natural phenomenon [112]".

media "the middle coat of the wall of a blood or lymph vessel consisting chiefly of circular muscle fibres – called also *tunica media* [112]".

membrane potential "the potential difference between the interior of a cell and the interstitial fluid beyond the membrane [112]".

metabolic autoregulation regulation of blood flow according to the degree of metabolism occurring in the neighbouring tissue.

metabotropic "relating to or being a receptor for glutamate that when complexed with G-protein triggers increased production of certain intracellular messengers [112]".

metabotropic glutamate receptors astrocyte glutamate receptor; involved in neurovascular coupling.

mGluR metabotropic glutamate receptors.

Michaelis-Menten kinetics model of enzyme kinetics; relates the reaction rate v to [S], the concentration of a substrate S.

MLCK myosin light chain kinase.

MLCP myosin light chain phophatase.

myogenic mechanism vascular mechanism that acts to counteract the normal fluctuations in arterial pressure that occur during normal activities.

myosin protein involved in muscle contraction; contraction occurs due to the interdigitation of myosin "heads" with actin filaments.

myosin light chain a subunit of myosin.

myosin light chain kinase MLCK; enzyme that phosphorylates the light chain (a subunit) of myosin, enabling the molecular interaction of myosin with actin.

myosin light chain phosphatase MLCP; enzyme that dephosphorylates the light chain (a subunit) of myosin, enabling the disruption of the molecular interaction of myosin with actin.

N-methyl-d-aspartate receptors neuronal ionotropic glutamate receptor; involved in NO-mediated neurovascular coupling.

Nernst potential reversal potential.

neuritic plaques plaques of amyloid-β-peptide found in the neuronal tissue of a brain affected by Alzheimer's disease.

neurodegenerative "relating to or marked by degeneration of nervous tissue [112]".

neurofibrillary tangle accumulation of abnormally formed tau protein that occurs in the neurons of those with Alzheimer's disease.

neuron "one of the cells that constitute nervous tissue, that have the property of transmitting and receiving nervous impulses [112]".

neuronal nitric oxide synthase enzyme found in neurons that is capable of producing vasodilatory nitric oxide.

neurotransmitter "a substance that transmits nerve impulses across a synapse [112]".

neurovascular coupling NVC; the intercellular communication system between cells comprising the neurovascular unit [54].

neurovascular signalling see **neurovascular coupling**.

neurovascular unit NVU; functional unit comprised of neurons, astrocytes and vascular cells.

nitric oxide NO; vasodilatory molecule; produced by neuronal nitric oxide synthase (nNOS) in neurons and endothelial nitric oxide synthase (eNOS) in endothelial cells.

NMDAR N-methyl-d-aspartate receptors.

nNOS neuronal nitric oxide synthase.

NO nitric oxide.

non-dimensionalization the process of removing units from a system of equations by making a series of substitutions for the variables; can be used to help uncover characteristic properties of the system (such as characteristic times or lengths) or to determine which terms of the equations significantly affect system behaviour.

normal "perpendicular to a tangent at a point of tangency [112]".

normal stress stress component normal to a surface.

numerical solution solution found by numerical mathematical methods.

NVC neurovascular coupling.

NVU neurovascular unit.

ODE ordinary differential equation.

oedema "an abnormal infiltration and excess accumulation of serous fluid in connective tissue or in a serous cavity – called also *dropsy* [112]".

Ohm's Law V=IR; "a law in electricity: the strength of a direct current is directly proportional to the potential difference and inversely proportional to the resistance of the circuit [112]".

ohmic of, or relating to Ohm's law, or a system component that is governed by Ohm's law.

ordinary differential equation ODE; a differential equation in which there is only one independent variable.

osmotic shrinkage shrinkage of one compartment due to the osmotic movement of water to a neighbouring compartment that has a higher solute (ionic) concentration.

overexpression "excessive expression of a gene by producing too much of its effect or product [112]".

paracrine "of, relating to, promoted by, or being a substance secreted by a cell and acting on *adjacent cells* – compare **autocrine** [112]".

parameter any of a set of physical properties whose values determine the characteristics or behavior of something [112].

partial derivative a derivative of a function of several variables.

partial differential equation PDE; "an equation containing at least one partial derivative [112]".

pathogenic "causing or capable of causing disease [112]".

pathology "the structural and functional deviations from the normal that constitute disease or characterize a particular disease [112]".

pathophysiology "the physiology of abnormal states; specifically: the functional changes that accompany a particular syndrome or disease [112]".

PDE partial differential equation.

PDEs phosphodiesterases.

perfusion "to force a fluid through (an organ or tissue) especially by way of the blood vessels [112]".

pericyte glial cell capable of altering the calibre of capillaries.

perivascular "of, relating to, occurring in, or being the tissues [or space] surrounding a blood vessel [112]".

PG prostaglandins.

pharmacological treatments drugs.

phenomenological models models formed by fitting equations to observed behaviour.

phosphatidylinositol 4 5 bisphosphate molecule from which many important signalling proteins are derived.

phosphodiesterases more specifically: cyclic nucleotide phosphodiesterases; a group of enzymes that degrade the phosphodiester bond in the second messenger molecules cAMP and cGMP.

Phospholipase C PLC; enzyme that cleaves PIP_2 to produce IP_3.

phosphorylate "to cause (an organic compound) to take up or combine with phosphoric acid or a phosphorus-containing group [112]".

physiological "characteristic of or appropriate to an organism's healthy or normal functioning [112]".

pial arteries arteries on the outside of the brain.

plasma membrane see **cell membrane**.

PLC Phospholipase C.

Poisson effect the effect observed when a deformable body is stretched in one direction: it tends to get thinner in the other two directions.

Poisson's ratio measure of the Poisson effect; it is the ratio of the strain in one direction to the strain in another direction.

posterior "situated behind [112]".

prostaglandins PG; arachidonic acid derivative which acts as a vasodilator.

protoplasmic astrocyte astrocytes with many branching processes [114].

proximal "next to or nearest the point of attachment or origin, a central point, or the point of view – compare **distal** [112]".

red blood cells "any of the haemoglobin-containing cells that carry oxygen to the tissues and are responsible for the red colour of vertebrate blood [112]".

reperfusion "restoration of the flow of blood to a previously ischaemic tissue or organ (as the heart or brain) [112]".

resistance "the opposition offered by a body or substance to the passage through it of a steady electric current [112]".

reversal potential the membrane potential at which there is no net flow from one side of the membrane to the other.

RK Runge-Kutta.

RKSUITE a robust mathematical solver that uses an embedded RK-45 method.

Runge-Kutta numerical method for finding a numerical solution that approximates the analytical solution of a differential equation.

SAC stretch-activated calcium ion channel.

sarcoplasmic reticulum "the endoplasmic reticulum of [muscle] that functions especially as a storage and release area for calcium [112]"; special form of "smooth" ER.

SD spreading depression.

sGC soluble guanylate cyclase.

shear stress stress component tangential to a surface.

sigmoidal behaviour behaviour that exhibits a progression from a small value that increases quickly and approaches a plateau over time; "S-shaped" behaviour; used to describe the opening of ion channels, among other things.

SMC smooth muscle cell.

smooth muscle cells cell that constitutes smooth muscle, a type of muscle that is a major component of arterial and arteriolar walls.

soluble guanylate cyclase intracellular receptor that binds nitric oxide; involved in NO-mediated vasodilation.

soma cell body.

spatial buffering mechanism for the regulation of extracellular potassium concentration by astrocytes.

spine see **dendritic spine**.

spreading depression SD; a slow spreading wave of depolarization of neurons and glial cells that is accompanied by changes in vascular tone, blood flow and metabolism [34].

SR sarcoplasmic reticulum.

strain a normalized measure of the size of the deformation/displacement of particles within a body relative to an initial or reference body size.

stress forces acting within a deformable body.

stress tensor mathematical grouping of stress components, usually into an array or matrix.

stroke cerebral infarction; where the blood supply to a part of the brain is interrupted by the rupture (haemorrhagic stroke) or the blocking (ischaemic stroke) of a blood vessel.

subarachnoid haemorrhage "haemorrhage situated or occurring under the arachnoid membrane in the brain [112]".

synapse "the place at which a nervous impulse passes from one neuron to another [112]".

synaptic cleft "the space between neurons at a nerve synapse across which a nerve impulse is transmitted by a neurotransmitter – called also *synaptic gap* [112]".

tangential "acting along or lying in a tangent [112]".

tensile stress acts to stretch a deformable body.

tone as in muscular "tonus;" see **vascular tone**.

transmural across the wall (of a blood vessel).

vascular relating to blood vessels.

vascular cells cells lining the lumen of blood vessels; these include smooth muscle cells and endothelial cells.

vascular tone the degree of tension or constriction the smooth muscle of a blood vessel has; muscular "tonus".

vasoconstriction constriction of a blood vessel.

vasoconstrictor "an agent (as a sympathetic nerve fibre or a drug) that induces or initiates vasoconstriction [112]".

vasodilation dilation of a blood vessel.

vasodilator "an agent (as a parasympathetic nerve fibre or a drug) that induces or initiates vasodilation [112]".

vasomodulator agent capable of modulating (inducing changes in) vascular tone.

vasomotion diameter oscillations of the arteries.

viscoelastic having both viscous and elastic properties.

viscoelastic model mathematical model consisting of springs (that represent the elastic response) and dashpots (that represent the viscous response) arranged in series and/or parallel.

VOCC voltage operated calcium channel.

voltage "electric potential or potential difference expressed in volts [112]".

VSM vascular smooth muscle.

VSMC vascular smooth muscle cell/s.

wall shear stress stress exerted on the vessel wall by flowing blood.

white matter "neural tissue especially of the brain and spinal cord that consists largely of myelinated nerve fibres bundled into tracts, has a whitish colour, and typically underlies the grey matter [112]".

WSS wall shear stress.

Young's modulus "the ratio of the tensile stress in a material to the corresponding tensile strain [112]".

Abstract

Functional hyperaemia is an important mechanism by which increased neuronal activity is matched by a rapid and regional increase in blood supply. This mechanism is facilitated by a process known as "neurovascular coupling" – the orchestrated communication system involving the cells that comprise the neurovascular unit (neurons, astrocytes and the smooth muscle and endothelial cells lining arterioles). Blood flow regulation and neurovascular coupling are altered in several pathological states including hypertension, diabetes, Alzheimer's disease, cortical spreading depression and stroke.

By adapting and extending other models found in the literature, we create, for the first time, a mathematical model of the entire neurovascular unit that is capable of simulating two separate neurovascular coupling mechanisms: a potassium- and EET-based and a NO-based mechanism. These models successfully account for several observations seen in experiment.

The potassium/EET-based mechanism can achieve arteriolar dilations similar in magnitude (3%) to those observed during a 60-second neuronal activation (modelled as a release of potassium and glutamate into the synaptic cleft). This model also successfully emulates the paradoxical experimental finding that vasoconstriction follows vasodilation when the astrocytic calcium concentration (or perivascular potassium concentration) is increased further. We suggest that the interaction of the changing smooth muscle cell membrane potential and the changing potassium-dependent resting potential of the inwardly rectifying potassium channel are responsible for this effect. Furthermore, our simulations demonstrate that the arteriolar behaviour is profoundly affected by depolarization of the astrocytic cell membrane, and by changes in the rate of perivascular potassium clearance or the volume ratio between the perivascular space and astrocyte.

In the modelled NO-based neurovascular coupling mechanism, NO exerts its vasodilatory effects via neuronal and endothelial cell sources. With both sources included, the model achieves a 1% dilation due to a 60-second neuronal activation. When the endothelial contribution to NO production is omitted, the arteriole is more constricted at baseline. Without the endothelial NO contribution, the arteriolar change in diameter during neuronal activity is greater (6%). We hypothesize that NO has a dual purpose in neurovascular coupling: 1) it di-

rectly mediates neurovascular coupling through release by neuronal sources, and 2) it indirectly modulates the size of the neurovascular coupling response by determining the baseline tone.

Our physiological models of neurovascular coupling have allowed us to replicate, and explain, some of the phenomena seen in both neurovascular coupling-oriented and clinically-oriented experimental research. This project highlights the fact that physiological modelling can be used as a tool to understand biological processes in a way that physical experiment cannot always do, and most importantly, can help to elucidate the cellular processes that induce or accompany our most debilitating diseases.

Chapter 1

Introduction

1.1 Overview

The human brain consumes an extraordinary 20% of the energy that is produced by the body. It receives a continuous supply of fuel and oxygen from blood, but if cerebral blood flow (CBF) is disrupted, brain function will cease within seconds and permanent damage to the cellular structures will occur within minutes [78]. Conversely, if blood supply is too plentiful, the brain will experience oedema (swelling). The brain therefore requires neither too much nor too little blood. To ensure that it receives just the right amount of blood, it has evolved a collection of protective, automatically regulated mechanisms.

A phenomenon known as *cerebrovascular autoregulation* constitutes one line of defence [78]. Arteries and arterioles within the brain make compensatory changes in radius in response to normal fluctuations in blood pressure and wall shear stress. When arterial pressure rises, arteries will constrict (their diameter will decrease) to counteract the increase in blood flow caused by the pressure rise. When arterial pressure drops, arteries will relax (their diameter will increase), allowing the passage of more blood. This process – termed *myogenic* regulation – ensures that a constant CBF can be maintained.

Another protective mechanism involves the distribution of blood according to the functional activity of different brain regions – a mechanism known as *functional hyperaemia*. Functional hyperaemia is essentially the process by which increased neuronal activity is matched by a rapid and regional increase in blood supply. Those familiar with fMRI will understand this in terms of the coloured "activated" areas overlaid on brain slices. Although investigations into functional hyperaemia began with the work of Roy and Sherrington [136] over 200 years ago, it is still unknown exactly what chemical species and cellular machinery are involved. However, a growing body of evidence indicates that neurons, astrocytes and vascular cells constitute an important entity (termed the *neurovascular unit* or NVU), which maintains homeostasis in the brain in a variety of different ways. It is believed that functional hyperaemia is achieved through

"*neurovascular coupling*" – the intercellular communication system between cells comprising the NVU [78].

The breakdown of the cell machinery that powers these defensive autoregulatory mechanisms leads to dysregulated cerebral blood flow and perfusion, which in turn leads to cellular injury, brain dysfunction and disease [78]. It is now believed that this cerebrovascular dysregulation is not only implicated in the development of cerebrovascular disease, such as stroke and atherosclerosis (hardening of the arteries), but also in neurodegenerative disorders, such as Alzheimer's disease (AD) [53, 59, 78] and cortical spreading depression (CSD) [98].

1.2 Motivations

Understandably, *neuronal* abnormalities have been the focus for neurodegenerative disease research for decades [107]. However, recent research into the nature and causes of neurological (and other) disorders has highlighted the importance of *vascular* pathology.

Impaired cerebrovascular autoregulation, as well as impaired autoregulation by functional hyperaemia, has been seen in "Alzheimer mice" (mice that overproduce the amyloid precursor protein, APP) [59, 119, 120, 122]. In light of such evidence, it has been hypothesized that vascular damage may actually *precede* the formation of the amyloid-β plaques and neurofibrillary tangles indicative of AD [78, 133]. It has also been shown that atherosclerosis and high cholesterol – essentially "bad" vascular health – increases the risk of developing AD [134, 148]. Other studies have localised neurodegenerative mechanisms down to specific defective ion channels in astrocytes or smooth muscle cells [108, 153, 165]. Finally, astrocytes (an integral part of the NVU) have also been implicated as major players in the progression of neurodegenerative diseases [107, 116]. Astrocytes – also known as the "housekeepers" of the brain – are known to "clean up" neuron-derived amyloid β material, which can eventually cause astrocytic cell injury and death [107].

The pathogenic gap between cerebrovascular disorders and other common diseases is also narrowing. AD [78], cortical spreading depression (CSD)[34] and diabetes [39, 156] all have a vascular component in their pathology. These vascular changes are not necessarily a side or secondary effect of the disease; vascular responses can play an integral part in the initiation, propagation or degeneration of the disease itself. Understanding the interplay between vascular and other components of a disease, and indeed developing new therapies to target these components, relies on the discovery and analysis of very complex and coupled cellular processes. Mathematical models that can describe cellular-level processes in detail will aid in this understanding and can provide a platform for predicting the effects that new pharmacological treatments could have [143]. Mathematical modelling has been used for hundreds of years

to help biological scientists better understand the mechanisms underlying their experimental results. These models have not only been used to validate existing hypotheses, but have also helped guide the creation of new and testable experimental pathways [155]. However, the process, and indeed the benefits, of creating a mathematical model are not well understood by the general scientific community. Care must be taken to ensure that they are presented in such a way that they can provide maximum value. Models need to be understood in terms of their scope, scale, strengths and limitations, and need to be presented so that every member of the interdisciplinary biological science community (experimentalists, clinicians and mathematicians) can understand the terminology [144]. This thesis must therefore include sufficient background information regarding physiological, clinical and mathematical concepts so that a person with knowledge only in one area could still understand this work as a whole.

1.3 Objective

The overall objective of this project is to build a mathematical model of neurovascular coupling and investigate the model's response to known physiological (and pathological) changes. In order to achieve these overall objectives, the following key goals were identified:

1. Conduct a review of the current neurovascular (smooth muscle, endothelial and astrocyte cell) models in the literature

2. Construct a working model of the neurovascular unit using previous cell models and additional physiological information

3. Analyze the contributions of two known neurovascular coupling mechanisms to blood flow regulation as a whole; namely, 1) a K^+- and EET- based mechanism and 2) a NO-based mechanism

4. Ensure that the model and its results are communicated in a format that is accessible to all members of the biological science community (experimentalists, clinicians and mathematicians)

Chapter 2

The Physics and Mathematics of Physiology

2.1 Introduction

The earliest physiological investigations were explorations into physical forces. They sought to understand "how chemical, electrical and mechanical forces are transmitted, transduced and processed in and around living organisms [19]." Or in other words:

> "La vie . . . n'est autre chose qu'un phenomen physique."
>
> —Lamarck [95]

Essentially: "Physiology is physics."

Physiology is a form of physics and physics can be translated into the language of mathematics. It is therefore natural to develop a mathematical approach to physiological study.

The aim of this project is to translate the physiology of neurovascular coupling into mathematical terms in the hope that the mathematics will help reveal the physiology. The following chapter endeavours to outline this translation process, beginning with very basic mathematical principles. Because this research sits evenly in the interstices between complex mathematics and complex physiology, it seemed important to describe both of these aspects so that a reader unknowledgeable in one aspect could understand the work as a whole. To this end, many of the mathematical ideas have been explained from very simple first principles (that is, assuming the reader has little training in mathematics). Furthermore, before we can explore the modelling that has already been done in the field of microvasculature research (Chapter 5), we must first understand what modelling is and how it adds value and insights to the research. Thus, it is useful to 1) explain the reasons why we make an effort to create mathematical (or *"theoretical"*) models and 2) to outline the differences between various different kinds of theoretical models.

2.2 Calculus and Differential Equations

Some scientific principles give information about the value of a variable at a given instant. Examples include Ohm's Law ($V = IR$) or Hooke's Law for Springs ($F = kx$). However, some laws of science do not provide direct information about the value of the variable which you want to measure. Take Newton's second law, for example:

$$\sum F = ma$$

Translated out of the language of mathematics this says: "The sum ($\sum$) of all the forces (F) acting on an object is equal to the mass (m) of that object multiplied by its acceleration (a)." You might be interested in the object's speed or its position in space, but the equation only gives you information about the acceleration. If you want to know about the velocity or position, you need a way to describe and manipulate change – that is, you need calculus, derivatives and differential equations. Things change. It is therefore important to have a mathematical way of talking about change. This is why differential equations appear throughout many branches of science – in physics, chemistry, economics, and, importantly (for the purposes of this project), physiology. The relationships between change, derivatives, differential equations and integration are outlined below.

2.2.1 Change

We can describe large changes and small changes. Let's start with large changes:

$$\frac{\text{change in } a}{\text{change in } b} = \frac{\Delta a}{\Delta b} \tag{2.1}$$

Equation 2.1 describes how much a changes with b. We can say that this is the change in *a with respect to b*.

Often we are interested in changes with respect to time. A change in the value of a variable K for a given time interval Δt is:

$$\frac{\text{change in } K}{\text{change in time}} = \frac{\Delta K}{\Delta t} \tag{2.2}$$

We are sometimes interested in changes across space. A change in the value of K with respect to its position x is described similarly:

$$\frac{\text{change in } K}{\text{change in } x} = \frac{\Delta K}{\Delta x} \tag{2.3}$$

Returning now to acceleration: the change in velocity with time (acceleration) can be described by:

$$\text{average acceleration over a time interval} = \frac{\text{change in velocity}}{\text{change in time}} = \frac{\Delta v}{\Delta t} \tag{2.4}$$

This equation will give us the average change in velocity (acceleration) in the time interval measured. If we want the acceleration at a given instant (the "instantaneous acceleration"), however, we must consider the change in velocity that occurs over the time interval of an "instant." To calculate this perfectly using perfect mathematics, we consider what the rate of change of velocity would "tend to" over a infinitesimal time interval (an interval so small it is almost zero: an "instant"). We compute the rate of change as the "limiting value of the ratio of the differences $\frac{\Delta v}{\Delta t}$ as Δt becomes infinitesimally small." *Differentiation* is a method of finding what the rate of change "tends to" at any given instant. The notation used to denote a very small (almost zero) change is d (this is sensible notation (as invented by mathematician Gottfried Leibniz) as the lowercase d is a "small" version of the uppercase greek "D", Δ). In Leibniz's notation, such an infinitesimal change in t is denoted by $\mathrm{d}t$, and the *derivative* of v with respect to t is written:

$$\text{instantaneous acceleration} = \frac{\mathrm{d}v}{\mathrm{d}t} \tag{2.5}$$

where $\frac{\mathrm{d}v}{\mathrm{d}t}$ is an example of a *first order* derivative.

As we know, velocity is another value that can be expressed in terms of change (it describes the change in position, x, with time). Velocity can therefore be expressed as a first order derivative itself:

$$\text{instantaneous value of velocity} = \frac{\mathrm{d}x}{\mathrm{d}t} \tag{2.6}$$

A *second order derivative* arises when we want to express acceleration in a different way: in terms of the position, x, rather than the velocity, v. If acceleration is the change in velocity with time, and velocity is the change in position with time, acceleration is the *change* in the *change* of position with respect to time, and is therefore given by:

$$acceleration = \frac{\mathrm{d}^2x}{\mathrm{d}t^2} \tag{2.7}$$

the *second* order derivative (demonstrated by the power of 2).

When first or second (or even higher order) derivatives are used in an equation, you have a *differential equation*. Differential equations involving derivatives of position and velocity with respect to time can be used in physiological or anatomical modelling to describe changes in the

position (displacement) of limbs, organs, vessels, muscles or cells. Other differential equations used in physiological modelling involve the changes in the chemical/ionic concentration inside or outside a cell with time. These equations appear when a mass balance is performed on the closed system of the cell. Mass balances are explained in the following section.

2.2.2 Mass Balances

> "The Law of the Conservation of Mass: Although matter may change its form or shape, its mass always remains the same."
>
> — Antoine-Laurent Lavoisier, French chemist (1743–1794)

In other words: The mass that enters a system must, by conservation of mass, either leave the system or accumulate within the system. In an equation:

$$\text{Input} = \text{Output} + \text{Accumulation} \tag{2.8}$$

Or, in the case where there is a chemical reaction or a change in state:

$$\text{Input} + \text{Generation} = \text{Output} + \text{Consumption} + \text{Accumulation} \tag{2.9}$$

Rearranging the simple balance (Equation 2.8) gives:

$$\text{Accumulation} = \text{Input} - \text{Output} \tag{2.10}$$

In the situation where we have a flow of mass entering and a flow of mass leaving a closed compartment, we can rewrite this equation as:

$$\text{change in mass inside the system per unit time} = \text{mass flowrate in} - \text{mass flowrate out} \tag{2.11}$$

This is shown graphically in Figure 2.1.

In physiological modelling, we are often concerned with the changing concentrations of ions and other chemical species inside the cell with time. We can write a mass balance for a specific ion or chemical (denoted by K) by replacing the accumulation or "change term" with a differential term. We get the following *differential* equation (DE):

$$\text{Accumulation of } K \text{ with time} = \frac{\mathrm{d}K}{\mathrm{d}t} = F_{in} - F_{out} \tag{2.12}$$

where t denotes time and where F_{in} and F_{out} are shorthand representations of the flowrate of

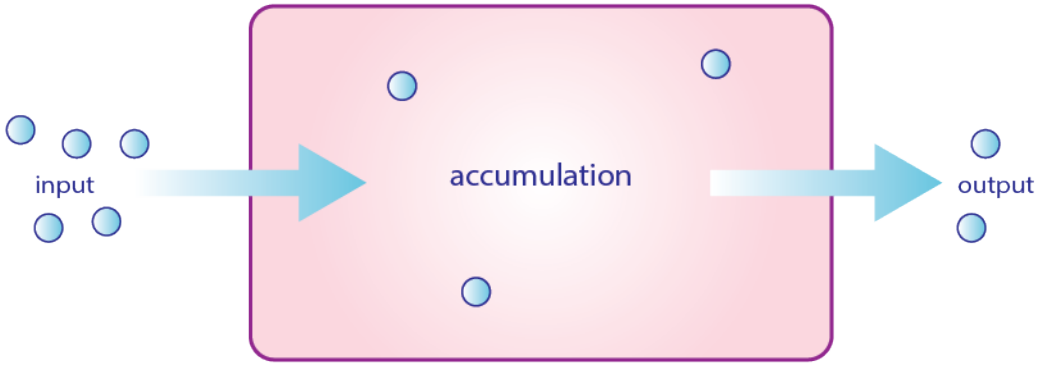

Figure 2.1 Accumulation of material inside a closed compartment. A flowrate of 5 dots per unit time in minus a flowrate of two dots per unit time out gives an accumulation in the system of 3 dots per unit time.

substance K in and out of the cell, respectively. Accumulation can actually be positive or negative. If positive, then Input is greater than Output, and K will literally "accumulate" in the cell. If the Accumulation term is negative, then Output is greater than the Input, and K will be "depleted" in the cell.

Note that sometimes the value of a variable changes with position *and* with time. This complicates the maths, and requires the use of *partial* derivatives (recognisable by the curly '∂' as opposed to the 'd' of an *ordinary* derivative). To simplify a model so that it is the type involving only ordinary derivatives, we can assume that variables do not change with their position in space. In the case of a model of a chemical K in a cell: if we assume the cell acts as a "well-mixed" compartment, we can assume that the value of the variable K is the same throughout the entire cell at a given instant. If a differential equation describes a change with respect to only one variable (like time t in Equation 2.12), then it is called an *ordinary differential equation* or ODE.

2.2.3 "Undoing" Differential Equations using Integration

To obtain the *solution* from a differential equation (that is, to find the value of the variable itself as opposed to the value of the *change* of the variable), you must "undo" the derivative using the process of *anti-differentiation* (or *integration*, for short). There are many different mathematical techniques involved in integration; the type of technique used depends on the particular mathematics used in the differential equation. In many situations, there will not be a technique available that is able to undo the differential equation perfectly. In this case, we would say that the analytical (or *exact*) solution cannot be found.

2.2.4 Solving Differential Equations Numerically

The physiological phenomena modelled in our system are complex and *non-linear* by nature; sigmoidal and exponential behaviour is very common in physiology. In addition, many of the equations that we use are *coupled* with other equations (certain variables depend on the values of other variables (for example: the membrane potential of a cell might depend on the concentrations of potassium K^+ and calcium Ca^{2+})). Finally, the different physiological processes we are trying to model operate on vastly different timescales (for example, the binding of the chemical glutamate at a receptor would occur much faster than muscle contraction would); this property creates what is known as a "stiff" system. Analytical solutions are not usually possible for complex, coupled or non-linear systems of differential equations (like those used in physiological modelling). *Numerical integration* techniques must therefore be used to find a solution that approximates the actual analytical solution. There are many numerical integration techniques that can be used; the choice of method depends on the nature of the equation set ("stiff" systems need certain techniques), the amount of error that can be tolerated and the computational expense of the method. In practice, higher order Runge-Kutta (RK) methods are used to solve such problems because of their superior convergence and stability features. *4th order explicit* RK methods are commonly used. A brief description of these methods, in the context of a system of ODEs, follows.

Say we have a collection of variables that describe our physiological system (let's assume the variables we are interested in are called y_1, y_2, y_3 and y_4). Rather than describe each variable and its corresponding differential equation separately, we can collect these variables together as an *array* – a collection of variables. This will help simplify the explanation. So our array would be $\mathbf{y} = \begin{bmatrix} y_1 & y_2 & y_3 & y_4 \end{bmatrix}$ or $\mathbf{y}(t) = \begin{bmatrix} y_1(t) & y_2(t) & y_3(t) & y_4(t) \end{bmatrix}$. Therefore, all the ODEs in our set (or *system*) will be of the form:

$$\frac{\mathrm{d}\mathbf{y}}{\mathrm{d}t} = f(t, \mathbf{y}(t)) \tag{2.13}$$

Here, the change in any one of the variables in the array $\mathbf{y}$ (i.e., y_1, y_2, y_3 or y_4) with respect to time t is described by a mathematical function f that could depend on the value of time t itself and/or the value of any one of the variables in the array $\mathbf{y}$ at time t. So, for example, the change in the variable y_1 may depend on time t and the components of the array $\mathbf{y}(t)$ in the following way:

$$\frac{\mathrm{d}y_1}{\mathrm{d}t} = f(t, \mathbf{y}(t)) = 3y_1(t)^2 + 2y_2(t) + 6y_3(t-4) + y_4(t)^3 \tag{2.14}$$

Note that $y_1(t)$, $y_2(t)$, $y_3(t)$, $y_4(t)$ and t don't all have to be involved in the DE. For example, the change in the variable y_1 at a certain time t may only depend on its own value, like in

Equation 2.15 below:

$$\frac{\mathrm{d}y_1}{\mathrm{d}t} = f(t, \mathbf{y}(t)) = 7y_1(t)^2 + 20 \tag{2.15}$$

We can think of t as some time between t_0 and t_f (the start and finish time of a time interval of interest, respectively). Let us assume that we know all the initial values ($\mathbf{y}_0$) of all of the variables in $\mathbf{y}(t)$ at the start time (t_0). That is:

$$\mathbf{y}(t_0) = \mathbf{y}_0 \tag{2.16}$$

If we know the initial value of all the variables, then the system of ODEs can be described as an *initial value problem*.

To find a numerical solution that approximates the analytical solution for this set of ODEs, we can first split the time interval of interest into N sections, each consisting of a small time step h. To solve an initial value problem like the one in Equations 2.13 and 2.16 you would take one variable at a time (starting with y_1) and use an explicit "sth" order RK method which would use the present value of the variable y at time step t (i.e., $y(t)$) to approximate $y(t+h)$, the value of y at the next time step $(t+h)$ using this general formula:

$$\begin{aligned} y^{(n+1)} &= y^n + b_1k_1 + b_2k_2 + b_3k_3 + \cdots b_sk_s = y^n + \sum_{i=1}^{s} b_ik_i \\ t^{n+1} &= t^n + h \end{aligned} \tag{2.17}$$

where

$$\begin{aligned} k_1 &= h\, f(t^n, y^n) \\ k_2 &= h\, f(t^n + c_2h, y^n + a_{21}k_1) \\ &\vdots \\ k_s &= h\, f(t^n + c_sh, y^n + a_{s1}k_1 + \cdots + a_{s,s-1}k_{s-1}) \end{aligned} \tag{2.18}$$

n is the nth, or previous, timestep; $(n+1)$ is the $(n+1)$th, or next/current, timestep; s is the number of stages (or the *order* of the RK method); the function f is the same function described in the system of ODEs (Equation 2.13), but different values are substituted into it (as shown) for each of k_1, k_2 and so on, up until k_s. Note that $\sum_{i=1}^{s} b_ik_i$ is a shorthand representation meaning "evaluate b_ik_i at all the values of i (starting at 1 and stopping at s), then add them all together." a_{ij} (for $1 \leq j < i \leq s$), b_i (for $i = 1, 2, \ldots, s$) and c_i (for $i = 2, 3, \ldots, s$) are special coefficients specific to the order of the method (found from a special mnemonic device known as a "Butcher Tableau" (Figure 2.2) – named after John C. Butcher, Emeritus Professor at the University of

Auckland, New Zealand).

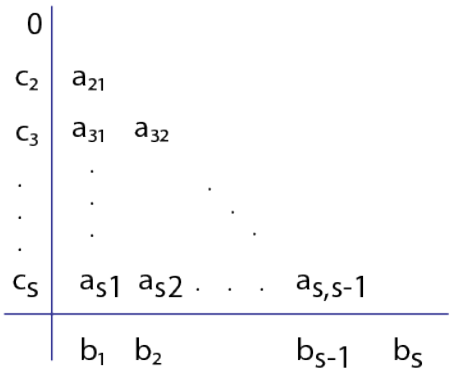

Figure 2.2 Butcher Tableau. Adapted from [1].

The Butcher Tableau for a fourth order RK method (RK4) is shown in Figure 2.3.

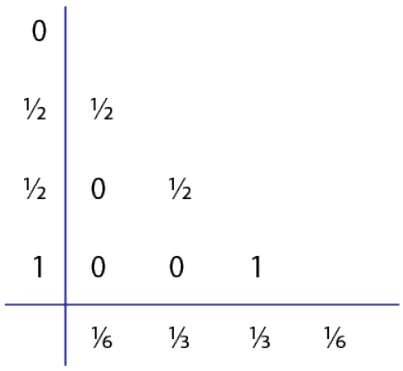

Figure 2.3 Butcher Tableau for RK4 method. Adapted from [1].

Obviously, it is less "expensive" (in terms of computational time) to have fewer, larger time steps. However, a larger step size (h) will produce a less accurate result. Ideally, you want the largest step size you can without allowing the solution to diverge from the actual solution (here you can define an acceptable error *tolerance* for your problem). This step size may need to be smaller or larger at different stages in a simulation or for equations with widely different timescales (*stiff* systems). *Adaptive* RK methods are used in these circumstances.

Adaptive methods produce an estimate of the local truncation error at a single step and then use that estimate to adjust the step size for the next iteration. The actual error between the calculated numerical solution and the actual solution cannot be calculated (as the actual

solution is not known). For the purposes of adaptive step size calculations, the exact solution is instead estimated as the solution gained using a RK method one order higher. An RK-45 method is a fourth order method that uses the fifth order calculation to help adjust the step size. This is done by having two methods in the tableau, one with order s and one with order $(s-1)$. The lower-order step (labelled using an *) is calculated:

$$y^{*n+1} = y^{*n} + \sum_{i=1}^{s} b_i^* k_i \tag{2.19}$$

where the k_i are the same as for the higher order method and b_i^* can be found from an extended version of the Butcher Tableau for this method.

The estimated error (at any given step) can be calculated as follows:

$$e^{n+1} = y^{n+1} - y^{*n+1} = h\sum_{i=1}^{s}(b_i - b_i^*)k_i \tag{2.20}$$

Now, if h_1 is the step taken by the solver to produce an error ε_1, then the step size h_0 that would have produced an error ε_0 can be calculated by

$$h_0 = h_1 \left| \frac{\varepsilon_0}{\varepsilon_1} \right|^{1/s} \tag{2.21}$$

Here ε_0 represents the desired accuracy or *tolerance* – this is decided before we begin. Thus, if $\varepsilon_1 > \varepsilon_0$ Equation 2.21 will calculate how much h_0 should decrease by, and if $\varepsilon_0 > \varepsilon_1$, it will calculate how much it should increase by. In this way, as solution progresses, the solver will adjust to smaller step sizes when the solution exhibits stiffness, and adjust to larger ones as the solution exhibits smoother behaviour.

In practice, systems of ODEs are solved using these types of numerical algorithms implemented on a computer system.

2.3 Sigmoidal Behaviour

Many natural processes, including the opening of ion channels in a cell, exhibit a progression from a small value that increases quickly and approaches a plateau over time. This "S-shaped" behaviour can be described by a sigmoidal function – Figure 2.4.

There are many ways to mathematically represent a sigmoidal function; some use the exponential function ($\exp(x)$) and some use the hyperbolic tan (tanh) function. For more information

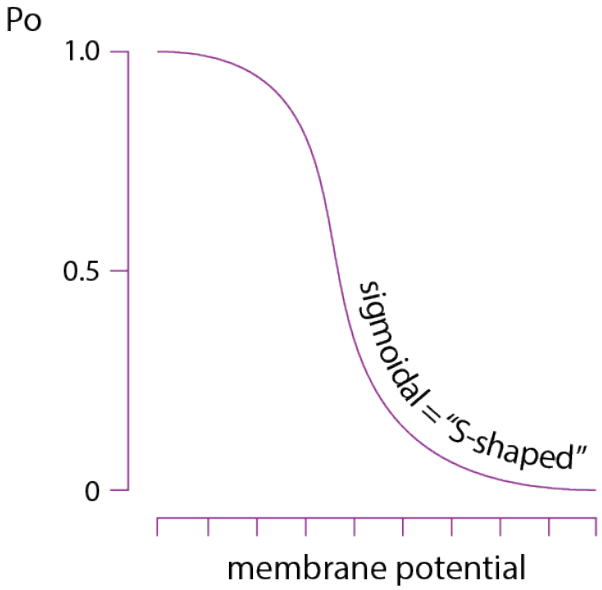

Figure 2.4 Example of sigmoidal behaviour: the fraction of open channels at different cell membrane potentials.

about these representations and how ion channels are represented by sigmoidal functions, see Appendix C.

2.4 Binding and the Hill Equation

The binding of a ligand to a receptor can be enhanced if there are already other ligands bound on the same receptor; this phenomenon is known as *cooperative* binding. The Hill equation can be used to characterize such binding behaviour (as a function of ligand concentration). It can be easily derived from the binding scheme below in which n molecules of ligand L bind to a receptor R [162]:

$$R + nL \underset{k_b}{\overset{k_f}{\rightleftharpoons}} RL_n \tag{2.22}$$

or

$$R + nL \overset{K_d}{\rightleftharpoons} RL_n \tag{2.23}$$

where the dissociation constant, which describes the tendency of a larger object to "break up" into smaller pieces, is given as $K_d \equiv \dfrac{k_b}{k_f}$. The Hill Equation is as follows:

$$\frac{\text{bound}}{\text{total}} = \frac{[L]^n}{K_d + [L]^n} \tag{2.24}$$

n (the Hill coefficient) provides a way to quantify the cooperativity of the binding. A coefficient greater than 1 indicates "positive cooperation" (that is, once one ligand is bound, the enzyme's affinity for other ligands *increases*). A coefficient less than 1 describes the opposite (that is, the affinity *decreases*). A coefficient equal to 1 indicates a "non-cooperative reaction" where the affinity is independent of prior ligand binding.

It is important to note that the reaction scheme (Equation 2.23) that gives rise to the Hill equation is a convenient mathematical simplification of binding that implies "simultaneous" binding; in reality, however, binding will occur in a sequential or independent fashion (Figure 2.5).

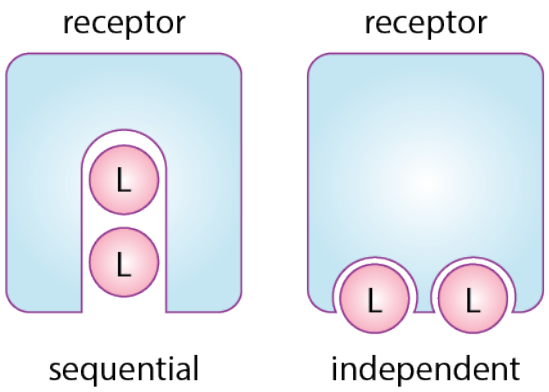

Figure 2.5 Schematic representation of a sequential vs. an independent ligand binding mechanism. L, ligand; R, receptor. Adapted from [162].

2.5 Michaelis-Menten Kinetics

"Michaelis-Menten kinetics" (named after German biochemist Leonor Michaelis and Canadian physician Maud Menten) can be used to describe enzyme and protein-protein interactions. The model consists of a single equation which describes the rate of an enzymatic reaction by relating the reaction rate V to $[S]$, the concentration of a substrate S. Its formula is given by:

$$V = \frac{V_{\max}[S]}{K_m + [S]} \tag{2.25}$$

$V_{\max}$ is the maximum rate achieved by the system at maximum (saturating) substrate concentrations. K_m is the substrate concentration at which the reaction rate reaches half of $V_{\max}$. A *small* K_m indicates that the substrate has a *high* affinity for the enzyme, so the reaction rate will approach $V_{\max}$ more quickly. As shown in Figure 2.6 below, the reaction rate increases with

substrate concentration $[S]$, and tends to its maximum rate $V_{\max}$ when all the enzyme is bound to the substrate.

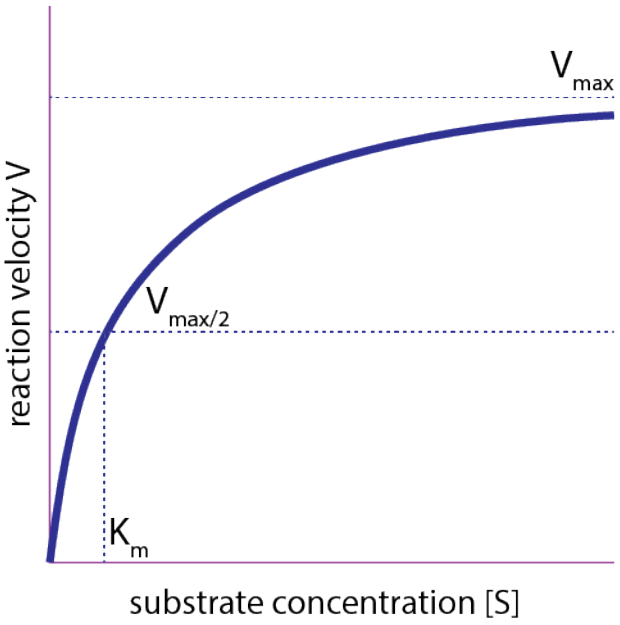

Figure 2.6 Michaelis-Menten kinetics and parameters. Adapted from [8].

2.6 Electrical Math

Cells in the human body are "powered" by electricity (Figure 2.7). This electricity has many similarities to the electricity that flows through the wires of an electrical appliance; therefore, with some adjustments, we can use the same equations for cell electricity as those used for standard electrical circuits. First: the definition of important terms and equations. Then: how to use them in the context of cell electricity.

Current (I) is the flow of electric charge through a medium. Commonly, we think of electrical charge travelling through a wire as negatively charged electrons, but electrical charge can travel in and out of cells as positively charged ions also. Voltage (V, also called *electromotive force*) is the potential difference between two points in an electrical field. As cells are usually more negative inside the cell membrane than they are outside, they have a membrane voltage (or membrane potential). The greater the voltage, the greater the flow of electrical current through a conducting medium for a given resistance (R) to that flow. This can be summarised

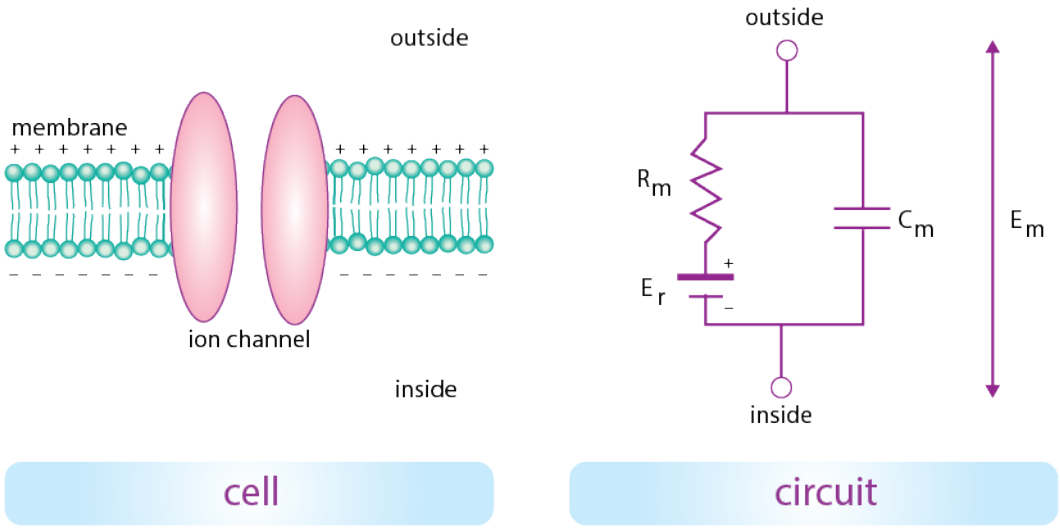

Figure 2.7 The origin of the electrical equivalent circuit of the cell membrane. Adapted from [21].

in Ohm's Law, the first important equation needed for cell electrical analysis:

$$V = IR \tag{2.26}$$

Capacitance (C) refers to the ability of a system (in this case, a cell membrane) to store electrical charge. It can be quantified as the ratio of charge (Q) to potential (V). Charge is not a useful measure for these purposes and it can instead be written in terms of current (as current (I) is the rate of change of charge (Q) with time (t)). That is:

$$I = \frac{dQ}{dt} \tag{2.27}$$

As $C = Q/V$ (or $Q = CV$), a small change in Q (δQ) will yield a corresponding small change in V (δV) to give:

$$\delta Q = C\delta V \tag{2.28}$$

Combining Equations 2.27 and 2.28 to obtain a more useful (and differential) form of the capacitance law gives:

$$C\frac{dV}{dt} = I \tag{2.29}$$

As there are many ion channels present in a cell membrane, there are many different currents. We therefore rewrite Equation 2.29 in terms of the *sum* of all the currents of ions through

all the membrane's N ion channels (Equation 2.30).

$$C\frac{dV}{dt} = \sum_{i=1}^{N} I_i \tag{2.30}$$

The current I_A through a generalized "A" ion channel can be expressed by a special form of Ohm's Law (Equation 2.31). Here, *conductance* g_A – the *ease* by which the channel conducts charge – is used instead of its reciprocal, resistance (a measure of how much the channel *resists* flow).

$$\text{Ohm's Law: } I = \frac{V}{R} \Rightarrow I_A = g_A a\,(V - V_A) \tag{2.31}$$

where g_A is the maximum conductance for all "A" ion channels in the cell, a is the fraction of open "A" channels, V is the membrane potential of the cell, and V_A is the reversal potential (or Nernst potential). The reversal potential (V_A) is the membrane potential at which there is no net flow of an ion from one side of the membrane to the other (an equilibrium state). Therefore, the terms $(V - V_A)$ constitute the "driving force" for ionic flow.

If an ion channel type selective to one species of ion dominates within the membrane of a cell (perhaps because this type is present in greater densities or because other ion channels are closed), then the cell's membrane potential will tend to equilibrate to the reversal potential for that ion.

2.7 Fluid Flow and Electricity

When a fluid in a pipe is subjected to a pressure gradient, it will flow along the pipe. The rate at which the fluid flows (Q) is proportional to the pressure gradient (ΔP) driving that flow. So,

$$Q \propto \Delta P \tag{2.32}$$

This flow will be met with a resistance (R), which gives:

$$Q = \frac{\Delta P}{R} \tag{2.33}$$

The flow of fluid through a pipe and the flow of charge through a circuit can be described in a similar way using the language of mathematics. In fact, the relationship between fluid flow and pressure in the pipe is analogous to Ohm's Law for electrical circuits:

$$I = \frac{\Delta V}{R} \tag{2.34}$$

Here, the *flow* of electrical current (I) is driven by a difference in electrical potential or voltage (ΔV) and is *resisted* by the resistance (R) of the electrical components in the circuit.

The resistance to *fluid* flow in a pipe results from 1) the friction between particles in the fluid (this is reflected in the *viscosity* of the fluid), and 2) the friction between the fluid and the pipe wall (which is determined by the pipe's length and radius). Resistance can therefore be represented mathematically by:

$$R = \frac{8\mu L}{\pi r^4} \tag{2.35}$$

where L is the length of pipe, μ is the viscosity, and r is the radius.

Equation 2.35 demonstrates that changes in the radius of the pipe can have a profound effect on fluid flow as the resistance to flow is inversely proportional to the *fourth* power of the radius. For example, halving the radius of a pipe increases the resistance to fluid movement by a factor of 16.

The combination of Equations 2.35 and 2.33 gives Poiseuille's Law:

$$\Delta P = \frac{8\mu L Q}{\pi r^4} \tag{2.36}$$

In the context of blood flow autoregulation modelling, we are interested in the relationship between compensatory blood vessel radius changes and the corresponding change in blood flow delivery to the tissue. In a rearrangement of Poiseuille's Law, the radius of a vessel r and the blood flow through that vessel Q, can be shown to be related by:

$$Q = \frac{\Delta P \pi r^4}{8\mu L} = \frac{\Delta P \pi}{8\mu L} r^4 = K r^4 \tag{2.37}$$

Here we simplify this relationship by assuming all the other components are constant and "lumping" them together as one term, K.

We are interested in the *changes* in r and Q and how they relate to one another and so we need to use derivatives of r and Q. They are related as follows:

$$\delta Q = \frac{\partial Q}{\partial r} \delta r \tag{2.38}$$

Differentiating Equation 2.37 with respect to r and substituting the result into Equation 2.38 yields Equation 2.39 below.

$$\delta Q = \frac{\partial Q}{\partial r} \delta r = 4 K r^3 \delta r = 4 K r^4 \frac{\delta r}{r} \tag{2.39}$$

As $Q = Kr^4$, Equation 2.39 becomes:

$$\frac{\delta Q}{Q} = 4\frac{\delta r}{r} \tag{2.40}$$

This means that the expected *relative* or *percentage* change in blood flow ($\frac{\delta Q}{Q}$) will be four times the percentage change in radius ($\frac{\delta r}{r}$) that causes it. For example, a 1% change in radius corresponds to a 4% change in blood flow through that vessel.

2.8 Muscles as Machines

Muscle converts the chemical fuel that we obtain from our food into the force and power needed to move parts of our body (like our legs, arms and importantly, the walls of our blood vessels). Our "muscle machinery" is comprised of myosin and actin proteins and the chemical fuel "burned" is in the form of ATP. Neither myosin nor actin has the ability to contract by itself. Contraction instead comes from the "interdigitation of myosin and actin [159]" which allows the filaments to ratchet along each other. This ratcheting action is analogous to hauling something toward you by pulling a long rope, arm over arm [159]. The "arms" here are thick protrusions from myosin filaments that attach (in a *crossbridge*), swing through an arc, detach and then reattach farther along the actin filaments. The swinging movement that occurs when they are attached is the motion that accomplishes contraction. The following questions remain:

- How do we quantify the movement of contraction?
- Are there other forces at play other than the active force of contraction?
- What equation/s are needed to describe these?
- How do we work with the cylindrical geometry of the smooth muscle layer in the arteriole?

The answers to these questions are not obvious, nor are they definite. In fact, different modellers use different models and/or model parameters depending on 1) their understanding of the mechanism involved, 2) the experimental data on which their contraction information is based, and 3) the assumptions and simplifications they define as part of the model development. One method of modelling vascular smooth muscle cell contraction begins by first considering a section of the arteriolar wall as a viscoelastic material (that is, a material that has both elastic and "viscous" (damped) properties), and then applying a force balance to it.

The active force that is provided by the crossbridges in the smooth muscle is not the only force that we need to consider. There is also the force provided by the pressure of blood acting

on the wall, the wall shear stress exerted by the flowing blood, and the viscoelastic forces exerted by the components of the wall. It helps to first have an understanding of the forces involved in this situation. The following sections describe the concepts and definitions needed to develop a model of muscle contraction (which we will do in Chapter 6).

2.8.1 Stress σ

A deformable body is a physical object that can be deformed; i.e., it will change its shape when an external force acts upon it. Stress is a measure of the *internal* forces acting *within* the body which are reactions to *external* forces applied *on* the body. *Tensile* stress acts to stretch while *compressive* stress acts to compress. Stress can be quantitatively described as the average internal force applied per unit area of a surface within the body. Therefore, the dimension of stress is that of pressure and has the (SI) unit of a pascal (symbol Pa). It is important to note here that although stress has the dimension of pressure, the external forces that act on the body do not have to be perpendicular (or *normal*) to the surface of the object. Forces can also be applied tangential to the body, as will be shown in a later section.

2.8.2 Strain ε

When a body is deformed, particles within the body are displaced from their original position. A strain is a normalized measure of the size of the deformation/displacement relative to an initial or reference body size. Strains are relative measures and are thus dimensionless. They are usually expressed as a decimal fraction, as a percentage, or in "parts-per" notation.

2.8.3 Measures of Stretchiness (Elasticity)

The relationship between tensile stress and strain in a deformable body is unique for each material and can be measured using a tensile test, where the amount of deformation (strain) is measured at known levels of stress. This data can be represented as a stress-strain curve (Figure 2.8). The elastic modulus of the body is the slope of this curve in the elastic deformation region (the region in which the body will still "spring back" to its initial shape after the force is removed). A stiffer material will have a higher elastic modulus. In the case of tensile elasticity, the elastic modulus is called the Young's modulus (E).

There are also other measures to describe elasticity. For example, when a body is stretched it tends to get longer in the direction of the stretch, but thinner in the other two directions

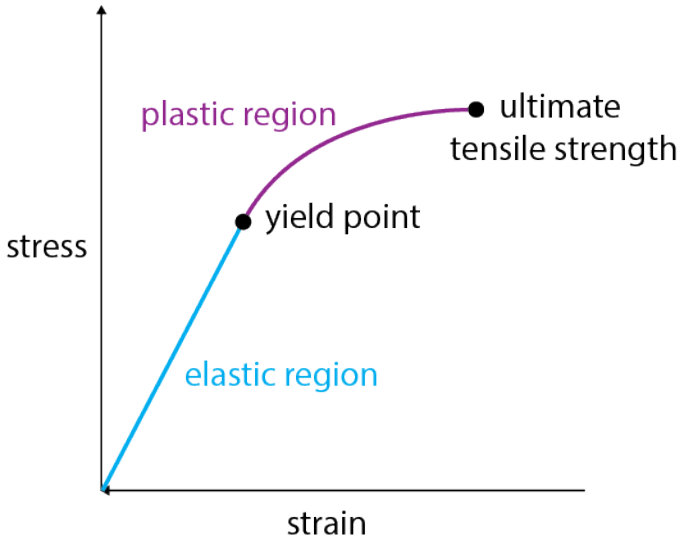

Figure 2.8 A stress-strain curve. The elastic modulus is the slope in the initial (elastic deformation) region. Adapted from [10].

(Figure 2.9). This phenomenon is the Poisson effect, which is quantified by Poisson's ratio, ν. The Poisson ratio is the ratio of the fraction of expansion divided by the fraction of compression.

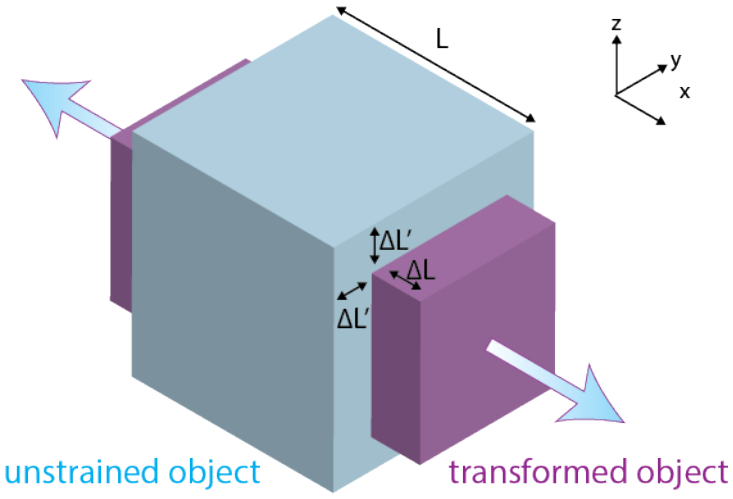

Figure 2.9 A cube with a Poisson's ratio of 0.5 and sides of length L is stretched along the x axis. The transformed cube is expanded in the x direction by ΔL and contracted in the y and z directions by $\Delta L'$. Adapted from artwork released into the public domain [3].

2.8.4 The Stress Tensor

One cannot describe a stress without first specifying the direction on which it acts. Stresses acting on a body can be resolved (split up) into three orthogonal (perpendicular) components: one component is normal to the surface and represents *normal* or *direct* stress and the other two components are tangential to the surface and represent *shear* stresses. Direct stresses will change the volume of the body; shear stresses will change the shape of the body, but the volume will remain unchanged.

In Cartesian ("xyz") coordinates, the stress at a single point inside the body can be represented by an infinitesimally tiny cube with the three stress components on each of its sides (one direct and two shear components for the top/bottom, left/right and front/back sides) – Figure 2.10. These nine components can be organized into a matrix: $\begin{bmatrix} \sigma_{xx} & \sigma_{xy} & \sigma_{xz} \\ \sigma_{yx} & \sigma_{yy} & \sigma_{yz} \\ \sigma_{zx} & \sigma_{zy} & \sigma_{zz} \end{bmatrix}$

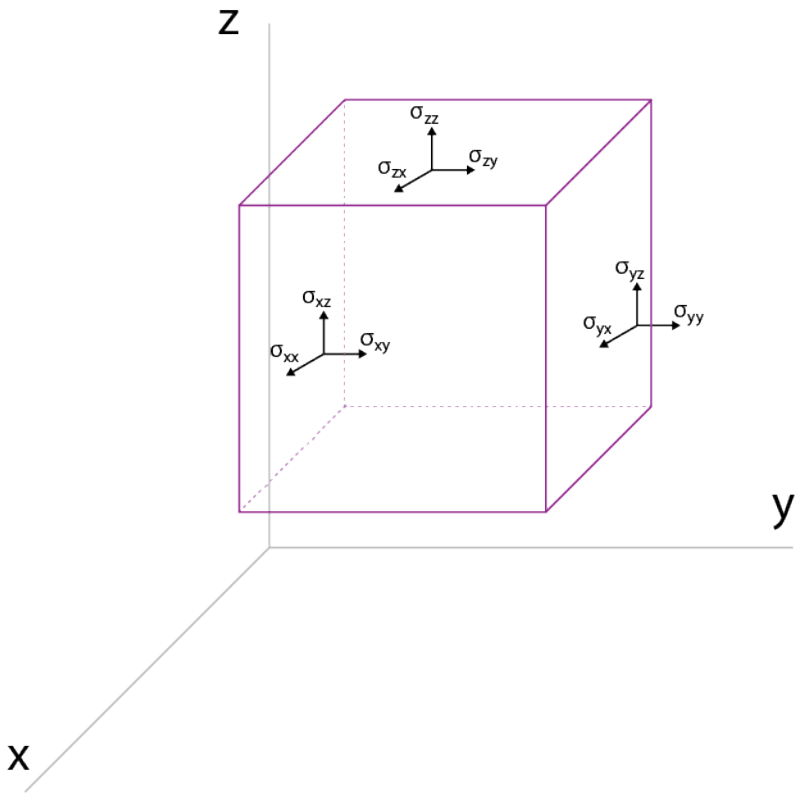

Figure 2.10 The nine stress components in a Cartesian coordinate system. Adapted from [5].

This special way of grouping the components together is known as the *stress tensor*.

Sometimes, the Cartesian coordinate system described above is not the most useful system to use. For example, the force applied to an arteriole wall can be decomposed more easily into components parallel to the *cylindrical* coordinates: r, z, and θ (Figure 2.11). These forces induce corresponding stresses within the body: *radial* stress, *axial* stress and hoop (or *circumferential*) stress, respectively.

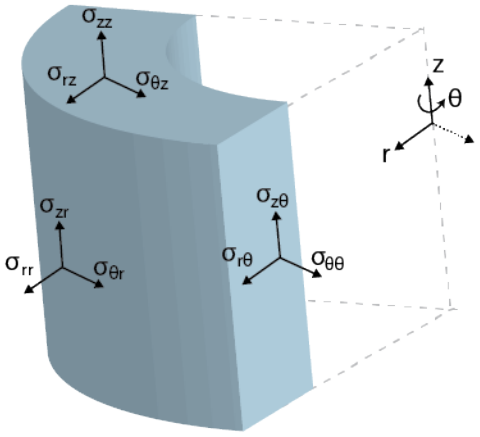

Figure 2.11 The nine stress components in a cylindrical coordinate system. Adapted from [7].

In both cases, there are nine possible stresses that can act on any internal point within the body. The sum of these stresses will determine how the body "deforms" (changes shape).

2.8.5 Models of Viscoelasticity

Several viscoelastic models exist and they are comprised of combinations of two main elements:

- a dashpot with viscosity η which obeys the relation $\sigma = \eta \cdot \frac{d\varepsilon}{dt}$
- a spring with elastic modulus E which obeys the relation $\sigma = E \cdot \varepsilon$

These elements are shown schematically in Figure 2.12.

Common viscoelastic models include the Kelvin-Voigt and the Maxwell models (Figures 2.13 and 2.14, respectively).

We can then make mathematical statements about the stresses (and strains) in the model of our choice. Let's take the Kelvin-Voigt model (Figure 2.13) as an example:

(a) dashpot

(b) spring

Figure 2.12 A dashpot with viscosity η and a spring with elastic modulus E

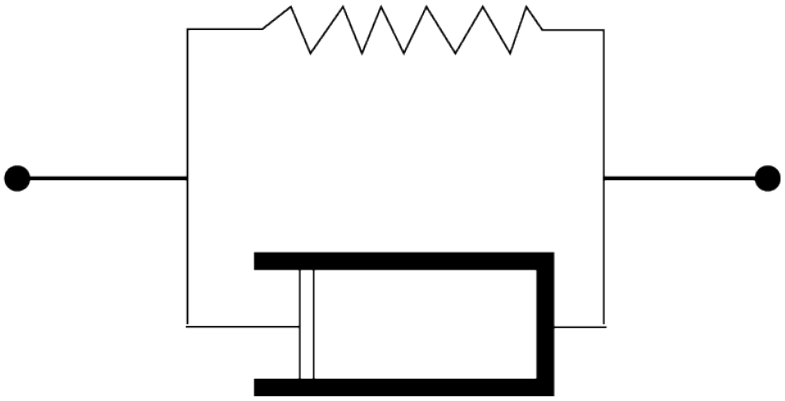

Figure 2.13 The Kelvin-Voigt model, which consists of a dashpot and a spring connected in parallel

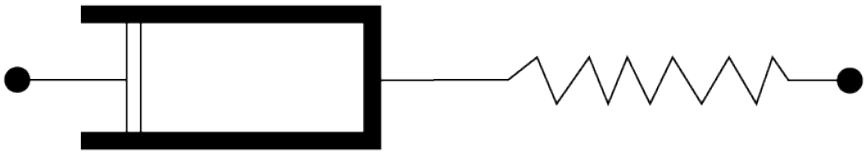

Figure 2.14 The Maxwell model, which consists of a dashpot and a spring connected in series

The two components of the model are arranged in parallel; as such, the strains in each component are identical:

$$\varepsilon_{total} = \varepsilon_{dashpot} = \varepsilon_{spring} \tag{2.41}$$

Similarly, the total stress will be the sum of the stress in each component (that is, the applied load is borne by the spring and the dashpot):

$$\sigma_{total} = \sigma_{dashpot} + \sigma_{spring} \tag{2.42}$$

From these equations and the two relations $\sigma = \eta \cdot \frac{d\varepsilon}{dt}$ and $\sigma = E \cdot \varepsilon$, we deduce, that in a Kelvin-Voigt material, stress σ, strain ε and their rates of change with respect to time t are determined by Equation 2.43:

$$\sigma(t) = E\varepsilon(t) + \eta \frac{d\varepsilon}{dt} \tag{2.43}$$

2.8.6 Laplace's Law for Thin-Walled Vessels

Laplace's Law states that if you have a larger vessel radius, you will need a larger wall tension to withstand a given internal fluid pressure. Arteries can be viewed as cylindrical thin-walled vessels and can be modelled by the Law of Laplace:

$$T = \frac{pr}{h} \tag{2.44}$$

where T=wall tension, p=pressure, r=radius, and h=wall thickness.

For a given internal fluid pressure, a larger vessel radius requires a larger wall thickness to accommodate a stable wall tension. Further, increases in the pressure load inside the vessel will necessitate an increase in the vessel wall thickness.

2.9 Mathematical Models

2.9.1 What Are Mathematical Models?

Mathematical modelling helps scientists better understand the mechanics and dynamics that underlie their experimental observations [155]. Simply put, a mathematical (or *theoretical*) model is a description of a physical system using mathematical language. Generally, a mathematical model includes a set of variables and a set of equations that relates the variables to one another.

Mathematical models can take many forms and can be classified in many ways. They can:

- be linear or non-linear
- have coupled or uncoupled variables

- be deterministic (with variables uniquely defined by parameters and initial values) or stochastic (with variables represented by probability distributions)
- be static or dynamic (a static model does not account for the element of time, while a dynamic model does)

Physiological models "specify how the concentrations of biochemical substances change in time, in and around cells, when influenced by the presence or absence of other molecules [155]". These models are comprised of a set of differential equations which encompass a variety of parameters, such as rate constants and thresholds, which need to be determined using appropriate experimental data [155].

2.9.2 Why Make Models?

> "The purpose of [mathematical] models is not to fit the data but to sharpen the questions."
>
> — Samuel Karlin, mathematician

It is easy to assume that the purpose of mathematical models is to simply calculate values that are in fitting with experimental data. However, fitting data is not particularly difficult and it provides little information. In fact, modelling is meaningless unless its value or its goal is explicitly stated at the outset. The first step to take in any modelling study is to therefore define the goals that are to be achieved. Bailey [16] provides the following collection of possible goals that arise from the question: Why make models?

- "to organize disparate information into a coherent whole
- to think (and calculate) logically about what components and interactions are important in a complex system
- to discover new strategies
- to make important corrections to the conventional wisdom
- to understand the essential qualitative features [16] "

So, why should we make *physiological* models? Because physiological modelling, in conjunction with experimental work, has the potential to overcome the difficulties we have in understanding multiplex physiological systems such as our circulatory system. Several hypothesized mechanisms can be integrated into a singular framework which can then be used to predict or

understand the overall behaviour of a larger system or behaviours at a lower level (cell, cells, segment, or segments level, in the case of blood flow regulation models). Further, the relative contributions of particular biological pathways can be assessed by removing them from the model, just as it is commonly done in experiment (except in a model, we are creating "mathematical knockouts" instead of physical ones) [143]. Essentially, models help us to organize our confused thoughts about complex biological phenomena. Indeed:

> "The essence of mathematics is not to make simple things complicated, but to make complicated things simple."
>
> — Stanley Gudder, mathematician

2.9.3 Types of Theoretical Models

Models can be roughly divided into two types: conceptual and phenomenological. Conceptual models are based on mathematical descriptions of underlying physical processes, whereas phenomenological models are formed by fitting equations to observed behaviour [144]. A brief description of the uses, benefits and weaknesses of these two model types follows.

2.9.3.1 Phenomenological Models

These models are not built upon descriptions of the underlying physical, mechanical or chemical processes. As such, these models cannot be used for simulations outside of the specific process or data set modelled. However, framing the data in a succinct mathematical construct in the making of these models can help to simplify complex data sets and can help to reveal statistical patterns [144].

2.9.3.2 Conceptual Models

These models are based on a conceptual understanding of the underlying physical mechanism that governs the behaviour. Some model parameters can be known *a priori* or can be scavenged from experimental data. Model results can be compared qualitatively or quantitatively to experimental observations for appropriate values of any unknown parameters. Discrepancies between model and observed behaviour could mean that the mechanism is not valid or that it has been poorly represented by its parameters. If there is agreement, the parameters can be optimized so that the model can obtain the best fit to experimental data. Parameter values outputted from this optimization can then be analyzed in terms of what they could mean in terms of the proposed mechanism. Those unfamiliar with theoretical modelling may judge the success of a model by the nearness of its fit to experimental data [144]. It is important to be aware that it is

not necessarily the case; in fact, a close fit to a set of experimental data does not guarantee the correctness of the proposed mechanism. A failure to achieve a close fit can reveal more to the modeller: the discrepancy can point out the areas in which an incorrect assumption has been made or may make it clear that not enough detail was included [144].

If we are fortunate enough to be modelling a system where the underlying mechanisms are well understood and well characterized, we can build a theoretical model where all the equations and parameters are known. The completed model can be validated against known experimental data, and can then be used to predict results in a computational "experiment." Often, a modeller's ultimate goal is the development of a model that can be extensively validated (compared) against experimental data. However, the value of a predictive sort of model exceeds this limited goal of merely reproducing what has been done before. A successful model could form a constituent of a larger multiscale project [144] or suggest novel experiments that could be used to help advance or reform the model [155]. Even better, it can be used to predict behaviours in conditions that have not yet been studied – or are difficult to study – experimentally. Many and varied computational experiments can be simulated in the time it would take to formulate and undertake a single physical experiment and can be performed without once lifting a scalpel.

2.10 Summary

Physiology is Physics. To understand physiology is to understand how chemical, electrical and mechanical forces are involved with the functioning of living cells and organisms.

Chemical reactions in the body occur in dependence upon the binding of substrates to enzymes. Chemical species can also bind to receptors on cells, initiating further chemical reactions. Differing concentrations of charged ions create a potential difference (voltage) across the membrane, fluxes of charged ions become electrical flux (or current), and the cell membrane itself acts as a capacitor. Mechanical stresses are exerted on deformable vascular walls by flowing blood, by myosin-actin crossbridges, and by viscoelastic wall components. All of these physiological phenomena can be simplified and be more easily understood using the mathematics. In fact, a physiological model is simply a description of a physiological system using mathematical language. Physiological models help us to organize and simplify complex information, think logically about what components are important in a system, and sharpen our research questions.

Chapter 3

Anatomy and Physiology

3.1 Introduction

> "The brain is the great receiving and distributing reservoir of vital electricity, just as the heart is the receiving and distributing reservoir of the blood."
>
> — Edward B. Foote, *Medical Common Sense*, 1866

The problem of the brain and its blood supply is a multiscale one, with scales spanning from the entire brain organ down to the level of ions and proteins that move within and between neuronal and glial cells. Macroscale events can affect systems in the microscale and microscale events can affect macroscale systems. The following chapter gives a brief overview of the important small and big "things" pertinent to this project. I will start with the big (brains and blood vessels) and progress to the small (cells, ions and proteins). A detailed description of the physiological processes involved in blood flow autoregulation and neurovascular coupling will then be given.

3.2 Blood Flow to the Brain – The "Big Things"

3.2.1 The Brain

The nervous system has three main functions: it 1) takes sensory inputs, 2) collates and processes them, and 3) provides motor output to muscle cells. The central nervous system (CNS) is responsible for *integrating* the information, while the network of nerves in the peripheral nervous system (PNS) *transports* sensory and motor signals between the CNS and the rest of the body.

3.2.1.1 Brain Regions

The brain is separated into two halves (the left and right hemispheres) which communicate through the corpus callosum, a thick band of nerve fibres. There are many parts of the brain (Figure 3.1) and each part is in charge of certain functions.

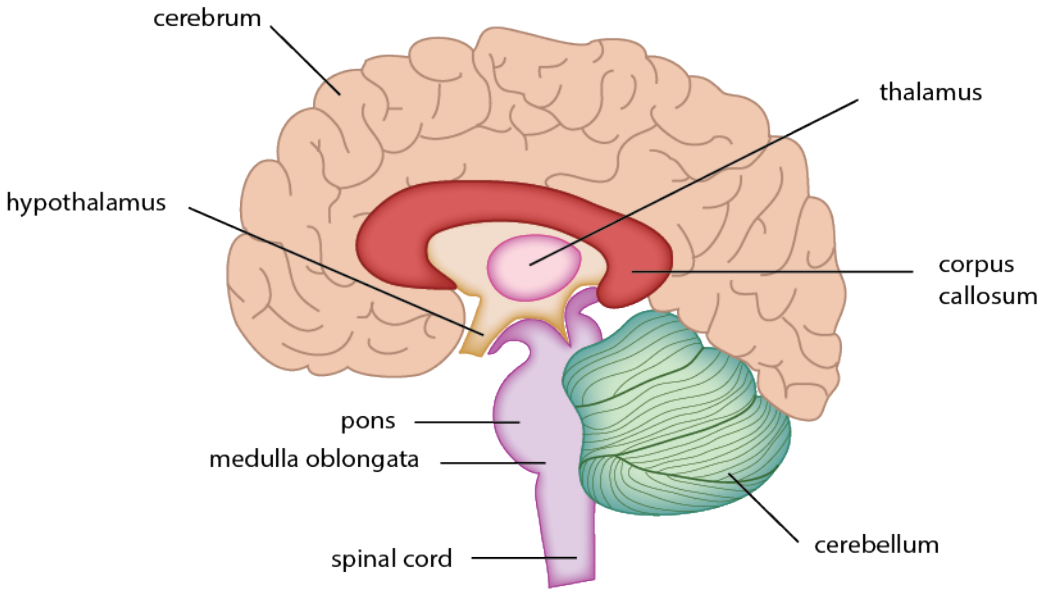

Figure 3.1 Main parts of the brain. Adapted from [12].

The brainstem (medulla oblongata, pons and midbrain) relays data and controls automatic activities essential for survival, such as heart rate, breathing and swallowing. The cerebellum controls movement and balance. The diencephalon consists mainly of two structures: the thalamus, which relays sensory input to the cerebral cortex, and the hypothalamus, which is responsible, among other things, for controlling the autonomic nervous system. The cerebrum interprets sensory impulses and controls conscious motor activity, emotion and intellectual processes. It folds in on itself, creating bulges (gyri) and crevices (sulci). The outer part of the cerebrum (known as the cerebral cortex) is made of gray matter, and the inner part is made of white matter. Gray matter is gray because it consists mainly of unmyelinated nerve cell bodies; white matter is white because it mainly consists of myelin-coated nerve cell fibre. The cerebral cortex can be further divided into four lobes: the frontal, parietal, occipital, and temporal lobes (Figure 3.2).

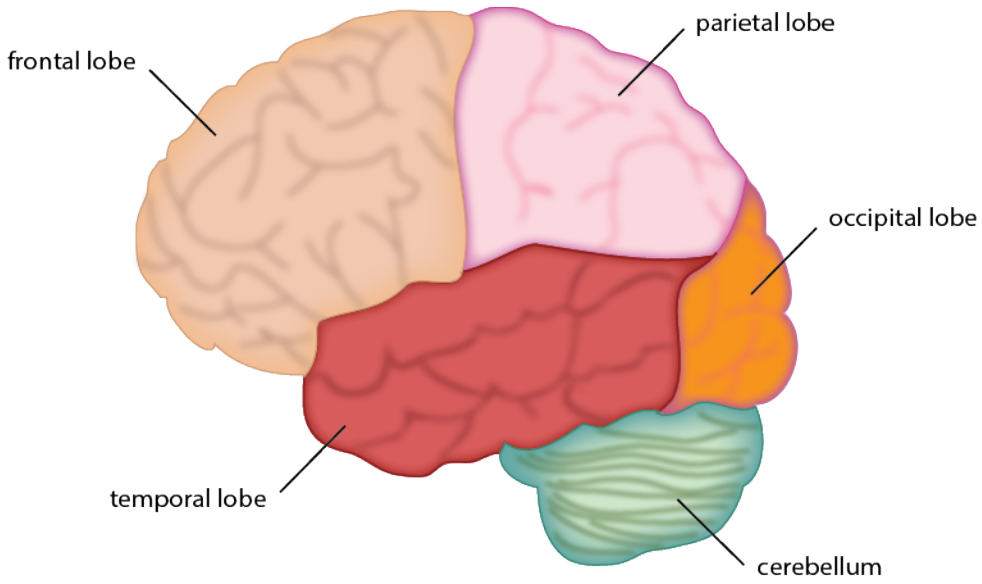

Figure 3.2 Lobes of the brain. Adapted from [12].

3.2.2 The Major Arteries of the Brain and the Circle Of Willis (CoW)

Blood flow to the brain is important, and as such, the brain is a highly vascularised organ. In fact, the brain is the only organ in the body that is supplied by four arteries: the two Vertebral Arteries (VAs) and the two Internal Carotid Arteries (ICAs). The VAs join together to form the Basilar Artery (BA) before they meet the ICAs in a ring-like structure called the Circle of Willis (CoW). The blood that enters the CoW is then distributed by the Anterior Cerebral Arteries (ACA), Middle Cerebral Arteries (MCA), and Posterior Cerebral Arteries (PCA). These arteries then bifurcate into smaller arterial branches. The Circle of Willis, with its ring-like conformation of branches, allows flow to be maintained in the case of impaired or blocked flow in one of the major afferent arteries. Essentially, as long as the "CoW is complete", if one artery is blocked, blood can still reach the brain tissue through an alternative CoW route. However, this "back-up system" is heavily dependent on the presence and/or size of all the CoW vessels and not everyone has a complete CoW (Figure 3.3). In fact, approximately half of the population has an incomplete CoW [89] – a fact that may not cause problems for a healthy individual, but may be very important for a person with cerebrovascular disease (see Chapter 4).

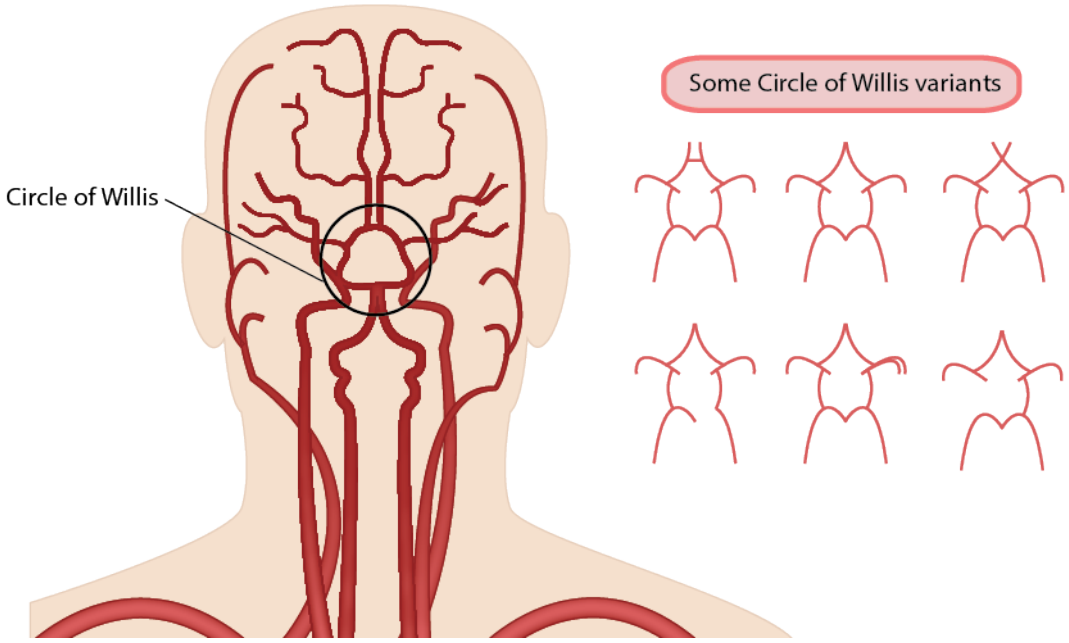

Figure 3.3 Arteries that surround and constitute the Circle of Willis in the brain. Image on left adapted from [6] and images on right adapted from [89].

3.2.3 Moving Down The Vascular Tree – From Arteries to Arterioles to Capillaries to the Tissue

From the heart to the tissue, blood vessels undergo repeated branching to progressively smaller sizes and increasing numbers. Blood vessels can be classified into *arteries, arterioles, capillaries, venules* and *veins*. For this study, we focus on the delivery of blood *to* the cerebral tissue and not its journey back to the heart via the venous system; as a result, we focus only on the structure and function of the arteries, arterioles and capillaries.

Blood flow velocity decreases significantly in the arterioles and is slowest in the capillaries due to the increase in total cross-sectional area that these vessel groups contribute. Blood pressure is the force exerted on the wall of the vessel and is determined in part by the pressure supplied by the heart, but also by the peripheral resistance of the arterioles, the "bottlenecks" of the circulatory system [32] – Figure 3.4.

The structure of a blood vessel (that is, the composition of its wall components) changes as we travel down the vascular tree. These structural differences correlate with their different functions. All vessels in the body, including the capillaries, have a tightly coupled endothelial cell layer that lines the lumen. Arteries, arterioles and veins have additional outer layers

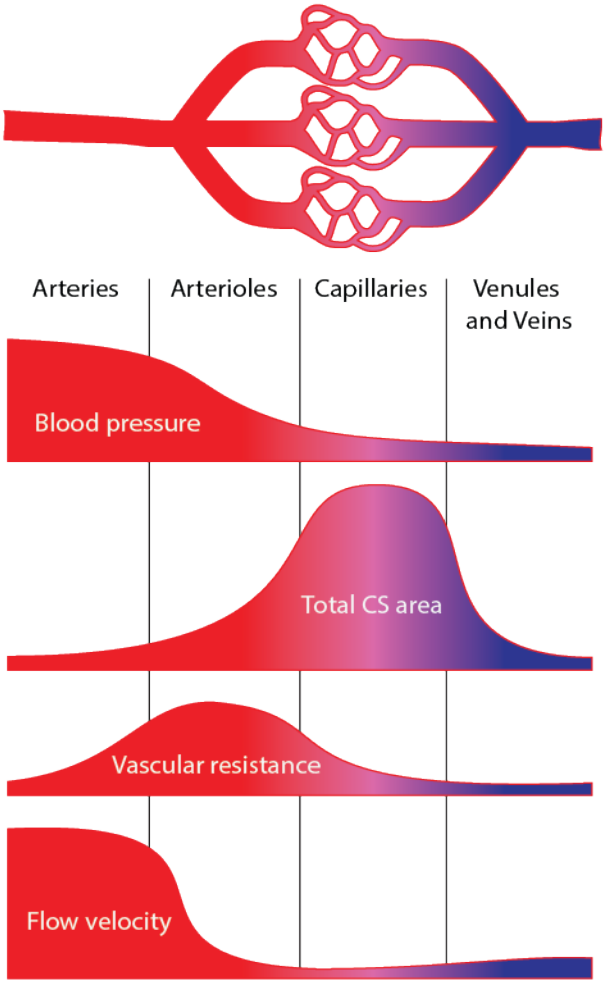

Figure 3.4 Blood pressure and velocity in, and the total cross-sectional area and resistance contribution of, the arteries, capillaries and veins of the circulatory system. Adapted from Figure 14.6 in [27].

composed of smooth muscle, elastic fibres and connective tissue (Figure 3.5).

Arteries have the thickest, strongest and springiest (most elastic) walls, so they can withstand the high blood pressure and fast blood flow that occurs there [32] (Figure 3.4). The transfer of nutrients between blood and the interstitial fluid surrounding tissue occurs across the thin walls of the capillaries – the low flowrates through the capillaries enhance this exchange (Figure 3.4). Capillary walls consist only of a single layer of endothelial cells and a *basement membrane*. The supply of blood to different organ and tissue regions is primarily governed by the variable constriction of sections of the arteriolar tree and by the closing and opening of sphincters that surround precapillary vessels.

The arterioles have relatively thick walls compared to their diameter as they have many layers of smooth muscle. The presence of large amounts of smooth muscle allows these ves-

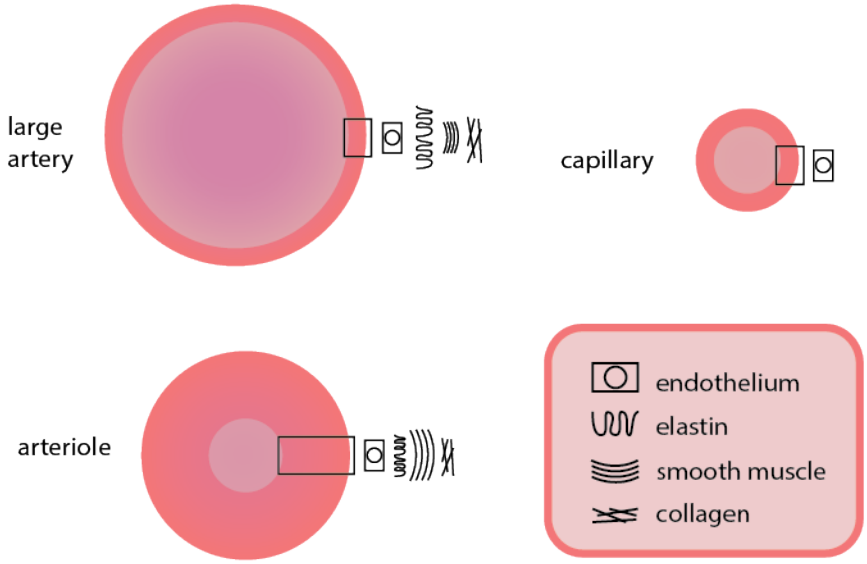

Figure 3.5 Structural differences between arteries, arterioles and capillaries. Adapted from Figure 14.4 in [27].

sels to significantly regulate their diameter and therefore change the resistance to blood flow [32]. For this reason, these vessels are often termed *resistance* vessels. Arterioles range from approximately 40 μm to as small as 9 μm in diameter, and have one to two layers of smooth muscle cells in their wall. Arterioles can, with their high *cumulative* resistance, be responsible for the majority of the control of the total vascular resistance of the tree [32].

The capillaries are the smallest vessels in the vasculature (about 7–9μm in diameter) and their purpose is to deliver nutrients to, and remove wastes from, the tissue. Red blood cells flow through most capillaries in a single file and frequently are folded and squeezed as they pass through the smaller diameter capillaries. Capillaries do not function independently; they form interconnected networks called capillary beds. Fat-soluble substances, such as oxygen and carbon dioxide, as well as small water-soluble molecules readily diffuse through the *plasma membrane*. Larger water-soluble substances must pass through the fenestrae or "gaps" between the endothelial cells. The tightly arranged endothelial cells form a barrier to the red blood cells themselves and to harmful substances. When people refer to the blood-brain barrier (BBB) they are referring to the tightly packed endothelial cells that act as permeability barriers to certain substances [32]. The BBB protects the brain from attack from harmful substances, but can also make it difficult to treat neurological diseases, as drugs must be capable of passing the barrier in order to have an effect on the diseased tissue.

Neurons are closely affiliated with cerebral blood vessels [46]. Pial arteries (those on the outside of the brain) are densely innervated (supplied) by nerve fibres that contain many vasodilators and constrictors. Small arteries and arterioles are generally innervated to a greater

extent than other blood vessel types and are contacted by neural processes that originate from local interneurons [78]. Local conditions in the neuronal tissue effect changes in the calibre (diameter) of the arterioles, adjusting the resistance of the tree, and hence altering the delivery of blood flow to that region. This local control ("autoregulation") ensures that there is adequate blood supply to meet the demand. The physiological processes involved in autoregulation are outlined later in this chapter.

3.3 Cells and Other Important "Small Things"

3.3.1 Cells

3.3.1.1 Major Cell Components

All cells are encapsulated by a selectively permeable membrane which is comprised of lipids and proteins. This membrane (also known as a *plasma* membrane) protects the cell's contents and allows an electrical potential to be maintained. It also facilitates the transport of important molecules in and out of the cell. Organelles ("miniature organs") can be found within the interior environment of the cell, the cytoplasm. There are many types of organelles (Figure 3.6) and each one has a specific role to play.

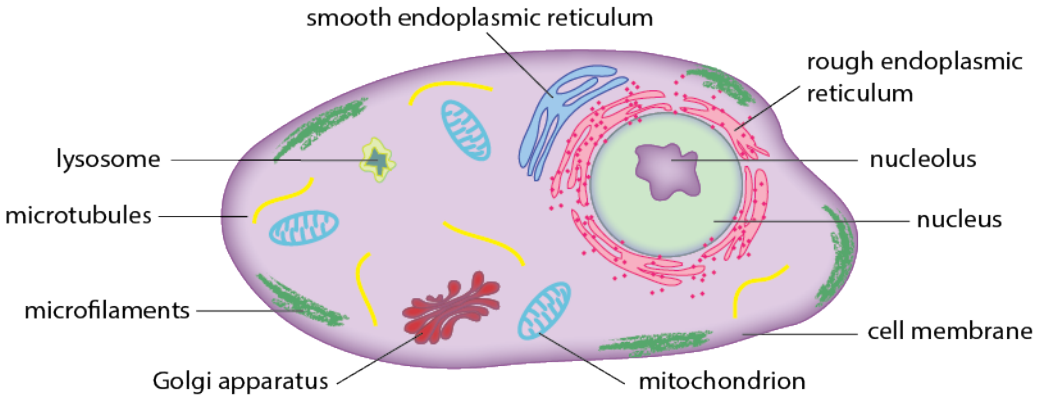

Figure 3.6 Organelles in an animal cell. Adapted from [4].

The cell **nucleus** is the cell's library – it holds all of the information the cell needs. This is where the cell's genetic material is stored and where most of DNA replication and RNA synthesis occurs. **Mitochondria** are responsible for generating the cell's energy by oxidative phosphorylation, using oxygen to release energy stored in cellular fuel (normally glucose) to generate ATP, a coenzyme capable of performing cellular work. The **endoplasmic reticulum**

(ER) constitutes the cell's "stores" or "holding area". It holds molecules requiring modification or transport. The ER has two forms: the rough ER and the smooth ER. The **sarcoplasmic reticulum (SR)** is a special type of smooth ER found in muscle. It is concerned only with calcium sequestration and release, processes that play a major role in muscle contraction (more on this in a later section).

3.3.1.2 Cells and Electricity

The human body runs on electricity. Electrical signals within cells are driven by ions (charged atoms). Some of the important ions in cellular biology are sodium Na^+, potassium K^+, calcium Ca^{2+} and chlorine Cl^-.

All animal cells maintain a voltage difference across the cell's plasma membrane; this is called the *membrane potential*. At rest, a cell has a *negative* membrane potential, meaning that there are more positive ions outside than there is inside. When the membrane potential undergoes a change in which it becomes less negative, this is called a depolarization. When the voltage becomes more negative, this is called a hyperpolarization. A change back to resting state after hyper- or depolarization is termed a repolarization. These different levels of polarization result from the operation of ion channels and ion pumps: protein structures that are embedded in the membrane.

Ion pumps use cellular energy (ATP) to continuously move ions in and out of the cell. They create concentration differences (between the inside and outside of the cell) by transporting ions against their concentration gradients (from regions of low concentration to regions of high concentration). Ion channels, on the other hand, transport ions "down" their concentration gradients (that is, from regions of high concentration to regions of low concentration). Ion pumps provide continuous transport, whereas ion channel fluxes are noncontinuous: they are "gated" by (open and close in response to) chemical and electrical (voltage) signals.

Ion channels are specially shaped proteins that contain a pore through which ions can travel. They are categorised by how they respond to signals from their environment. For example, there are voltage-gated channels which open and close in response to the voltage across the membrane. Ligand-gated channels open and close in response to the binding of a ligand (signal-triggering) molecule, such as a neurotransmitter. Some channels can be both ligand- and voltage- gated. Ion channels can also open and close in response to mechanical forces, such as pressure or shear stress.

Most channels are specific for one ion, even though cell ions can be approximately the same size and charge (like potassium (K^+) and sodium (Na^+), for example). A channel may have several different states (corresponding to different conformations of the protein), but each

such state is either open or closed. When we create equations to describe the behaviour of ion channels, we refer to the *probability distribution* of channels in an open state. It is called a *probability* distribution because it describes the proportion of channels that are *likely* to be open at a given voltage. These distributions can be shifted due to the presence of ligands and also due to ionic concentrations inside or outside the cell.

The resting (*equilibrium* or *Nernst*) potential of an ion channel is the potential at which no ions feel compelled to pass through it (that is, the electric force generated by diffusional movement of the charged ion down its concentration gradient becomes equal to the molecular force of that diffusion). The equilibrium potential for any ion can be calculated using the Nernst equation.

Like an electrical circuit, the cell membrane has a capacitance, which is a measure of how much charge must be passed across the membrane in order to produce a given change in membrane potential. Each different ion channel has a different electrical resistance associated with it. In physiological modelling, it is common to use conductance (the inverse of resistance) to describe the "difficulty" by which open ion channels pass charge in and out. The size of the ionic flux through an open channel is determined by the maximum channel conductance and the electrochemical driving force for that ion (the difference between the actual membrane potential and the resting potential) – see Chapter 2 for further explanation.

Another important electrical cellular event is known as the action potential, which involves the transport of Na^+ and K^+ across the membrane. Action potentials occur in many different types of animal cells, but they exist in neurons as a mechanism for cell-cell communication. An action potential (or "depolarizing wave") in the neuron is a "transient ($<$1 millisecond) reversal in the polarity of the membrane potential which then moves from its point of initiation, down the axon, to the axon terminals [17]".

3.3.2 Cells in the Brain

Brain tissue is composed of neurons and supporting cells (glia). Neurons create and transmit signals. Glia support, insulate and protect neurons. We are particularly interested in the glial cell called the astrocyte, as it is known to have an important role in the control of *vascular tone* (the degree of tension/constriction an arteriole possesses).

Vascular tissue (also found in the brain, in the blood vessels that perfuse brain tissue) contains endothelial cells (ECs) and smooth muscle cells (SMCs).

Finally, blood, a connective tissue, circulates through the lumen (inside) of brain blood vessels, and contains a collection of ions and proteins, nutrients, metabolic waste products, hormones, and respiratory gases.

3.3.2.1 Neurons

A neuron (Figure 3.7) consists of a cell body (or *soma*), dendrites, and an axon. An axon is a part of the neuron that extends out like a thin strand from a lump at the cell body (the axon hillock). Dendrites are also filaments (strands) that protrude from the cell body. They branch extensively, giving rise to a complex dendritic "tree." A dendritic spine (or simply *spine*) is a small protrusion from a neuron's dendrite that typically receives input from a single synapse of an axon. A neuron can have many dendrites, but only one axon. Axons are commonly surrounded by myelin sheaths. The sheaths are formed by glial cells, and they enable action potentials to travel faster whilst using less energy. The myelin sheath is interrupted at intervals by *nodes of Ranvier* which contain a high density of voltage-gated ion channels [32].

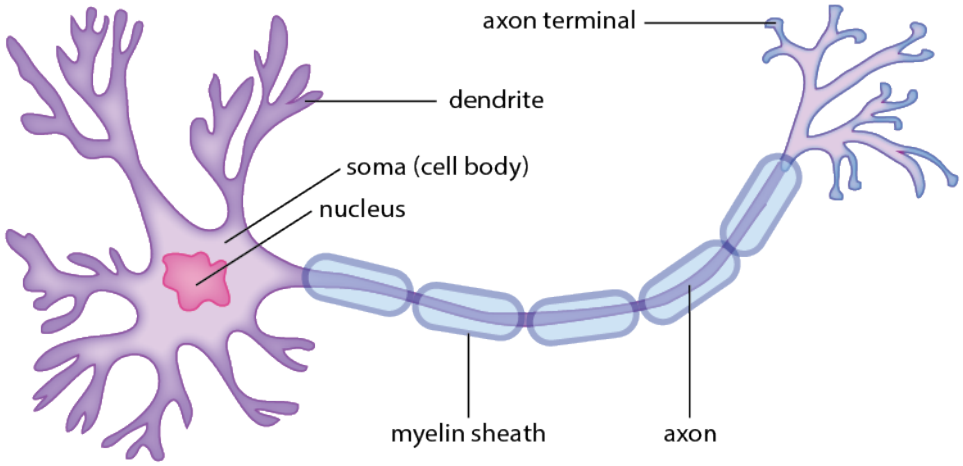

Figure 3.7 A neuron. Adapted from [9].

Chemical signaling between neurons occurs via synapses. Signals from one neuron to others are transmitted from the axon to the soma and dendrites. A synapse, therefore, is the place at which the axon of one neuron comes into contact with the dendrite or soma of another. The process of synaptic communication begins with an action potential (described earlier). When an action potential reaches the axon terminal, it opens voltage-gated calcium channels, allowing calcium ions to enter the terminal. Calcium causes vesicles (membranous bubbles) filled with neurotransmitter molecules to fuse with the membrane, releasing their contents into the synaptic cleft [32]. The neurotransmitters diffuse across the synaptic cleft and activate receptors on the postsynaptic neuron (neuron at the opposing end of the synapse) or on neighbouring glia.

Neurotransmitter receptors can be classified into *ionotropic* or *metabotropic* receptors.

Ionotropic receptors form an ion channel pore; when they are activated, they allow ions to flow. A metabotropic receptor does not form a channel pore; instead, when a metabotropic receptor is activated, a series of events involving intracellular second messenger chemicals is triggered. These events can culminate in ion channel opening but do so *indirectly*, through signal transduction pathways (often involving G-proteins).

No neuron is like another; they come in a wide variety of shapes and sizes and have diverse electrochemical properties [32]. They also tend to specialise in a particular task. For example, sensory neurons respond to stimuli (like light, sound and touch) and send signals to the spinal cord and brain. Motor neurons work in the opposite direction; they receive signals from the brain and spinal cord and cause muscle contractions and changes in glands. Interneurons connect neurons to other neurons.

3.3.2.2 Glia – Astrocytes and Pericytes

Historically, astrocytes, as well as other glia, were believed to be structural cells [107]; that is, their main function was to "glue" the neurons in place. It is now known, however, that astrocytes serve many functions and are responsible for maintaining the neuronal environment. This includes clearing away excess potassium and neurotransmitters, providing important support molecules to synapses, and contributing to the health of the BBB (blood brain barrier) [160]. Astrocytes also regulate cerebral blood flow in periods of changing neuronal metabolism [107]; in other words, they are involved in "neurovascular coupling" – the process that is investigated in this thesis.

Astrocytes were once viewed as a largely homogeneous cell population defined by their characteristic "star-shape." They were divided only into two subpopulations based on their location and morphology: *fibrous* and *protoplasmic* for astrocytes in the white and gray matter, respectively [114] (Figure 3.8). Protoplasmic astrocytes were thought to have many branching processes that surround synapses with endfeet that impinge upon blood vessels, and fibrous astrocytes: long, thin, unbranched processes whose endfeet envelop nodes of Ranvier. However, this nomenclature (fibrous and protoplasmic) is not sufficient to describe the vast anatomical diversity seen in astrocytes. Advanced electrophysiological, molecular, and genetic tools have now revealed that astrocytes represent a "complex and diverse population of cells with numerous functions [160]. "

The astrocyte's plasma membrane folds into both complex *lamellae* (thin flat layers) and *fibre* (thread-like) forms, which arrange themselves around networks of neural synapses (Figure 3.9). The degree at which the astrocytes wrap around these forms depends on their location in the brain. For example, in the hippocampus, only 57% of the synapses have astrocytic pro-

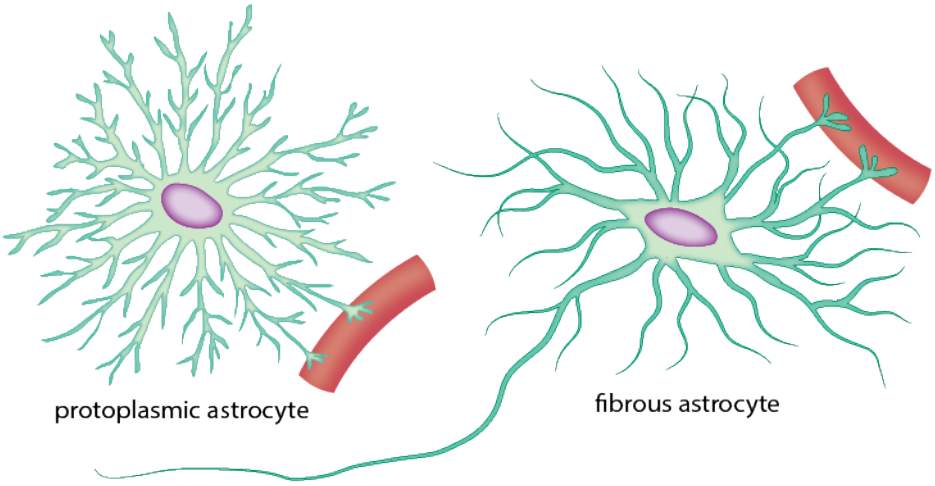

Figure 3.8 Glial cells are morphologically diverse; some are more *fibrous* (have long, thread-like branches) and some are more *protoplasmic* (have many branches). Adapted from [11].

cesses positioned around them. In the cerebellum, the special neurons known as Purkinje cells, can be surrounded 67% or 94% of the time, depending on the type of neuron that provides their excitatory input [160]. The complex contortion of the astrocytic membrane results in the presence of glial microdomains (spatially exclusive regions), which have been observed in cerebellar and hippocampal astrocytes using electron microscopy [30, 63, 68]. These compartments consist of thin membrane sheets, as well as mitochondria. It is possible that an astrocyte may consist of hundreds of separate compartments, each capable of independently interacting with the synapses that it surrounds. These microdomains can restrict the spread of Ca^{2+} waves in response to neuronal stimulation [63]. Mature astrocytes are also organised in non-overlapping domains and make contacts with many thousand synapses [30, 67]. This allows a one astrocyte to one synapse communication, which inhibits the problem of information mismatch.

It has long been assumed that neurovascular coupling could only be effected by the change in tone (tension/constriction) of smooth muscle that surrounds the arterioles. Capillaries – with their lack of smooth muscle – were never thought to be able to contribute. However, it has recently been discovered that pericytes – glial cells present at regular intervals along capillaries – can adjust the calibre of the capillary due to the contractile proteins that they possess [69]. The importance of pericyte capillary control for regulating cerebral blood flow is yet to be determined, as it has not yet been demonstrated *in vivo* in *physiological* conditions [69] (although it does occur after *ischaemia* [172]). The importance of the pericyte effect also depends on the fraction of the total vascular resistance that the capillaries actually contribute (this could be between between 16% and 70% [102, 103]).

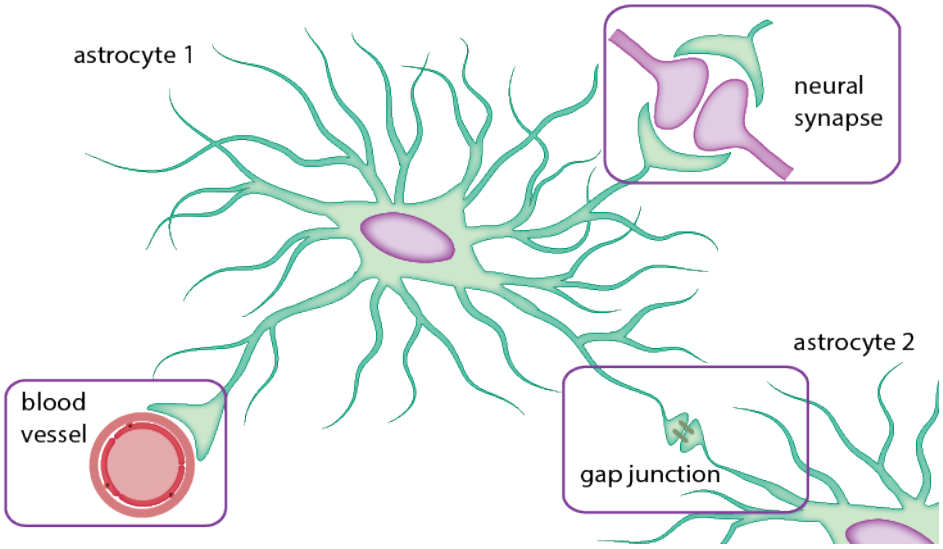

Figure 3.9 Astrocytes arrange themselves around synapses and blood vessels. They also can communicate with each other via gap junctions.

3.3.2.3 Smooth Muscle Cells and Smooth Muscle Contraction

Layers of smooth muscle cells (SMCs) line the walls of various organs and 'tubes' in the body. These cells are 'smooth' because they lack the striations (stripes) of skeletal and cardiac muscle. Furthermore, unlike skeletal muscle, the level of tone in smooth muscle is not under voluntary control – it is instead controlled by hormones and other chemical signals. A change in membrane potential, for example, often triggers contraction [161].

Smooth muscle contains thick and thin filaments. Thin filaments consist of a 'rope' made of actin strands and regulatory protein, while thick filaments are arrays of myosin molecules [32]. During contraction, thick and thin filaments form cycling crossbridges, which act to progressively "ratchet" the smooth muscle together, causing the filaments to slide past one another, shortening the muscle.

Contraction of smooth muscle is first initiated with a change in Ca^{2+}. Cytosolic Ca^{2+} increases due to Ca^{2+} release from intracellular stores (the sarcoplasmic reticulum) as well as entry from extracellular space through Ca^{2+} channels (which is often instigated by the changes in membrane potential mentioned above). This additional Ca^{2+} combines with the protein calmodulin to form a complex which activates the enzyme myosin light chain kinase (MLCK) to phosphorylate (add a phosphate group to) the "light chain" (a subunit) of myosin, enabling myosin to form a molecular 'bridge' with actin. The cycling of these bridges provides contraction. Therefore, the degree of contraction in smooth muscle is directly determined by the degree of phosphorylation of the myosin light chains. In some smooth muscle cells, the phos-

phorylation state is maintained at a low level in the absence of stimuli [161]. This essentially means that the smooth muscle is always slightly constricted – this is known as "basal tone."

It is important to note that the action of muscle is always to contract. Muscles can only extend passively [32], by "relaxation." Smooth muscle relaxation occurs either as a result of 1) the removal of a contracting stimulus or 2) by the action of a substance that actually *inhibits* the contractile machinery (i.e., a vasodilator). Either way, relaxation is dependent on a decreased cytosolic Ca^{2+} concentration, and the increased activity of myosin light chain *phosphatase* (MLCP, an enzyme that *dephosphorylates* the myosin light chain). Again, membrane Ca^{2+} channels facilitate the decrease in Ca^{2+} [161].

3.3.2.4 Blood

Blood is a type of tissue consisting of several kinds of cells suspended in a liquid, plasma. The three main types of cells contained in blood are erythrocytes (or *red blood cells* – used to help transport oxygen and carbon dioxide), leukocytes (or *white blood cells* – necessary for defense and immunity) and platelets (for blood clotting). Plasma is essentially a carrier fluid that is made up mostly of water, but which also contains ions and proteins, nutrients, waste products, hormones, and respiratory gases (oxygen and carbon dioxide).

3.3.2.5 The Neurovascular Unit (NVU)

Neurons, astrocytes, and the endothelial and smooth muscle cells surrounding blood vessels comprise what is known as the neurovascular unit (NVU). Figure 3.10 demonstrates their positions in the cerebrovasculature.

3.4 The Physiology of Autoregulation

The brain demands a constant supply of oxygenated blood. Changes within the brain must not affect the supply of blood reaching the brain tissue. Blood vessels within the brain are known to make compensatory changes in radius in response to local changes by several autoregulation mechanisms. These mechanisms include blood pressure, wall shear stress and metabolic-mediated mechanisms [47].

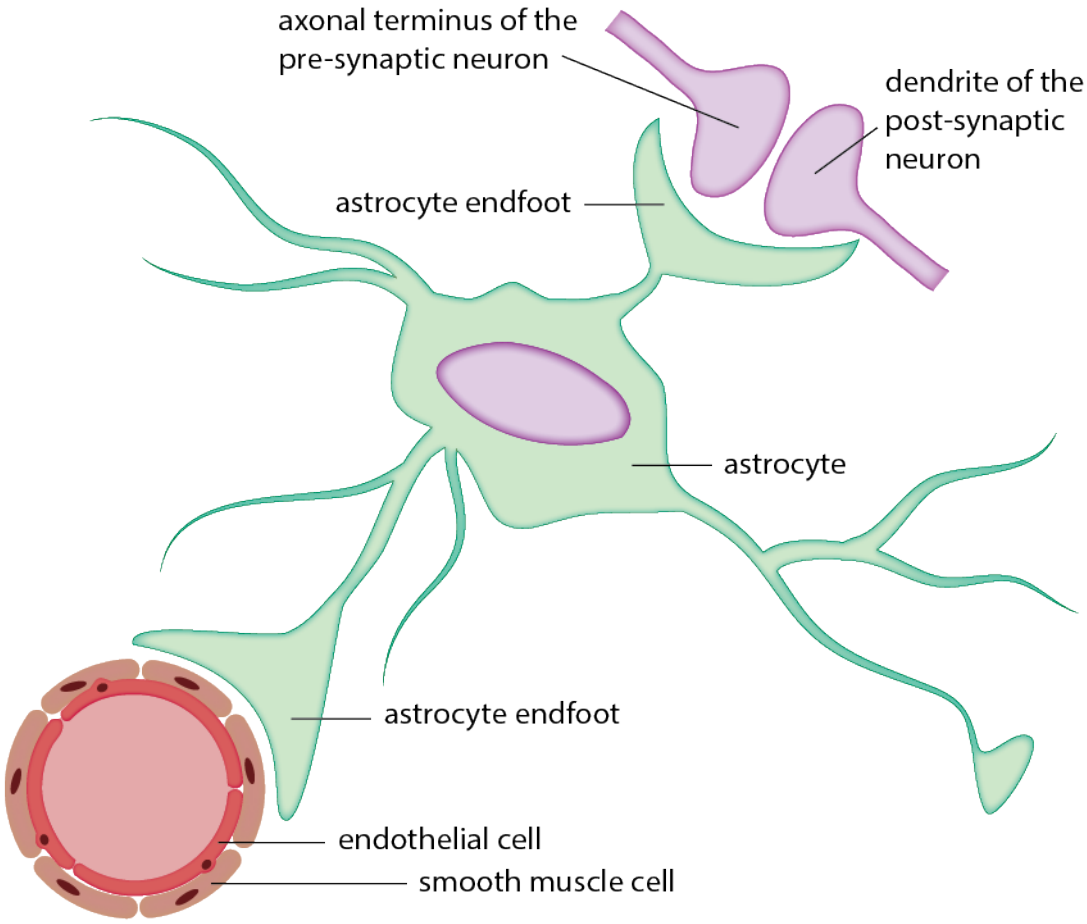

Figure 3.10 Cells comprising the neurovascular unit.

3.4.1 Cerebrovascular Autoregulation – Myogenic (Pressure) and Wall Shear Stress Mechanisms

The myogenic (pressure-based) mechanism counteracts the effects of the normal fluctuations in arterial pressure that occur during everyday activities (like moving from sitting to standing). Cerebral arteries relax to counteract arterial pressure decreases, and constrict to combat arterial pressure rises [78]. This mechanism is effected by stretch activated channels in the SMCs that "sense" the increases in pressure and flow and effect ionic changes in the cell that induce contraction. The flowrate through the vessel at varying blood pressures is demonstrated below (Figure 3.11). Note that not all vessels are able to react to changes in pressure. For those vessels that do, there exists a range or "autoregulated region" of normal physiological blood pressures for which these mechanisms work; however, these processes do not function in the pathological ranges of hypotension (low blood pressure) and hypertension (high blood pressure).

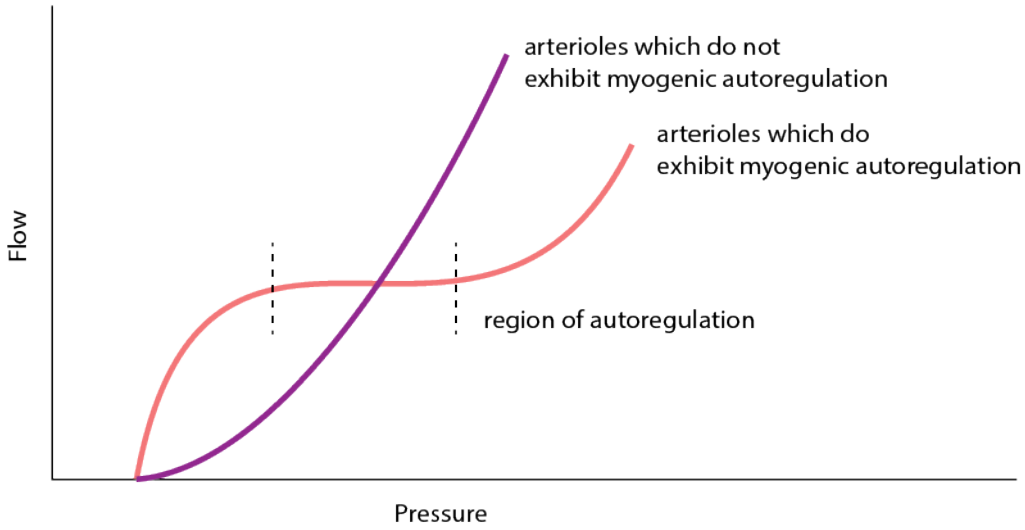

Figure 3.11 Autoregulation of blood flow with changing pressure. Some vessels, such as those in the brain and the kidneys, have the ability to autoregulate, whereas others do not. Adapted from Figure 14.13 in [27].

Vascular smooth muscle tone also depends on the shear stress exerted on vascular walls by flowing blood. Increased wall shear stress initiates the synthesis of vasodilatory nitric oxide (NO) by the enzyme endothelial NO synthase (eNOS). It is believed that while heightened blood pressure causes arterial smooth muscle to contract, higher wall shear stress acts as a counterbalance to this response, causing arterial walls to dilate [38, 128].

3.4.2 Metabolic Autoregulation Mechanisms

Our understanding of metabolic autoregulation is changing constantly. Historically, it was believed that a negative feedback system existed, where activated neurons generated a metabolic signal (such as a fall in O_2 or ATP or a rise in CO_2 concentration) which then triggered a rise in CBF that would rectify the metabolic signal by supplying the required metabolite (Figure 3.12(a)). This hypothesis was supported by results such as those in Yaksh and Anderson [168], where exogenous CO_2 caused vasodilations. Several investigations (reviewed in [13]) have since shown that tissue O_2, glucose and CO_2-based mechanisms do not regulate blood flow in a negative feedback process.

Metabolic signals don't need to be tissue-based; they can arise from the lumen "side", and not the tissue "side", of the vessel wall. In a recent review, Ellsworth et al. [50] argue that erythrocytes, through their oxygen-dependent release of the vasodilator ATP, can act as metabolic sensors and effectors of changes in vascular tone. Figure 3.13 details the basic pathways by

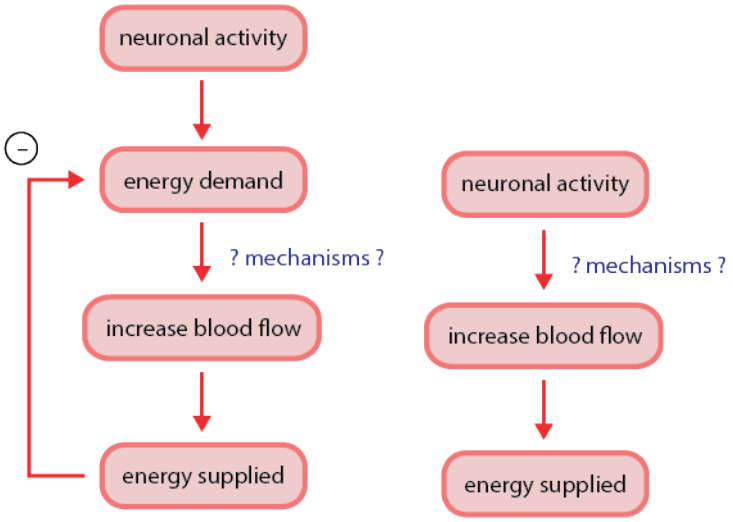

(a) Negative-feedback hypothesis (b) Feedforward hypothesis

Figure 3.12 Metabolic autoregulation – feedback or feedforward? Adapted from [13].

which erythrocytes can increase CBF. In short, the entrance of erythrocytes into tissue regions with a high oxygen demand (characterised by a decreased oxygen tension (PO_2)) results in diffusion of oxygen to the tissue and a decrease in the oxygen saturation (SO_2) of the haemoglobin within erythrocytes. This decrease in SO_2 stimulates the release of ATP, which interacts with endothelial receptors, resulting in the production of mediators that initiate vasodilation in the nearby SMCs. This vasodilation is conducted upstream along the blood vessel, resulting in increased blood flow to the areas of increased oxygen demand.

The feedback and metabolic signal-based pathways described have recently been superseded by a feedforward hypothesis (Figure 3.12(b)) following the discovery that glutamate, a neurotransmitter released by active neurons, is capable of regulating blood flow via a signaling pathway involving neurons and astrocytes (the mechanism known as *neurovascular coupling*). This signal is capable of increasing or decreasing blood flow depending on the local O_2 concentration. A metabolic signal (i.e., the O_2 concentration) is still involved in the process; however, it is not that which actually *initiates* the request for changes in CBF. In this *feedforward* mechanism, *activation* itself is the initiating signal, *not* the changing tissue metabolism associated with the activation. The next section provides a more detailed description of neurovascular coupling.

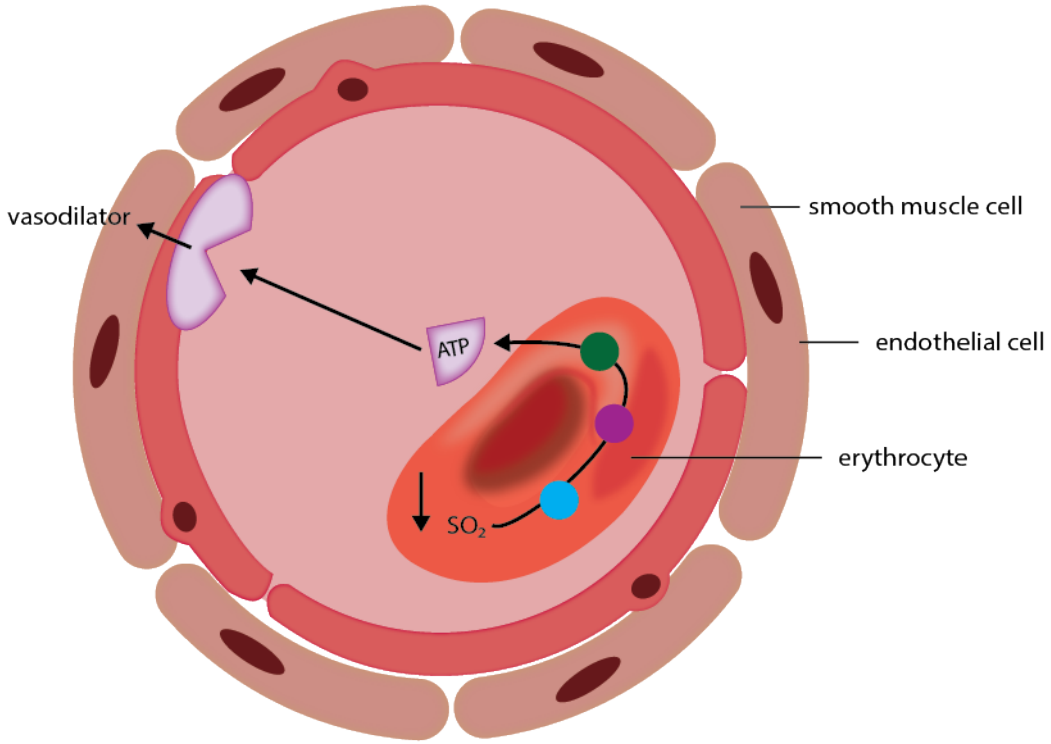

Figure 3.13 Erythrocytes as oxygen sensors and effectors of vasodilation. Adapted from [50]. Note that, for simplicity, many of the intermediate pathways have not been shown in detail and are instead represented schematically by coloured circles.

3.4.2.1 Neurovascular Coupling – Astrocytic and Neuronal Control of Blood Flow

The processes, major cells and chemical species known to be involved in the neurovascular coupling (NVC) mechanisms described are shown in Figure 3.14.

Synaptically released glutamate acts on both neurons and astrocytes. In neurons, glutamate attaches to N-methyl-d-aspartate receptors (NMDAR) to raise neuronal Ca^{2+}, causing neuronal nitric oxide synthase (nNOS) to release NO, which acts via sGC and cGMP in SMCs to dilate vessels. Raised Ca^{2+} may also generate arachidonic acid (AA), which is converted to vasodilatory prostaglandins (PG). In astrocytes, glutamate raises Ca^{2+} by activating metabotropic glutamate receptors (mGluR), generating arachidonic acid and three types of AA metabolite (Figure 3.15): PGs and EETs in astrocytes, which dilate vessels, and 20-HETE in smooth muscle, which constricts vessels.

There is a high expression of voltage-dependent, calcium-activated potassium (or “BK”) channels in astrocytic endfeet processes, with higher densities in areas close to synapses and blood vessels. These channels are also activated by EETs [73]. Activation of these channels

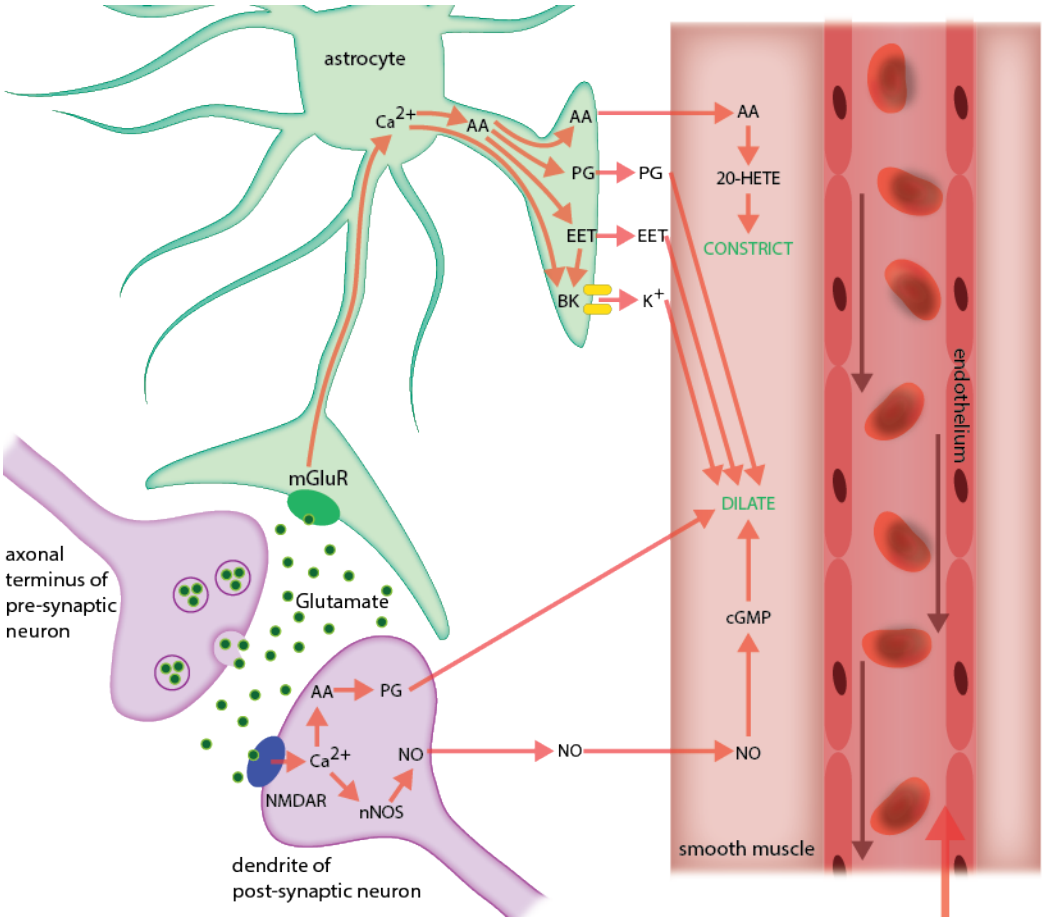

Figure 3.14 Neurovascular coupling: an overview. Adapted from Attwell et al. [13].

following glutamate-induced calcium and EET increases results in the rapid efflux of potassium into the perivascular space [55]. Increases in extracellular potassium concentration ($[K^+]$) can lead to vasodilation (and in higher concentrations, paradoxically, vasoconstriction) [31, 48, 60, 94, 111]. Filosa et al. [56] and others [37, 81, 84, 117] have proposed that the release of K^+ ions from astrocyte endfeet and the subsequent activation of inwardly rectifying potassium (KIR) channels on vascular SMCs comprises a rapid mechanism of arteriolar dilation.

It is difficult to assess the relative contributions of these signalling pathways to functional hyperaemia, as they all interact with each other: NO, O_2, lactate and adenosine concentrations affect neurovascular coupling at low O_2 concentrations [13], NO inhibits the production of both vasoconstricting 20-HETE and vasodilating EET [135], and O_2 is needed for the synthesis of NO as well as the vasomodulatory AA metabolites [70].

It is also important to note that the collection of possible NVC pathways shown in Figure 3.14 is not exhaustive. The exact interactions between pathways are also not well understood. Peng et al. [127] studied changes in CBF in rats (induced by forepaw stimulation)

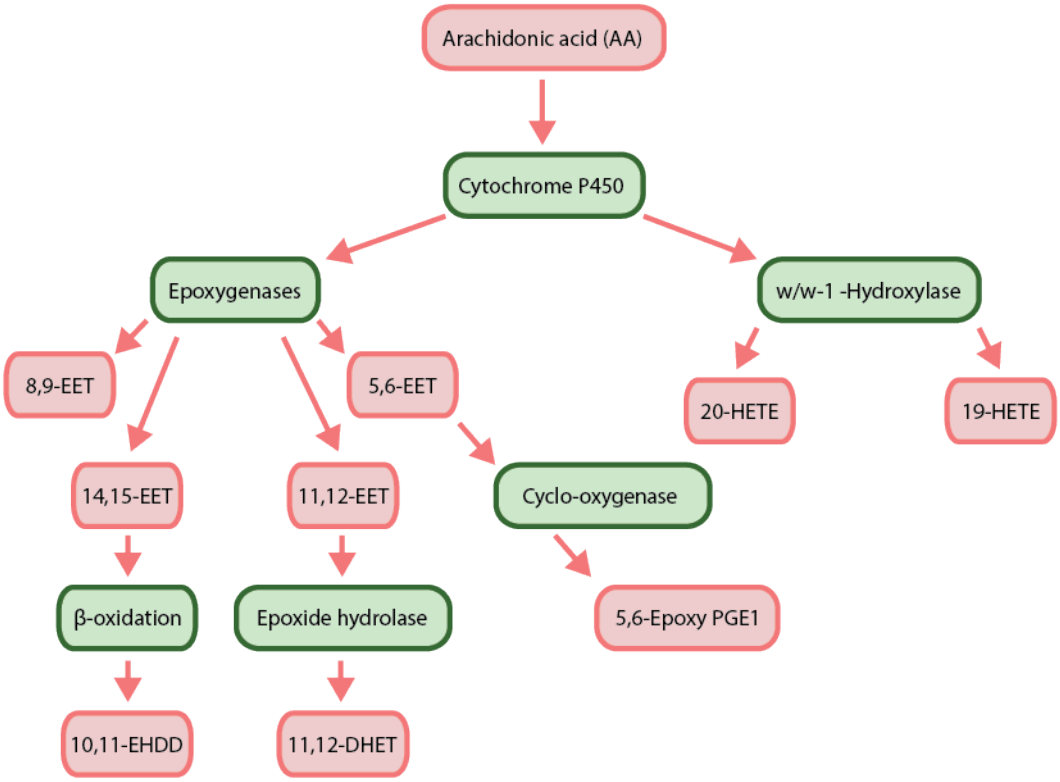

Figure 3.15 Metabolites of arachidonic acid (AA). Adapted from Fleming [57].

whilst blocking the NO and K^+/EET pathways. Blocking either pathway reduces the increase in cerebral blood flow (CBF) by about 60%. Paradoxically, when both pathways are blocked the decrease is still 60%. Shi et al. [145] also examine the effect of blocking K^+/EET and measure a 50% decrease in CBF response. They also observe a similar, non-additive, effect when blocking metabotropic glutamate receptors (mGluRs) and adenosine A_{2B} receptors, where the CBF response still only decreases by 50%.

3.5 Summary

The problem of the brain and its blood supply is a multiscale one, with scales spanning from the big to the very small. This thesis focuses on the blood flow autoregulation mechanism known as neurovascular coupling: the system by which neuronal activity triggers a rapid and regional increase in blood supply. Although the exact pathways of neurovascular coupling are still not completely understood, it is known that the neurotransmitter glutamate operates in a feedforward manner to generate activity-induced blood flow and that astrocytes mediate this blood flow control. Glutamate released by active neurons acts on both neighbouring neurons

and astrocytes, initiating the production of various vasomodulatory compounds including NO, EETs, PGs, 20-HETE, and K^+.

Chapter 4

Neurovascular Coupling in Disease

4.1 Introduction

The process of neurovascular coupling is altered in several pathological conditions. These alterations disrupt the delivery of blood and nutrients to, and impair the removal of waste and toxic products from, active brain cells. Subsequent disruptions to the brain's microenvironment can lead to neurodegeneration, disability, and death. In this section, we will focus on the cerebrovascular, astrocytic and neuronal dysfunction that occurs in diseases and disorders such as hypertension, diabetes, Alzheimer's disease (AD), spreading depression (SD) and stroke.

4.2 Neurovascular Changes in Normal Aging

Aging is known to affect the structure and mechanics of cerebral blood vessels. In aged rats, it has been shown that during aging, cerebral arterioles undergo atrophy (waste away) and have reduced distensibility (capacity to stretch or dilate) [66].

4.3 Stroke and Ischaemia

A stroke, or *cerebral infarction*, is an event where the blood supply to a part of the brain is interrupted by the rupture (haemorrhagic stroke) or the blocking (ischaemic stroke) of a blood vessel. The lack of blood supply to the brain (cerebral *ischaemia*) not only causes damage to neuronal tissue, but can exert profound effects on normal blood flow regulation.

After ischaemia, and during reperfusion of the affected tissue area, there is a transient increase in flow, followed by a period of reduced flow. During this time, the cerebral circulation abides in paralysis. In addition, the reactivity to vasomodulatory stimuli changes, autoregulation is impaired and the process of functional hyperaemia is compromised [59]. Certain cell

componentry important for vasomodulation can also be damaged following stroke: vascular KIR and BK channel function is impaired in ischaemia/reperfusion [108] and subarachnoid haemorrhage conditions [88], respectively.

4.4 Hypertension

Hypertension (high blood pressure) is a medical condition that causes many deleterious effects on circulation in the brain. It affects vascular *structure* causing enlargement and remodelling of the cells in the vascular wall, which reduces the maximum dilatation of cerebral arterioles [52]. Major causes of stroke are also associated with hypertension. These include increased blood coagulability and occlusion of the larger cerebral arteries due to atherosclerotic growth. Hypertension also impairs the *function* of cerebral blood vessels – it reduces endothelium-dependent responses to agonists [52] and alters cerebrovascular autoregulation profiles [152] (Figure 4.1). Evidence also suggests that hypertension alters functional hyperaemia in mice and in humans [59].

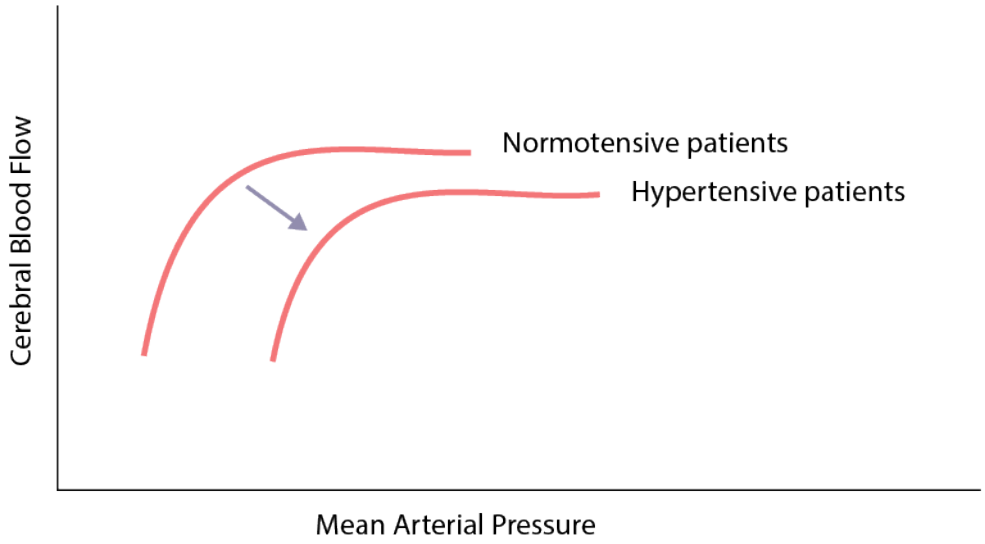

Figure 4.1 Autoregulation profile for normotensive and hypertensive patients. Adapted from [152].

4.5 Neurovascular Regulation in Alzheimer's Disease

Alzheimer's disease (AD) is the commonest form of dementia and is characterised by the deposition of amyloid-β-peptide (Aβ) in neuronal tissue (neuritic plaques) and blood vessels (cerebral amyloid angiopathy (CAA)), and by the accumulation of altered neurofilaments (neurofibrillary tangles). Aβ has long been identified as a major malefactor in AD, but, importantly, it is *vascular* factors that have only recently been implicated in AD progression [59].

4.5.1 Vascular Factors Involved in AD

Cerebrovascular disease and AD share common risk factors (such as hypertension, diabetes, and hypercholesterolaemia [43]), which suggest that their pathogenic mechanisms are similar. Furthermore, AD patients have more severe atherosclerosis in arteries of the Circle of Willis than age-matched controls without AD [134]. The occlusions caused by these atherosclerotic plaques limit cerebral blood supply.

Cerebrovascular structure and function is significantly affected by AD, with cerebral microvessels reducing in number, endothelial cells flattening, and smooth muscle cells degenerating [53]. Both resting CBF, and the increase in CBF produced by activation (functional hyperaemia) are impaired [59]. Importantly, this cerebrovascular dysfunction often *precedes* the noticeable symptoms of cognitive impairment, suggesting that it could play a role in the underlying mechanisms of the dementia [78].

4.5.2 How Aβ Affects the Cerebrovasculature

A closer look at the vascular biology involved is necessary for us to understand the involvement of these "vascular factors" in AD. Aβ is produced when amyloid precursor protein (APP) – a protein that is present in most cells – is cleaved by enzymes known as secretases [78]. In mouse models of AD, mutated APP is overexpressed to increase Aβ levels. These "Alzheimer mice" develop cognitive impairments at 6 months of age supposedly due to the arrival of the insoluble forms of Aβ (neuritic plaques) [163]. However, it is the cerebral *circulation* that is first affected, at 2–3 months of age [119, 122]. In these mice, endothelium-dependent vasomodulation is affected [79], and responses to vasoconstrictors are exaggerated [121]. Cerebrovascular (myogenic) autoregulation is severely diminished [119], and functional hyperaemia is impaired [122].

Aβ affects not only the contractile machinery of the vessels (through SMC and EC damage), but also, by promoting oxidative stress [125], inhibits the production of vasodilators [13],

such as neuronal nitric oxide synthase (nNOS) [154].

Multiple pathogenic events, in either the capillaries or larger vessels, can initiate the breakdown of the neurovascular unit (Figure 4.2). These events include insufficient angiogenesis (growth of new vessels) and atherosclerosis, cerebral amyloid angiopathy (CAA), or faulty clearance of Aβ across the blood-brain barrier (BBB). Even normal healthy aging causes changes in the cerebrovasculature that can trigger a pathogenic cascade. These cascades can initiate the breakdown of communication between elements of the neurovascular unit (neurovascular *un*coupling), leading to hypoperfusion, vessel inflammation, BBB compromise and reduced control of the neuronal microenvironment. These changes result in, or exacerbate, neuronal and glial dysfunction, eventually culminating in cell injury or death [174].

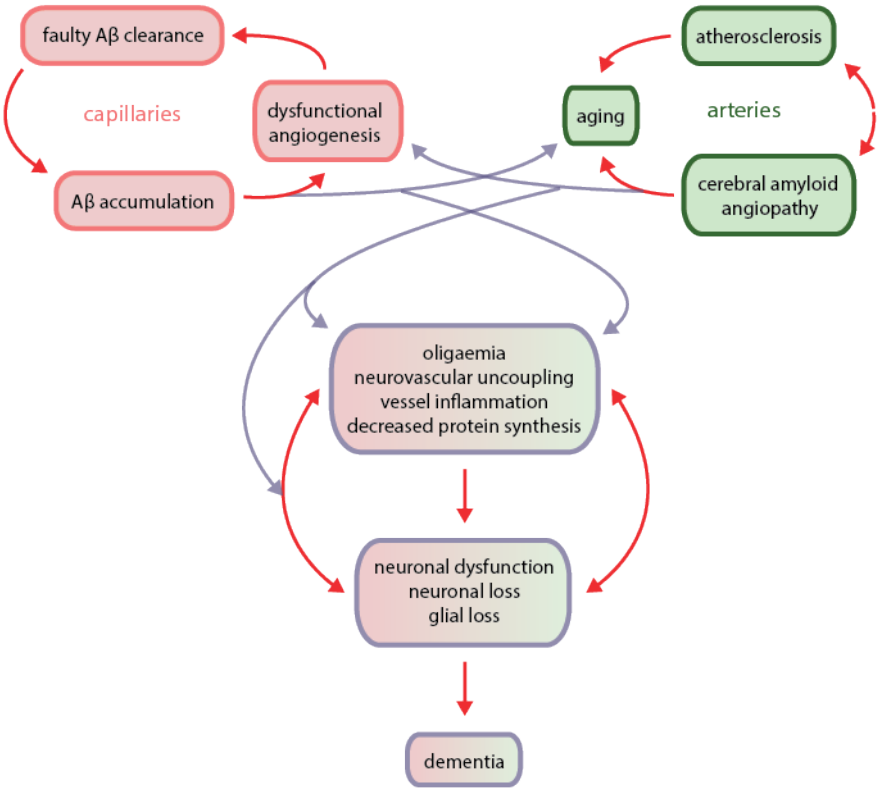

Figure 4.2 Changes to capillaries and arteries in AD and their associated vascular, neuronal and cognitive effects. Adapted from [174].

Interactions of Aβ with atherogenesis and cholesterol metabolism can potentially explain the increased atherosclerosis seen in patients with AD.

In AD, large arteries can develop atherosclerotic plaques that can produce thrombi; intracerebral arteries experience CAA, develop amyloid lesions and a thinning SMC layer. At the

capillary and tissue level, amyloid lesions develop, endothelial cells (and hence the BBB) degenerate, the basement membrane thickens, and microglia and astrocytes are activated [174] – Figure 4.3.

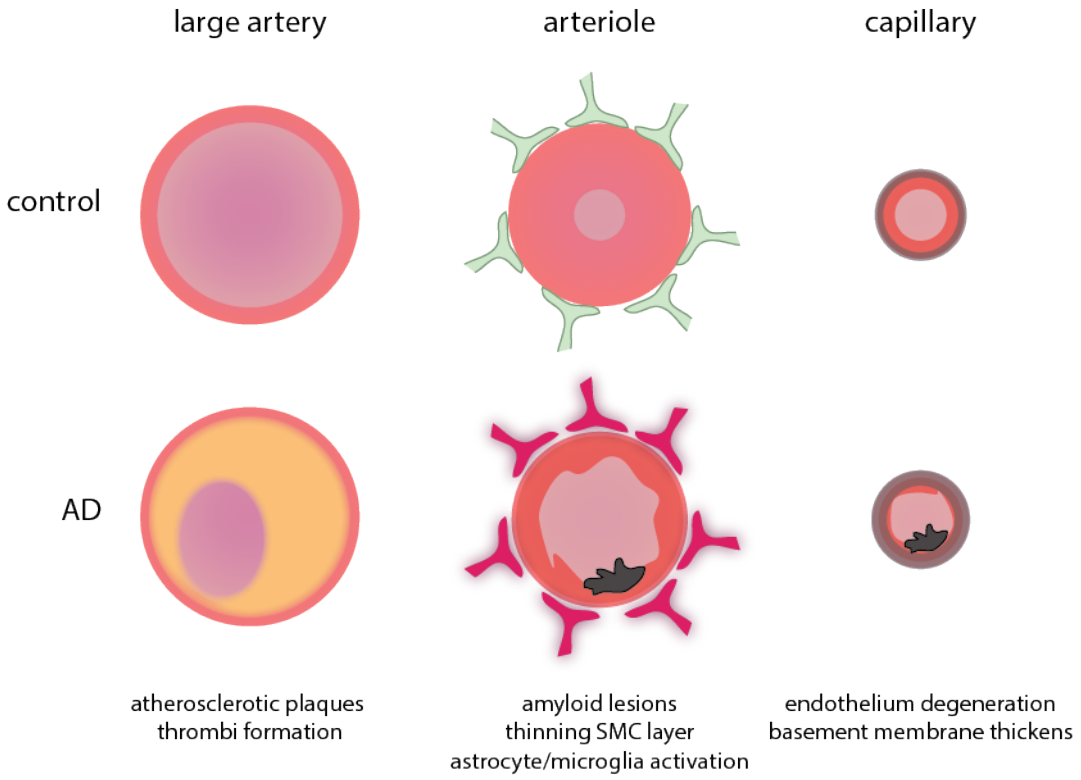

Figure 4.3 Comparison of healthy and AD-afflicted cerebral blood vessels. Adapted from [174].

4.5.3 Interactions Between Vascular and Amyloid Factors in AD

It is very difficult to separate the vascular and amyloid factors involved in AD, as they are closely coupled. Aβ induces the early vascular dysregulation which leads to a deficient blood supply (oligaemia). Oligaemia affects protein synthesis, which facilitates the further production of Aβ. A sluggish blood supply also causes a reduced clearance of Aβ, resulting in aggregation. Accumulated Aβ then promotes the formation of atherosclerotic plaques which further reduces the blood supply by occluding large cerebral arteries. Aβ, with its ability to affect synaptic function, and oligaemia, with its effects on protein synthesis, contribute to dementia early in AD. As the disease progresses, neurons (as well as as SMCs, ECs and astrocytes) can no longer withstand the amyloid accumulation and lack of blood supply, and are subsequently

destroyed [78]. The hypothetical time course of the disease may therefore be represented by Figure 4.4. There is a latent, asymptomatic phase where the initial vascular dysregulation occurs (from 1–2). Cognitive impairments then result when Aβ-induced neuronal dysfunction and sluggish blood supply begin to affect cell functioning (from 2–3). As the disease progresses, cerebrovascular regulation deteriorates at a similar rate to cognitive function. In the final stages, neurons and vessels degenerate and brain function is maximally compromised.

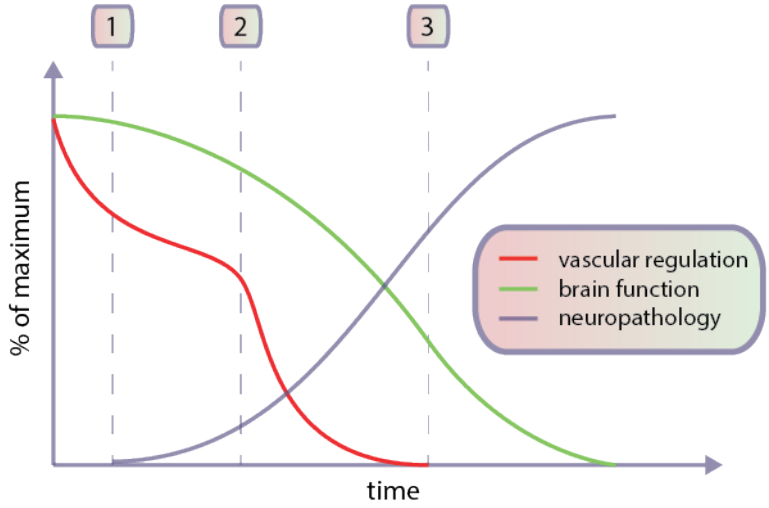

Figure 4.4 Proposed time course of Alzheimer's disease. Adapted from [78].

4.5.4 Astrocyte Dysfunction in AD

So far we have focused on the neuronal and vascular pathology of AD. However, the astrocyte, an integral part of the neurovascular unit, has also been implicated. Activated astrocytes are found close to Aβ plaques in the brain tissue of AD sufferers [167]. This suggests a causal relationship between Aβ and alterations in astrocyte function. Astrocytes, in the process of performing their many housekeeping chores, may accumulate neuron-derived amyloid material that has been released from degenerating neurons. If they accumulate enough toxic debris they may too undergo cell death, resulting in the formation of another type of amyloid plaque [116].

Mouse models of AD also tend to have "hyperactive" astrocytes; that is, astrocytes with increased intercellular calcium wave signalling [91]. Calcium oscillations are also altered in cells expressing the familial AD presenilin 1 mutation [82]. Astrocytes are important for maintaining the neuronal environment; if they are operating and communicating in a dysfunctional manner, this could lead to neuronal dysfunction. It is not only Alzheimer's disease where astrocyte dysfunction is known to be affected. Astrocyte changes have been observed and implicated in the

pathology of amyotrophic lateral sclerosis (ALS) and Huntington's, Parkinson's and Alexander disease [107].

4.6 Vascular Responses to Spreading Depression

Spreading depression (SD) is defined as "a slowly propagated wave of depolarization of neurons and glial cells, followed by a subsequent sustained suppression of spontaneous neuronal activity, accompanied by complex and variable changes in vascular calibre, blood flow, and energy metabolism [34]." Other phenomena associated with this process include cellular swelling, the release of neurotransmitters, and dramatic fluxes of ions in and out of cells [34]. Of particular interest to us, as NVC researchers, is the release of the known NVC mediators, K^+ and glutamate, and the vascular changes associated with them. Figure 4.5 gives an overview of some of the causes and effects of the SD-related K^+ and glutamate releases.

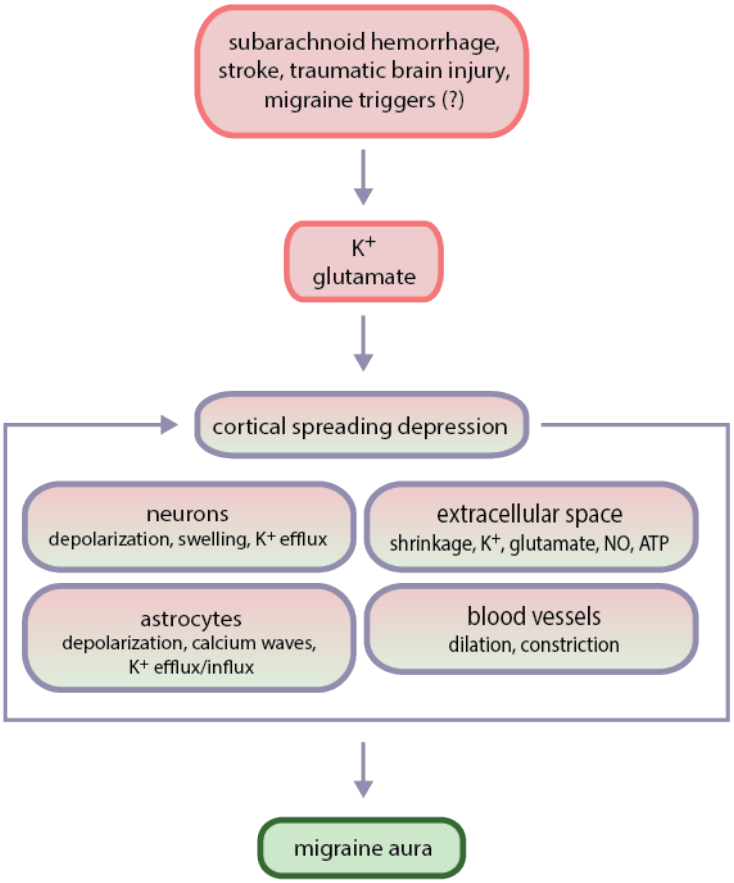

Figure 4.5 Basic mechanisms of CSD (cortical spreading depression) development and its consequences using migraine with aura as an example. Adapted from [34].

Experimental vascular responses to SD are complex and variable, depending on the experimental conditions. The original paper describing CSD in the rabbit reported a transient vasodilation, followed in some cases by a more sustained and less pronounced vasoconstriction [97]. In both mouse and rat, there is an initial dilation of arterioles and an accompanying increase in blood volume [15, 28]. However, in the mouse, this initial dilation is followed by a profound constriction of vessels and then *another* dilation, whereas in the rat the initial dilation is sustained [15, 28, 118]. Therefore, under some conditions, the predominant vascular response may be vasodilation, whereas under other conditions it may be vasoconstriction. The variability of vascular responses to SD may depend on a number of factors including: resting vascular tone, sensitivity of the vessels to extracellular K^+, tissue oxygenation, and basal and evoked levels of NO [34]. It is important to note that vascular responses in SD are not merely passive reactions to fluctuating K^+ and glutamate concentrations. One of the earliest studies of SD by Leao and Morison [98] indicated that blood vessels may play an *active* role in the propagation of SD. Vascular changes may even precede and condition SD [98].

Functional hyperaemia would be an extremely useful mechanism for preventing neuronal damage in pathological conditions in which metabolism is raised. Unfortunately, it is often in these conditions that this mechanism fails. This is so for spreading depression. In SD, there is an increase in brain energy use (presumably due to the increases in the concentration of glutamate, an excitatory neurotransmitter). As a result, the cerebral tissue consumes more O_2 and glucose, and the extracellular concentrations of these species decrease. The failure of neurovascular coupling to provide adequate blood flow to match this increased consumption may cause the neurological deficiencies associated with SD after subarachnoid haemorrhage [13].

The mechanism by which SD affects (or *disables*) NVC responses is not well understood. A possible pathway may lie with the impairment of the NO system [51, 141]. Remember that NO can dilate vessels directly or suppress 20-HETE-effected constrictions (see Chapter 3). In addition, NO both requires O_2 for its production *and* causes the vasodilations that would increase it. This could form a damaging feedback loop: SD-related increases in energy consumption cause low O_2 concentrations, which decrease NO formation, thereby reducing NO-dependent vasodilations (and hence blood flow), which decreases O_2 further [13]. It is also possible that the failure of neurovascular coupling in SD can be attributed to the very unusual vascular responses to extracellular K^+ (vasodilations in low concentrations of K^+, but *vasoconstrictions* in high concentrations of K^+).

Clearly, from a clinical point of view, understanding SD is essential, as SD has been shown to play a role in many pathological conditions such as migraine, haemorrhagic and ischaemic stroke, subarachnoid haemorrhage, traumatic brain injury, and epilepsy [34]. From a NVC

research point of view, understanding SD is also important, as the phenomenon's distinctive features may provide insights into the mechanisms of signalling between neurons, astrocytes, and vascular cells in normal brain function [34].

4.7 Diabetes and Vascular Disease

Diabetes (*Diabetes Mellitus*) is a metabolic disease characterized by hyperglycaemia (high blood sugar). It affects millions of people worldwide and will affect many million more in the years to come [166].

The connection between diabetes and vascular disease is not a trivial one: vascular diseases are the leading causes of death and disability in people with diabetes and can manifest as macrovascular consequences, such as atherosclerosis and hypertension, as well as microvascular consequences, such as retinopathy and nephropathy (responsible for blindness and end-stage renal failure, respectively) [39, 156]. The exact pathogenesis of vascular disease in diabetes is still unclear – there are many possible links between the metabolic abnormalities that characterize diabetes and the cellular mechanisms that affect the function and integrity of blood vessels [39] (some of which are displayed in Figure 4.6).

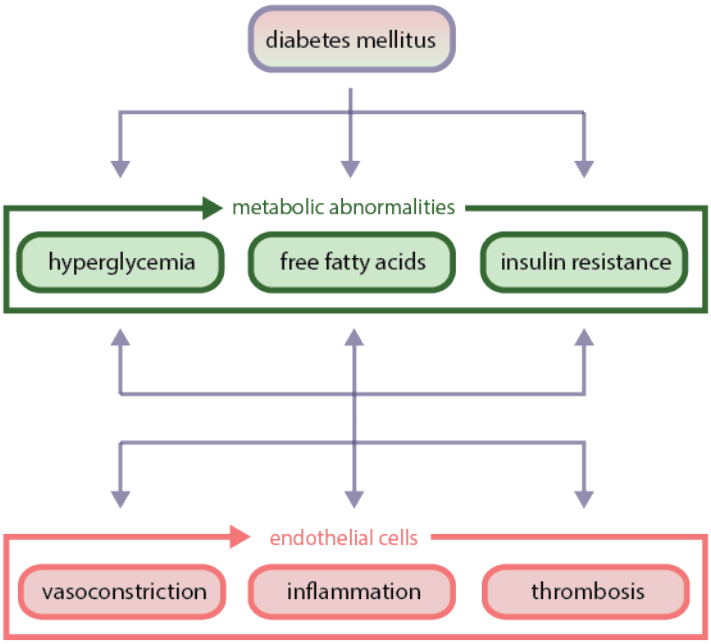

Figure 4.6 Abnormalities that occur in diabetes (hyperglycemia, free fatty acids, and insulin resistance) provoke endothelial cell dysfunction. Adapted from [39].

It is important to note that ECs, positioned between the flowing blood and the vessel wall, are well-placed to regulate vascular function and structure. When functioning normally, they synthesize and release substances that ensure adequate blood flow while preventing thrombosis. NO is just one of the many important molecules that the EC produces and its availability is used as a sign of vascular health. NO causes vasodilation by acting directly, and indirectly via cGMP, on adjacent SMCs. In addition, NO protects the blood vessel from atherosclerotic injury by mediating signals that prevent platelet and leukocyte interactions with the vessel wall. Endothelial dysfunction, manifesting as impaired NO-mediated relaxation, occurs in experimental models of diabetes. Further, experimental evidence supports the idea that hyperglycaemia decreases EC-produced NO [39]. The excellent review by Traub and Van Bibber [156] examines the role of NO in the development of vascular disease in diabetes.

Studies have also found a weak association between diabetes and Alzheimer's disease and a strong association between diabetes and stroke-associated dementia [105]. The relationship between diabetes and Alzheimer's disease is difficult to determine; however, it is possible that glycoxidation, glycation-related oxidative processes that occur in both AD and diabetes, forms the biochemical link [139, 147].

4.8 Prospects For New Therapies

Cerebrovascular disorders and neurological/neurodegenerative disorders do not exist as mutually exclusive phenomena – often they are coupled. Vascular cell integrity can be affected in many conditions associated with neurological deficits and cognitive decline (such as AD [174], ischaemia/reperfusion [108] and subarachnoid haemorrhage [88]). Furthermore, decreased or dysfunctional vascular responses can initiate, exacerbate or propagate the damage caused by other pathological pathways (as in AD [78], SD [34], and hypertension [45]). Having an understanding of the cellular mechanisms that underlie the blood flow dysregulation in pathological conditions allows us the opportunity to identify and develop therapies that could be of help.

Cerebrovascular disease and AD share common risk factors (such as hypertension, diabetes, and hypercholesterolaemia [43]). Reducing these risk factors through early treatment or preventative measures (such as lifestyle changes) may reduce the development of AD. Also, a useful adjuvant approach could be formed when treatments that rescue blood flow responses act in tandem with the treatment of other disease processes.

According to the neurovascular hypothesis put forth by Zlokovic [174] (shown in Figure 4.2), physiologically altered ECs, SMCs, and glia are important targets for controlling the cerebrovascular disorder in AD. Research into genes and other pathways that cause predisposition for neurovascular degeneration might also provide new leads for AD therapies [174].

Further, therapeutic agents that provide protection for stressed and ischaemic endothelial cells and neurons could protect the NVU from the combined attack of Aβ and hypoxia that is seen in AD [174].

Evidence also suggests that NO metabolism and vascular responses to NO are altered in diabetes [156]. There is also a documented NO system impairment in SD [51, 141]. Therapies that address pathogenic NO deficiencies may therefore benefit these patients.

Development of new therapies relies on the discovery and analysis of very complex and coupled cellular processes. Mathematical models that can describe cellular-level processes in detail will aid in the understanding of the stages of disease initiation, progression and degeneration. More than that, they can provide a mathematical framework for predicting the effects that potential pharmacological mediators could have [143].

4.9 Summary

The pathogenic gap is narrowing between cerebrovascular disorders and other common diseases. Stroke, Alzheimer's disease, spreading depression and diabetes all have vascular components in their pathology. These vascular changes are not necessarily a side or secondary effect of the disease; vascular responses can play an integral part in the initiation, propagation or degeneration of the disease itself.

Understanding the interplay between vascular and non-vascular components of a disease, and indeed developing new therapies to target these components, relies on the discovery and analysis of very complex and coupled cellular processes. Mathematical models that can describe cellular-level processes will aid in this understanding [143].

Chapter 5

Literature Review

5.1 Introduction

The problem of blood flow control is not a new one; it has been studied since the late 1800s. Since then, the mechanisms involved have been extensively researched, and include: pressure-dependent, shear-dependent, metabolic and propagated vessel responses, to name but a few. However, although the individual mechanisms are reasonably well characterized, the process in which the various mechanisms combine and counteract each other to produce flow and perfusion control as a whole is not. The problem is a complex one. The vascular system is comprised of many interconnected vessels. The flow through each branch is dependent on the flow resistance of that branch as well as the resistance of the many vessels connected to it. The many regulatory mechanisms act in varying degrees on different sections of the vascular tree and depend on variables, like pressure and metabolic rates, that are actually dependent on flow themselves – they form a closed loop. Information is exchanged in a variety of different ways, and many cells – smooth muscle, endothelial, erythrocyte, glial and neuronal – contribute to this complicated information exchange. Blood flow regulation is therefore multiplex and theoretical models can help us to analyze and understand these physiological intricacies.

This chapter gives a brief review of the smooth muscle, endothelial and astrocyte cell models, as well as whole vessel models, that have been developed and published in the literature. Each model is briefly summarized under its own heading and compared to other models.

Whilst reading this review, it is perhaps useful to remain mindful of two of the main objectives of this study: to 1) construct a working model of the neurovascular unit (SMC, EC and astrocyte), and 2) analyze the contributions of two known neurovascular coupling mechanisms – namely, a K^+- and EET-based mechanism and a NO-based mechanism – to blood flow regulation. Blood flow regulation as a whole – and even neurovascular coupling by itself – constitutes a large, complex and contentious area, and cannot all be reviewed here. Many aspects of the research have been necessarily omitted. For example, models of neuronal cell processes are

not reviewed here, as this lies outside the scope of this research (that is, we consider chemical processes relevant to neurovascular coupling occurring within the synapse but not within the neuron itself, at least at this stage).

5.2 Smooth Muscle Cell and Contraction Models

Arteriolar diameter (or arteriolar "tone") is adjusted by smooth muscle cells (SMCs). The magnitude of the adjustment generated by the SMC is dependent on many factors, including the SMC's length or tension, metabolite concentrations, the presence of other signalling molecules, and neural inputs. Of course, the consummate model of blood flow autoregulation would include SMC responses to all of these stimuli. Currently, such an integrated model does not exist; however, particular components of these cellular responses have been considered, and to varying degrees, modelled.

5.2.1 Gonzalez-Fernandez and Ermentrout [61]

The model of Gonzalez-Fernandez and Ermentrout [61] attempts to simulate the cellular processes underlying, firstly, stationary vasomotion (diameter oscillations), and secondly, the myogenic response, in a small artery. They use a system of 7 differential equations to accomplish this. These equations incorporate ionic movements, the SMC membrane potential, muscle contraction, and the mechanics of a thick-walled cylinder. Gonzalez-Fernandez and Ermentrout [61] show that the interaction of potassium and calcium fluxes (mediated by BK and VOCC channels, respectively) brings about cyclical changes of the ion transports. This causes periodic changes in the SMC cytosolic calcium, myosin light chain phosphorylation, and cross-bridge formation (with corresponding muscle stress development). The vessel's transmural pressure provides a circumferential stress which, together with the elastic and muscle stresses, determines the rate of change of the vessel's diameter. Further, they hypothesize that the relationship between calcium-channel openings on voltage is shifted by changes in transmural pressure (indeed, this is how they simulate a myogenic effect in their model). This allows the experimentally determined myogenic response (decreasing of vessel diameter with increasing pressure) to be reproduced.

This model introduced a number of useful concepts, including the mechanical representation of the arterial wall as a three-element model (with active muscle elements in series and parallel with non-linear "spring" elements). Limitations include the omission of SMC KIR channels and endothelial cell effects on the smooth muscle cell dynamics, and the assumption

that myogenic effects rely solely on pressure changes (ignoring the potential contributions of wall stress).

5.2.2 Yang et al. [170] and Yang et al. [171]

In their earlier publication, Yang et al. [170] develop a mechanistic model of the vascular smooth muscle cell (VSMC), which provides descriptions of:

1. ionic transmembrane currents
2. cytoplasmic Ca^{2+} regulation, and
3. Ca^{2+}-catalyzed MLC phosphorylation, crossbridge and force development

This work is very similar to the work of Gonzalez-Fernandez and Ermentrout [61] just described. Hodgkin-Huxley representations are used to describe voltage changes and the mechanical model is much the same, but is extended to include a viscoelastic element in series with the active contraction element. However, the mathematical description of myosin phosphorylation differs. In Gonzalez-Fernandez and Ermentrout [61]'s model, it is simply assumed that the dependence of phosphorylation on calcium is sigmoidal and approximates the relationship found at equilibrium, but in Yang et al. [170]'s model, calcium and force generation are related by the crossbridge phosphorylation and latch-state model of Hai and Murphy [65] (depicted in Figure 5.1). Their four-state model is more physiologically correct than the phenomenological description proposed by Gonzalez-Fernandez and Ermentrout [61] (although more complex models have since been developed in [64]). Further, Yang et al. [170] do include the contributions of KIR channels to SMC dynamics.

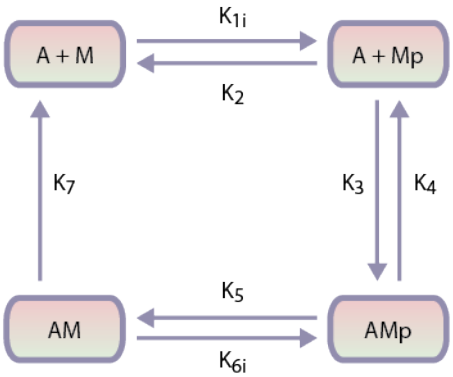

Figure 5.1 Crossbridge phosphorylation and latch-state model of Hai and Murphy [65]. Adapted from [65].

Their SMC model [170] is then incorporated into a vessel model of the myogenic response [171].

5.2.3 Yang et al. [169]

In a later study, Yang et al. [169] utilize their VSMC model and incorporate the signal transduction of vasodilatory NO/cGMP pathways, which includes model descriptions of:

1. sGC activation by NO,
2. sGC-catalyzed cGMP production,
3. cGMP- and NO- mediated intracellular Ca^{2+} regulation, and
4. cGMP-modulated MLC phosphorylation and VSMC contraction [169]

In this study, they identify many different mechanisms by which NO can act on cell machinery (through cGMP-dependent and -independent pathways) (Figure 5.2).

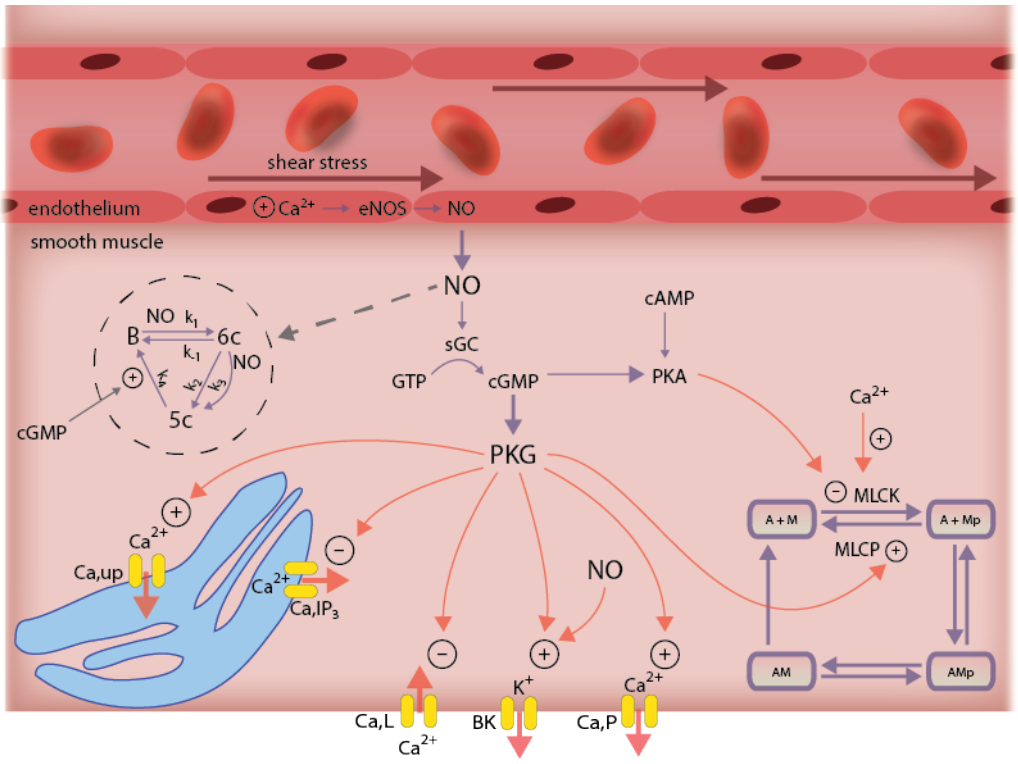

Figure 5.2 Diagram of endothelium-derived smooth muscle relaxation via NO/cGMP pathways as modelled by Yang et al. [169]. Adapted from [169].

A limitation in this model is that the arteriolar diameter (or subsequent blood flow) changes are not calculated so that they can be compared to experimental data. Furthermore, the mechanisms by which NO is actually generated (by neuronal or endothelial NOS) are not modelled in Yang (SMC NO concentration is simply an input). NO generation has, however, been considered theoretically by other groups [35, 38] and will be discussed further in a later chapter (Chapter 8).

5.2.4 Koenigsberger et al. [86]

The model of Koenigsberger et al. [86] uses a system of 14 differential equations to describe vasomotion in a small arteriole (56.3 μm). The fundamental difference between this model and those already described is that this one includes the ionic transports in both SMCs *and* ECs. Koenigsberger et al. [86] successfully reproduce the synchronous calcium oscillations that cause vasomotion, as well as the myogenic response. Further, as they include ECs in the model they are also able to show how the presence of ECs modulate the results obtained only with SMCs.

The calcium dynamics of an SMC are described in [86] by five variables: the calcium concentration in the cytosol c_i, the calcium concentration in the sarcoplasmic reticulum s_i, the cell membrane potential v_i, the open channel probability of voltage and calcium-activated (BK or K_{Ca}) potassium channels w_i, and the IP_3 concentration I_i. The dynamics in an EC are modelled similarly using four variables: cytosolic calcium concentration $\widetilde{c}_j$, endoplasmic reticulum calcium concentration $\widetilde{s}_j$, cell membrane potential $\widetilde{v}_j$, and the IP_3 concentration $\widetilde{I}_j$. Channel openings are modelled stochastically.

Cells are connected to their nearest neighbours via gap junctions, which allow electrical, calcium and IP_3 coupling. The model includes both *hetero*cellular coupling (coupling between *different* cell types, i.e., an SMC and EC pair) and *homo*cellular coupling (coupling between the *same* cell type, i.e., an SMC-SMC or EC-EC coupling).

The effects of SMC vasoconstrictors can be simulated using this model. Increases in vasoconstrictor concentration effect an increase in the PLC rate (a term in the differential equation for IP_3 concentration, I_i).

For the development of vessel tone, like Yang et al. [170], Koenigsberger et al. [86] use the crossbridge phosphorylation and latch-state model of Hai and Murphy [65]. The vessel radius in this model is then computed by considering the balance of circumferential forces in the wall and using Laplace's Law: $pr/h = \sigma_p + \sigma_a + \sigma_v$, where σ_p, σ_a and σ_v are the parallel elastic, active and viscous stress components of a viscoelastic model, respectively (see Chapter 2 for an explanation of viscoelastic models). Here, p is the pressure exerted on the

wall and h is the thickness of the arteriole. Viscous stress is represented by $\sigma_v = \eta \frac{dr}{dt}$, where η is the wall viscosity coefficient. The differential equation for the vessel radius (r) can therefore be represented by Equation 5.1:

$$\frac{dr}{dt} = \frac{1}{\eta}\left(\frac{pr}{h} - \sigma_p - \sigma_a\right) \tag{5.1}$$

Active stress (σ_a) is assumed to be directly proportional to the fraction of attached crossbridges ($[AMp] + [AM]$). They also assume that the vessel wall volume remains constant.

The equations were incorporated on a cylindrical grid of rectangular SMCs superimposed on a cylindrical grid of ECs. ECs are arranged parallel and SMCs perpendicular to the vessel axis. Each cell is connected via gap junctions with its nearest neighbours on the same layer and with the cells on the other layer directly across from it. SMCs and ECs are different sizes. In this model, each SMC has six nearest-neighbour SMCs and 5–6 nearest-neighbour ECs, and each EC has six nearest-neighbour ECs and approximately 15 nearest-neighbour SMCs. Koenigsberger et al. [86] first omit the population of ECs to analyze the effects of stress only on SMCs. Once the ECs are added, it was shown that they have only a modulating effect.

The work of Koenigsberger et al. [86] therefore describes a model that extends on its predecessors by including the important contributions of coupled ECs. It is essential to include ECs as they facilitate not only wall shear stress mediated-mechanisms, but potentially many other vasomodulatory mechanisms that are effected from the "blood" or lumen side of the neurovascular unit.

5.2.5 Kudryashov and Chernyavskii [92]

In their study, Kudryashov and Chernyavskii [92] model a "biological active tube," or arteriole. They are primarily interested in modelling the two main mechanisms of local autoregulation, the myogenic and wall shear stress mechanisms, while accounting for the non-linear viscoelastic behaviour of the vessel wall and the diffusion and kinetics of the key agents: NO, Ca^{2+} and phosphorylated myosin. The mechanism by which wall shear stress exerts an effect on vessel muscle relaxation in their model is as follows: 1) an increase in wall shear stress on the surface of the endothelial cells opens the calcium channels, which 2) leads to an increase in NO synthesis from L-Arginine; 3) NO then diffuses across the intima (EC and elastic) layer to smooth muscle cells in the media layer; 4) NO is taken up by the smooth muscle cells and initiates the synthesis of cGMP; 5) cGMP stimulates the outflow of intracellular calcium ions (Ca^{2+}); 6) the Ca^{2+} concentration decreases, reducing the concentration of contracting myosin-actin complexes, which 7) causes SMC relaxation (Figure 5.3). They assume that there is a linear

dependence of the muscular force on the phosphorylated myosin concentration and that the rate of NO production in the ECs is proportional to shear stress.

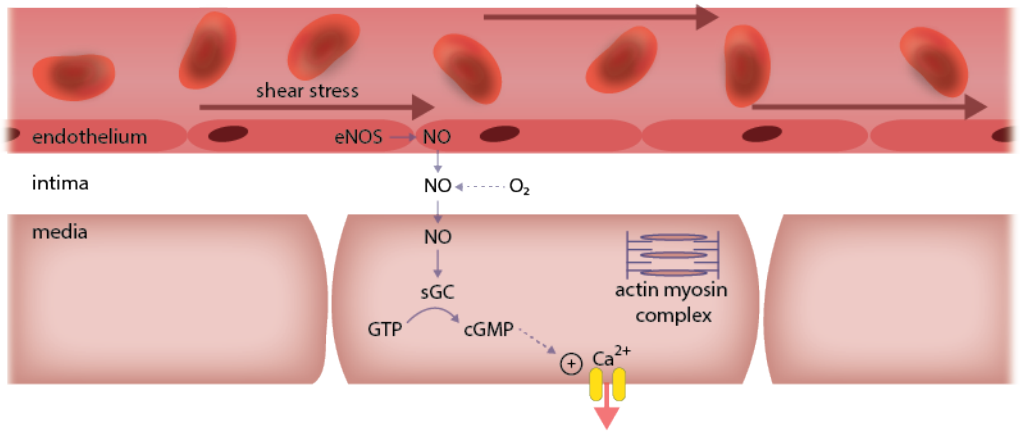

Figure 5.3 Diagram of the autoregulation process modelled by Kudryashov and Chernyavskii [92]. Adapted from [92].

Kudryashov and Chernyavskii [92] then use a Kelvin-Voigt type model to describe the viscoelasticity of the arterial wall, with an active force in parallel with the spring and damper (dashpot). This basic Kelvin-Voigt representation is adjusted by Kudryashov and Chernyavskii [92] in a number of ways. Namely:

- the passive elastic force is assumed to be weakly nonlinear with a quadratic correction
- the active force is assumed to be linearly proportional to the average concentration of phosphorylated myosin along the vessel
- the Young's Modulus, E, is also a function of phosphorylated myosin (as the "stiffness" of the wall changes as more crossbridges are formed)

This model is similar to that of Yang et al. [169] in that it incorporates NO mechanisms which act upon SMCs to cause dilation. However, the mathematical descriptions of the NO and cGMP processes involved here are largely phenomenological – this model does not include equations for important ion channels or ionic transports or gap junction coupling between EC and SMC layers. The viscoelastic model of the arteriolar wall is, however, more sophisticated than that in Yang et al. [169].

5.2.6 Summary of Smooth Muscle Cell and Contraction Models

These models typically include a description of the ionic transports and calcium dynamics that occur within a SMC, as well as equations that relate those changes in cytosolic calcium to the development of myosin-actin crossbridges and force development which effect changes in the vessel's dynamics.

For the purposes of our study, we require a SMC model that incorporates all known important ionic transports and chemical species involved in the major neurovascular coupling mechanisms – SMC KIR channels, EC-SMC interactions, and NO-cGMP pathways – but we also need a model that includes a physiological description of crossbridge formation and the non-linear viscoelastic properties of the vessel wall. Although models in the literature include pieces of this "ideal" model, no one incorporates a full description.

5.3 Astrocyte Models

Astrocytes, as well as other glia, were once believed to be only the "glue" that held neurons together [107]. It is now known that astrocytes serve multiple functions and are responsible for aiding in the process of neurovascular coupling. However, this relatively recent discovery means that our understanding of the cellular processes involved in astrocyte-aided neurovascular coupling is formative at best. This fact is both a disadvantage and an advantage for the theoretical modeller interested in understanding more about neurovascular coupling. On the one hand, it is difficult to model a process that is not well characterized by experimental studies. On the other hand, a theoretical modeller is well placed to help analyze, and in doing so, elucidate, the mechanisms that are truly at play.

There are few astrocyte models in the literature. Three different models, with very different goals and outcomes, are presented below.

5.3.1 Chen and Nicholson [36]

"Spatial buffering" by K^+ channels in glia is the focus of this mathematical model by Chen and Nicholson [36]. Although the scope of our research includes the mechanisms by which K^+ is released by astrocytes to SMCs during neurovascular coupling, this does not necessarily mean we are interested in spatial buffering. Spatial buffering is an ambiguous term, and different groups utilize different definitions. In the model of Chen and Nicholson [36], spatial buffering refers to the phenomenon of "spatial potassium concentration gradients in extracellular space

(ECS)" and their dissipation via "glial intracellular pathways" [36]. Their mechanism is as follows:

1. due to increased neuronal activation, K^+ ions are released into the interstitial spaces between cells and local $[K^+]_o$ (extracellular potassium) rises
2. this causes local depolarization of glial membranes that can be propagated along the cell and to other neighbouring cells, via gap junctions
3. there now exists a spatial distribution of membrane potentials along the length of the glial cell,
4. which elicits a local current that mediates either:
    - an influx of K^+ into the region of the cell where $[K^+]_o$ is locally raised, or
    - an efflux of K^+ from other glial cells that have low local $[K^+]_o$

Chen and Nicholson [36] use a two-part model, consisting of an extracellular space compartment and an intracellular glial compartment, together with the coupled partial differential equations describing the distribution of intra- and extra- cellular K^+ and membrane potential varying across space and time. Passive uptake by KCl was assumed to be the dominant method by which the cell sequestered its K^+ ions. Therefore, to estimate how the glial intracellular potassium $[K^+]_i$ varies with $[K^+]_o$, the dynamics of intracellular $[Cl^-]_i$ and extracellular $[Cl^-]_o$ are modelled. The $Na^+/K^+/2Cl^-$ co-transporter, the active Na^+/K^+ pump, and the change in ECS volume due to osmotic water movement were not considered. Chen and Nicholson [36] analyzed the effect that distributions of KIR channels (in endfooted and non-endfooted membranes) had on spatial buffer currents and $[K^+]_o$. They also analyzed the effects of glial geometry. Finally, they discussed whether their mechanism was able to efficiently transport K^+ over longer (multiple cell length) distances.

Although this model begins to analyze potassium processes that potentially form an important part of one known NVC pathway, it is not a NVC model. Important pieces of the K^+-based NVC mechanism are missing entirely, as they are not central to the understanding of spatial buffering, the primary focus for this group.

5.3.2 Bennett et al. [20]

The cell model of Bennett et al. [20] is based on the work of Lemon et al. [99]. Bennett's model, used to describe blood volume changes in microvessels as a result of glutamate release at

neuronal synapses, is depicted in Figure 5.4. Essentially, they are trying to model the following processes:

1. Synaptic glutamate, through its actions on metabotropic receptors, triggers a calcium transient in the astrocyte;
2. calcium changes generate the production of EETs that activate BK and K_{ATP} (ATP-activated K^+ channels) in the smooth muscle cells of adjacent arterioles; and,
3. this leads to SMC hyperpolarization and relaxation, and increases in blood flow.

It is important to note here that Bennett et al. [20] assume that EETs act on SMC channels and not on astrocyte channels (i.e., they work in a paracrine, rather than autocrine, manner). They also do not include the interactions of K^+ and EET mechanisms.

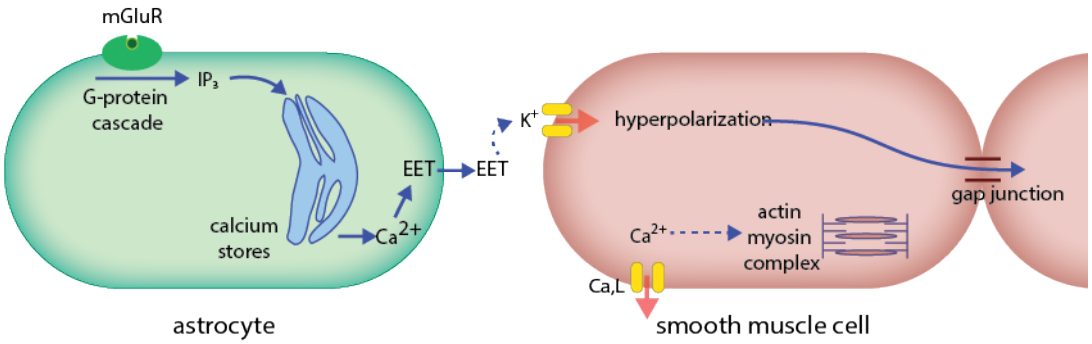

Figure 5.4 Major processes modelled by Bennett et al. [20] in an astrocyte and a smooth muscle cell. In the astrocyte, receptor binding initiates a G-protein cascade and production of IP_3 which elicits the release of Ca^{2+} from the ER and EETs from the astrocyte. In the smooth muscle cells, EETs cause a hyperpolarization leading to the closure of voltage operated calcium channels (VOCCs) and relaxation. Adapted from [20].

The equations are then integrated into a three-dimensional grid with several cells modelled (a representative two-dimensional cross-section is shown in Figure 5.5). They therefore model the *spatial variation* of chemical species throughout their grid.

This work is the first to attempt to model the neurovascular unit as a whole (in fact, they are modelling several adjacent neurovascular units at once). However, in their case, the neurovascular unit is comprised of an astrocyte and a SMC and does not include ECs. This omission limits their model in two ways: 1) the modulatory effects of ECs cannot be included, and 2) other, potentially interacting, pathways of arteriolar tone control that are elicited through ECs (such as wall shear stress-related pathways) cannot be incorporated into this model at a later

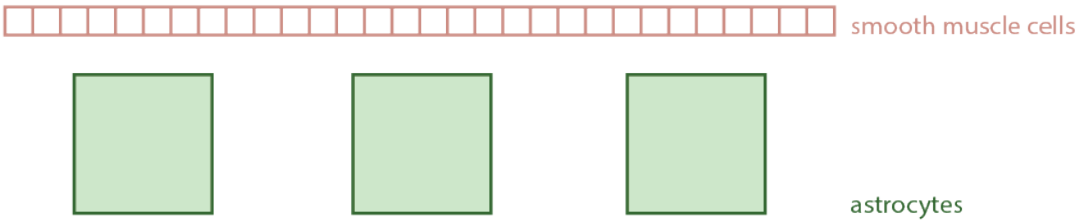

Figure 5.5 Geometric arrangement of astrocytes and smooth muscle cells in the model of Bennett et al. [20]. Astrocytes are represented by cubes of side length 25μm. Smooth muscle cells are cuboids with a square cross section of side length 5μm; they wrap twice around an arteriole of 14 mm diameter. The endfeet of astrocytes are about $10-20\mu$m long and cover one to two smooth muscle cells. Adapted from [20].

stage. Further, although astrocyte processes are well described in this model, the processes occurring in the SMCs are not. The EET targets (ion channel/s) that actually effect the SMC membrane voltage change are not modelled in Bennett et al. [20]. Instead, they assume a simple relationship for the SMC membrane potential: that the voltage change is directly proportional to the EET concentration. The SMC Ca^{2+} and VOCCs are, however, modelled. The Hai and Murphy [65] model is used to describe the dynamics of the myosin-actin interactions; although here a simplified three state ([M], [Mp] and [AMp]) version was used. Bennett et al. [20] state that the "contraction of the muscle cell is taken to be proportional to [AMp]" and also that the "change in cell length is translated into a change in arteriole diameter and hence by integration to a change in blood volume." The details of this method, however, are not given; they are also not apparent from the reference given ([157]).

In summary, this work, although commendable in many ways, lacks the physiological complexity required. It is pertinent to reiterate here that cellular-level modelling is particularly useful for understanding the effects of pharmacological mediators [143]; if insufficient molecular targets are modelled (or are modelled in too simplistic, or too phenomenological, a fashion) it will be impossible to investigate these mediators.

5.3.3 Østby et al. [124]

Shrinkage of the extracellular space (ECS) occurs when neuronal activity is increased. Østby et al. [124] outline a mathematical model that attempts to explain the main mechanisms behind ECS shrinkage (Figure 5.6). They note that this shrinkage accompanies the potassium clearance undertaken by astrocytes, and as such, they model the relationships between potassium clearance, water transport, and ECS shrinkage. They investigate, among other things, water transport via aquaporins in astrocytes, cotransporters and their involvement in potassium clearance, and the effects of particular knockouts on ECS shrinkage.

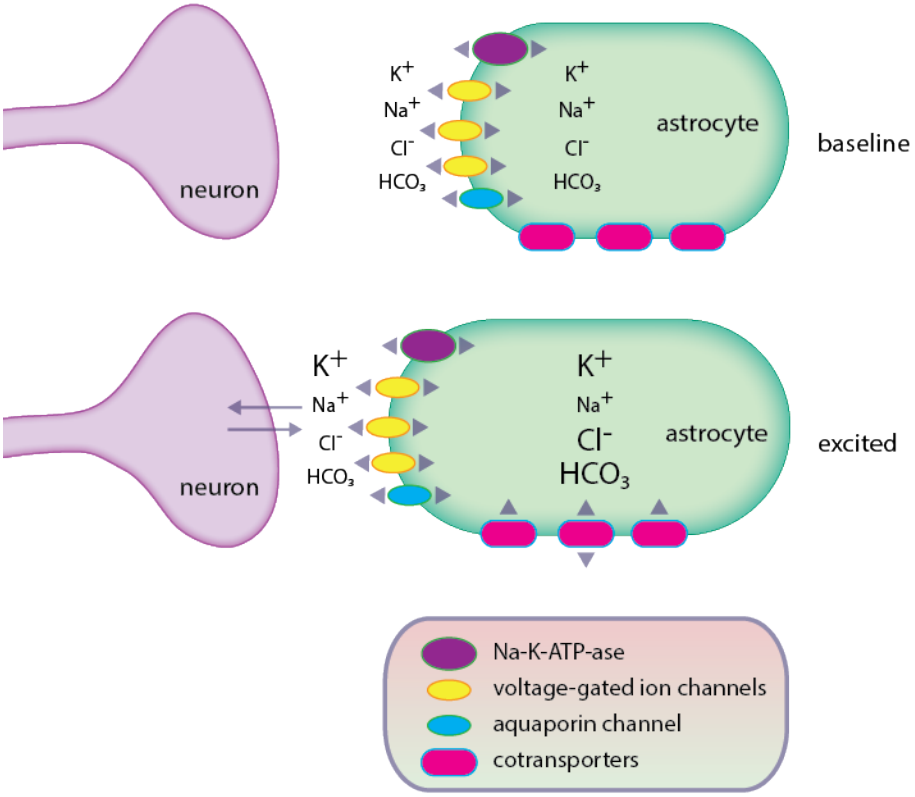

Figure 5.6 Outline of the basic model of Østby et al. [124]. In the baseline state, the neuron is "silent." In the excited state, the neuron contributes to changes in ECS and astrocyte volumes by generating potassium and sodium fluxes during firing. The changes in font and astrocyte size indicate the changes from the baseline to the excited state. Adapted from [124].

Although this work focuses mainly on the phenomenon of ECS shrinkage (which they successfully simulate), the model, with the inclusion of important ionic transports, could be used to investigate other phenomena, such as potassium spatial buffering and K^+-based neurovascular coupling.

5.3.4 Summary of Astrocyte Models

There are few astrocyte models in the current literature. Although some are interested in the analysis of neurovascular coupling mechanisms, many are interested more in the (albeit related) areas of potassium buffering and ECS shrinkage.

We require a model that describes glutamate receptor activation, the production of IP_3 and release of Ca^{2+} from internal stores, and the subsequent astrocyte-based NVC pathways that are elicited as a result (such as the K^+ and EET related pathways). Again, as it was with the SMC models currently in the literature, current astrocyte models do not contain all

the necessary components of the sort of physiological and flexible model that we require in order to investigate several NVC pathways operating in unison. Furthermore, only one model [20] attempted to link the astrocyte model with an SMC/vessel model, and none attempt to include the dynamics occurring within an EC. We aim to build a model that fully describes the important cellular processes occurring in *all* cells of the neurovascular unit.

5.4 Summary

In this review, it has been shown that although aspects of the cellular responses involved in neurovascular coupling (and indeed other metabolic autoregulatory pathways) have been modelled already, they have not been integrated into one complete coupled model. A coupled model contains all components of the neurovascular unit so that cells can communicate to one another and so that many different autoregulatory signals (those originating from the neuron side *or* the blood side) can be built in and can coexist and interact.

Essentially, there is a need for a model that:

- incorporates all cells of the NVU (astrocyte, SMC and EC) and the spaces between them
- contains all the important cell machinery that "powers" these cells (ion channels, pumps, receptors)
- describes a vessel that incorporates anatomically correct viscoelastic properties
- contains enough of the important cell equipment and chemical species to serve as a general framework for studying a variety of vasomodulatory mechanisms
- is physiologically correct, not just phenomenologically correct
- simulates small (single cell) changes as well as big (whole vessel) changes that can be separately compared with relevant experimental data

Chapter 6

Model Development

6.1 Introduction

The major aim of this research project is to create a theoretical model of neurovascular coupling (NVC) working within an entire neurovascular unit (NVU). Although there are many possible pathways involved in NVC, this project will focus on two: 1) K^+- and EET-mediated, and 2) NO-mediated pathways. This chapter outlines and explains the "foundation" NVU model, whereas the following two chapters are devoted to the extensions of the model and the obtained results for the two mechanisms.

It is important to note here that theoretical models do not follow a single accepted format. Some are phenomenological, some not; some use many sources of experimental data, some don't; some have simplifications and assumptions that others don't have, and some incorporate physical laws or mathematical concepts in subtly different ways to their predecessors. Therefore, to describe this model correctly and unambiguously – and indeed to get a "feel" for exactly what sort of model we are dealing with – the following points outlined in [144] must be addressed in this chapter:

- type of model (phenomenological or conceptual)
- scale(s) to which the model applies
- number of parameters and whether they are known *a priori*, fitted to data, or simply assumed
- experimental data used (for the formation of model parameters or for comparing to model results)

6.2 The Neurovascular Unit Model – General Overview

6.2.1 Model Type

The model presented in this thesis is of the quantitative conceptual model type (see Chapter 2). A "conceptual" model is based on the underlying physical mechanism that governs the behaviour. The "quantitative" component of this type arises from the fact that the description of the mechanism is fully parameterized. The model parameters are mostly scavenged from experimental data. Model results can be compared quantitatively to experimental observations for suitable values of the unknown parameters. Discrepancies between model and observed behaviour could mean that the mechanism is not valid or that it has been poorly represented by its parameters. If there is agreement, the parameters can be optimized so that the model can obtain the best fit to experimental data. The resulting parameter values can then be analyzed in terms of what they represent in the proposed mechanism.

6.2.2 Scale of the Model

This model applies in the scale range of a cell to a single vessel level. We focus first on the changes occurring in the cells of one neurovascular unit (namely, an astrocyte, a smooth muscle cell and an endothelial cell) during the process of functional hyperaemia. However, because it is important for us to understand if these cellular changes adequately account for the blood flow changes seen in experimental measures, we must also calculate the change in diameter of a model vessel. We can then translate these modelled changes in vessel diameter into an estimate of the blood flow change that could be expected (relative change in blood flow is approximately 4 times the relative change in diameter – see Equation 2.40 in Chapter 2). Note that these calculations of blood flow change apply only for a vessel considered in isolation; the calculation of the true physiological value of the blood flow change in a brain vessel would require a model that was incorporated into a large vascular tree network.

6.2.3 Experimental Data and Model Parameters

Model parameters are taken, where possible, from many different sources from the literature. Where there is insufficient (or non-existent) experimental data, we have had to make model estimations. All parameters are either referenced to their data source or labelled as estimations in the parameter tables (Appendix B).

The ideal experimental data set to use for parameterization of our model would:

- include the concentrations of all pertinent ionic and chemical species in all pertinent cells at rest and during varying "intensities" of neuronal activation, *and*
- include the consequent changes in myosin phosphorylation, crossbridge formation, muscular stress, arteriolar radius, pressure, blood flow, and wall shear stress, *and*
- would be conducted in a human
- in the cerebral vasculature *and*
- would be captured *in vivo*
- in real time.

Unfortunately, such a data set does not, and potentially never will, exist. We therefore collect our parameters not from one cohesive data set, but instead in pieces from experiments in which one ion channel or one cell or one ionic concentration is measured. Often the experiments are working in the coronary vasculature instead of the cerebral vasculature. Sometimes experiments are done on intact arterioles. Other times, they are performed on denuded arterioles (those lacking ECs). Often the cell has been removed from a live source and is then studied *in vitro*; some experiments are done on cultured cells. It is extremely rare to find data from human cell studies.

Further, there is not often the opportunity to validate one source of experimental data with another. The concentrations of the species in the solutions that the cells are grown in or are studied in vary between studies, which may have an effect on the quality or magnitude of the observed behaviour. Also, the expression of cellular entities (such as ion channels, for example) change throughout the lifetime of the animal; some studies are performed on developing/juvenile animals and others on fully-grown animals.

As there is little experimental data to work with, we must assume that the experimental conditions employed in the studies are as close as possible to those experienced by the cell *in vivo*. Additionally, as most studies are performed on non-human cells, we also assume that the properties of ion channels and other cellular machinery in the vasculature of other animals can be used to approximate the properties in the human cerebrovasculature.

6.2.4 Model Assumptions

Assumptions will be stated as they are made in the model development. However, some general assumptions to consider before we begin are:

- that 1) K^+- and EET- mediated and 2) NO-mediated pathways are the dominant mechanisms employed in NVC
- ion channel properties to do not change appreciably between different cells and species
- concentrations of ionic species are uniform throughout the compartment in which they reside (they are well mixed compartments – no spatial variation is considered)
- compartments have a constant volume – no osmotic shrinkage effects occur
- ionic species in the extracellular medium (except for K^+, explained in the following chapter) are approximately constant
- the Ca^{2+} concentration in the cytosol is buffered
- EET affects the voltage- and calcium- gated potassium (BK) channels on the astrocyte endfoot and does not diffuse across to the SMC
- there is two point sources for NO: NO is produced in the EC by eNOS and in the neuron by nNOS
- there exists fast binding kinetics of glutamate to mGluR receptors and G-protein activation in the astrocyte
- there is no depletion of PIP_2 and no catalytic effect of Ca^{2+} on IP_3 production in astrocyte
- there is an approximate 1 SMC : 1 EC : 1 astrocyte ratio
- cytosolic Ca^{2+} is contributed to by SR Ca^{2+}-release in the SMC (this is termed "Ca^{2+}-induced Ca^{2+}-release" (CICR))
- we assume that Ca^{2+}-dependent phosphorylation is the only mechanism of myosin phosphorylation present in the smooth muscle cell
- only attached crossbridges contribute to active force generation in the arteriole
- crossbridge attachment increases the stiffness of the active layer of the arteriole
- the populations of crossbridges are all identical to one another and are identically formed (heterogenous)
- we have an axially symmetric and viscoelastic artery
- blood is an incompressible and viscous fluid

- the flow is quasi-stationary
- the transmural pressure (difference of the pressures acting on the vessel wall, approximately equal to blood pressure) is constant

6.2.5 Model Schematics

A summary of the model – and the data, concepts and assumptions that it is built from – is given in Figure 6.1.

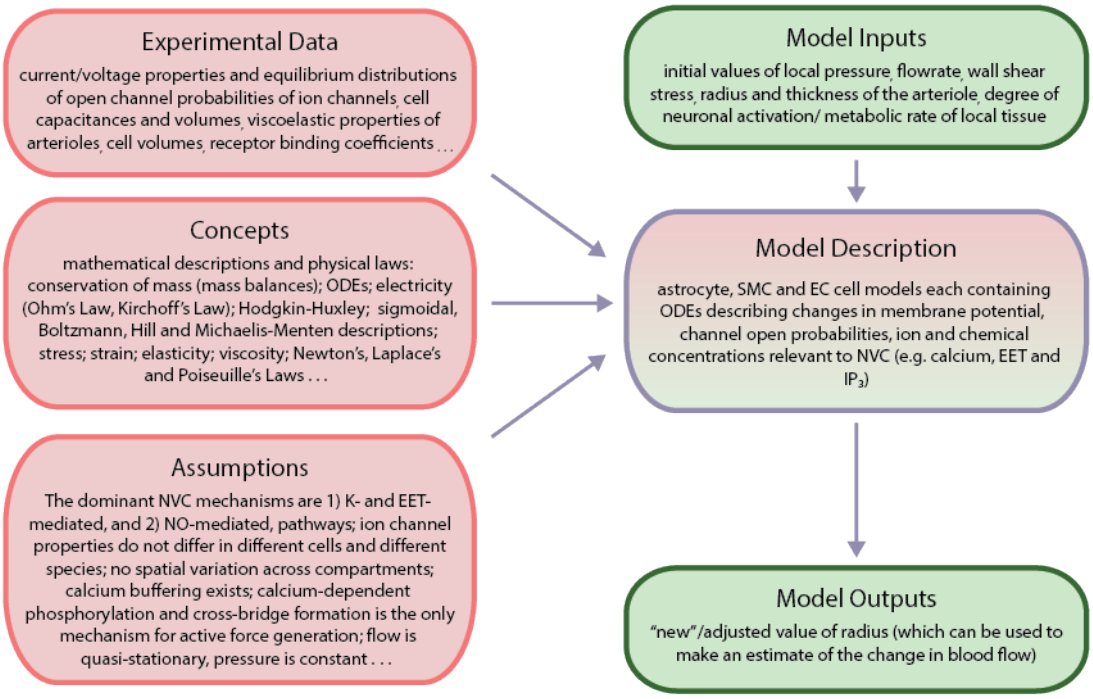

Figure 6.1 Non-mathematical overview of the neurovascular unit model.

The pathways that are modelled in this thesis are shown in Figure 6.2.

6.3 Description of the Basic Model

We develop here a model of the entire neurovascular unit, including the synaptic cleft, astrocyte, perivascular space and both active layers of the arteriole (smooth muscle cells (SMCs) and endothelial cells (ECs)). There have been several models produced of the component parts of the neurovascular unit (see Chapter 5) and we extend and adapt some of these. We use the

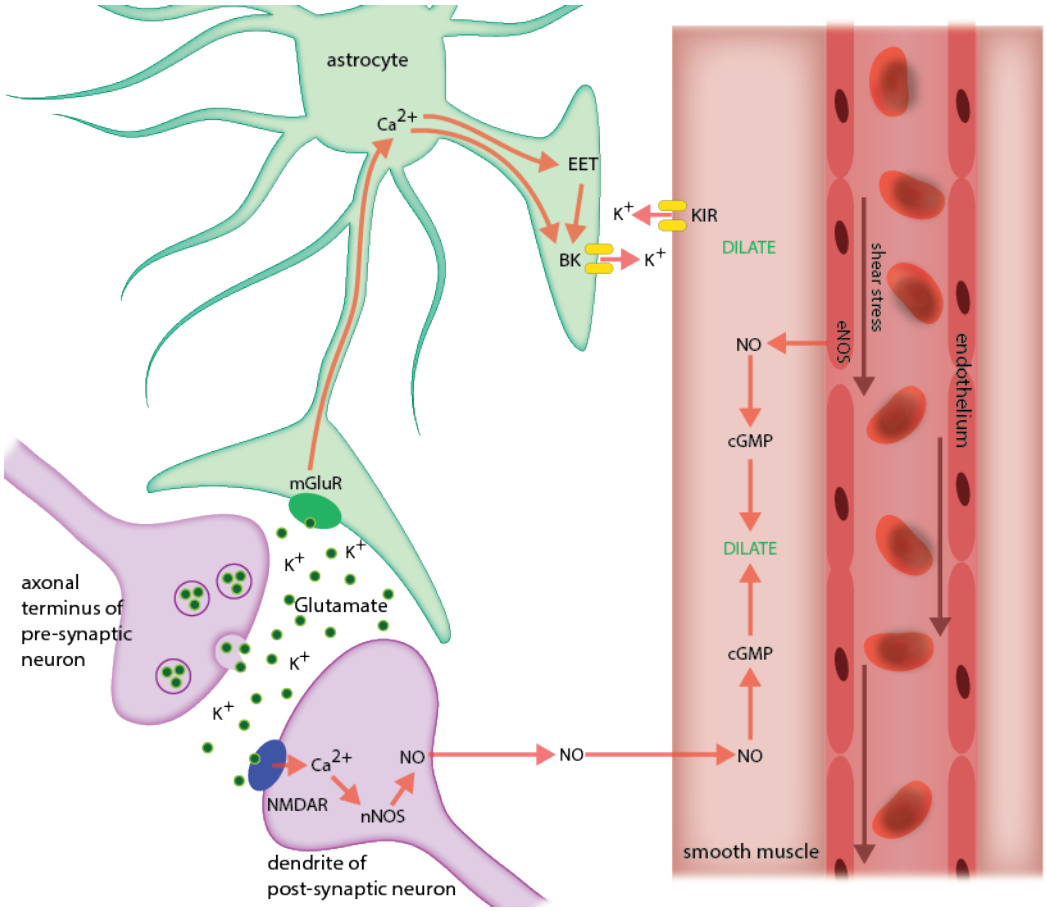

Figure 6.2 Aspects of neurovascular coupling studied in this thesis. Note here the NO produced by nNOS in the neurons and also by eNOS in the endothelial cells. Refer to Figure 3.14 for the full collection of known NVC mechanisms.

models of Koenigsberger et al. [86] for our coupled EC and SMC layers of the arteriole, with extensions to include the SMC KIR channels and EC eNOS activation needed as part of our model. The neurovascular unit model of Bennett et al. [20] includes only the EET (and not the K^+) mechanisms, and both Koenigsberger et al. [86] and Bennett et al. [20] use simplistic (first order or proportional) models of muscle contraction. We therefore use only the astrocyte equations of Bennett et al. [20], extending them to include potassium signalling. Finally, we further develop the muscle contraction equations of Kudryashov and Chernyavskii [92] to produce a more physiologically correct model that takes into account the multilayer structure of the arterial wall and the nonlinear viscoelastic properties of the wall material. Furthermore, in contrast to other autoregulation models [20, 61] who consider only the dynamics in the SMC component of the wall; we include a coupled SMC and EC cell layer. An illustration of how these existing models are included and extended is given in Figure 6.3.

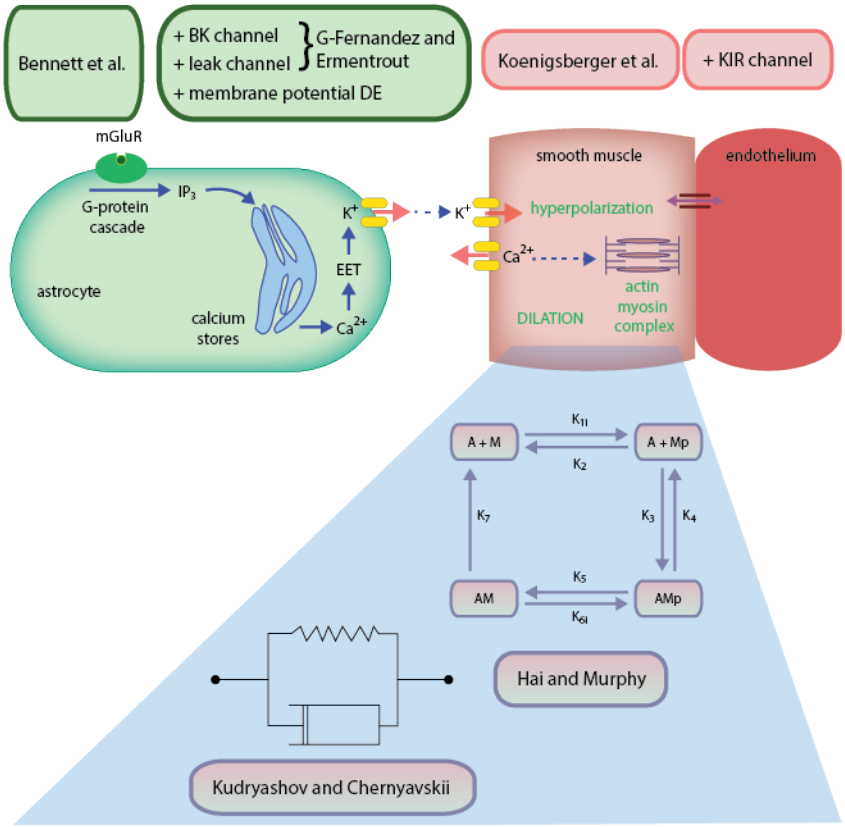

Figure 6.3 Building blocks of the neurovascular unit model.

6.3.1 Dimensional Consistency and Unit Conversions

This model uses equations from sources in the literature (Figure 6.3). The models in these sources have different focuses and goals and derive their parameters from a variety of different experimental data. For these reasons, the equations in these sources have a variety of units. For example: some will describe ionic fluxes in terms of an electrical current (with units of coulombs per second, Cs^{-1}, or amps, A) and others will describe the size of the fluxes in terms of the change in concentration that they cause when they enter or leave the cell (units of μMs^{-1} or mMs^{-1}). In order for these dimensionally inconsistent equations to be used together in our model, model parameters must be first converted to common units using certain physical laws or additional parameters taken from the literature. For example: to convert a parameter with units of Cs^{-1} to that of μMs^{-1}, we need to have an understanding of the relationship between electricity and chemistry, or more specifically: the relationship between charge and concentration. We therefore need to use concepts borrowed from Faraday's electrochemical laws to relate the amount of charged ions to the number of the chemical species (mols) and we will also need to have an estimation of the volume of the cell taken from the literature (to get

the molar *concentration* in μmol L^{-1} (equivalent to μM)). The working for this is as follows:

$$\begin{aligned} \left[\text{electrical flux in } \frac{\text{C}}{\text{s}}\right] \times \frac{1}{k_1}\frac{\text{mol}}{\text{C}} \times \frac{1}{k_2}\frac{1}{\text{L}} \times \frac{10^6\ \mu\text{M}}{1\ \text{M}} &= \left[\text{molar flux in } \frac{\mu\text{M}}{\text{s}}\right] \\ \therefore \quad \left[\text{electrical flux in } \frac{\text{C}}{\text{s}}\right] \times \left(\frac{10^6}{k_1 k_2}\right) &= \left[\text{molar flux in } \frac{\mu\text{M}}{\text{s}}\right] \end{aligned} \tag{6.1}$$

where k_1 is the valency/charge of the ion (i.e., Ca^{2+} has a valency of 2 and K^+ has a valency of 1) multiplied by Faraday's constant (96500 C mol^{-1}) and k_2 is the volume of the cell or space described by the equation (in L). To convert from a value in Cs^{-1} to one in μM s^{-1}, we must multiply by the "conversion factor" of $10^6/(k_1k_2)$.

The conventional units for physiological measures of pressure or stress are mmHg or dyne cm^{-2}, so many model parameters also need to be converted from these into the SI units of Pa for dimensional consistency. A simple relationship between these units exists:

$$1\ \text{mmHg} = 1333\ \text{dyne cm}^{-2} = 133.3\ \text{Pa} \tag{6.2}$$

An even simpler conversion is required when model equations are described by parameters or variables that differ only in an order of magnitude. For example, one equation may describe concentration changes in μMs^{-1} and another may be expressed in mMs^{-1}. These equations differ only by a factor of 1000 and can therefore be easily converted using the following relationships:

$$\begin{aligned} \frac{1\ \mu\text{M}}{s} \times \frac{1\ \text{mM}}{1000\ \mu\text{M}} &= \frac{0.001\ \text{mM}}{s} \\ \frac{1\ \text{mM}}{s} \times \frac{1000\ \mu\text{M}}{1\text{mM}} &= \frac{1000\ \mu\text{M}}{s} \end{aligned} \tag{6.3}$$

There are many equations in this model where this sort of conversion has been applied. These simple conversions will not be mentioned specifically in this text, but parameters listed throughout the main thesis body and especially in Appendix B will be listed in their converted units, as they were used in model equations.

As a guide, here is a list of the common units that will be used throughout the model development:

- Ionic fluxes and changes in concentration are usually expressed in μMs^{-1} or mMs^{-1} (mMs^{-1} is used for K^+ concentrations and neuronal Ca^{2+}; otherwise μMs^{-1} is used)
- Glutamate concentrations are in nM

- Voltages/membrane potentials are in mV (this is the convention for cellular measurements)
- Pressures and stresses are in Pa except in cases where the units will cancel within an equation to produce a dimensionless quantity (in which case, units of mmHg used in the original sources are used)
- Temperatures are in K
- Time and rate constants are in s and s^{-1}, respectively
- Some conductance values are given in the parameter tables as electrical conductances (pS) instead of molar conductances (μM mV^{-1} s^{-1}). Similarly, cell capacitances are given in pF (a farad, F, can be represented as a coulomb per volt, C V^{-1}). The equations that utilize these electrical units possess a conversion factor within them that produces molar values. These equations and their conversion factors will be explained as they are introduced in this thesis.

6.3.2 Astrocyte

Voltage-operated calcium channels (VOCCs) are expressed in cultured astrocytes, and Filosa and Blanco [55] include these channels as an important entity in their hypothesized process of neurovascular coupling. However, Carmignoto et al. [33] show that VOCCs may not necessarily be responsible for the propagating calcium waves involved as part of neurovascular coupling. We therefore exclude these channels in this model. We do, however, include a general "leak" term. The equations and parameters for the leak current are those of Gonzalez-Fernandez and Ermentrout [61].

The voltage- and calcium- operated potassium channel (BK) and the "inwardly-rectifying" potassium- and voltage-gated potassium channel (KIR) are both expressed in astrocyte processes surrounding synapses and arterioles [72, 129]. However, according to Zhou and Kimelberg [173], astrocytes can be divided into two classes: variably-rectifying astrocytes (VRA) and outwardly-rectifying astrocytes (ORA), where only VRA seem suited for uptake of extracellular potassium via KIR channels. We assume then that ORA are therefore responsible for "pushing" potassium out via BK channels, and VRA for "pulling" it back in again via KIR channels, and together they cooperate to move potassium in and out of extracellular spaces ("potassium buffering"). As we are not investigating the process of potassium buffering at this time, we will look only at the ORA, and as such will only include the BK channels in the astrocyte.

The foundation for this model of the astrocyte cell processes is that of Bennett et al. [20]. We further develop their equations with additions and adaptations to include a differential equation for the astrocyte membrane voltage, which includes ohmic relationships for BK and leak fluxes. The BK channel flux is modelled from Gonzalez-Fernandez and Ermentrout [61], with a voltage shift term that is dependent on the EET concentration.

The differential equations describing the dynamics in the astrocyte are as follows. Here c_k is the cytosolic Ca^{2+} concentration, v_k is the membrane voltage, s_k is the concentration of Ca^{2+} in the endoplasmic reticulum (ER), h_k is the inactivation variable for IP_3, i_k is the concentration of IP_3 and eet_k is the concentration of EETs.

Calcium moves between the cytosol and the ER, and the cytosol and the extracellular space surrounding the astrocyte, by several mechanisms. We denote the calcium flux from the ER to the cytosolic volume through IP_3 receptor/channels (IP_3R) by J_{IP_3}, the leakage flux from the ER to the cytosol as $J_{ER_{leak}}$ and the ATP-dependent pump flux from cytoplasm to ER as J_{pump}. Thus we can write:

$$\frac{dc_k}{dt} = B_{cyt}\left(J_{IP_3} - J_{pump} + J_{ER_{leak}}\right) \tag{6.4}$$

The constant B_{cyt} is a steady state approximation for buffering in the cytosol [20] and is a dimensionless quantity. J_{IP_3}, J_{pump} and $J_{ER_{leak}}$ are molar fluxes in μMs^{-1}.

The astrocyte membrane voltage changes due to fluxes of ions leaving the astrocyte: the potassium flux through *BK* channels (J_{BK_k}) and a *general* leak flux (J_{leak_k} – not to be confused with $J_{ER_{leak}}$). Note that we have assumed that Ca^{2+} does not enter or leave the astrocyte cell itself; it only enters and leaves the internal cell stores (the ER). We can therefore state the relationship:

$$\frac{dv_k}{dt} = \frac{1}{C_{ast}}\left(-J_{BK_k} - J_{leak_k}\right) \tag{6.5}$$

where C_{ast} is the astrocyte cell membrane capacitance (in pF). J_{BK_k} and J_{leak_k} are "electrical currents" (in fA). This gives the desired units of mVs^{-1} for the change in voltage with time.

s_k, the concentration of calcium in the ER, was assumed to be constant in the original model [20]. In order to be able to investigate this variable further, we incorporate the following differential equation:

$$\frac{ds_k}{dt} = \frac{-1}{VR_{ERcyt}}\left(\frac{dc_k}{dt}\right) \tag{6.6}$$

where VR_{ERcyt} is the ratio of ER volume to cytosolic volume.

The flux J_{IP_3} is taken from Li and Rinzel's simplification [100] of the De Young and Keizer [44] model of the IP_3R. The IP_3 receptor/channel can be represented by three identical subunits, which each contain one IP_3 binding site, one Ca^{2+} activation site, and one Ca^{2+} inactivation

site, hence the following formulation:

$$J_{IP_3} = J_{max}\left[\left(\frac{i_k}{i_k + K_I}\right)\left(\frac{c_k}{c_k + K_{act}}\right)h_k\right]^3 \times \left[1 - \frac{c_k}{s_k}\right] \tag{6.7}$$

J_{max} is the maximum rate in μMs^{-1}, K_I is the dissociation constant for IP_3 binding to an IP_3R (in μM) and K_{act} is the dissociation constant for Ca^{2+} binding to an activation site on an IP_3R (also in μM). The cubic power arises from the fact that the receptor/channel conductance was experimentally determined to be at its highest when all three subunits experience binding [44]. The Ca^{2+} inactivation variable h_k is modelled as a dynamic variable:

$$\frac{\mathrm{d}h_k}{\mathrm{d}t} = k_{on}\left[K_{inh} - (c_k + K_{inh})\,h_k\right] \tag{6.8}$$

Here k_{on} is the rate of Ca^{2+} binding to the inhibitory site on the IP_3R ($\mu\text{M}^{-1}\text{s}^{-1}$) and K_{inh} is the corresponding dissociation constant (μM). $J_{ER_{leak}}$ is determined by:

$$J_{ER_{leak}} = P_L\left(1 - \frac{c_k}{s_k}\right) \tag{6.9}$$

where P_L is determined from the steady state calcium balance (μMs^{-1}), and J_{pump} is:

$$J_{pump} = V_{max}\frac{c_k^2}{c_k^2 + k_{pump}^2} \tag{6.10}$$

V_{max} is the maximum pumping rate (μMs^{-1}) and k_{pump} is the dissociation constant (μM). For IP_3, we have:

$$\frac{\mathrm{d}i_k}{\mathrm{d}t} = r_h G - k_{deg} i_k \tag{6.11}$$

where r_h is the maximum rate of IP_3 production in the astrocyte due to glutamate attachment at metabotropic receptors (μMs^{-1}), k_{deg} is the rate constant for IP_3 degradation in the astrocyte (s^{-1}), and G is the ratio of active G-protein to total G-protein, and satisfies:

$$G = \frac{\rho + \delta}{K_G + \rho + \delta} \tag{6.12}$$

ρ is the ratio of bound to total glutamate receptors on the synapse end of the astrocyte, and K_G is the G-protein dissociation constant (dimensionless). δ is the ratio of the activities of the unbound and bound receptors. The inclusion of δ allows for there to be background activity even in the absence of ligand binding (i.e., unbound receptors can still activate a small amount of G-protein). This behaviour is more fully described in the work of Lemon et al. [99].

Finally, Ca^{2+}-dependent EET production is described with the simple relationship:

$$\frac{\mathrm{d}eet_k}{\mathrm{d}t} = V_{eet}\left(c_k - c_{k,min}\right) - k_{eet}eet_k \tag{6.13}$$

$c_{k,min}$ is the minimum Ca^{2+} concentration required for EET production (μM). V_{eet} and k_{eet} are the rate constants for EET production and EET degradation, respectively; these both carry units of s^{-1}. Degradation is assumed to follow first order kinetics.

6.3.2.1 Dimensional Consistency in Astrocyte Equations

Many of the parameters listed in the tables in Bennett et al. [20] were dimensionally inconsistent with their own equations. We therefore have had to estimate values for any unusable parameters in Bennett et al. [20] (i.e., V_{eet}, k_{eet}, r_h, and k_{deg}). We have estimated values that give approximately the same concentration changes for IP_3 and EET as those showed in the results of Bennett et al. [20].

6.3.2.2 BK Channel Model

J_{BK_k} in Equation 6.5 can be described by the ohmic relationship:

$$J_{BK_k} = g_{BK_k} n \left(v_k - v_{BK_k}\right) \tag{6.14}$$

where g_{BK_k} is the conductance (in pS), v_{BK_k} is the Nernst reversal potential (in mV) and n is the open BK channel probability (dimensionless). BK channel equations and parameters are taken from the SMC model of Gonzalez-Fernandez and Ermentrout [61], with the exception of the conductance which is a model estimation (the astrocyte BK channel conductance has not been experimentally determined as yet).

Work by Lu et al. [104] shows that both EETs and EET-derived dihydroxyeicosatrienoic acids (DHETs) act as potent activators of BK channels, where DHETs were shown to shift the voltage at which the channel open probability was half-maximal. We therefore incorporate a EET-dependent voltage shift (eet_{shift}) into the relationship given by Gonzalez-Fernandez and Ermentrout [61], to get n_∞, the *equilibrium* distribution of openings for the BK channel:

$$n_\infty = 0.5\left(1 + \tanh\left(\frac{\left(v_k + eet_{shift}eet_k\right) - v_3}{v_4}\right)\right) \tag{6.15}$$

The time course of the fraction of BK channel open states, n, is described, after Morris and

Lecar [115], by the first-order kinetics of opening:

$$\frac{\mathrm{d}n}{\mathrm{d}t} = \phi_n \left(n_\infty - n\right) \tag{6.16}$$

where the rate constant associated with the opening of these channels, ϕ_n, is based on statistical considerations [49]:

$$\phi_n = \psi_n \cosh\left(\frac{v_k - v_3}{2v_4}\right) \tag{6.17}$$

$$v_3 = -\frac{v_5}{2}\tanh\left(\frac{c_k - Ca_3}{Ca_4}\right) + v_6 \tag{6.18}$$

In this case, ψ_n is a characteristic rate (s^{-1}) and v_3 incorporates a calcium-dependent shift on the distribution of BK channel open states with respect to membrane voltage. v_3 is the voltage associated with the opening of half the population and v_4 is a measure of the spread of the distribution. v_5, determines the range of the shift of n_∞, as calcium varies. Constants v_3 to v_6 carry units of mV. Ca_3 and Ca_4 describe the shift in this distribution with calcium; these have units of μM.

Note: Unlike Bennett et al. [20], we assume that the astrocyte-derived EETs do not diffuse through the perivascular space to the arteriole, but act primarily upon the BK channels at the astrocytic endfeet (that is, we assume that diffusion processes occur over much longer timescales than the interactions between EETs and the nearby astrocyte BK channels). It is possible that EETs or other AA-derived metabolites act on the SMCs themselves [13], but at this stage, for simplicity, we only look at EET interactions within the astrocyte itself.

6.3.2.3 "Leak" Channel Model

The relationship for J_{leak_k} is also taken from Gonzalez-Fernandez and Ermentrout [61].

$$J_{leak_k} = g_{leak_k}\left(v_k - v_{leak_k}\right) \tag{6.19}$$

Here J_{leak_k} carries the unit of fA, and g_{leak_k} (pS) and v_{leak_k} (mV) are assumed to be constant.

6.3.3 Smooth Muscle and Endothelial Cells

The foundation for this model of the smooth muscle and endothelial cell processes follows that of Koenigsberger et al. [86] (full equation set in Appendix A). We add a KIR channel flux in the SMCs, which is modelled similarly to that of the BK potassium channels described above. We use the following relationship for the time course of the fraction of open KIR channel states, k:

$$\frac{\mathrm{d}k}{\mathrm{d}t} = \frac{1}{\tau}(k_\infty - k) \tag{6.20}$$

τ is a characteristic time (in s) associated with the opening of these channels and k_∞ is the equilibrium distribution of open states.

J_{KIR_i} is incorporated into the SMC voltage differential equation in the following form:

$$J_{KIR_i} = g_{KIR_i} k (v_i - v_{KIR}) \tag{6.21}$$

Again, here g_{KIR_i} is the membrane conductance (in pS) for the KIR current and v_{KIR} is the corresponding Nernst reversal potential (given in mV).

Patch clamp experiments by Kurachi [93] give a kinetic model for the opening of the KIR channel. The time constant associated with the change in the fraction of the open channels (τ) is the "balance" of the two opening and closing constants, α and β (as described in Appendix C and below).

$$\tau = \frac{1}{\alpha + \beta} \tag{6.22}$$

with:

$$\alpha = \frac{1020}{1 + \exp\left(\frac{v_i + 18}{6.8}\right)} \tag{6.23}$$

$$\beta = 26.9 \exp\left(0.06(v_i + 18)\right) \tag{6.24}$$

α and β are time constants and possess units of seconds. v_i is the membrane potential minus v_{KIR} (the reversal potential) – both of these are measured in mV.

The equilibrium open channel probability (a dimensionless quantity) is given by the (sigmoidal) relation:

$$k_\infty = \frac{\alpha}{\alpha + \beta} \tag{6.25}$$

v_{KIR} (the Nernst reversal potential for the KIR channel) increases with $[\mathrm{K}^+]_o$ (the perivascular potassium concentration in mM). Using the data from Oonuma et al. [123], and assuming a linear relationship in their $[\mathrm{K}^+]_o$ range, we obtain:

$$v_{KIR} = K_{KIR_1} \left[\mathrm{K}^+\right]_o - K_{KIR_2} \tag{6.26}$$

Finally, Quayle et al. [130] gives the change in inward rectifier conductance with changes in $[\mathrm{K}^+]_o$:

$$g_{KIR_i} = 145 \sqrt{[\mathrm{K}^+]_o} \tag{6.27}$$

where $[K^+]_o$ is in mM. We assume a conductance coefficient of 7250 pSmM$^{-0.5}$ (50 times higher than the 145 pSmM$^{-0.5}$ value given by Quayle et al. [130]) as the density of inward rectifier potassium current (in single cells from pig coronary arteries) can vary by a factor of up to 50 times if it is taken from a small arteriole as opposed to a larger artery [130].

6.3.3.1 Dimensional Consistency in the SMC/EC Equations

A scaling factor is needed to convert between the electrical conductance (g_{KIR_i}, in pS) given in Equation 6.27 to a molar conductance (in μMs^{-1}) for use with the SMC equations of Koenigsberger et al. [86]. We could use the conversion described in Equation 6.1 using Faraday's constant and the volume of the SMC. However, in this case, we don't need to find the volume of the SMC, as we can apply another conversion using parameters from the SMC models of Gonzalez-Fernandez and Ermentrout [61] and Koenigsberger et al. [86]. We use the "cell capacitance coefficient" from [61] ($z_1 = 1.9635 \times 10^{-14}$ C/mV) and the "scaling factor relating net movement of ion fluxes to the membrane potential" from [86] ($z_2 = 1970\text{mV}/\mu\text{M}$) to obtain the appropriate scaling factor ($1/(z_1 z_2 \times 10^{15})$), as shown below:

$$\begin{aligned} 1\text{ pS} &= 10^{-12} \times 1\text{ S} \\ &= 10^{-12} \times \frac{1\text{ C}}{1\text{ Vs}} \\ &= 10^{-12} \times \frac{1\text{ C}}{1\text{ Vs}} \times \frac{1\text{ V}}{10^3\text{ mV}} \\ &= \frac{10^{-15}\text{ C}}{1\text{ mVs}} \times \frac{1}{z_1}\frac{\text{mV}}{\text{C}} \times \frac{1}{z_2}\frac{\mu\text{M}}{\text{mV}} \\ &= \left(\frac{1}{z_1 z_2 \times 10^{15}}\right)\frac{\mu\text{M}}{\text{mV}} \end{aligned} \tag{6.28}$$

6.3.4 Calcium-Dependent Crossbridge Formation

The cellular calcium concentration and the subsequent development of myosin-actin crossbridges in SMCs is related by the crossbridge phosphorylation and latch-state model of Hai and Murphy [65] (Figure 6.4). In their model, an elevation of calcium induces contraction through the formation of crossbridges between myosin and actin. Myosin can be in four possible states: free non-phosphorylated crossbridges [M], free phosphorylated crossbridges [Mp], attached phosphorylated crossbridges [AMp], and attached dephosphorylated crossbridges ("latchbridges") [AM].

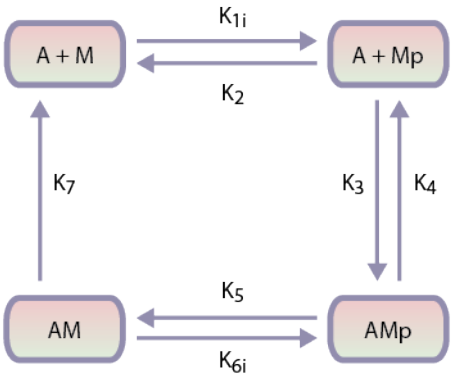

Figure 6.4 Crossbridge phosphorylation and latch-state model of Hai and Murphy [65]. Adapted from [65].

Four differential equations are used to model the fraction of myosin in each of the four states (Appendix A). The conversion to and from each state is described using 7 rate constants (Figure 6.4). K_{1_i} and K_{6_i} depend on the cytosolic calcium concentration of the SMC (or c_i). That is:

$$K_{1_i} = K_{6_i} = \gamma c_i^n \tag{6.29}$$

where γ represents the *sensitivity* of the contractile apparatus to calcium.

6.3.5 Muscle Stress Development and Vessel Calibre Changes

Equations describing the motion of the arterial wall are modified from the model of Kudryashov and Chernyavskii [92], who use a Kelvin-Voigt type of viscoelastic model (described in Chapter 2). The hoop (circumferential) stress acting upon the arteriolar wall, $\sigma_{\theta\theta}$, can be described as follows:

$$\sigma_{\theta\theta} = E\varepsilon + \mu\frac{\mathrm{d}\varepsilon}{\mathrm{d}t} + f_a \tag{6.30}$$

where E and μ are the Young's (elastic) modulus and viscosity of the viscoelastic arteriolar wall, respectively. f_a is the active force supplied by contraction of smooth muscle in the wall and ε represents the strain (a measure of how much a material has been elongated with reference to its original length). In the case of an arteriole, we are interested in how much the circumference (L) can be stretched from the basal circumference (L_0). So, in more useful terms (i.e., in terms of the radius of the vessel, R):

$$\varepsilon = \frac{\Delta L}{L_0} = \frac{L - L_0}{L_0} = \frac{2\pi R - 2\pi R_0}{2\pi R_0} = \frac{R - R_0}{R_0} \tag{6.31}$$

where R_0 is the basal radius of the arteriole.

The term $\frac{d\varepsilon}{dt}$ in Equation 6.30 can also therefore be written in terms of R:

$$\frac{d\varepsilon}{dt} = \frac{d\left(\frac{R-R_0}{R_0}\right)}{dt} = \frac{d\left(\frac{R}{R_0}\right)}{dt} - \frac{d\left(\frac{R_0}{R_0}\right)}{dt} = \frac{1}{R_0}\frac{dR}{dt} - \cancelto{0}{\frac{d1}{dt}} \tag{6.32}$$

The second term cancels to zero as constants always differentiate to give zero.

Rewriting Equation 6.30 in terms of R:

$$\sigma_{\theta\theta} = \frac{E}{1-\nu^2}\frac{R-R_0}{R_0} + \frac{\mu}{R_0}\frac{dR}{dt} + f_a \tag{6.33}$$

(Note that in transforming from strain to circumferential stress the transformation constant is given (for an isotropic material) as $\frac{1}{1-\nu^2}$, where ν is Poisson's ratio. See Equations 2.4 and 2.20 in [90]).

The representation in Equation 6.33 is adjusted by Kudryashov and Chernyavskii [92] in a number of ways. Namely:

- they simplify the $\frac{\mu}{R_0}$ to a viscosity *coefficient*, ϕ
- the passive elastic force is assumed to be weakly nonlinear with a quadratic correction, so $\frac{R-R_0}{R_0}$ becomes $\left[\frac{R-R_0}{R_0} + c_1\left(\frac{R-R_0}{R_0}\right)^2\right]$, where c_1 is a constant
- the active force, f_a, is assumed to be linearly proportional to the average concentration of phosphorylated myosin along the vessel (F), giving $f_a = c_2F$, where c_2 is a constant
- the Young's Modulus, E, is also a function of F (i.e., E(F)) as the "stiffness" of the wall changes as more crossbridges are formed

This gives their final representation of $\sigma_{\theta\theta}$:

$$\sigma_{\theta\theta} = \frac{E(F)}{1-\nu^2}\left[\frac{R-R_0}{R_0} + c_1\left(\frac{R-R_0}{R_0}\right)^2\right] + \phi\frac{dR}{dt} + c_2F \tag{6.34}$$

Finally, Kudryashov and Chernyavskii [92] apply a force balance to the wall. They consider a wall element of mass Δm, density ρ_w , thickness h, radius R, and length Δx. The two forces acting on the wall are f_r, a force proportional to the tangential stress tensor, $\sigma_{\theta\theta}$, and f_p, the force exerted by blood pressure. These are given by Equations 6.35 and 6.36 respectively.

$$f_r = -\sigma_{\theta\theta}2\pi h_0\Delta x \tag{6.35}$$

$$f_p = \Delta p 2\pi R \Delta x \tag{6.36}$$

where Δp is the transmural pressure. R_0 and h_0 are the basal radius and thickness of the arteriole, respectively.

Using Newton's second law of motion for the wall:

$$\Delta m \frac{\mathrm{d}^2 R}{\mathrm{d}t^2} = f_r + f_p \tag{6.37}$$

where Δm can be defined as:

$$\Delta m = \rho_w 2\pi R_0 \Delta x h_0 \tag{6.38}$$

Kudryashov and Chernyavskii [92] make the assumption that $\frac{R}{R_0} = \frac{h_0}{h}$ or $R \cdot h = R_0 \cdot h_0$. In words, this relationship means that as the radius increases from its basal state (stretches), the thickness decreases (is pulled tighter and thinner) by the same ratio. Finally, by cancelling the common term Δx, and defining a radius perturbation, η, as:

$$R = R_0(1+\eta) \tag{6.39}$$

they obtain the following differential equation for η:

$$\rho_w h_0 R_0 \frac{\mathrm{d}^2\eta}{\mathrm{d}t^2} + \phi h_0 \frac{\mathrm{d}\eta}{\mathrm{d}t} + \frac{h_0 E(F)}{R_0(1-\nu^2)}\left[\eta + c_1\eta^2\right] = \Delta p\,(1+\eta) - \frac{h_0}{R_0} c_2 F \tag{6.40}$$

Firstly, it must be noted that in [92] there was a mathematical "cancelling" error (or perhaps a simple typographical error) in the equation where the term $\Delta p\,(1+\eta)$ is listed as Δp. Secondly, the second order term in Equation 6.40 is actually very small and only has an effect when looking at very small timescales. As our interest is confined to times much greater than those dominated by the second derivative, we ignore this term and reduce the DE to a first order equation instead (Equation 6.41). Finally, it is important to understand that the perturbation η is actually the same quantity as the strain ε. We assume the authors define the "new" variable η so as to be specific about the particular strain they are referring to. We use η throughout this thesis to achieve some consistency with [92].

The simplified and rearranged ODE for η is:

$$\frac{\mathrm{d}\eta}{\mathrm{d}t} = \frac{1}{\phi h_0}\left(\Delta p\,(1+\eta) - \frac{h_0}{R_0} c_2 F - \frac{h_0 E(F)}{R_0(1-\nu^2)}\left[\eta + c_1\eta^2\right]\right) \tag{6.41}$$

We also make the following further adjustments to Equation 6.41:

1. It is the fraction of myosin in the two attached states (AM and AMp described in the previous section) that determines the active stress, and hence the contraction that can be effected in the arteriolar wall. Kudryashov and Chernyavskii [92] define the active force on smooth muscle due to muscular tonus as c_2F (where c_2 is a constant and F is the concentration of contracting actin-myosin filaments). To fit better with the proposed crossbridge model above, we instead define F as F_A, the total fraction of attached crossbridges, i.e:

$$F_A = [AMp] + [AM] \tag{6.42}$$

   Maximal active stress in [86] was given as 1.8×10^5 Pa. Gore and Davis [62] stated a value of maximal active stress (for second order arterioles from hamster cheek pouches) of 3.9×10^5 Pa. We chose a value of 2.25×10^5 Pa for c_2 (the maximal active stress) in our model.

2. In $\sigma_{\theta\theta}$ (Equation 6.34), $E(F)$ (Pa) represents Young's modulus, a measure of the "stiffness" of the cell wall material. We take Young's modulus to be an exponential function of F, as we assume that the cell wall material becomes increasingly (and exponentially) stiff when more crossbridges are in the attached state (see similar assumption in [61]).

$$E(F) = E_0 \left(1 + \varepsilon \exp\left(\frac{F}{F_{max}}\right)\right) \tag{6.43}$$

   Here E_0 (Pa) and ε (dimensionless) are estimated constants and F_{max} is the maximum fraction of attached crossbridges (0.8 from [65] – See Appendix A) and ε is an estimated stiffness coefficient.

3. The value of the viscosity coefficient is ambiguously described in the work of Kudryashov and Chernyavskii [92]. It does not appear to have been taken from experiment; instead it is calculated based on the desired characteristic timescale for vessel calibre change. We want to formulate a model that is as anatomically correct as possible; as such, we obtain a viscosity value from the literature and scale it for our purposes:

   The viscosity of the pulmonary artery wall of a sheep is given in [22] as $(2.1 \pm 1.4) \times 10^{-1}$mmHg s mm^{-1}. Based on these units, we assume that this "viscosity" is actually a viscosity *coefficient* as in [92] (i.e., $\lambda_{sheep} = \frac{\mu}{R_{sheep}}$). Applying the conversion factor

1 mmHg = 133.3 Pa, we obtain:

$$\begin{aligned}\lambda_{sheep} &= \frac{\mu}{R_{sheep}} \\ &= \frac{(2.1 \pm 1.4) \times 10^{-1} \text{ mmHg s}}{1 \text{ mm}} \times \frac{1000 \text{ mm}}{1 \text{ m}} \times \frac{133.3 \text{ Pa}}{1 \text{ mmHg}} \\ &= \frac{(2.8 \pm 1.9) \times 10^{4} \text{ Pa s}}{\text{m}}\end{aligned}$$

So for our model we can use:

$$\lambda = 2.8 \times 10^4 \times \frac{R_{sheep}}{R_0} \frac{\text{Pa s}}{\text{m}}$$

If we assume the pulmonary artery radius of the sheep (R_{sheep}) is approximately 10 mm and the basal arteriolar radius for our model (R_0) is 10 μm, we get $\lambda = 2.8 \times 10^7$ Pa s m^{-1} (which is 20 times smaller than the (appropriately rescaled for radius) parameter given by Kudryashov and Chernyavskii [92]).

F

6.3.6 Model Scope Boundaries and Limitations

As stated, the blood flow problem is a complex one and this project attempts to understand a small piece of this larger problem: the interactions that occur within and between the cells in one neurovascular unit. Therefore, at this stage, we exclude the following:

- other mechanisms of metabolic autoregulation such as those involving CO_2, H^+, HCO_3 or ATP
- NVC mechanisms driven by direct neural innervation of vessels
- spatial variations of chemical species (i.e., there is no diffusion terms or partial differential equations)
- stochastic opening of ion channels
- homocellular coupling between adjacent SMCs and ECs in the same vessel or a neighbouring vessel in a vascular tree
- conducted signal responses along a vessel or between branches of the vascular tree
- networks of NVUs

Further identified limitations include:

1. This foundation model contains 22 differential equations and approximately 100 parameters. In models containing large numbers of parameters (all of which have error tolerances) there exists the possibility of large total errors (especially due to the non-linear interactions between parameters). Reducing both the number of "free" parameters and their respective error tolerances reduces the possibility of non-physiological model solutions.

2. The mechanisms by which potassium is released and/or taken up by astrocytes is still very much in dispute [56, 87, 113, 126]. We will only attempt to explore one or two of the possible hypothesized mechanisms (in Chapter 7).

3. Ca^{2+}-induced Ca^{2+} release (CICR) is the process by which the release of Ca^{2+} from intracellular stores triggers a positive feedback mechanism, whereby more store channels are opened, accelerating the rate of Ca^{2+} release. Capacitative calcium entry (CCE) is a similar mechanism where the release of Ca^{2+} from stores can also stimulate influx of Ca^{2+} across the plasma membrane [128]. The exact mechanism of action of both CICR and CCE is unclear and a variety of different explanations have been suggested in the literature. We model CICR in the astrocyte and SMC as they have been modelled in [20] and [86], respectively, but do not model CCE. This may later limit our understanding of the NO-based NVC pathway as CCE appears to be inhibited by cGMP (which is produced as a part of the NO signalling cascade) [128].

4. In our model, we assume that Ca^{2+}-activated MLC phosphorylation is the major pathway for contraction, but alternative, more complex, pathways are known to exist [149].

6.4 Summary

In this chapter, we develop a model of the component cells of the neurovascular unit including the astrocyte and both active layers of the arteriole (smooth muscle cells (SMCs) and endothelial cells (ECs)). To accomplish this, we both adapt and extend on previous models found in the literature. We mainly use Koenigsberger et al. [86] for our coupled EC and SMC cell pair, the astrocyte equations of Bennett et al. [20], the myosin-actin crossbridge model of Hai and Murphy [65], and the viscoelastic models and muscle stress development equations developed by Kudryashov and Chernyavskii [92]. We extend these models to incorporate missing, physiologically important equations, such as those representing the SMC KIR channels and astrocyte BK channels. This model, with the important cells and cell components included, forms a

physiologically sound foundation on which any number of hypothesized or known regulatory pathways can be incorporated and analyzed. This sort of model, with this level of physiological complexity, is truly necessary to help elucidate the complex mechanisms at play in neurovascular coupling, a phenomenon not well characterized by experimental or theoretical work. In the following chapters, we will explore the contributions that two major pathways – K^+/ EET- and NO- mediated – make to metabolic autoregulatory control.

Chapter 7

Models of Neurovascular Coupling via K^+ and EET Signalling

7.1 Introduction

There have been many astrocyte-derived vasoactive signals identified, including NO, ATP and arachidonic acid (AA) metabolites (such as epoxyeicosatrienoic acids (EETs)) [59]. Numerous studies have also documented that increases in extracellular K^+ concentration ($[K^+]_o$) can lead to vasodilation (and in higher concentrations, vasoconstriction) [31, 48, 60, 94, 111]. Further studies by Filosa et al. [56] and others [37, 81, 84, 117] have proposed that the release of K^+ ions from astrocyte endfeet and the subsequent activation of KIR channels on vascular smooth muscle cells (SMCs) comprises a rapid mechanism of arteriolar dilation. There has long been an argument for chemical versus electrical signalling in neurovascular coupling, and it has still not been determined if it is these biochemical signals that modulate arteriolar diameter and hence blood flow, or if it is the "electric" signal in the form of a flux (current) of positive K^+ ions. Filosa and Blanco [55] suggest that both of these mechanisms coexist and interact, with the chemical signals being better suited to maintaining changes in vessel tone in response to sustained neuronal activation and K^+ fluxes being more appropriate for eliciting the rapid response following the onset of neuronal activation. In keeping with these hypotheses we include aspects of both of these signals in the form of K^+ fluxes and EET release.

It is important at this point to make a distinction between the mechanism known as 'K^+ siphoning' and the mechanism that we are proposing. The 'K^+ siphoning' hypothesis states that K^+ released from active neurons depolarizes astrocytes, leading to K^+ efflux from astrocyte endfeet [126]. This mechanism of neurovascular coupling has been tested by depolarizing astrocytes and measuring neighbouring blood vessel diameter simultaneously [113]. Depolarization fails to dilate blood vessels, proving that K^+ siphoning does not contribute to vasodilation. In our mechanism, K^+ is pumped into the astrocyte via the Na^+-K^+ pump (causing an overall depolarization), but is released by endfoot BK channels due to the action of EETs on

them, not due to the depolarizing membrane. Therefore, we have two independent mechanisms controlling the influx and efflux of K^+ in our model astrocytes.

7.2 Model

7.2.1 Overview of the Model

The presented model includes all major mechanisms that occur in the neurovascular coupling process as proposed by Filosa and Blanco [55], starting with the release of glutamate at the synapse due to neural activity and ending with the dilation of an arteriolar segment. Figure 7.1 shows the major cells and processes involved. They are modelled as follows: (1) neural activity causes the release of K^+ and glutamate into the synaptic space; (2) K^+ is taken into the astrocyte cytosol via the Na-K pump, while glutamate binds to metabotropic receptors on the top "arm" of the astrocyte leading to the release of IP_3 into the cytosol of the astrocyte; (3) IP_3 stimulates the release of calcium from intracellular stores via PLC, causing a rise in cytosolic calcium. AA-derived EETs are also produced due to this rise in calcium; (4) both EETs and increases in cytosolic calcium gate the "BK" K^+ channels that are present in the endfeet of the astrocyte causing a release of K^+ into the perivascular space between the smooth muscle cells surrounding the arteriole and the endfoot; (5) the rise in K^+ in the perivascular space further gates the "KIR" K^+ channels in the smooth muscle cells (SMCs), causing them to open, extruding further K^+ into this perivascular space, hyperpolarizing the SMC membrane in doing so; (6) this hyperpolarization closes voltage-operated calcium channels in the SMCs, preventing the influx of Ca^{2+}; (7) the decreased SMC cytosolic calcium then mediates the dilation of the arteriole through the consequent detachment of myosin-actin crossbridges and relaxation of smooth muscle.

During the neurovascular coupling process described above, K^+ accumulates within the perivascular space, and is removed by a process known as "K^+ buffering" [36]. To properly develop a model of K^+ buffering, an interacting network of NVUs would need to be established. We therefore do not attempt to model K^+ buffering at this time, but instead look only at the uptake of K^+ from the synaptic cleft and the extrusion of K^+ into the perivascular space. We also do not take into account the small (2%) extracellular space shrinkage that occurs as a result of extracellular ionic concentration changes [87]; all intracellular and extracellular compartments are assumed to possess constant volume.

Diffusion processes are known to occur as a part of neurovascular coupling; in particular, calcium increases are known to propagate down from the synaptic arm of the astrocyte to the endfeet as a "calcium wave." We do not however a spatial distribution of chemical species

throughout any of the cells; rather, we adopt a lumped parameter approach and model each cell as a well mixed compartment.

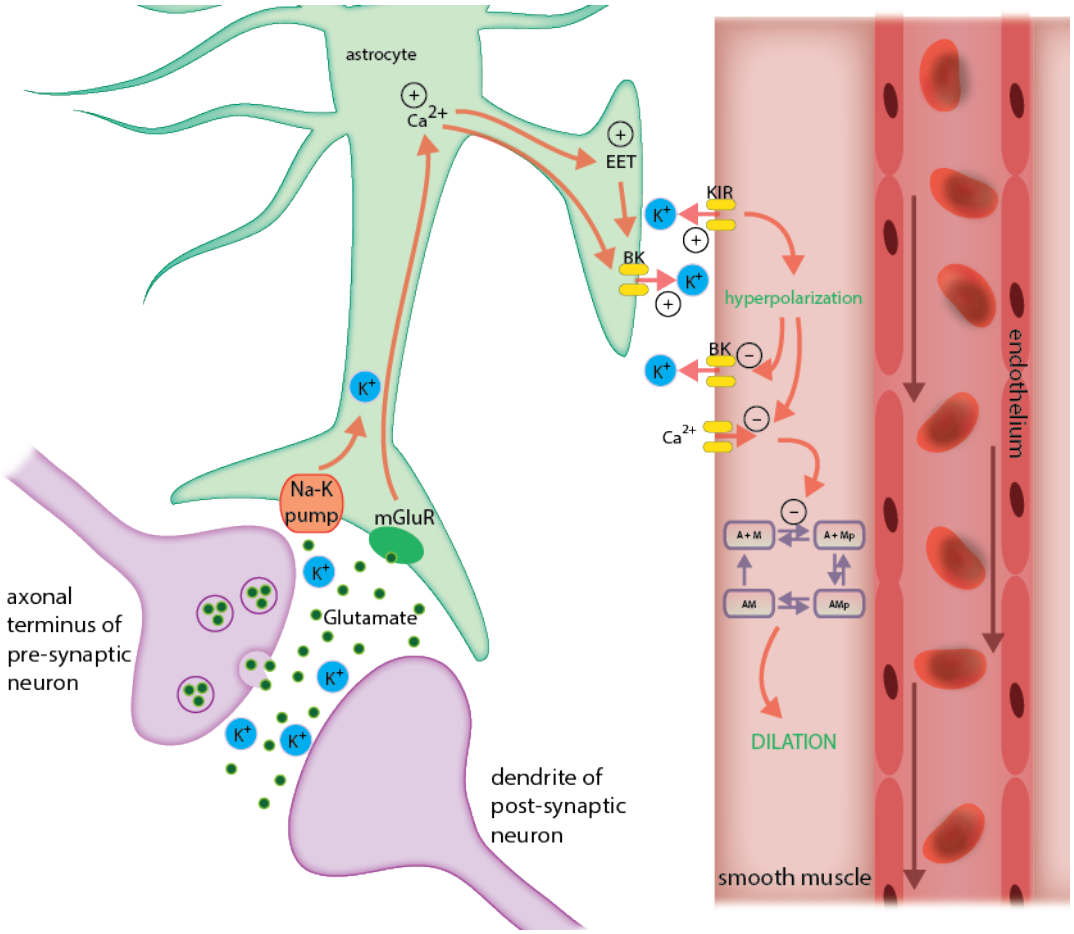

Figure 7.1 Neurovascular coupling via K^+ and EET Signalling: an overview.

7.2.2 Extensions to the Foundation Model

The release of K^+ into the synaptic and perivascular spaces is crucial for the K^+/EET NVC mechanism. Therefore, we extend the NVU model described in the previous chapter (Chapter 6) by adding equations describing the concentrations of K^+ in these spaces (Figure 7.2).

7.2.2.1 Potassium in the Synaptic Cleft

We adopt a very simple model for the concentration of K^+ in the synaptic space K_s. K^+ is released into this space by the neurons only during neuronal activation, and is constantly

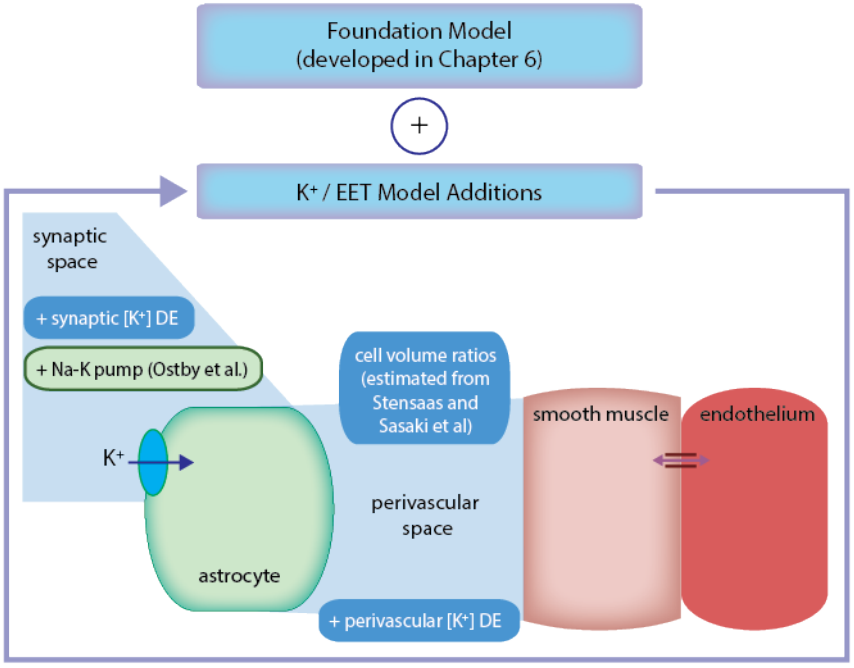

Figure 7.2 Extensions to the "foundation" NVU model that are described in this chapter. Authors of the model components are shown in brackets where applicable.

removed from the space via the Na-K pump positioned on the top "arm" of the astrocyte. The smooth "pulse" of K^+ release during neuronal activation is represented by J_{K_s}, and the Na-K pump flux is denoted by J_{NaK_s}. The concentration of K^+ in the synaptic cleft is therefore the difference of these two fluxes, as described in Equation 7.1.

$$\frac{dK_s}{dt} = J_{K_s} - J_{NaK_s} \tag{7.1}$$

J_{K_s} and J_{NaK_s} carry units of mMs^{-1}. J_{K_s} is estimated and the formulation for J_{NaK_s} is taken from Østby et al. [124]:

$$J_{NaK_s} = J_{NaK_{max}} \left(\frac{K_s}{K_s + KKo_a} \right) \left(\frac{{Nai_a}^{1.5}}{{Nai_a}^{1.5} + {KNai_a}^{1.5}} \right) \tag{7.2}$$

$J_{NaK_{max}}$ is the maximum pump flux (in mMs^{-1}) and KKo_a and $KNai_a$ are the threshold values for the extracellular (synaptic) K^+ concentration (K_s) and intercellular Na^+ concentration (Nai_a), respectively. These concentrations are given in mM and Nai_a is assumed to be constant for simplicity.

The influx of K^+ into the astrocyte from the Na-K pump changes the astrocyte membrane voltage. We therefore need to add this flux term into the astrocyte membrane voltage ODE that

was developed in the last chapter (Equation 6.5). However, before we can do this we need to convert the J_{NaK_s} *molar* flux (expressed as the change in concentration of K^+ in the synaptic cleft per unit time in mMs^{-1}) to an *electrical* flux J_{NaK_k} (expressed as the number of charged particles entering the astrocyte per unit time in fCs^{-1} or fA). This sort of conversion has been explained in Equation 6.1, but is also shown below for completeness.

$$\begin{aligned} J_{NaK_s} \text{ in } \frac{\text{mM}}{\text{s}} &= J_{NaK_s} \text{ in } \frac{\text{mmol}}{\text{Ls}} \\ J_{NaK_s} \text{ in } \frac{\text{mmol}}{\text{Ls}} \times v_{cleft} \text{ L} &= J_{NaK_s} \text{ in } \frac{\text{mmol}}{\text{s}} \\ J_{NaK_s} \text{ in } \frac{\text{mmol}}{\text{s}} \times F \frac{\text{C}}{\text{mol}} &= J_{NaK_s} \text{ in } \frac{\text{mC}}{\text{s}} \\ J_{NaK_s} \text{ in } \frac{\text{mC}}{\text{s}} \times \frac{10^{12} \text{ fC}}{1 \text{ mC}} &= J_{NaK_s} \text{ in } \frac{\text{fC}}{\text{s}} \\ \therefore \quad J_{NaK_s} \text{ in } \frac{\text{mM}}{\text{s}} \times \left(v_{cleft} \times F \times 10^{12}\right) &= J_{NaK_k} \text{ in } \frac{\text{fC}}{\text{s}} \end{aligned}$$

where v_{cleft} is the volume of the synaptic cleft in L (calculated from the cube of the synaptic cleft width from [140]) and F is Faraday's constant.

J_{NaK_k} is now ready to be incorporated into the astrocyte voltage ODE, as follows:

$$\frac{\mathrm{d}v_k}{\mathrm{d}t} = \frac{1}{C_{ast}} \left(-J_{BK_k} - J_{leak_k} + J_{NaK_k}\right) \tag{7.3}$$

7.2.2.2 Potassium in the Perivascular Space

We adopt a simple model for the concentration of K^+ in the perivascular space K_p at this stage, assuming that the accumulating K^+ is removed by a K^+-dependent decay term. K^+ enters the perivascular space via astrocyte BK channels, SMC KIR and SMC BK channels, with corresponding fluxes (in mMs^{-1}) denoted by $\widetilde{J}_{BK_k}$, $\widetilde{J}_{KIR_i}$ and $\widetilde{J}_{BK_i}$, respectively. The balance of these fluxes, along with the decay term, gives the following differential equation:

$$\frac{\mathrm{d}K_p}{\mathrm{d}t} = \frac{1}{VR_{pa}} \left(\widetilde{J}_{BK_k}\right) + \frac{1}{VR_{ps}} \left(\widetilde{J}_{KIR_i} + \widetilde{J}_{BK_i}\right) - R_{decay} \left(K_p - K_{p_{min}}\right) \tag{7.4}$$

Here R_{decay} is the estimated K^+ clearance rate from the extracellular space (in s^{-1}) and $K_{p_{min}}$ is the equilibrium K^+ concentration in the perivascular space (in mM). VR_{pa} and VR_{ps} are the estimated volume ratios of perivascular space to astrocyte and to SMC, respectively. There are very few histological experiments done on astrocytes; it is therefore particularly difficult to estimate the relative volumes of the perivascular space, whole astrocyte and astrocyte endfoot.

Figure 7.3 shows the relative size of the perivascular space and the astrocyte endfeet sur-

rounding a small arteriole in the white matter of a newborn rabbit.

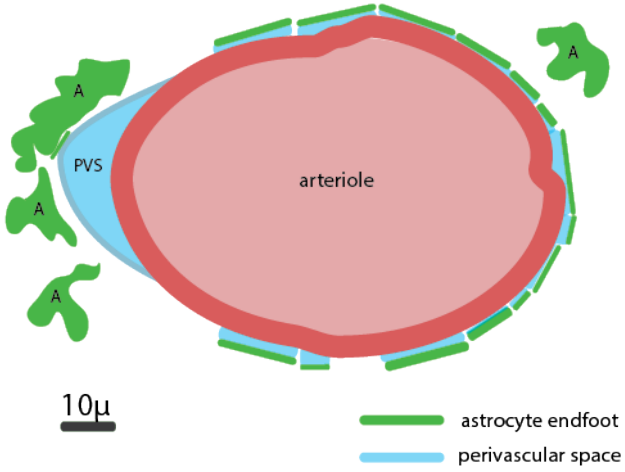

Figure 7.3 An arteriole in the white matter of a newborn rabbit is surrounded by a small perivascular space (PVS), astrocytes (A) and astrocyte end-feet (as indicated by the thin green rectangles). Adapted from schematic in [150].

In Figure 7.3, it is clear that the size of the perivascular space can be relatively large, like the one denoted by "PVS", or relatively small, like those indicated by the small blue shapes underneath the other astrocyte endfeet. If we assume the volume of the large "PVS" is a cube of width 10 μm in size, and the volume of one of the smaller perivascular spaces is a cuboid of 5 μm by 1 μm by 1 μm, we obtain a range of PVS sizes of approximately 5–1000 fL. Dividing the numbers in this range by the astrocyte volume (v_{ast}) of 38,000 fL from [124] gives a range of VR_{pa} of approximately 0.0001–0.02.

Recall that *astro*cytes are *star*-shaped and have many branching processes. This means that the volume of the astrocyte endfoot compared to the whole astrocyte volume is not easily obtained from Figure 7.3. The outlines of the astrocytes shown are not necessarily indicative of the volume of a whole astrocyte (it is not clear if the outlines show the astrocyte soma or simply a wider branch of the astrocyte). It is also difficult to ascertain a three-dimensional estimate from a two-dimensional schematic. Perhaps a better appreciation of the relative scales of astrocyte and endfoot can be gained instead from Figure 7.4. This figure shows that the volume of the endfoot (and hence the perivascular space that it contacts) is a very small fraction of the whole astrocyte volume.

To summarize: it is difficult to ascertain an accurate VR_{pa} from the experimental data available (Figures 7.3 and 7.4). At best, we can take a sensible value that can provide a significant model response and then investigate the importance of changes in this parameter in a sensitiv-

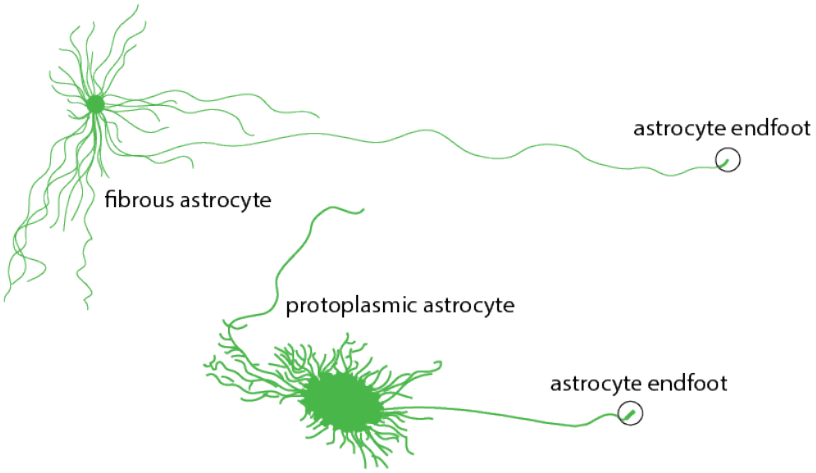

Figure 7.4 Indication of the relative sizes of astrocyte endfeet compared to the entire astrocyte. Both a fibrous and protoplasmic astrocyte are shown. It is important to understand here that astrocytes constitute a heterogenous cell population, the morphology of which can lie anywhere in a continuum between the two types shown here. This figure is a simplified tracing of those in [138].

ity analysis (in Results section of this chapter) – we therefore use a value of 0.0009 for our simulations.

Important comments about dimensional consistency in Equation 7.4:

- J_{BK_k} (described in Equation 6.14) possesses units of fA. This value needs to be converted to $\widetilde{J}_{BK_k}$ (with units of mMs^{-1}) before it can be used in the ODE for perivascular potassium (Equation 7.4). This was done using the following conversion:

$$\begin{aligned} J_{BK_k} \text{ in fA} &= J_{BK_k} \text{ in } \frac{\text{fC}}{\text{s}} \\ J_{BK_k} \text{ in } \frac{\text{fC}}{\text{s}} \times \frac{1 \text{ C}}{10^{15} \text{ fC}} &= J_{BK_k} \text{ in } \frac{\text{C}}{\text{s}} \\ J_{BK_k} \text{ in } \frac{\text{C}}{\text{s}} \times \frac{1}{F} \frac{\text{mol}}{\text{C}} \times \frac{1}{v_{ast}} \frac{1}{\text{L}} &= J_{BK_k} \text{ in } \frac{\text{M}}{\text{s}} \\ J_{BK_k} \text{ in } \frac{\text{M}}{\text{s}} \times \frac{10^3 \text{ mM}}{1 \text{ M}} &= \widetilde{J}_{BK_k} \text{ in } \frac{\text{mM}}{\text{s}} \\ \therefore \quad J_{BK_k} \text{ in fA} \times \left(\frac{1}{F \times v_{ast} \times 10^{12}} \right) &= \widetilde{J}_{BK_k} \text{ in } \text{mMs}^{-1} \end{aligned}$$

  where v_{ast} is the volume of the astrocyte in L (from [124]) and F is Faraday's constant.

- $\widetilde{J}_{KIR_i}$ and $\widetilde{J}_{BK_i}$ also need to possess units of mMs^{-1} for use in Equation 7.4. J_{KIR_i} and

J_{BK_i} carry units of μMs^{-1}, and so the following conversions apply:

$$J_{KIR_i} \text{ in } \frac{\mu\text{M}}{\text{s}} \times \frac{1 \text{ mM}}{10^3\ \mu\text{M}} = \widetilde{J}_{KIR_i} \text{ in } \frac{\text{mM}}{\text{s}}$$
$$J_{BK_i} \text{ in } \frac{\mu\text{M}}{\text{s}} \times \frac{1 \text{ mM}}{10^3\ \mu\text{M}} = \widetilde{J}_{BK_i} \text{ in } \frac{\text{mM}}{\text{s}}$$

7.2.3 Solution Methodology

Neuronal activation was simulated by a release of glutamate and K^+ into the synaptic cleft. This was achieved by assuming a smooth pulse (amplitude 0.07) for ρ (the fraction of bound glutamate receptors) and for the synaptic cleft K^+ influx ($J_{K_s} = 0.7$ mMs^{-1}) for 60 seconds. All 24 differential equations representing the entire neurovascular unit (ODEs in Chapters 6 and 7 and Appendix A) were then solved using the solver RKSUITE, a robust mathematical solver written by Brankin et al. [26]. RKSUITE uses the embedded RK pair BS(4,5) method derived by Bogacki and Shampine [24]. It has a fifth order accuracy and uses an adaptive step size method where the new step size (h_0) is calculated using the algorithm: $h_0 = h_1 \left|\frac{\varepsilon_0}{\varepsilon_1}\right|^{1/p}$ where p is the order (5), and h_1 and ε_1 are the previous step size and error, respectively. ε_0 is the desired accuracy (or *relative error tolerance*) that we set to be 1×10^{-6}. Using RKSUITE, the production of 800 seconds of model data for all 24 equations took 10.989 seconds of CPU time.

We also varied perivascular K^+ concentration within the physiological range of values, and solved only the EC and SMC equations at each of these values. According to experiment, a modest increase of K^+ should induce vasodilation [84, 94, 111], but, paradoxically, a further increase in perivascular K^+ should then cause vasoconstriction [77, 84]. A similar effect (vasodilation followed by vasoconstriction) is observed in Girouard et al. [58] when astrocyte cytosolic calcium is varied. We therefore manually altered the astrocyte cytosolic calcium in our model equations so that we could compare to these experiments.

Simple sensitivity analyses were also performed on a subset of the parameters by 1) adjusting the parameter, 2) solving the set of equations again with the new parameter, and 3) plotting the "new" results alongside the results found using the "old" value of the parameter. Solutions for 3–4 different variations of each parameter were usually calculated. The following parameters were chosen either because they were estimated or because they differed across different literature sources:

- g_{BK_k} (conductance of the astrocyte BK channel – Equation 6.14)
- R_{decay} (the rate of K^+ clearance from the perivascular space – Equation 7.4)
- VR_{pa} (the volume ratio between perivascular space and astrocyte – Equation 7.4)

- γ and n (the power *and* coefficient of the phosphorylation rate constant equation for K_{1_i} and K_{6_i} – Equation 6.29)
- eet_{shift} (the shift in the distribution of open BK channel states along the voltage axis due to EET – Equation 6.15)
- G_{stretch} (the conductance of the stretch-activated Ca^{2+} channel (channel responsible for the myogenic response in the model of Koenigsberger et al. [86] – Equation A.33)

We will also further investigate the mechanism by which K^+ is taken up and released by astrocytes in this model. Amongst experimentalists, the mechanism is still in dispute. The 'K^+ siphoning' hypothesis assumes that K^+ effluxes from neurons causes astrocyte depolarization, which leads to a K^+ efflux from astrocyte endfeet. Our model incorporates a different hypothesis: that K^+ is pumped into the astrocyte from the synaptic cleft via the Na-K pump (causing astrocyte depolarization), but is released by endfoot BK channels due to the action of EETs on them, not due to the depolarizing membrane. Essentially, we have two independent mechanisms controlling the fluxes of K^+ in and out of our model astrocytes. However, it is still possible that depolarization will influence the BK channels to a certain degree. To explore the relative effects that the depolarization and EET have on NVC, we compare model results with EET present and EET absent (thus allowing us to observe the depolarization effect alone).

For simplicity, we consider one NVU only (that is, one synaptic space, one astrocyte and one arteriolar segment which will be represented as a set of identical smooth muscle cell-endothelial cell pairs heterogeneously coupled via IP_3 and electrical coupling (see Equations A.35 – A.38).

7.3 Results and Discussion

7.3.1 Overall Model Behaviour

Figure 7.5 shows the response of modelled astrocyte variables to a 60-second "neuronal activation" (starting at Time=0). The increase in calcium in the cytosol, and the subsequent increase in EETs, gate the BK channels in the astrocyte causing a large increase in the open channel state probability (not shown), which then allows the release of a large K^+ flux into the perivascular space (pvk). The astrocyte cell membrane undergoes a transient hyperpolarization during this process (see "voltage" plot). The changes in perivascular K^+ gate KIR channels on the vascular SMCs concluding in the dilation of the arteriole (shown here in the "diameter" plot). It is difficult to see here whether or not EET lags calcium (as it is known to do). We can do a simple analysis to determine this (see Appendix D). If we assume that the increase in calcium

after activation occurs in a linear fashion, we find that as long as $\frac{1}{k_{eet}} < \frac{1}{V_{eet}} + 1$ (which it is for our model) then EET will *always* lag calcium.

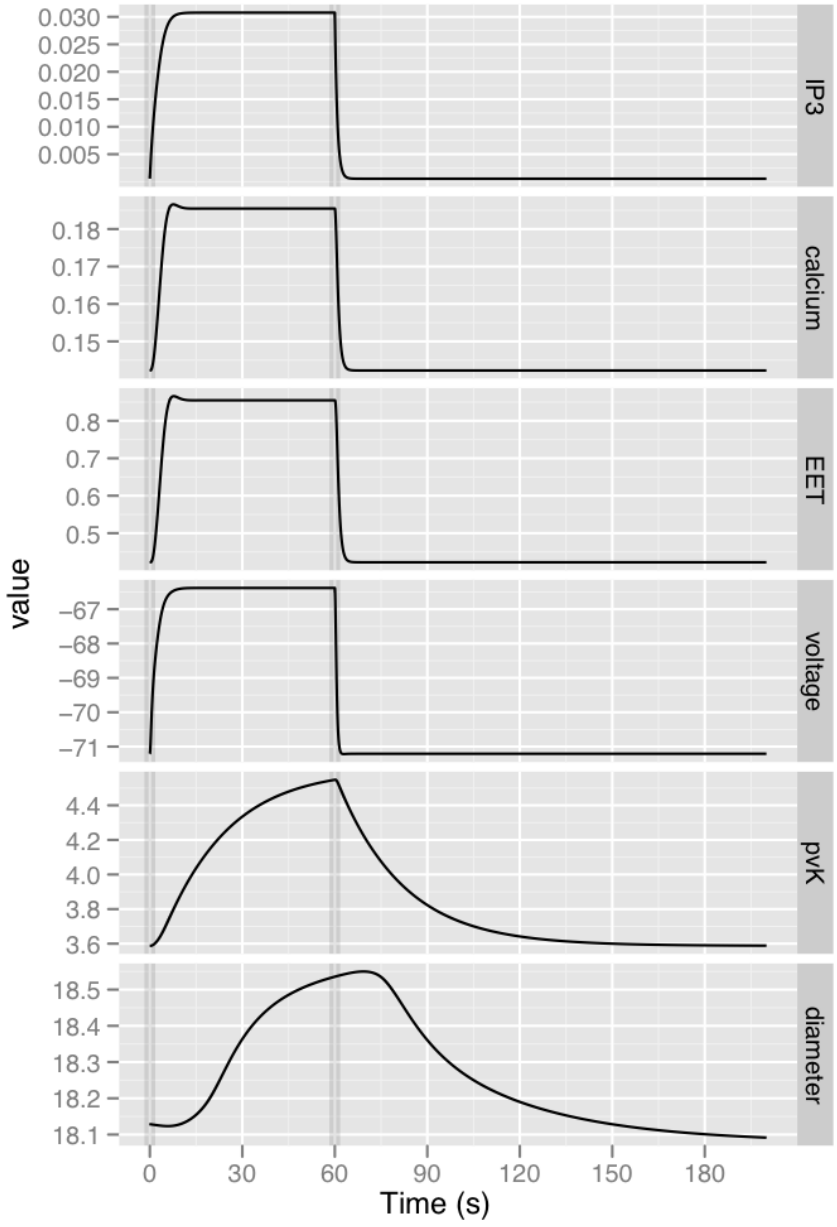

Figure 7.5 Summary of the neurovascular response to a 60-second neuronal activation (shown here are the glutamate-induced increases in astrocytic IP3, calcium and EET concentrations (μM), and their effect on the astrocyte membrane potential or "voltage" (mV), as well as subsequent increases in perivascular K^+, pvK (mM), and arteriolar diameter (μm).

The change in diameter is modest: an approximate 3% change in diameter (which corresponds to an approximate 12% change in blood flow). The timescale of the arteriolar diameter

change is much slower than the timescales of the other variables shown in Figure 7.5; the arteriole doesn't respond to changes in pvk (perivascular K^+) until 15s after the onset of neuronal activation. The reasons for this slow response will be analyzed in the next section.

These results successfully support the hypothesis of K^+- and EET-mediated signalling from astrocyte to arteriole (proposed by Filosa and Blanco [55]). We show (Figure 7.5) that synaptic glutamate- and K^+- induced astrocytic changes can gate BK channels in the astrocyte such that K^+ is released into the perivascular space, causing a dilation.

Although we are able to achieve a diameter change similar in magnitude to the flow changes seen in the experimental work of Shi et al. [145] (approximately 15% flow change corresponding to an approximate 4% diameter change), we are unable to emulate the speed of the response. Maximum flow changes are reached in less than 5 seconds from the onset of stimulation in the experiments of Shi et al. [145], but only occur after 30 seconds in our model solution. Shi et al. [145] also show that blood flow changes occur in the presence of EET antagonists, proving that EET mechanisms are certainly not the only mechanisms working to achieve successful functional hyperaemia. A recent (and excellent) review on the regulation of blood flow via neurons and astrocytes by Attwell et al. [13] describes these other mechanisms, including those involving O_2 and NO. The arteriolar response to neuronal activation is therefore the sum of many such signals, some of which are faster than others. For example, it is known that NO is capable of diffusing rapidly over fairly long distances and is produced at many locations in the NVU (by neuronal NOS and endothelial NOS) meaning that its concentration at any given point is determined by the sum of all NO sources [29]. NO may be better placed to elicit the initial, rapid blood flow response, whereas the EET/K^+ signals may control dilations over more sustained activations. The dynamics of the O_2 and NO pathways are therefore of great interest in the next stage of developing a model capable of the rapid metabolic autoregulation seen in experiment.

7.3.2 Potassium Effects

Figure 7.6 compares the changes in SMC membrane potential ("voltage')' at different perivascular K^+ concentrations for our model and the experimental data of Edwards et al. [48]. This experimental data looks at proximal and distal segments of the middle cerebral artery (MCA).

The same general trend can be seen in both the model and experimental data; that is, increasing the perivascular K^+ concentration causes a hyperpolarization, and then a depolarization in SMC membrane potential. However, there is a clear difference in the membrane potential of the SMC at the resting value of K^+ (3mM) in the model data and even between

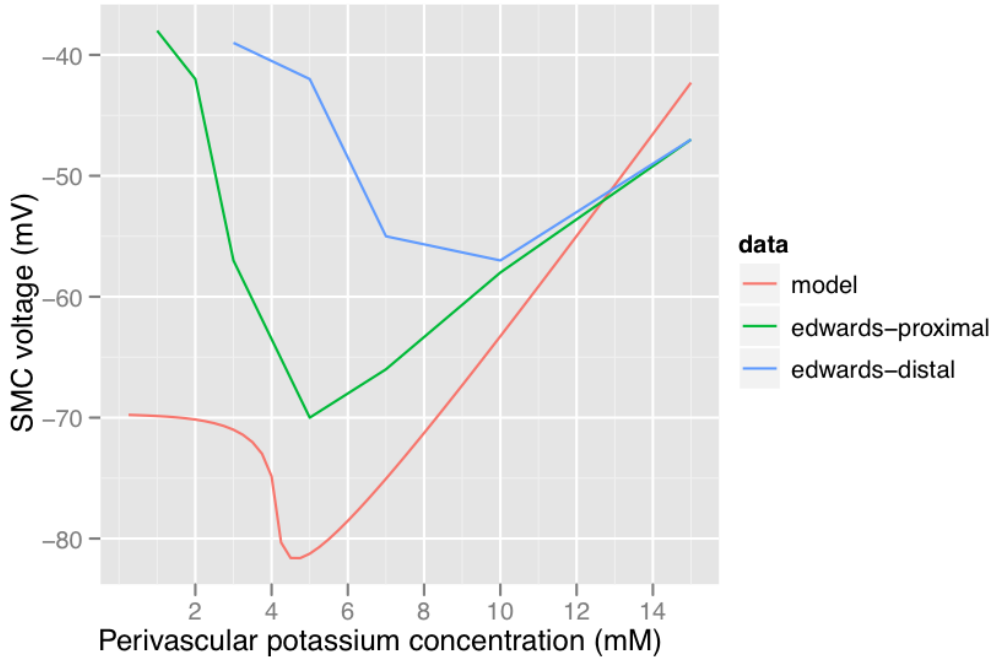

Figure 7.6 Change in SMC membrane potential due to changing perivascular K^+ concentration.

different sets of experimental data (seen as an offset between each curve). This is unsurprising as it is known that there is a variable distribution of resting membrane potentials [80, 146] and ion channel expression [130] throughout the vasculature, just as there is very different structural and signalling specialisations underlying how blood flow is locally regulated at different levels of the vascular tree [25]. However, if our model SMC *did* possess a membrane potential of approximately -40 mV at the perivascular K^+ concentration of 3mM (i.e., a membrane potential similar to the experimental values at that concentration – Figure 7.6), there would be a much larger hyperpolarization (-40 mV to -70 mV) with neuronally-activated perivascular K^+ rises (from 3 to 6 mM). This larger hyperpolarization would induce larger changes in SMC cytosolic Ca^{2+} resulting in much larger dilations.

In general, SMC hyperpolarization causes vasodilation and depolarization causes vasoconstriction. Therefore, following the result shown in Figure 7.6, model simulations produce vasodilation at lower K^+ concentrations and vasoconstriction at higher K^+ concentrations (Figure 7.7).

The paradoxical, but experimentally observed, effect where increased K^+ causes first an increase and then a decrease in diameter is successfully simulated (Figure 7.7). The mechanisms behind this phenomenon have never been fully elucidated, although it has previously

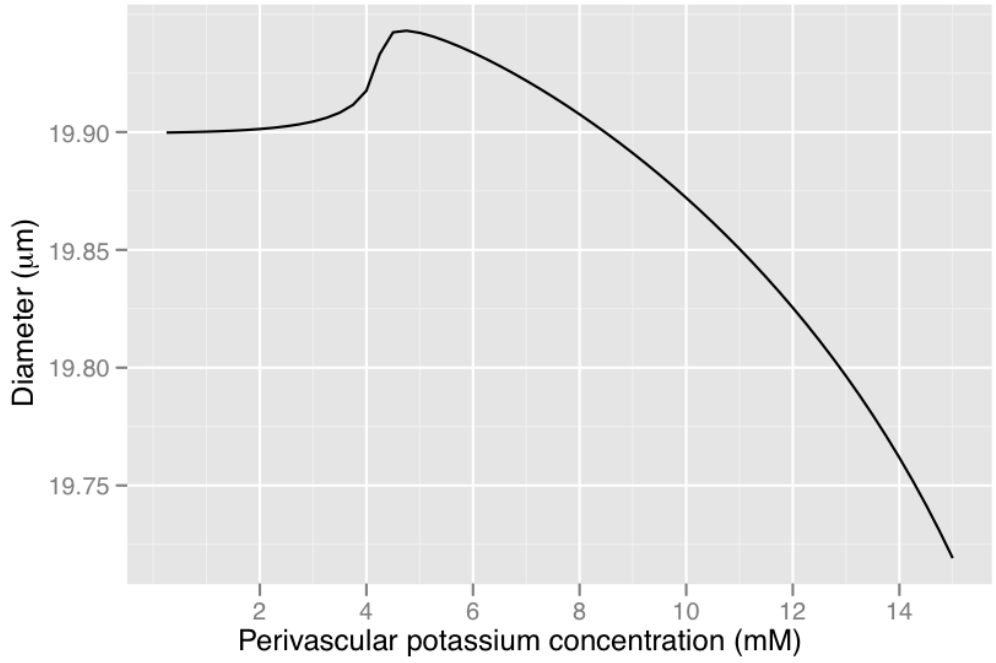

Figure 7.7 Change in diameter due to changing perivascular K^+ concentration.

been attributed to the interactions of SMC Na-K pumps and KIR channel currents [111, 131].

The trend seen in Figure 7.6 (and the subsequent trend in Figure 7.7) can be best explained by observing the behavior of v_{KIR} (the KIR Nernst reversal potential) and k (the fraction of open KIR channels) as K^+ in the perivascular space increases – shown in Figure 7.8.

Our investigations into the cause of this trend (Figures 7.8A and B) point to the interactions between the fraction of open KIR channels (k) and the changing value of the K^+-dependent resting potential of the KIR channel (v_{KIR}). These peculiar interactions cause the KIR channels to exhibit an "all-or-nothing" effect. The KIR channels will always attempt to bring the SMC membrane potential back (or "rectify") to v_{KIR} by passing K^+ in or out of the cell[1]. The size of the K^+ current passed is the product of the membrane potential "driving force" (the difference between the SMC membrane potential and the reversal potential) and the fraction of open KIR channels (Equation 6.21). Figure 7.8A shows that the driving force is very large at lower concentrations of K^+, and the SMC membrane potential should attempt to hyperpolarize so as to return to the reversal potential. However, because there is only a very small fraction of channels open at more depolarized membrane potentials (Figure 7.8B), only very small

[1]The naming of the KIR channels (or "inwardly rectifying" potassium channels) can lead to confusion. "Inwardly" makes it seem as if they can only pass potassium ions into the cell. However, they can actually pass ions both in and out of the cell; they are just able to pass ions into the cell *more readily* (i.e., with less resistance).

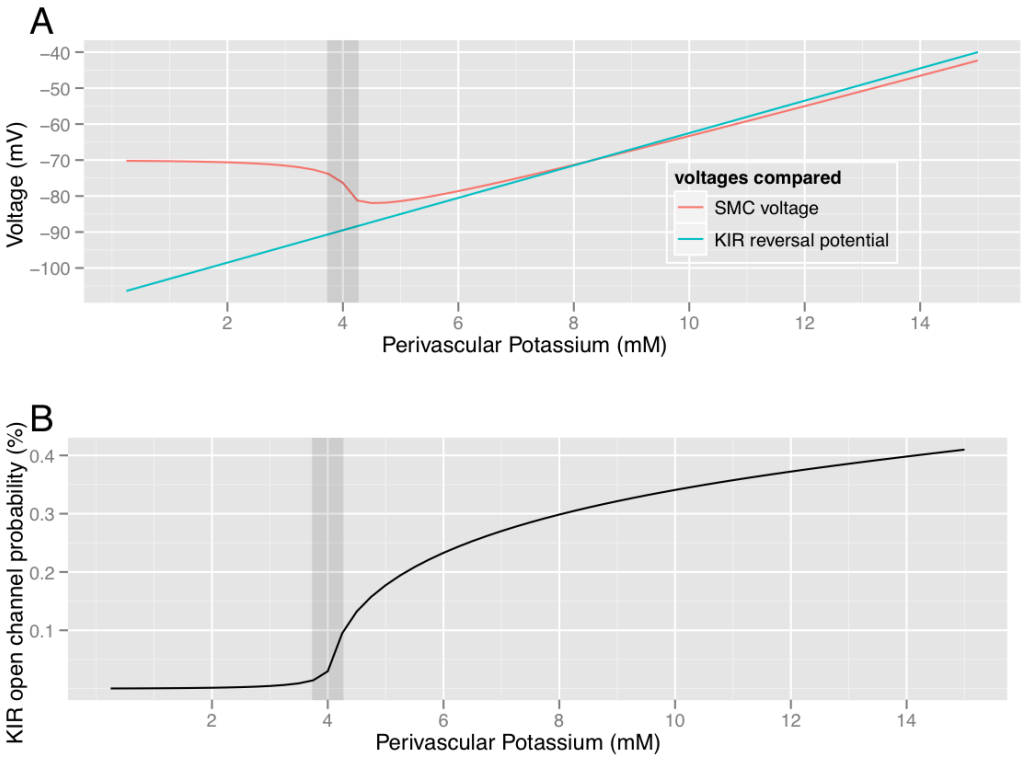

Figure 7.8 Comparison of v_{KIR}, k and voltage relationships and perivascular K^+ concentration.

fluxes of K^+ can pass through the KIR channels. The small fluxes of K^+ leaving through the KIR channels do eventually cause the SMC membrane potential to hyperpolarize to the critical "gating" membrane potential (≈ -75 mV) at which KIR channels open rapidly. The rapid increase in channel openings allows large fluxes of K^+ to exit via the KIR channels; rapidly *hyperpolarizing* the SMC membrane. The SMC membrane potential then *depolarizes* at higher K^+ concentrations in an attempt to rectify to the changing v_{KIR} (Figure 7.8A).

Another paradoxical effect (this time: vasodilation followed by vasoconstriction with increasing endfoot *calcium* concentrations) seen in the work of Girouard et al. [58] is successfully emulated in our model simulations also (Figure 7.9); these results were generated by manually altering the astrocyte cytosolic Ca^{2+} in the model equations. It is important to note, however, that the calcium concentration at which the "switch" (from dilation to constriction) occurs is higher in our results ($\approx$ 1000 nM) than in the work of Girouard et al. [58] ($\approx$ 500 nM).

The cellular mechanisms behind this experimental phenomenon can perhaps be explained now that we have an appreciation of the SMC KIR channel dynamics (Figure 7.8). Endfoot calcium begins the vasomodulatory signal by determining the BK release of K^+ from astrocytes; SMC KIR channels then "read" this signal and determine whether to constrict or dilate, and

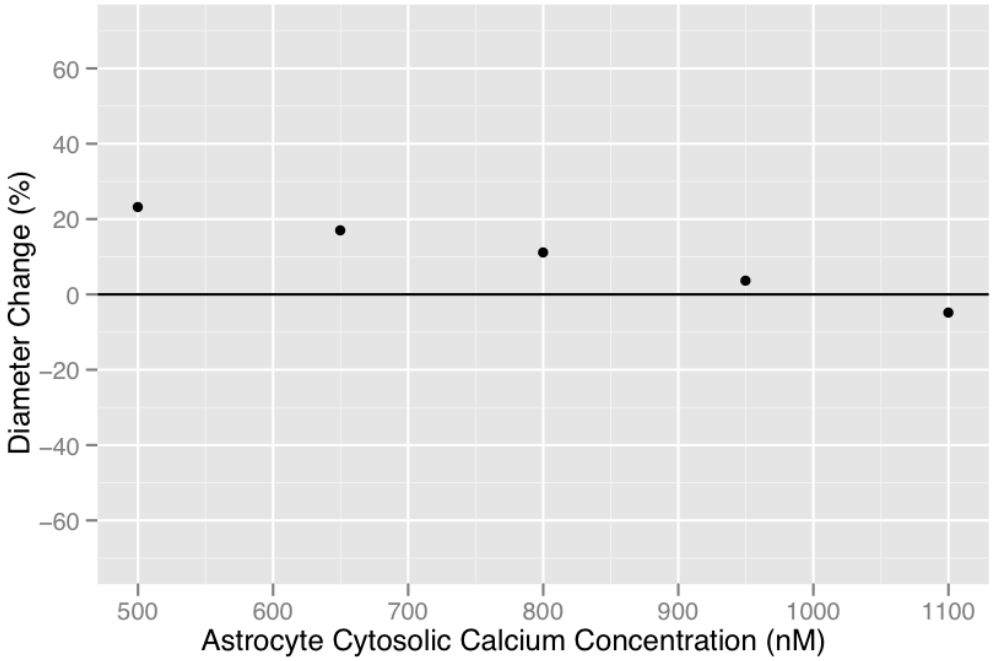

Figure 7.9 Endfoot calcium determines both arteriolar constriction and dilation.

by how much. Therefore, these model investigations, like the experimental results of Girouard et al. [58], support the concept that endfoot BK and smooth muscle KIR channels act in series, together forming a signalling module.

Figure 7.10 shows the simulated changes in perivascular K^+ (A) and diameter (B) when different estimates for the astrocyte (whole cell) BK channel conductance were used for a 60-second neuronal activation. The larger the conductance, the larger the flux of K^+ from astrocyte to perivascular space. *The higher the concentration of* K^+ *in the perivascular space*, the larger the dilation and the longer the vasodilation is sustained.

Figure 7.11 shows the simulated changes in perivascular K^+ (A) and diameter (B) when different estimates for the 'K^+ clearance rates' were used for a 60-second neuronal activation. *The longer* K^+ *is allowed to remain in the perivascular space*, the larger the dilation, and the longer the vasodilation is sustained.

Figure 7.11B also shows that the K^+ clearance rate determines what sort of vessel response is achieved (dilation or constriction), as well as the size of that response (large or small). Furthermore, the K^+ clearance rate affects the equilibrium value of the perivascular K^+ concentration and the value of the resting ("basal") arteriolar tone. Why? Because as long as there is K^+ in the perivascular space, SMC KIR channels will be affected (even if there is no neuronal

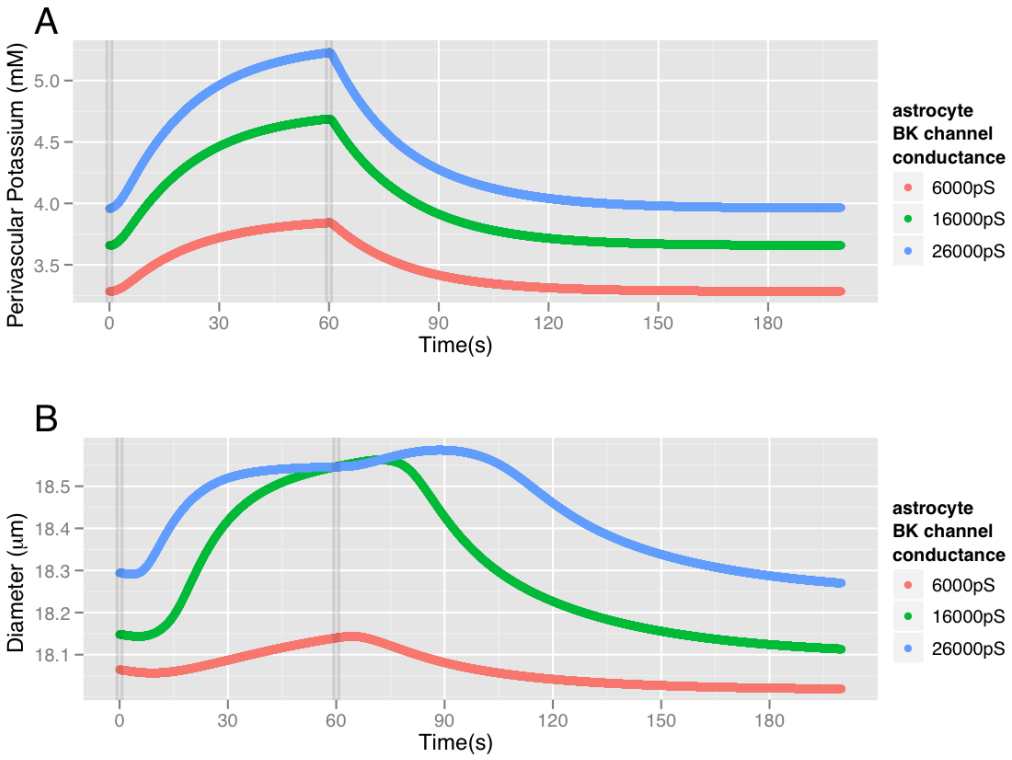

Figure 7.10 Model perivascular K^+ concentration (A) and diameter (B) changes for various estimates of the astrocyte whole cell BK channel conductance.

activation at that time), K^+ will be released from SMCs, changing both the perivascular K^+ concentration and the level of tone (through membrane potential and Ca^{2+}-mediated steps).

The results presented in this section highlight the potential importance of controlling not only the release of K^+ into the perivascular space but also the clearance of K^+ from it – if K^+ is not cleared at the appropriate rate, arterioles may exhibit the incorrect behaviour (constrict instead of dilate or not dilate to a large enough degree or dilate longer than is necessary for efficient blood flow autoregulation). This current model does not include the important physiological mechanisms involved in K^+ clearance (i.e., 'K^+ buffering' via VRAs); these mechanisms need to be added to the model in a future revision.

As discussed earlier in this chapter, the ratio of perivascular space to astrocyte volume is difficult to calculate from experimental data. Figure 7.12 shows the effect that changing this parameter has on NVC. The larger the perivascular space – essentially, the larger the "reservoir" for ion accumulation – the lower the concentration of K^+ for a given ion "release." A smaller change in perivascular K^+ effects a smaller change in diameter and blood flow.

We hypothesize that the slow timescale of the arteriolar response is due to slow K^+ release

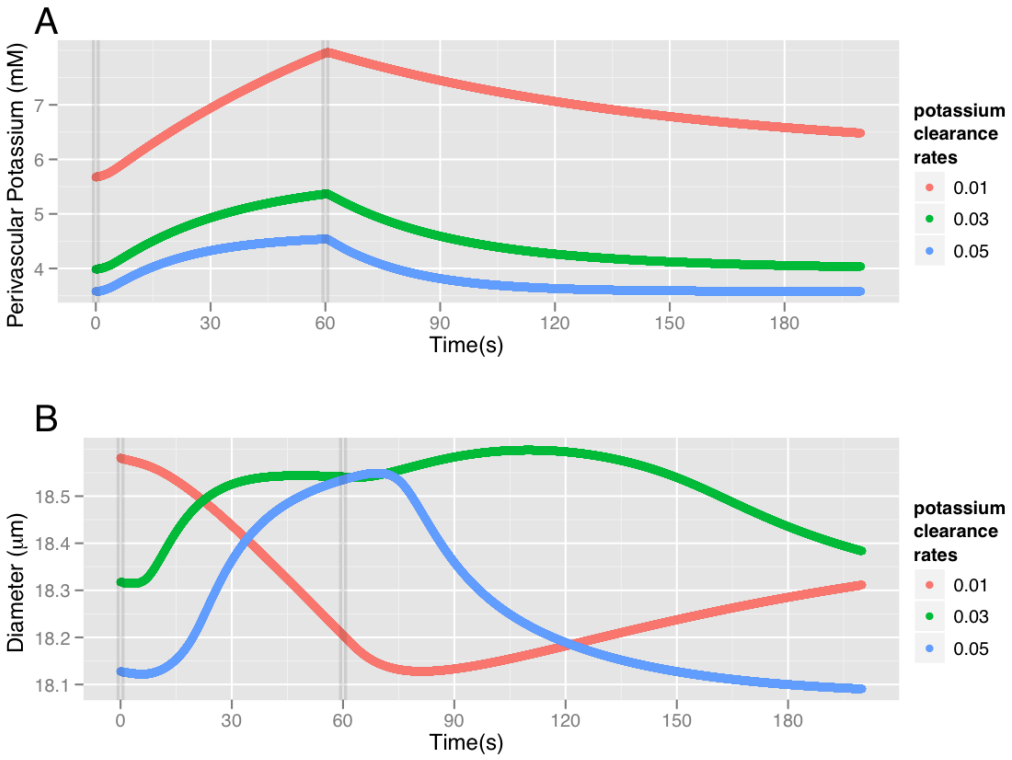

Figure 7.11 Model perivascular K^+ concentration (A) and diameter (B) changes for various 'K^+ clearance rates.'

by the SMC KIR channels due to the "gated" behaviour of the KIR channels (i.e., that the KIR channels only open and release sufficient K^+ after a critical K^+ concentration is reached – see Figure 7.8). An analysis of the important K^+ fluxes is shown in Figure 7.13 along with the pvK, SMC membrane potential and diameter changes. Included are jbkk (the K^+ efflux to the perivascular space from the BK channels in the astrocyte endfoot), jkiri (the K^+ efflux to the perivascular space via SMC KIR channels) and jbki (the K^+ efflux to the perivascular space from the BK channels in the SMC) as all these contribute to the perivascular K^+ concentration. Here, the K^+ flux from the astrocyte (jbkk) is very rapid ($\approx$ 2 s), but the flux from the KIR channels (jkiri) is comparatively slow to reach its maximal value ($\approx$ 10 s). SMC KIR channels form the only signalling link between the astrocyte's "initiating" NVC signal (K^+ release into the perivascular space) and the final "concluding" signal in the SMC (membrane potential and calcium changes and subsequent dilation). We therefore hypothesize that all other SMC cellular processes (membrane potential, calcium, myosin phosphorylation and crossbridge attachment, and vessel relaxation/dilation) are "waiting" for the KIR flux that "calls them to action." Note also that jbki (the K^+ efflux from the BK channels in the SMC) is negligible compared to jkiri

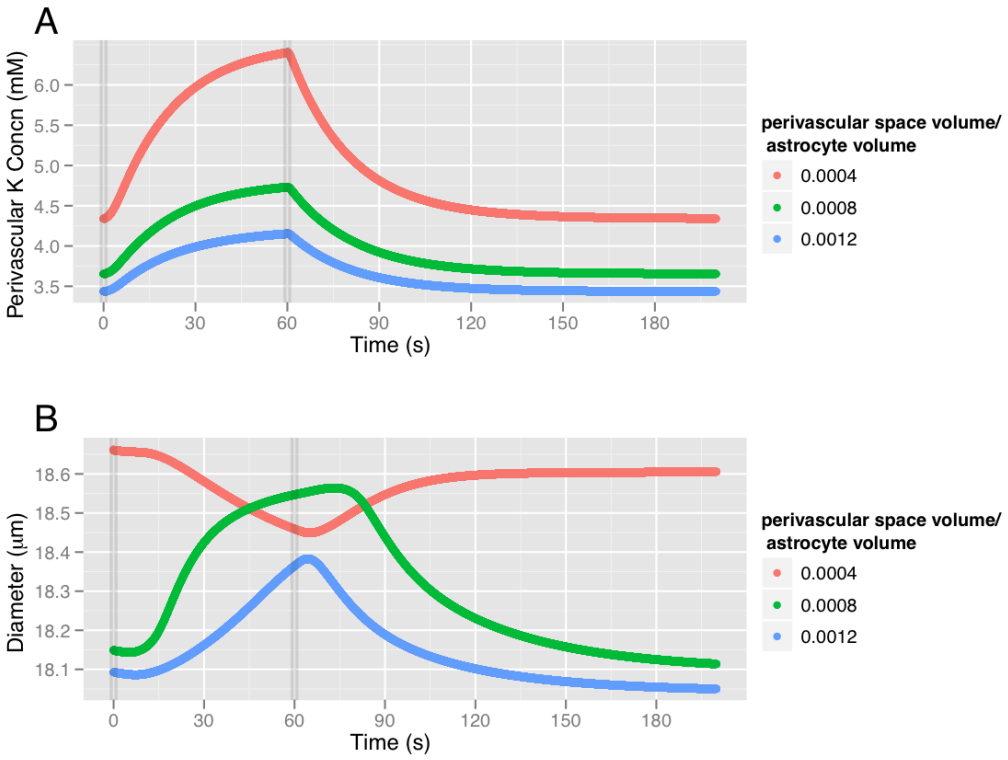

Figure 7.12 Changing the ratio of perivascular volume to astrocyte volume affects the perivascular K^+ concentration (A) and subsequently the diameter of the neighbouring arteriole (B).

(the K^+ efflux via SMC KIR channels) and could be excluded to simplify the model.

The perivascular K^+ concentration (pvk) would have to increase to above the KIR's "gating" level much faster to stimulate a faster arteriolar response. If K^+ was instantaneously released from astrocyte BK channels into the perivascular space the NVC response would be that of Figure 7.14 (these results were simulated assuming an instantaneous rise (and fall) or perivascular K^+ from 3–6 mM for the 60 s "activation" period). Here, KIR channels open immediately, rather than "waiting" until the K^+ concentration in the perivascular space has reached the critical value. The latency (time to onset of the arteriolar response) in Figure 7.14 is approximately 5 s, much smaller than the 30 s in the "non-forced case" (Figure 7.5). The rise time (time to maximal dilation) is 60 s, exactly the time when the perivascular K^+ is forced back to its resting concentration. In the non-forced case, the rise time is $\approx$ 70 s; this is possibly due to "lingering" perivascular K^+ (that which has not yet cleared from the perivascular space) continuing to exert its effects on SMC processes even after the activation period has ceased.

Obviously, K^+ release into the perivascular space cannot be instantaneous (as simulated in Figure 7.14). However, it is unclear what the timescale of the perivascular K^+ concentra-

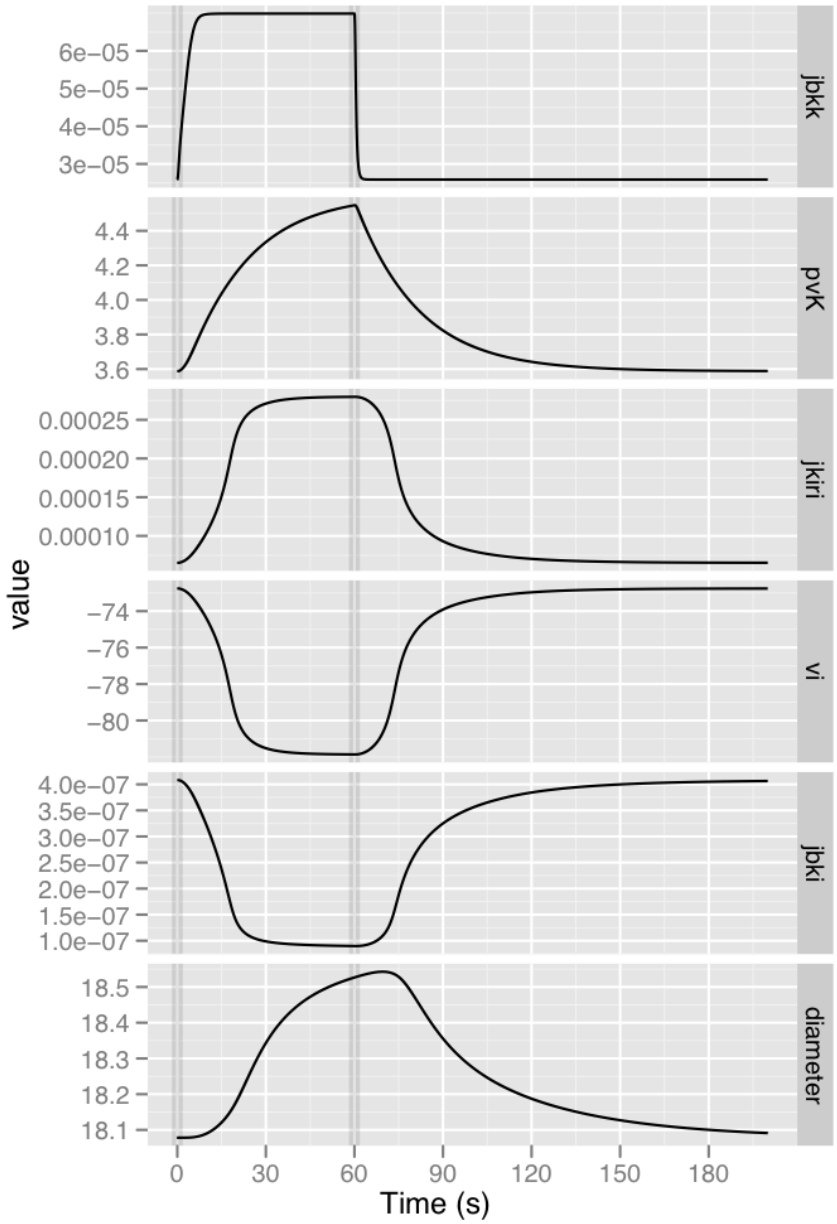

Figure 7.13 Important contributors to the perivascular K^+ concentration (pvk in mM) and hence the arteriolar diameter change (in μm): jbkk (the K^+ efflux from the BK channels in the astrocyte endfoot), jkiri (the K^+ efflux via SMC KIR channels) and jbki (the K^+ efflux from the BK channels in the SMC) (these all in mMs^{-1}). SMC membrane potential vi (mV) is shown here for completeness.

tion change should be. D'Ambrosio et al. [41] and Holthoff and Witte [76] experimentally investigate $[K^+]_o$ increases after neuronal stimulation but find very different response times. D'Ambrosio et al. [41] find a rise time of approximately 40 s (close to the response time of our model) whereas the time acquired by Holthoff and Witte [76] is much quicker at approximately 6 s.

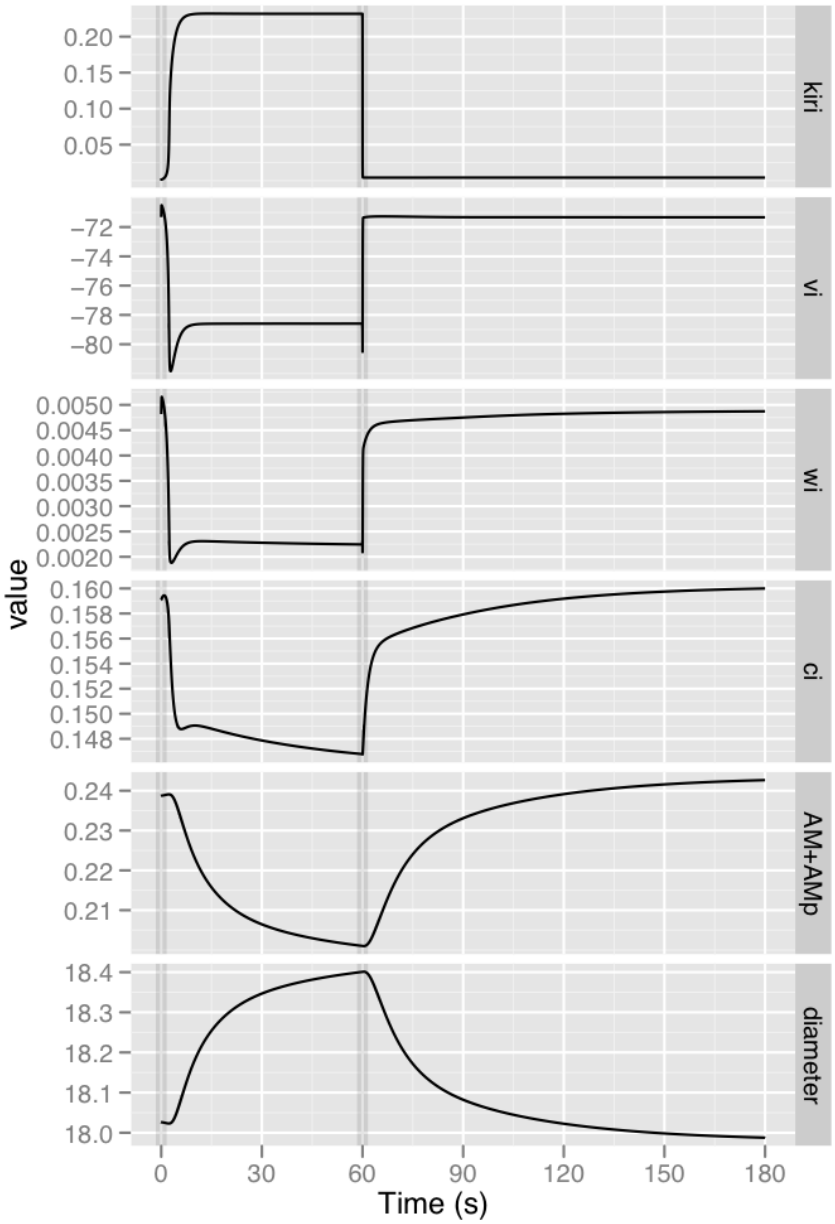

Figure 7.14 SMC response when perivascular K^+ is "forced" to 6 mM for 60 s. Shown here are kiri (open channel probability for the SMC KIR channel), vi (SMC membrane potential) in mV, wi (open channel probability for the SMC BK channel), ci (cytosolic Ca^{2+} concentration) in μM, AM+AMp (the fraction of attached myosin-actin crossbridges), and arteriolar diameter in μm.

In another study, Hillman et al. [74] investigate the response of pial arterioles to a 4 s forepaw stimulation. Arterioles in this study begin to respond within 1 s.

In our model, even if K^+ was *instantaneously* released into the perivascular space, the arteriolar response is still slower than that seen in experiment [74]). Referring back to Figure 7.14,

we can see that when K^+ is "instantaneously" released there is corresponding fast responses for KIR (kiri), membrane potential (vi), BK (wi) and calcium (ci) in the SMC. However, the changes in crossbridge attachment (AM+AMp) are much slower and the arteriolar response follows. This discovery prompted us to analyze the crossbridge model further (as follows).

The myosin phosphorylation and crossbridge model is that of Hai and Murphy [65]. Previous models [20, 86, 170] have used Hai and Murphy [65], but all with different choices of parameters. In particular, there seems to be a large variation in the coefficient (γ) and power (n) used in the myosin phosphorylation rate constants (K_{1i} and K_{6i}); remember that $K_{1i} = K_6 = \gamma c_i^n$. Bennett et al. [20] use $\gamma = 80\ \mu\text{M}^{-4}\text{s}^{-1}$ and $n = 4$ and Koenigsberger et al. [86] uses $\gamma = 17\ \mu\text{M}^{-3}\text{s}^{-1}$ and $n = 3$. Yang et al. [170] uses a Hill model (with Hill coefficient= 2) to describe K_{1i} and K_6 (therefore: $K_{1i} = K_6 \in [0,1]$). Tables 7.1 and 7.2 summarize the effects that changing these parameters has on the model response during a simulated 60 s neuronal activation.

γ	n	D_i	%ΔD
17	1	13.4	0.3
17	2	14.7	1.4
17	3	18.1	2.2
17	4	20	5.0

Table 7.1 Summary of model responses during a simulated 60 s neuronal activation with varying phosphorylation constant *powers* (n). Tabulated here are the coefficient (γ in $\mu\text{M}^{-3}\text{s}^{-1}$) and power ($n$) used in the myosin phosphorylation rate constants (K_{1i} and K_{6i}), the baseline arteriolar tone (D_i, in μm) and the maximum change in arteriolar diameter (%ΔD, in %)

γ	n	D_i	%ΔD
1	3	20.3	2.0
10	3	18.9	1.9
100	3	14.8	3.0

Table 7.2 Summary of model responses to changes in phosphorylation constant *coefficient* during a simulated 60 s neuronal activation. Tabulated here are the coefficient (γ in $\mu\text{M}^{-3}\text{s}^{-1}$) and power ($n$) used in the myosin phosphorylation rate constants (K_{1i} and K_{6i}), the baseline arteriolar tone (D_i, in μm) and the maximum change in arteriolar diameter (%ΔD, in %)

Altering the power (n) and coefficient (γ) of the phosphorylation rate constants K_{1i} and K_6 affects the resting tone and the size of the dilation due to neuronal activation (Tables 7.1 and 7.2), albeit by a small degree. However, the speed of the arteriolar response (at least for the parameter variations simulated here) does not increase to the speed that we require for this

model to be physiologically accurate (i.e., for all parameter variations, the time to half maximal dilation exceeded 30 s). It is important to remember that K_{1i} and K_6 are not only a function of n and γ but are also Ca^{2+}-dependent; therefore, Ca^{2+} can also determine the size and the *speed* of the response. We can also observe in Figure 7.14 that the change in SMC calcium concentration (c_i) is relatively small (as it has been in all simulations thus far) – only 0.01 μM. Figure 7.15 shows the crossbridge formation and arteriolar changes that would occur when the Ca^{2+} is altered manually from a resting concentration of 0.16 μM to 0.10 μM for 60 s.

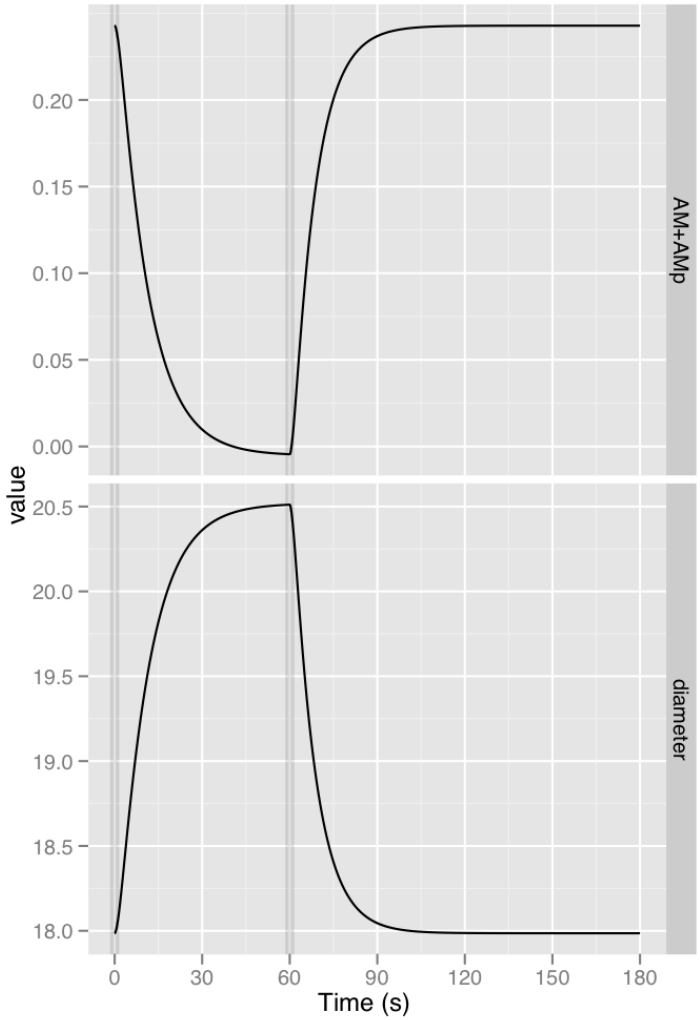

Figure 7.15 Model response when SMC cytosolic calcium is "forced" from 0.160 μM to 0.100 μM for a 60 s simulation. Phosphorylation rate constants are that used in Koenigsberger et al. [86] ($\gamma = 17\ \mu M^{-3}s^{-1}$ and $n = 3$).

Figure 7.15 demonstrates that much larger changes in diameter can occur with a larger decrease in SMC cytosolic Ca^{2+} ($\approx$ 14% compared to the $\approx$ 3% in Figure 7.5). A larger change in Ca^{2+} may be induced if SMC hyperpolarization was more profound (as it might be if

the resting potential of the SMC at the resting perivascular K^+ concentration (3 mM) was closer to that determined experimentally – see Figure 7.6). The rise time (time to maximal dilation) is still 60 s (the end of the activation period), however, the time to half maximal dilation is $\approx$ 10–15 s (as opposed to $\approx$ 30 s in Figure 7.5). Therefore, larger calcium changes can effect a faster response, although 10–15 s is still considerably slower than the physiological speed. More investigation into the myosin phosphorylation and crossbridge attachment model is needed to determine its suitability, and indeed its physiological accuracy, for use in the NVC model. The mechanisms for phosphorylation and crossbridge attachment described in the original Hai and Murphy [65] model are far from exhaustive; there is evidence to suggest that there are alternative mechanisms of myosin phosphorylation [149], some of which have been modelled more recently [64].

Spreading depression (SD – see Chapter 4) is defined as "a slowly propagated wave of depolarization of neurons and glial cells, followed by a subsequent sustained suppression of spontaneous neuronal activity, accompanied by complex and variable changes in vascular calibre, blood flow, and energy metabolism [34]." Interestingly, one other major hallmark of the phenomenon is an extremely large K^+ efflux which increases the extracellular K^+ concentration from a resting level of 3–4 mM to $>$ 40mM [14]. Having created a vessel model capable of reacting to changing $[K^+]_o$, we wanted to examine how the SMC and vessel model would respond to the pathophysiological extracellular K^+ concentrations implicated in SD. Figure 7.16 demonstrates the NVC model responses that occur at the pathophysiological perivascular K^+ concentrations of 10 mM and 40 mM (simulated by again "forcing" the perivascular K^+ to these values for the 60 s activation period).

Experimental vascular responses to SD are complex and variable and depend on the experimental conditions. The original paper describing CSD in the rabbit reported a transient vasodilation, followed in some cases by a more sustained and less pronounced vasoconstriction [97]. In both mouse and rat, there is an initial dilation of arterioles, and an accompanying increase in blood volume [15, 28]. However, in the mouse, this initial dilation is followed by a profound constriction of vessels and then *another* dilation, whereas in the rat, the initial dilation is sustained [15, 28, 118]. Therefore, under some conditions, the predominant vascular response may be vasodilation, whereas under other conditions, it may be vasoconstriction. The variability of the vascular responses to SD may depend on a number of factors including: the resting vascular tone, sensitivity of the vessels to extracellular K^+, tissue oxygenation, and basal and evoked levels of NO [34].

Previously, we have shown that our model achieves vasodilations in the lower range of physiological $[K^+]_o$ (Figure 7.7 and also Figure 7.14). Here, in Figure 7.16, we show that in

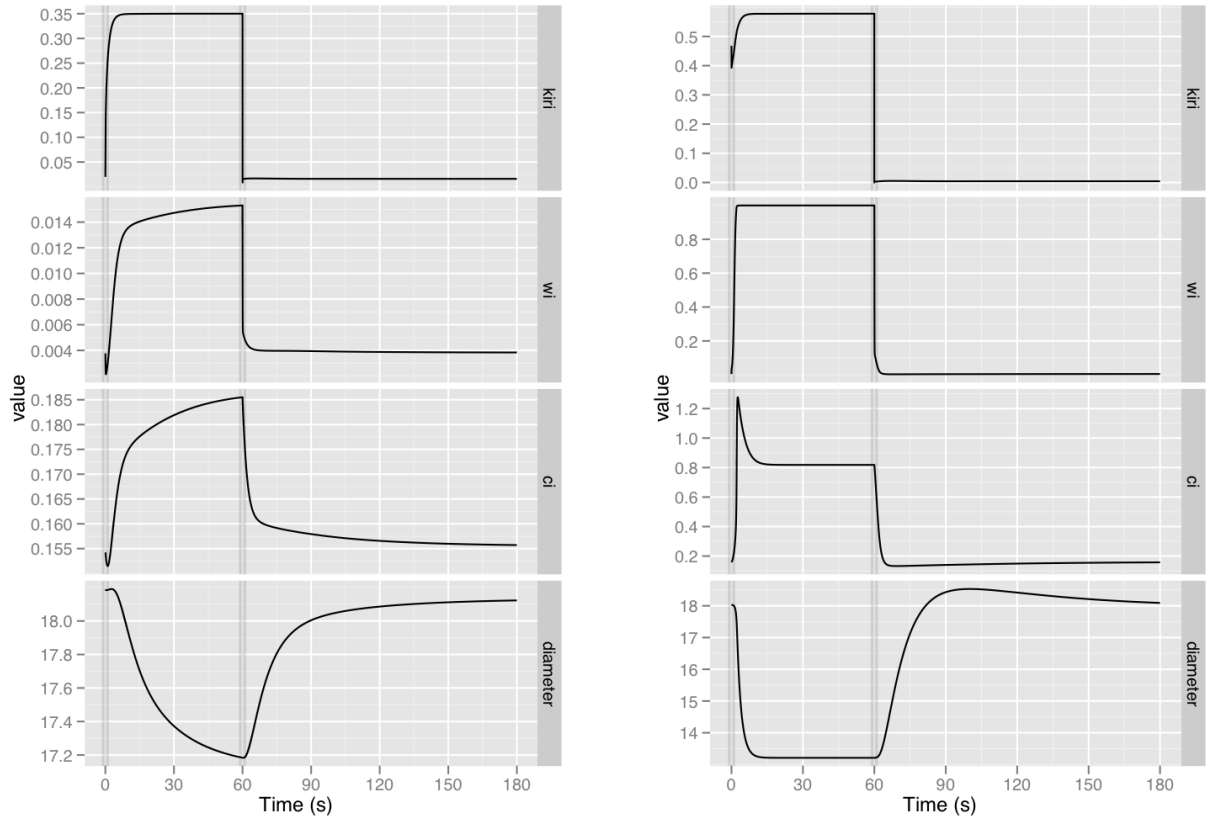

Figure 7.16 SMC response when perivascular K^+ is "forced" to concentrations of 10 mM (left) and 40 mM (right), respectively, for 60 s. Shown here are kiri (open channel probability for the SMC KIR channel), wi (open channel probability for the SMC BK channel), ci (cytosolic Ca^{2+} concentration) in μM, and arteriolar diameter in μm.

the upper ranges of physiological $[K^+]_o$ (10 mM), the model arteriole exhibits small constrictions, and in pathophysiological $[K^+]_o$ (40 mM), the model arteriole exhibits profound (and very rapid) constrictions. This is an interesting result, and not unlike the experimental SD observations in the mouse [28], where initial dilation is followed by constriction. It is important to note here that if we had not set the change of $[K^+]_o$ to be a Heaviside function from 3 mM to the higher concentration (10 or 40 mM) at $t = 0$ and instead allowed the concentration to gradually increase through the lower $[K^+]_o$ levels first, we would have seen the arteriole first progressing through the initial dilation seen in Figure 7.14. Please note that the value of the K^+-dependent KIR Nernst potential used for the simulations in Figure 7.16 is taken again from [123], using their log relationship for values in the upper $[K^+]_o$ levels.

It is clear that vascular responses occur as a part of SD, but it would be unwise to assume that the vasculature responds only passively. One of the earliest studies of SD by Leao and Morison [98] indicated that blood vessels may play an active role in the propagation of

SD. Vascular changes may even precede and condition SD [98]. Vascular responses to SD are therefore important to understand, both from a clinical point of view (because vascular responses contribute to SD and the pathological conditions, like migraine, that arise from it), but also from an NVC research point of view (because the behaviour of neurons, astrocytes and blood vessels during SD could provide insight into the workings of the NVU in normal brain function).

Our current model does not include a physiologically correct model of K^+ clearance. We have shown earlier in this section that the arteriolar behaviour is very sensitive to both the rate of clearance of K^+ in the perivascular space (Figure 7.11) and indeed the volume of the perivascular space (Figure 7.12). It is therefore possible that insufficient control of these two variables could play a contributing role in SD. An improved understanding of SD and its accompanying vascular responses could be achieved through the power of a theoretical model that included physiologically accurate K^+ buffering and clearance mechanisms.

7.3.3 EET Effects

The parameter eet_{shift} determines to what degree the BK channels are gated by EET (i.e., it determines the size of a voltage-dependent shift in the BK channel open probability distribution when EET is produced in the astrocyte cytosol – see Equation 6.15). Figure 7.17 shows the effect that changing this parameter has on both the BK channel open probability (BKPo) and the corresponding arteriolar diameter when a 60 second neuronal activation is simulated.

As would be expected, increasing the parameter eet_{shift} (applying a larger voltage shift to the BK open channel probability) effects a larger change in the fraction of open BK channels in the astrocyte (Figure 7.17A), releasing larger fluxes of K^+ into the perivascular space (not shown). The rate of K^+ deposition (by astrocyte BK channels) into the perivascular space, determines the "polarity" of the vessel response that is achieved (dilation or constriction), as well as the size of that response (large or small) (Figure 7.17B). Further, when there is more astrocyte BK channels open at rest, the equilibrium value of the perivascular K^+ concentration is higher, which affects the value of the resting ("basal") arteriolar tone. This behaviour is similar to that shown in Figure 7.11, in which changes in the perivascular K^+ *clearance* rate also affects the magnitude and polarity of the arteriolar response.

The value for eet_{shift} that we use in our model (2 mV/mM) shifts the BK open channel probability distribution so that BKPo increases by approximately 125% during neuronal activation (Figure 7.17). This increase corresponds well to the BKPo increase seen for EET application in Lu et al. [104]. Increasing eet_{shift} further can cause BKPo changes greater than this (BKPo

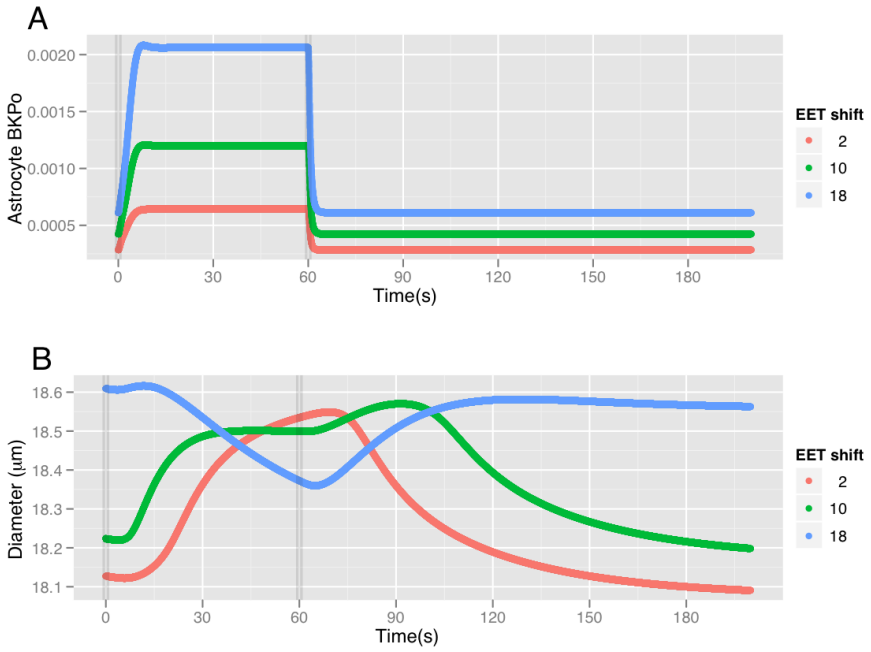

Figure 7.17 Sensitivity analysis for parameter eet_{shift}. Shown here are the changes in the fraction of open astrocytic BK channels (BKPo) and arteriolar diameter during a 60 s neuronal activation.

changes seen in Lu et al. [104] due to the application of the EET-derived metabolite DHET reaches much higher values). Further experimental work is needed to better characterize 1) the amount of AA, EET and DHET that is produced during neuronal activation, and 2) the effects that these molecules have on astrocyte endfoot channels, and hence NVC.

To explore further the relative effects that (synaptic K^+-induced) astrocyte depolarization and (synaptic glutamate-induced) EET production have on the K^+/EET pathway, we compare model results 1) when EET alone is allowed to exert its effects on astrocyte BK channels (the depolarization signal is silenced), and 2) when the astrocyte depolarization is allowed to exert its effect on astrocyte BK channels (with the EET signal silenced) – Figure 7.18.

Recall that the 'K^+ siphoning' hypothesis states that K^+ released from active neurons depolarizes astrocytes, leading to K^+ efflux from astrocyte endfeet [126]. This mechanism of neurovascular coupling has been tested by depolarizing astrocytes while measuring blood vessel diameter [113]; depolarization fails to dilate blood vessels, proving that K^+ siphoning does not contribute to vasodilation. In our model mechanism, K^+ is pumped into the astrocyte via the Na-K pump (causing a depolarization), and is released by endfoot BK channels due to, we assumed, the action of EETs on them, not due to the depolarizing membrane. However, in Figure 7.18 it is apparent that both the depolarization of the astrocyte membrane *and* the

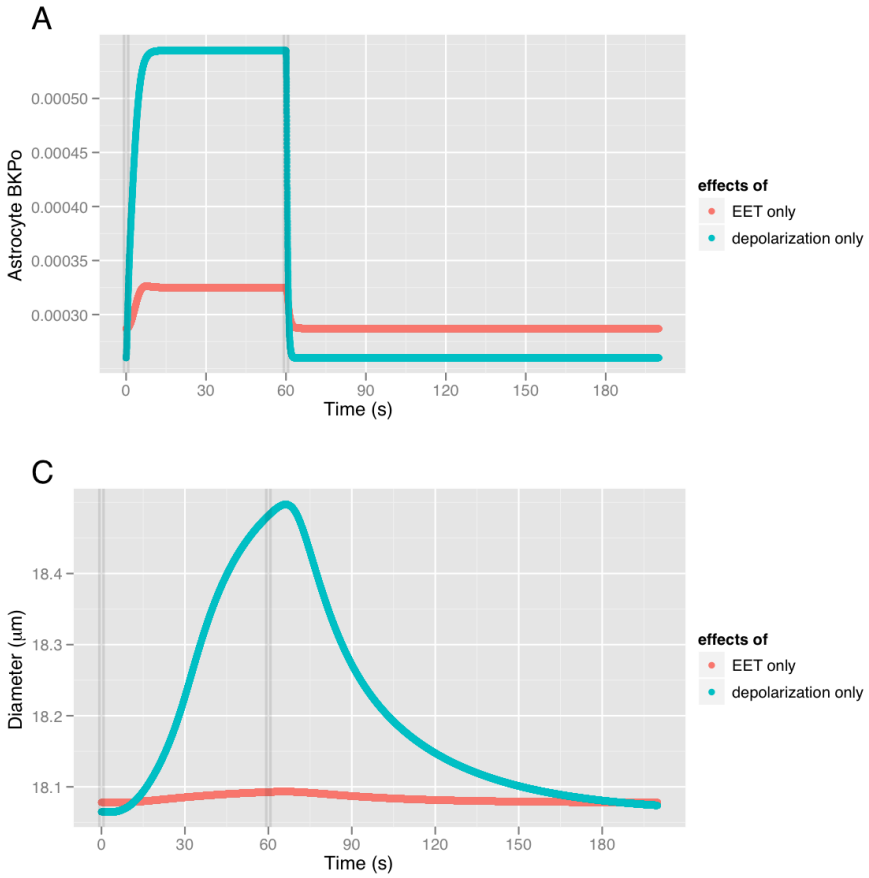

Figure 7.18 Is the depolarization of the astrocyte the major mediating signal responsible for vasodilation in the arteriole? Or is it the EET signal? Shown here are the changes to the astrocyte BK channel open probability (Astrocyte BKPo) and arteriolar diameter (μm) during a 60 s neuronal activation when depolarization and EET signals are silenced in turn.

produced EETs act on endfoot BK channels to cause K^+ efflux into the perivascular space, with the "depolarization only" effect taking an overwhelming dominance.

7.3.4 Stretch-Activated Channel Effects

The stretch-activated Ca^{2+} channel (SAC: channel responsible for the myogenic response in the model of Koenigsberger et al. [86]) is potentially important for determining tone-dependent vascular responses (more on this in Chapter 8). Therefore, we briefly analyze the effects that changing the conductance of this channel (G_{stretch}: a "model estimation" in [86]) would have on the model response (Figure 7.19).

The size of the SAC channel conductance affects the magnitude and polarity of the arteriolar response, as well as the resting tone of the arteriole. Increasing G_{stretch} ensures that the

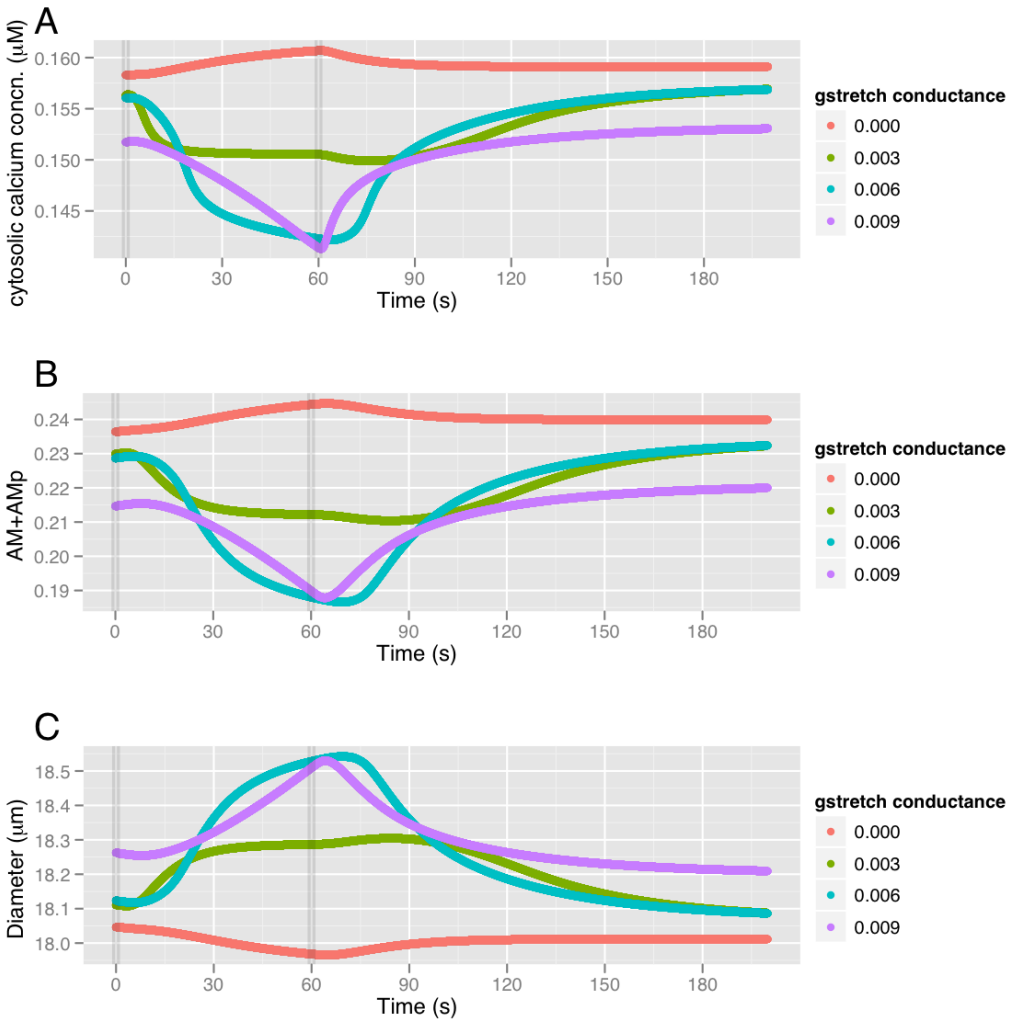

Figure 7.19 Changes in the SMC model response to a neuronal activation of 60 s when the conductance of the stretch activated calcium channel (G_{stretch}) is altered. Shown here are cytosolic calcium concentration (in μM), AM+AMp (the fraction of attached myosin-actin crossbridges), and arteriolar diameter (in μm).

balance of ionic fluxes in the SMC is more heavily influenced by the activity of the SAC channel. In general, the larger the value of G_{stretch}, the larger the Ca^{2+} efflux from SMCs (J_{stretch_i}), the less Ca^{2+} in the SMC to cause myosin phosphorylation and crossbridge formation, and hence: the larger the relaxation/dilation.

7.4 Verification of the Model Code

The code used to produce the results given in this chapter was verified by Kristina Raba, a summer scholarship student, whose project involved the non-dimensionalisation of the model equations outlined in Chapters 6 and 7.

Throughout the course of her 3 month project, she:

1. non-dimensionalized the model equations
2. checked the validity of the code used for this thesis by comparing the thesis results to her non-dimensionalized results (which were also obtained using the RKSUITE ODE solver)
3. simplified the model by removing any terms that were more than two orders of magnitude smaller than the largest term in the equation they belonged to

Her verification showed no significant difference between the non-dimensionalized solution and the solution found using the thesis source code (see Appendix E for details of the code developed for this thesis).

7.5 Summary

Our mathematical model simulates neurovascular coupling using EET and K^+ as the major signalling pathways. Important steps in this process are the production of EETs in the astrocyte and the release of K^+ into the perivascular space via BK and KIR channels. Constructing a model of sufficient physiological complexity has allowed us to not only support experimentally observed observations, but actually investigate the causes of them, such as the effect where increased perivascular K^+ causes first an arteriolar dilation and then a constriction. We suggest that the interaction of the changing smooth muscle cell membrane potential and the changing K^+-dependent resting potential of the KIR channel is responsible for this effect.

We were able to achieve vasodilations (and vasoconstrictions) similar in magnitude to those seen in experiment [58, 145]. However, the latency and rise time of the arteriolar response is slower than that observed [74, 145]. We believe that the introduction of other known major neurovascular coupling pathways (especially those of NO and 20-HETE) may be capable of producing a response closer to the physiological speed required. We will explore the NO-mediated neurovascular mechanism in the next chapter (Chapter 8).

We also looked more closely at the specific effects that EET and K^+ have on the complex NVC mechanism modelled. In the literature, differing views exist about the exact mechanism and effects of K^+ movement in and out of the extracellular space surrounding neurons and glia [56, 73, 113, 126]. We developed this model with the intention that (synaptic glutamate-induced) EET production and not (synaptic K^+-induced) astrocyte depolarization would be responsible for the activation of astrocyte BK channels and the subsequent release of K^+ into the perivascular space. Closer examinations of the model have shown that both the depolarization of the astrocyte membrane *and* the produced EETs act on endfoot BK channels to cause

the K^+ efflux, with the depolarizing effect taking dominance. This analysis will further add to the ongoing debate and discussion that surrounds the seemingly separate but inexorably intertwined phenomena known as K^+ siphoning, K^+ buffering and K^+-mediated neurovascular coupling.

Our investigation into the vascular responses that occur during Spreading Depression (a pathological process characterized by large rises in perivascular K^+), led to results that support experimental observations in the mouse [28]: that dilations can give way to constrictions. We also postulate that control of the deposition and removal of K^+ into the perivascular space is vital for the K^+-mediated NVC mechanism as the behaviour of the arteriole is profoundly affected if the rate of clearance of K^+ from the perivascular space is altered. Even the volume of the perivascular space can affect the arteriolar behaviour – vasodilation can be abolished if the volume ratio between the astrocyte and perivascular space changes. This demonstrates that a well-controlled mechanism that works to maintain K^+ homeostasis in the extracellular environment of the brain could be very important for not only successful neurovascular coupling, but also successful recovery from Spreading Depression.

Chapter 8

Models of Neurovascular Coupling via Nitric Oxide Signalling

8.1 Introduction

Neuronal activation and the subsequent release of glutamate (Glu) into the synapse activates neuronal NMDA receptors, resulting in an influx of Ca^{2+} into the neuron and the activation of neuronal nitric oxide synthase (nNOS). nNOS releases nitric oxide (NO), a vasodilator. Experimental inhibition of nNOS in the cortex reduces functional hyperaemia [106], suggesting a role for NO in neurovascular coupling (NVC). This response is, however, restored by the addition of NO donors, which provide a constant concentration of NO. This indicates that NO *is* an important *contributor* to neurovascular coupling, but the dynamic rise in NO caused by neuronal activation itself does not *directly* mediate the message between neuron and blood vessel. Perhaps then, at least in the cortex, NO is needed to modulate other vasomodulatory pathways, such as those involving K^+ or EET. In any case, the exact role of NO in NVC is unclear. This chapter is devoted to extending the mathematical framework we have created in the past two chapters to include NO-driven signals of NVC.

8.2 Model

8.2.1 Overview of the Model

The NO-driven mechanism we propose is as follows: a) glutamate binding activates NMDA receptors in the neuron causing Ca^{2+} entry; b) Ca^{2+} forms a complex with calmodulin (CaM) which c) activates neuronal nitric oxide synthase (nNOS). There is also NO production in the endothelial cells (ECs) lining the neighbouring arteriole due to activation of endothelial nitric oxide synthase (eNOS) by the wall shear stress (WSS) exerted by flowing blood. The NO produced by nNOS and eNOS then d) diffuses to the vascular smooth muscle cell (SMC) and

activates soluble guanylate cyclase (sGC), which e) catalyses the formation of cyclic guanosine monophosphate (cGMP), which in turn causes f) vessel dilation by:

1. opening BK (voltage- and calcium- activated K^+) channels, which decreases SMC membrane potential and effects a *decreased* influx of Ca^{2+} through voltage operated calcium channels (VOCCs) into the cell, and

2. increasing the rate of myosin light chain dephosphorylation (MLCP) (effectively *desensitizing* the contractile system to the effects of Ca^{2+})

An overview of the cells, chemical species, and cell componentry involved in this model is shown in Figure 8.1.

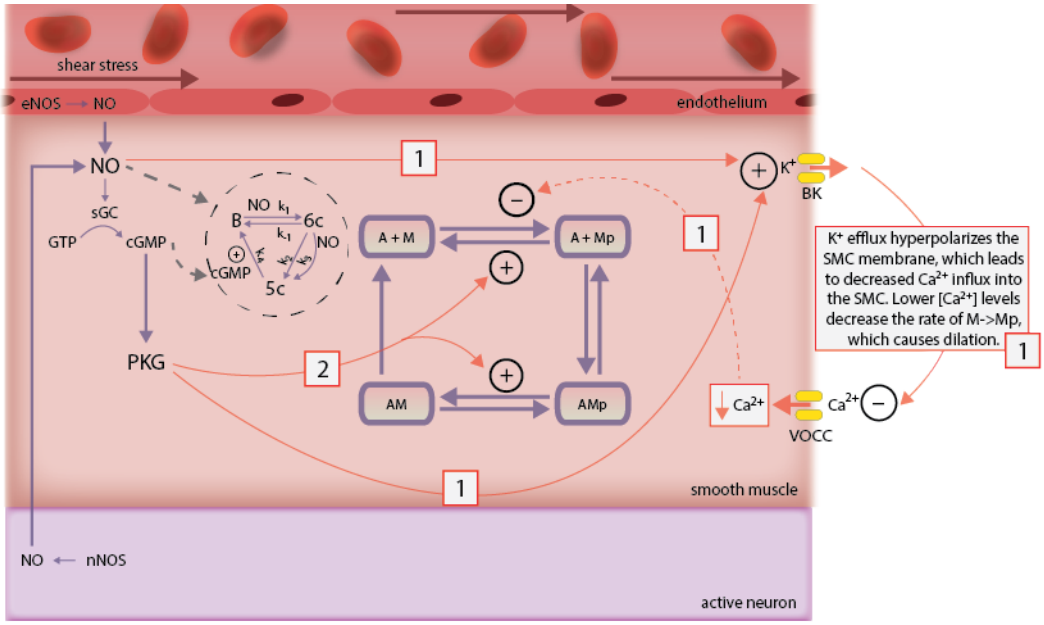

Figure 8.1 NO production and action in the neurovascular unit. NO is produced by nNOS in active neurons and by eNOS in ECs. NO from these two sources then diffuses into the SMC and activates sGC from its basal state, *B*, to its active state, *6c*. The active sGC then converts GTP to cGMP which acts via protein kinase G (PKG). Our model focuses on two vasodilatory pathways: 1) the effect of cGMP (via PKG) and NO on the BK channel open state probability, and 2) the effect of cGMP (via PKG) on the rate of MLC dephosphorylation. These are numbered on the diagram as described. Adapted from [169].

Note that there are other proposed means (in addition to those shown in Figure 8.1) by which cGMP acts on various other cell components (such as the VOCCs) to bring about relaxation; we focus on the two pathways described because they are those investigated by Yang et al. [169]. Any effect that NO has on EET concentration is ignored.

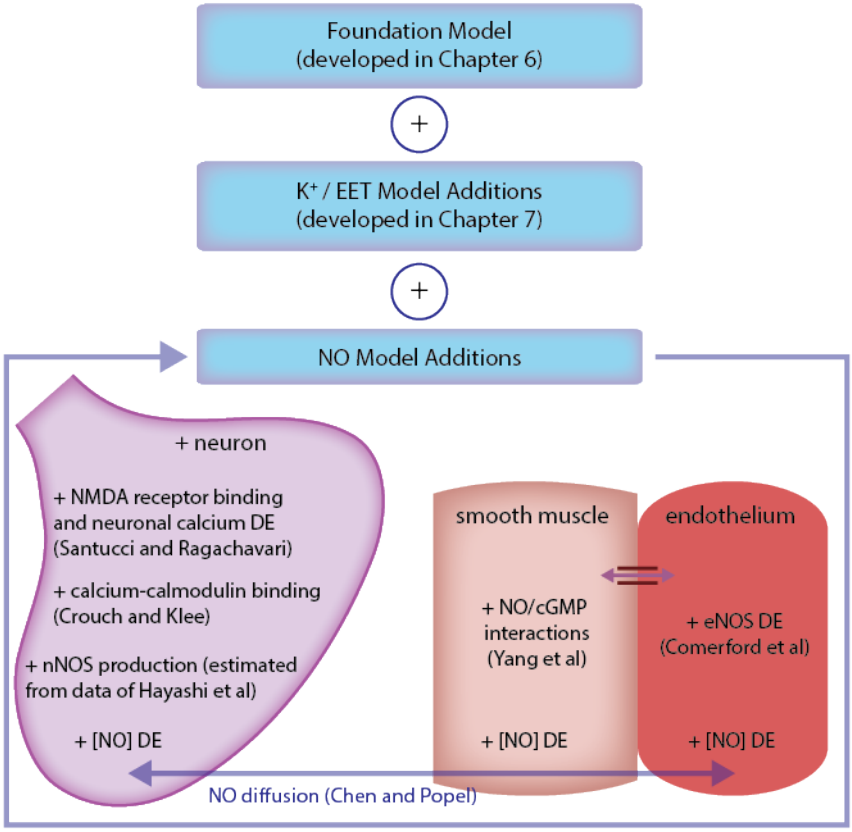

Figure 8.2 Extensions to the NVU model to include NO equations. Authors of the model components are shown in brackets where applicable.

Figure 8.2 provides an overview of the components that constitute the NO model extension described in this chapter.

8.2.2 Glutamate Release and NMDA Receptor Binding

The presented model of glutamate binding to NMDA receptors is based on that of Santucci and Raghavachari [137]. They state that the majority of NMDA receptors in the mammalian brain are either of an NR2A or NR2B subtype with an average of 0.63 (NR2A) and 11 (NR2B) receptors per synapse, respectively. The fraction of open NR2A NMDA receptors (P_{NR2A-O}) is dependent on the synaptic glutamate concentration, as follows:

$$P_{NR2A-O} = \frac{[Glu]}{\beta_A + [Glu]} \tag{8.1}$$

Similarly, the fraction of open NR2B NMDA receptors (P_{NR2B-O}) is:

$$P_{NR2B-O} = \frac{[Glu]}{\beta_B + [Glu]} \tag{8.2}$$

where β_A and β_B are 0.41 nM and 1.02 nM, respectively.

8.2.3 Calcium Influx and Calmodulin Binding

The inward calcium current *per* open NMDA receptor is given by Santucci and Raghavachari [137]:

$$I_{Ca} = \frac{4VG_M(P_{Ca}/P_M)(Ca_{ex}/M)}{1+\exp(-0.08(V+20))} \frac{\exp(2VF/RT)}{1-\exp(2VF/RT)} \tag{8.3}$$

where G_M is the conductance of the NMDA channel (pS); P_{Ca}/P_M is the relative conductance of the NMDA channel to Ca^{2+} compared to monovalent ions (dimensionless); Ca_{ex} is the external calcium concentration (mM); M is the concentration of monovalent ions (mM), T is temperature (K); R is the gas constant ($Jmol^{-1}K^{-1}$) and F is Faraday's constant ($Cmol^{-1}$). V is the neuronal membrane potential (voltage) and is assumed to be approximately constant. In reality, the neuron hyperpolarizes and repolarizes many times during the action potentials that occur in periods of activation. This model does not include equations describing this "spiking" activity and so we take an approximate average voltage that occurs during this period. Note that this assumption means that, in this model, calcium currents in the neuron depend purely on the concentration of glutamate in the synapse. This is a very simplified mathematical description of the complex dynamics that actually occur in the neuron but is suitable for our purpose (as we are focusing on glutamate-effected calcium changes in the neuron).

Note about dimensional consistency in Equation 8.3: The expression $2VF/RT$ requires V to have units of V (volts) in order to be dimensionally consistent. However, this equation has been fitted to data measured in mV, and so the term $\exp(-0.08(V+20))$ actually requires units of mV. To obtain I_{Ca} in our desired units of fA, the V term in the numerator of the equation also needs to be in mV. Therefore, for dimensional consistency, Equation 8.3 should really be written as the following equation:

$$I_{Ca} = \frac{4VG_M(P_{Ca}/P_M)(Ca_{ex}/M)}{1+\exp(-0.08(V+20))} \frac{\exp(2VF/1000RT)}{1-\exp(2VF/1000RT)} \tag{8.4}$$

where V is in mV.

The total inward calcium current for *all* open NMDA receptors (I_{Ca_T}) is the calcium current for *one* open receptor (I_{Ca}) multiplied by the *total* number of open receptors. As there are two types of receptor, NR2A and NR2B, that are each present in different densities (0.63 (NR2A)

and 11 (NR2B) receptors per synapse, respectively), we obtain (in fA):

$$I_{Ca_T} = I_{Ca}\,(0.63P_{NR2A-O} + 11P_{NR2B-O}) \tag{8.5}$$

The change in neuronal cytosolic Ca^{2+} (in mMs^{-1}) was also given by Santucci and Raghavachari [137] as the ordinary differential equation:

$$\frac{\mathrm{d}[Ca^{2+}]_n}{\mathrm{d}t} = \frac{(I_{Ca_T}/(2Fv_{spine} \times 10^3)) - \kappa_{ex}([Ca^{2+}]_n - Ca_{rest})}{1+\Lambda} \tag{8.6}$$

v_{spine} is the volume of the neuronal dendritic spine (in L), Ca_{rest} is the resting calcium concentration (mM), Λ is the buffer capacity (dimensionless), and κ_{ex} is the decay rate constant of the internal calcium concentration (s^{-1}). The $(2Fv_{spine} \times 10^3)$ term is required here to convert between the electrical flux (in fA) given in Equation 8.5 and the molar flux (in mMs^{-1}) required by Equation 8.6 – see Equation 6.1 in Chapter 6 for a more complete explanation of this conversion.

nNOS activation depends on the concentration of calcium-calmodulin complexes (Ca^{2+}-CaM) present in the neuron. To relate the neuronal calcium changes described in Equation 8.6 to changes in the calcium-calmodulin complex concentration ([Ca^{2+}- CaM] or [CaM] for short), we can use the Ca^{2+}-CaM kinetics of Crouch and Klee [40]. Each calmodulin can bind a maximum of four Ca^{2+}. The number of Ca^{2+} bound per calmodulin, N, is given by Crouch and Klee [40] as:

$$N = \frac{[Ca^{2+}]_n}{\phi}\frac{\mathrm{d}\phi}{\mathrm{d}[Ca^{2+}]_n} \tag{8.7}$$

where ϕ describes the sum of all the states of bound Ca^{2+} (i.e., 1, 2, 3 or 4 Ca^{2+} bound) with respect to free Ca^{2+}. ϕ is given as the following function:

$$\phi = 1 + Q_1[Ca^{2+}]_n + Q_1Q_2[Ca^{2+}]_n^2 + Q_1Q_2Q_3[Ca^{2+}]_n^3 + Q_1Q_2Q_3Q_4[Ca^{2+}]_n^4 \tag{8.8}$$

Q_1–Q_4 (mM^{-1}) are constants describing the degree in which Ca^{2+} associates with each of the four binding sites on the CaM molecule. Note that the binding of Ca^{2+} to CaM is a positively cooperative process; i.e., Ca^{2+} binding to one site on CaM increases the affinity for Ca^{2+} on another binding site.

8.2.4 Nitric Oxide in the Neuron

Hayashi et al. [71] have shown experimentally how nNOS activation depends on the concentration of [CaM] when nNOS is overexpressed in the bacteria *E. Coli*, and they list Michaelis-

Menten kinetic constants (i.e., $V_{max_{NOS}}$ and $K_{act_{NOS}}$) that relate nNOS activity and [CaM] for unphosphorylated and phosphorylated nNOS. However, the units used in [71] for $V_{max_{NOS}}$ are nmol/min/mg of bacteria, when we require units of μMs^{-1} in our equations. The nNOS enzyme is also overexpressed in *E. Coli* making the $V_{max_{NOS}}$ value unrepresentative of the rate of NO production that would occur in a neuron. For these reasons, we must estimate a value for $V_{max_{NOS}}$ (in μMs^{-1}) that will give physiological values for [NO]. We do however use the value of $K_{act_{NOS}}$ for unphosphorylated nNOS (in mM) that is given in [71].

We also assume that no nNOS activity occurs before a threshold concentration of [CaM] ($[\text{CaM}]_{thresh}$, in mM) is reached (otherwise vasodilatory NO would be produced continuously and arteriolar homeostasis would be difficult to maintain). As such, we develop the following kinetic scheme for nNOS production in the neuron, NO_{nNOS} (in μMs^{-1}):

$$NO_{nNOS} = V_{max_{NOS}} \frac{([\text{CaM}] - [\text{CaM}]_{thresh})}{K_{act_{NOS}} + ([\text{CaM}] - [\text{CaM}]_{thresh})} \tag{8.9}$$

where [CaM] is defined by:

$$[\text{CaM}] = \frac{[\text{Ca}^{2+}]_n}{N} \tag{8.10}$$

N is given in Equation 8.7.

We formulate the differential equation for neuronal NO by taking the amount of NO produced from nNOS (Equation 8.9), and subtracting that which is lost by diffusion and that which is scavenged by O_2 (the formulations and parameters for the latter two terms are taken from Chen and Popel [35]). We therefore describe NO concentration changes (in μMs^{-1}) by:

$$\frac{\text{d}[\text{NO}]_n}{\text{d}t} = NO_{nNOS} - \frac{[\text{NO}]_n - [\text{NO}]_i}{\tau_{ni}} - k_{O_2}[\text{NO}]_n^2[\text{O}_2]_n \tag{8.11}$$

The first term in Equation 8.11 represents the synthesis of NO by nNOS (from Equation 8.9), the second represents that which diffuses to the smooth muscle cell (as indicated by the subscript i) and the third represents that which is scavenged by O_2 in the neuronal tissue. **A note about the form of the second (diffusion) term:** Describing the diffusion process accurately would necessitate differential equations that describe variations in space and time (i.e., partial differential equations, PDEs). These equations would complicate the solution of the equation set considerably. So that we can keep a simpler ODE formulation, we represent diffusion using a simple relationship: the difference between NO concentrations at two point sources (the neuron $[NO]_n$ and the SMC $[NO]_i$) determines the "driving force" for diffusion (and thus the size of the diffusive flux) and τ_{ni} determines the characteristic time for diffusion. In other words, τ_{ni} represents the approximate time taken for NO to diffuse the distance h_1 between the neuron

(subscript n) and the smooth muscle cell (subscript i). Mathematically:

$$\tau_{ni} = \frac{h_1^2}{D_{NO}} \tag{8.12}$$

where D_{NO} is the diffusion coefficient for NO used in the NO diffusion model of Chen and Popel [35], and h_1 is estimated as 6 μm.

8.2.5 Nitric Oxide in the Endothelial Cell

NO is also produced in the endothelial cells in response to shear stress exerted on the wall by flowing blood.

The changes in NO in the endothelial cell (in μMs^{-1}) can be described by:

$$\frac{\text{d}[\text{NO}]_j}{\text{d}t} = \frac{\text{d}eNOS_{act}}{\text{d}t} - \frac{[\text{NO}]_j - [\text{NO}]_i}{\tau_{ji}} - k_{o_2}[\text{NO}]_j^2[\text{O}_2]_j \tag{8.13}$$

This formulation is similar to that in Equation 8.11; the first term represents the production of NO by eNOS, the second is the NO which is lost by diffusion to the SMC and the third is that which is lost by reaction with oxygen.

Equation 8.14 represents the activation and deactivation of eNOS to produce NO and is taken from the model of Comerford et al. [38]. The endothelial NOS is activated by cytosolic free calcium c_j (μM) at a maximum rate K_{dis} (μMs^{-1}) and deactivated at constant rate μ_2 (s^{-1}). This equation also includes a source term, $g_{max}F(\tau_\omega)$, for activation of eNOS directly by WSS.

$$\frac{\text{d}eNOS_{act}}{\text{d}t} = \frac{K_{dis}c_j}{K_{eNOS} + c_j} - \mu_2[\text{NO}]_j + g_{max}F(\tau_\omega) \tag{8.14}$$

where

$$F(\tau_\omega) = \frac{1}{1 + \alpha\exp(-W(\tau_\omega))} \tag{8.15}$$

and

$$W(\tau_\omega) = W_0\frac{(\tau_\omega + \sqrt{16\delta_{WSS}^2 + \tau_\omega^2} - 4\delta_{WSS})^2}{\tau_\omega + \sqrt{16\delta_{WSS}^2 + \tau_\omega^2}} \tag{8.16}$$

Equations 8.15 and 8.16 are those in Wiesner et al. [164] where τ_ω is the wall shear stress (Pa) and δ_{WSS} is the membrane shear modulus (also in Pa). Also:

$$\tau_{ji} = \frac{h_2^2}{D_{NO}} \tag{8.17}$$

where h_2 is the approximate distance between the SMC (subscript i) and the EC (subscript j). We assume this distance is the same as h_1 for simplicity (6 μm).

8.2.6 Nitric Oxide in the Smooth Muscle Cell

The rate of change of the NO concentration in the smooth muscle cell (in μMs^{-1}) is given by:

$$\frac{\mathrm{d}[\mathrm{NO}]_i}{\mathrm{d}t} = \frac{[\mathrm{NO}]_n - [\mathrm{NO}]_i}{\tau_{ni}} + \frac{[\mathrm{NO}]_j - [\mathrm{NO}]_i}{\tau_{ji}} - k_{dno}[\mathrm{NO}]_i \tag{8.18}$$

Here, the first and second terms are the diffusive fluxes from the neuron and EC, respectively. The third term, $k_{dno}[\mathrm{NO}]_i$, is the scavenging term resulting from NO binding to proteins – the formulation and parameter value for this term is taken from [35].

8.2.7 Overview of NO/cGMP Interactions in the Smooth Muscle Cell

Some of the actions performed by NO/cGMP in the SMC were shown in Figure 8.1. The following sections describe how these processes are described mathematically in this model. As indicated in Figure 8.2, the mathematical descriptions for NO/cGMP interactions are taken directly from Yang et al. [169], with adaptations to ensure they are compatible with the SMC model that we are using.

8.2.7.1 sGC Activation

sGC is the only known receptor for NO. Activation of sGC produces cGMP and PKG (species that act on SMC components to bring about vasodilation). sGC is therefore an important component of NO-mediated vasodilation. The kinetics involved in sGC activation are shown in Figure 8.3.

Essentially, in the smooth muscle cell, NO binds to sGC in the following reactions formulated by Yang et al. [169], where:

- B is the basal state of sGC
- $6c$ is the intermediate form
- $5c$ is the fully activated form
- E is the fraction of each form

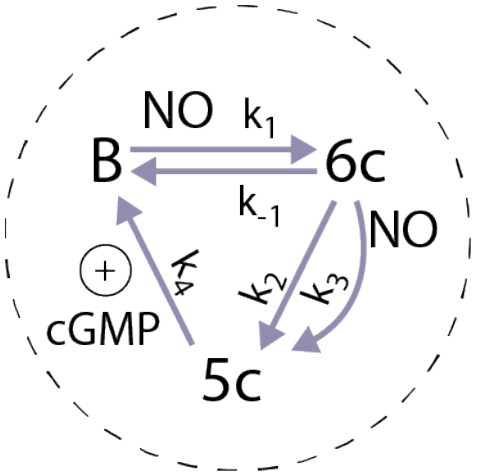

Figure 8.3 The kinetics of sGC activation. NO activates sGC by transforming it from its basal state, *B*, to the active state, *5c*, via the intermediate form *6c*. cGMP can also have a negative feedback effect on its own production by inactivating sGC to its *B*-form again. This detail from Figure 8.1 is adapted from [169].

- k_1, k_2, k_3, k_4, and k_{-1} are rate constants

First *B* is activated by NO to form *6c*:

$$\mathrm{E_b} + \mathrm{NO} \underset{k_{-1}}{\overset{k_1}{\rightleftharpoons}} E_{6c}$$

There is an NO-independent decay of *6c* to *5c* described by:

$$\mathrm{E_{6c}} \xrightarrow{k_2} E_{5c}$$

There is also a NO-dependent scheme:

$$\mathrm{E_{6c}} + \mathrm{NO} \xrightarrow{k_3} E_{5c} + \mathrm{NO}$$

The dissociation of NO from sGC, and hence the recovery to basal sGC conditions, is described by:

$$\mathrm{E_{5c}} \xrightarrow{k_4} E_b + \mathrm{NO}$$

where

$$k_4 = C_4[\mathrm{cGMP}]^m \tag{8.19}$$

C_4 is a constant and m reflects the strength of feedback from cGMP. For simplicity, we assume $m = 0$ (i.e., there is no feedback from cGMP).

These interactions give the following set of differential equations:

$$\frac{\mathrm{d}E_b}{\mathrm{d}t} = -k_1 E_b[\mathrm{NO}]_i + k_{-1}E_{6c} + k_4 E_{5c} \tag{8.20}$$

$$\frac{\mathrm{d}E_{6c}}{\mathrm{d}t} = k_1 E_b[\mathrm{NO}]_i - k_{-1}E_{6c} - k_2 E_{6c} - k_3 E_{6c}[\mathrm{NO}]_i \tag{8.21}$$

$$\frac{\mathrm{d}E_{5c}}{\mathrm{d}t} = k_3 E_{6c}[\mathrm{NO}]_i + k_2 E_{6c} - k_4 E_{5c} \tag{8.22}$$

8.2.7.2 cGMP Production

The rate of cGMP production from GTP (guanosine-5'-triphosphate) is dependent on E_{5c}. The rate of cGMP degradation is dependent on cyclic nucleotide phosphodiesterases, PDEs, which hydrolyze cGMP to GMP. The reactions are modelled by Yang et al. [169] as:

$$\mathrm{GTP} + \mathrm{E_{5c}} \rightleftharpoons \mathrm{GTP \cdot E_{5c}} \longrightarrow \mathrm{cGMP} + \mathrm{E_{5c}}$$
$$\mathrm{cGMP} + \mathrm{PDE} \rightleftharpoons \mathrm{cGMP \cdot PDE} \longrightarrow \mathrm{GMP} + \mathrm{PDE}$$

under the assumption that GTP is abundant and that cGMP production foremost depends on sGC concentration. Under the assumption that [PDE] is constant, the following equation arises:

$$\frac{\mathrm{d}[\mathrm{cGMP}]}{\mathrm{d}t} = V_{max,sGC}E_{5c} - \frac{V_{max,pde}[\mathrm{cGMP}]}{K_{m,pde} + [\mathrm{cGMP}]} \tag{8.23}$$

where $V_{max,sGC}$ is the maximum cGMP production rate when $E_{5c} = 1$ and

$$V_{max,pde} = k_{pde}[\mathrm{cGMP}] \tag{8.24}$$

In our simulations, we use the parameters $V_{max,sGC}$, k_{pde}, and C_4 from Yang et al. [169] (who fitted these equations to experimental data).

8.2.7.3 cGMP and NO Effects on BK Channels (Mechanism 1)

The BK channel open probability distribution can be shifted due to the effects of NO and cGMP (via PKG) [151] – see Figure 8.4. These shifts act to open BK channels, increasing the efflux of K^+ from the SMC, hyperpolarizing the membrane. Voltage-operated Ca^{2+} channels (VOCCs) close in response to this shift in the membrane potential (or "voltage"), restricting the access of Ca^{2+} into the SMC, leading to a decrease in MLC phosphorylation, crossbridge attachment, and force development, causing muscle relaxation and vasodilation.

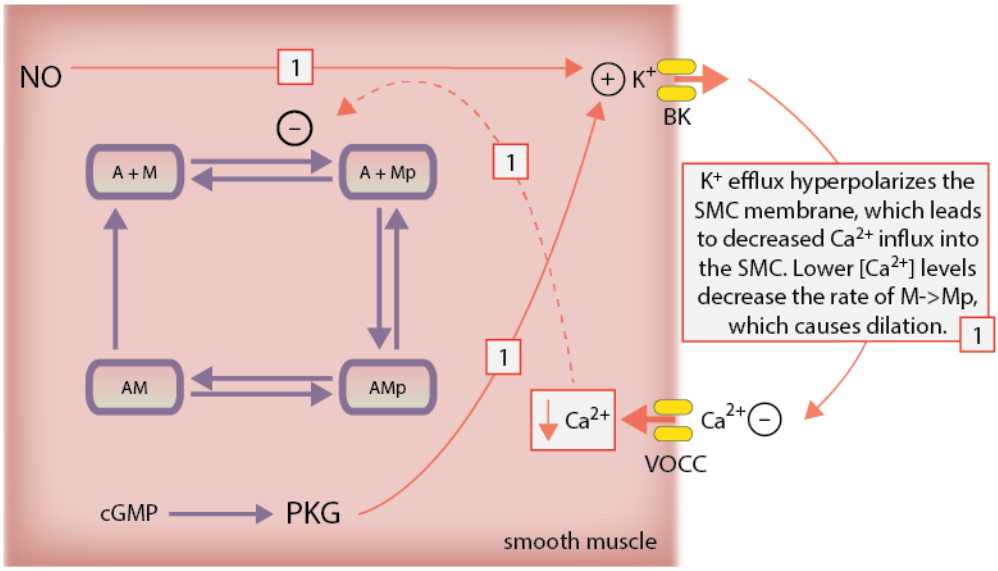

Figure 8.4 Mechanism 1: NO and cGMP act to increase the BK channel open probability. This leads to K^+ efflux, hyperpolarization, decreased Ca^{2+} influx, decreases in the rate of MLC phosphorylation, and vasodilation. Detail from Figure 8.1.

The regulatory effect of cGMP on the BK channel open probability is described by the Hill function:

$$R_{cGMP}(K_{m,cGMP}, n_{H,cGMP}) = \frac{[\text{cGMP}]^{n_{H,cGMP}}}{[\text{cGMP}]^{n_{H,cGMP}} + K_{m,cGMP}^{n_{H,cGMP}}} \tag{8.25}$$

There is also a direct effect of NO on the open probability. It is modelled in a similar way:

$$R_{NO}(K_{m,NO}, n_{H,NO}) = \frac{[\text{NO}]^{n_{H,NO}}}{[\text{NO}]^{n_{H,NO}} + K_{m,NO}^{n_{H,NO}}} \tag{8.26}$$

The effect of NO/cGMP on the BK channel open probability, P_o, is described in Equation 8.27, which is of the same *formulation* as that which we use in the SMC model of the previous chapters (see Equation A.25), but with parameters adjusted to fit the experimental data from Stockand and Sansom [151]. The closeness of fit is shown in Figure 8.5.

$$P_o(c_i, v_i) = K_{activation_i} = \frac{(c_i + c_{wi})^2}{(c_i + c_{wi})^2 + \beta_i \exp\left[-(v_i - v_{Ca_3})/R_{K_{fit}}\right]} \tag{8.27}$$

where

$$v_{Ca_3} = V_{cGMP} R_{cGMP}(K_{m,cGMP}, n_{H,cGMP}) - V_{NO} R_{NO}(K_{m,NO}, n_{H,NO}) - V_b \tag{8.28}$$

v_i is the SMC membrane potential (mV) and c_i is the SMC cytosolic calcium concentration

(μM). We adjusted the parameters V_{cGMP}, V_b and $R_{K_{fit}}$ (all in mV) to provide the best model fit to the experimental data (Stockand and Sansom [151]). We **do not** use the formulations for the BK channel P_o described in Yang et al. [169], because they use a different SMC model to us – using the formulation by Yang et al. [169] would result in discrepancies between the models that we are attempting to combine together.

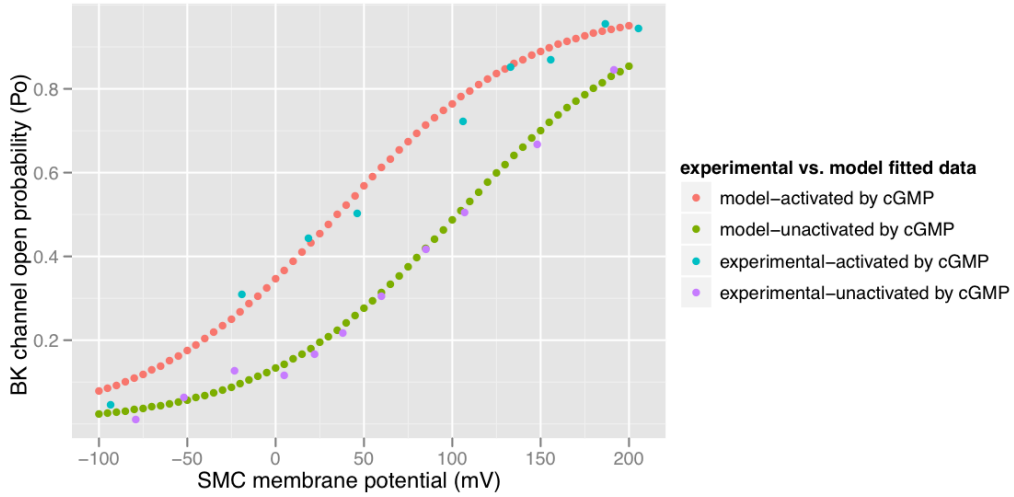

Figure 8.5 BK channel open probability (Po) as a function of SMC membrane potential (v_i) – fitted to the experimental data of Stockand and Sansom [151].

8.2.7.4 cGMP Effect on MLC Phosphorylation Sensitivity (Mechanism 2)

cGMP can increase the rate of myosin light chain (MLC) dephosphorylation. This is also known as "Ca^{2+} desensitization" because the process of MLC phosphorylation becomes less "sensitive" to the level of Ca^{2+}. The MLC is then less likely to be attached at the current Ca^{2+} level and will hence generate a smaller contractile force, resulting in smooth muscle relaxation and vasodilation [169]. This mechanism is shown graphically in Figure 8.6.

Essentially, Mechanism 2 involves *increasing* the rate at which MLC is *de*phosphorylated. In Figure 8.6, you can see that cGMP (via PKG) acts on both dephosphorylation operations (M ⟵ Mp and AM ⟵ AMp). Yang et al. [169] use the crossbridge model of Hai and Murphy [65], as do we. This allows us to use the same equations for Mechanism 2 that are provided by Yang et al. [169]. The two rate constants for dephosphorylation, K_2 and K_5, are dependent on cGMP concentration in the following way:

$$K_2 = K_5 = k^b_{mlcp} + k^c_{mlcp} R_{cGMP}(K_{m,mlcp}, n_{H,mlcp}) \tag{8.29}$$

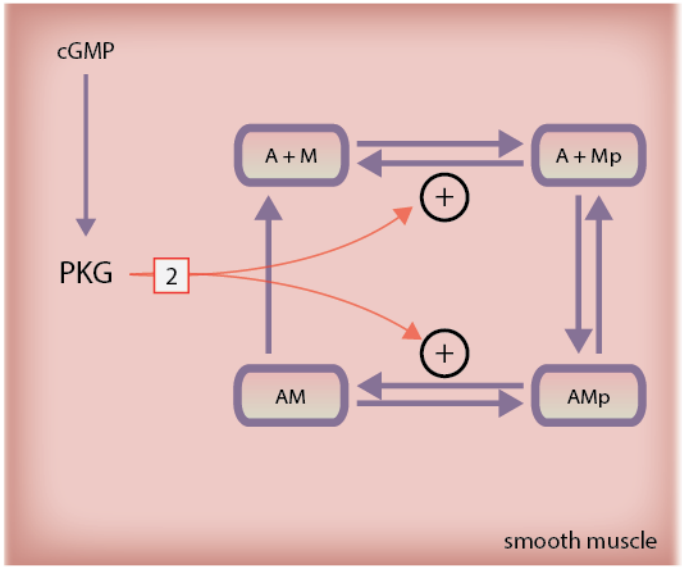

Figure 8.6 Mechanism 2: cGMP (via PKG) can cause vasodilation by increasing the MLC dephosphorylation rate (desensitizing the SMC contractile system to the effects of Ca^{2+}). Detail from Figure 8.1.

where k^b_{mlcp} is the basal MLC dephosphorylation rate constant and k^c_{mlcp} is the first order rate constant for cGMP-regulated MLC dephosphorylation (both in s^{-1}). $R_{cGMP}(K_{m,mlcp}, n_{H,mlcp})$, the regulatory effect of cGMP on myosin dephosphorylation, is again expressed as a Hill function:

$$R_{cGMP}(K_{m,mlcp}, n_{H,mlcp}) = \frac{[\text{cGMP}]^{n_{H,mlcp}}}{[\text{cGMP}]^{n_{H,mlcp}} + K^{n_{H,mlcp}}_{m,mlcp}} \tag{8.30}$$

Figure 8.7 graphically shows the mathematical relationship described in Equations 8.29 and 8.30.

With this shift in sensitivity, MLC is more likely to be dephosphorylated at a given Ca^{2+} concentration. This drives a further shift in the conformation of myosin-actin crossbridges to a more detached / less attached state; a smaller contractile force is generated and the vessel relaxes.

8.2.8 Solution Methodology

All the equations described in this chapter are combined with all the other equations for the NVU previously developed in Chapters 6 and 7. All equations are again solved using RKSUITE (details of which have already been given in Chapter 7) assuming a 60 s neuronal activation (simulated as a rapid sigmoidal increase in synaptic glutamate from 0 μM to 0.75 μM as per [75]). Once again, we consider an arteriole with a 10 μm radius and a wall thickness of 4 μm.

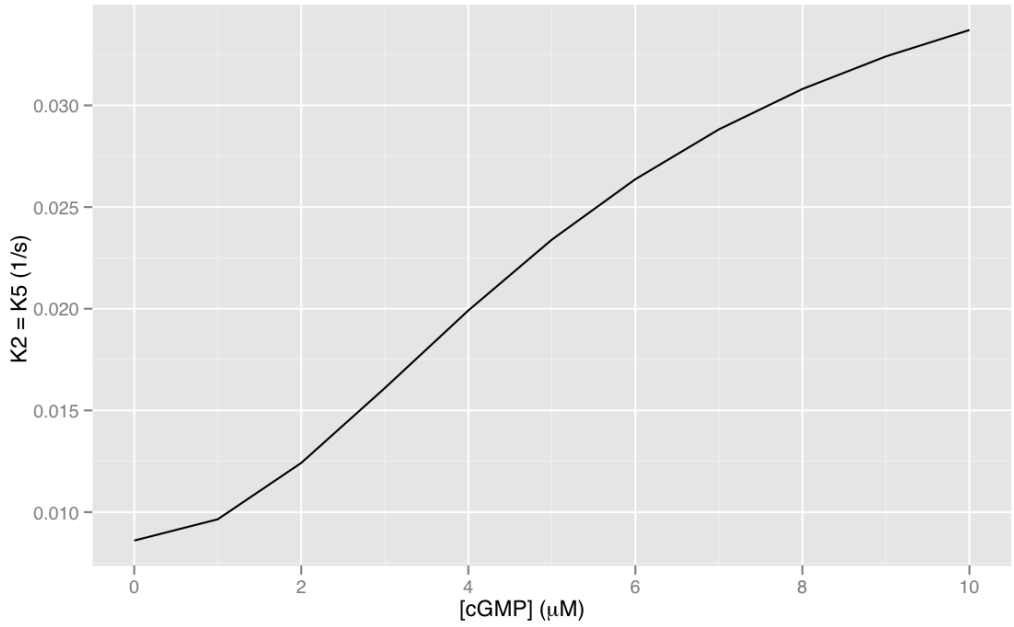

Figure 8.7 Effect of cGMP concentration [cGMP] on the dephosphorylation rate constants K_2 and K_5.

The pressure is set at 30 mmHg, the O_2 concentration is set at 200 μM (as per Chen and Popel [35]) and the level of wall shear stress is assumed to be 1.82 Pa [132].

In this chapter, we are focusing mostly on NO- (and cGMP-) mediated NVC and therefore want to analyze it first in isolation. To this end, we initially ignore the K^+/EET signals that we previously developed in Chapter 7. Mathematically, we "silence" the K^+/EET mechanism by omitting their "triggers" (bound astrocyte metabotropic glutamate receptors (mGluR) and synaptic K^+ release). We will then reintroduce the K^+/EET signals (by reincorporating their triggers) so that we can analyze the NVC response when both pathways (NO-mediated *and* K^+/EET-mediated vasodilation) operate in tandem. The production of 800 seconds of model data for all equations in the combined model took 15.448 seconds of CPU time.

8.3 Results and Discussion

The first section demonstrates the model response when only the NO-mediated mechanism acts upon the NVU system. These results are then compared to the response obtained when only the K^+/EET-mediated signals act upon the NVU. The final results simulate a NVU system with both NO-mediated *and* K^+/EET-mediated NVC.

8.3.1 NO-Mediated Neurovascular Coupling

8.3.1.1 Overall Model Behaviour

Following synaptic glutamate release (starting at t=0) there is a very rapid ($<$ 1s) rise in NO concentration in all the cells modelled (not shown). Of the three cell types modelled, the neuron had the highest maximum NO concentration (0.20 μM) followed by the SMC (0.18 μM) and the EC (0.16 μM). The NO changes in the SMC are due to diffusion from the neighbouring neuron and EC. The NO concentrations achieved in our model differ considerably from that of the NO diffusion model of Chen and Popel [35]. Their simulations show a maximum NO value of 6 nM (which equates to 0.006 μM; about 30 times lower than in our simulation). However, Mashour and Boock [109], in their study of WSS-induced NO levels in human cerebral endothelial cells (in an artificial capillary system) report EC NO concentrations of 0.57 ± 0.0067 μM (at the WSS value of 1.35 Pa); these values align more closely with our model results. Note that we used a very simple model for diffusion so that we did not have to incorporate partial differential equations (PDEs) into our equation set. Adding PDEs (like those used in the study of Chen and Popel [35]) will allow the NO diffusion process to be more accurately modelled.

A summary of the effects of the NO model on the NVU is given in Figure 8.8. Note that the NO/cGMP dynamics model we use is that of Yang et al. [169], a group that has also formulated a myogenic and vessel model [170, 171]. Curiously, they don't analyze diameter or blood flow changes caused by NO/cGMP, despite having the means to do so through their vessel model. The following results therefore constitute the first attempt at simulating these NO/cGMP equations in a full vessel model. Here, an SMC NO concentration change from 0.1 to 0.18 μM causes an increase in diameter of 1% (Figure 8.8), equating to an approximate 4% change in blood flow through that vessel (when considering a vessel in isolation).

In the SMC, an increase in NO concentration leads to a cGMP concentration increase from 9 μM to 12 μM (a 33% increase), when both neuronal and endothelial NO sources are included (see Figure 8.8). NO acts directly (and indirectly, via cGMP) on BK channels, rapidly increasing their open channel probability (BKPo) by a small amount (0.0060 – 0.0085). The SMC Ca^{2+} concentration (ci) does decrease slightly (by only $4 \times 10^{-5} \mu$M) and at a much slower timescale than the BKPo change. The changes in SMC BK open channel probability (BKPo), SMC Ca^{2+} concentration (ci), and SMC membrane potential (vi) are very small, suggesting that Model Mechanism 1 (NO- and cGMP- mediated BK channel opening) does not contribute greatly to NO-mediated NVC. The (small) arteriolar change (1%) is likely due to Model Mechanism 2 (cGMP-mediated Ca^{2+} desensitization of the contractile system).

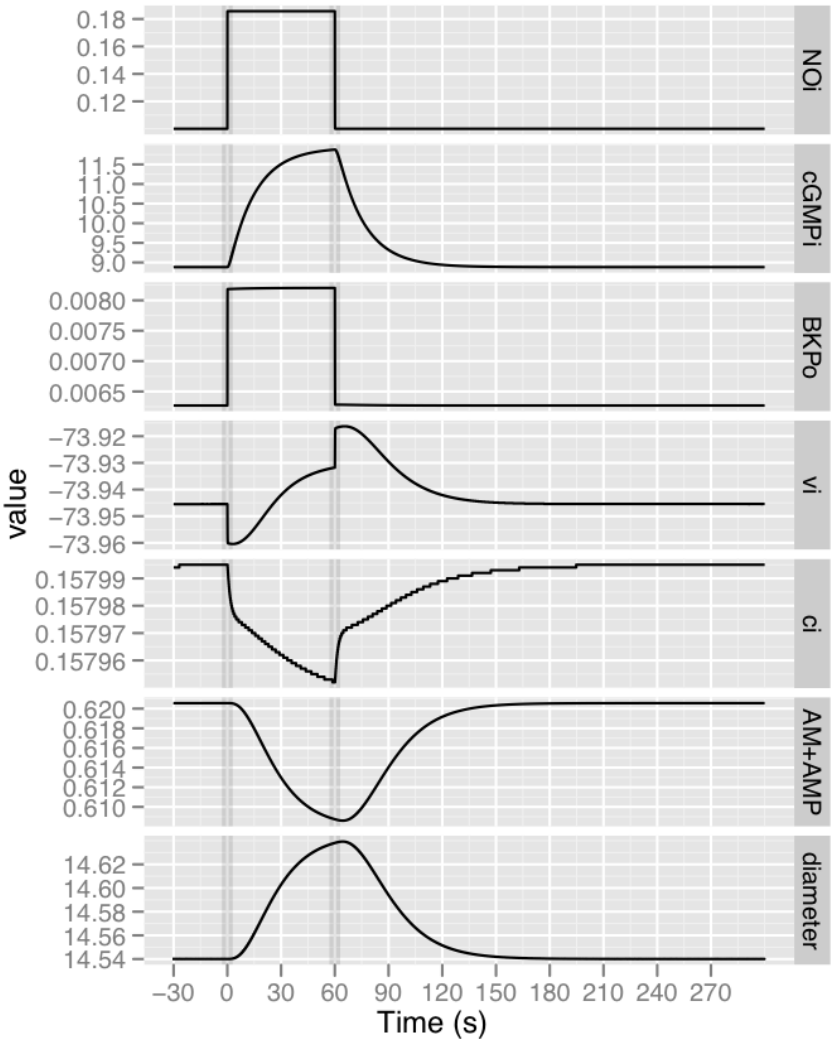

Figure 8.8 Arteriolar response to NO-mediated NVC mechanisms. Shown here are SMC NO concentration changes (in μM), SMC cGMP concentration (in μM), SMC membrane potential (vi, in mV), SMC Ca^{2+} concentration (ci, also in μM), SMC BK channel open probability (BKPo), AM + AMP, the fraction of attached crossbridges (the states generating a contractile force), and finally, the arteriolar diameter (in μm). A NO change from 0.1 to 0.18 μM causes an increase in diameter of approximately 1%. Note that these results do not include simulations of the K^+/EET pathways involving the astrocyte.

The failure of Model Mechanism 1 to produce the expected changes in arteriolar tone highlights an important issue that physiological modellers need to be aware of. If you describe and/or analyze a mechanism in isolation (as was done in [169]) and don't incorporate it into a model of the "bigger picture" (a vessel or tree model), you may run the risk of making hypotheses or conclusions based on only a small "zoomed-in" section of a much larger system. In this case, it seemed Mechanism 1 was a promising pathway for successful NO/cGMP-mediated NVC – after all, cGMP did significantly alter the BK channel probability in experiment –

however, when incorporated into our NVU model it did not have any significant effect on arteriolar tone. If we examine Figure 8.5 again more closely, it is apparent why Mechanism 1 (NO/cGMP-mediated BK channel opening) does not contribute to NO-mediated NVC. cGMP can produce profound increases in the fraction of open BK channels (BKPo), but not at the membrane potential our model SMC is operating at (≈ -74 mV). As we explored in the previous chapter (in Figure 7.6), if our model SMC *did* possess a membrane potential of approximately -40 mV at "rest" (i.e., a membrane potential similar to the experimental values shown in Figure 7.6), we may see a more significant change in BKPo, and hence arteriolar diameter. There are also many other potential cellular targets for NO, cGMP and their molecular derivatives; these are reviewed in [169] and include the voltage-dependent Ca^{2+} channels (VOCCs) themselves, as well as the Ca^{2+}-ATPase pump (that pumps Ca^{2+} into the sarcoplasmic reticulum, the SMC Ca^{2+} stores). Future extensions to this model will include these potentially important targets.

When the eNOS contribution to NO production is omitted, as shown in the right hand plot of Figure 8.9, the arteriole is more constricted at baseline (13.7 μm) than when the eNOS contribution is included (14.54 μm), as shown in the left hand plot of Figure 8.9. Without the EC NO contribution, the change in arteriolar diameter during neuronal activity is about 6% (compared to 1% with EC NO contributions). The reason for his effect is unclear, but it is possible that when the constant supply of vasodilatory NO (from ECs) is no longer present, the arteriole will develop a more constricted resting tone. Then, during neuronal activation, when a "burst" of NO is produced, there is a larger dilation because the arteriole has more "room to move" (more room to dilate) if the arteriole is already in a more constricted state. This "tone-dependent" dilation will be discussed more in the next section.

8.3.1.2 Wall Shear Stress and O_2 Effects

WSS/O_2 and arteriolar tone/blood flow changes are connected in a complex loop. First: WSS and O_2 concentration determine the levels of NO in the EC/SMC and hence the tone of the arteriole and the blood flow through it. Then: the changed blood flow determines a new flow profile (with a new WSS value) and increased perfusion (with a new O_2 concentration). The new WSS and O_2 concentration closes the loop. We do not attempt to model this feedback at this stage – this is better left to be incorporated into a larger tree model where flow, pressure, WSS and perfusion will be more accurately calculated as part of a cooperating whole. We instead do a simple sensitivity analysis so we can start to understand how the NO model is affected by different background values for WSS (Figure 8.11) and tissue O_2 concentration (Figure 8.10). As in Chapter 7, simple sensitivity analyses are performed by 1) adjusting the

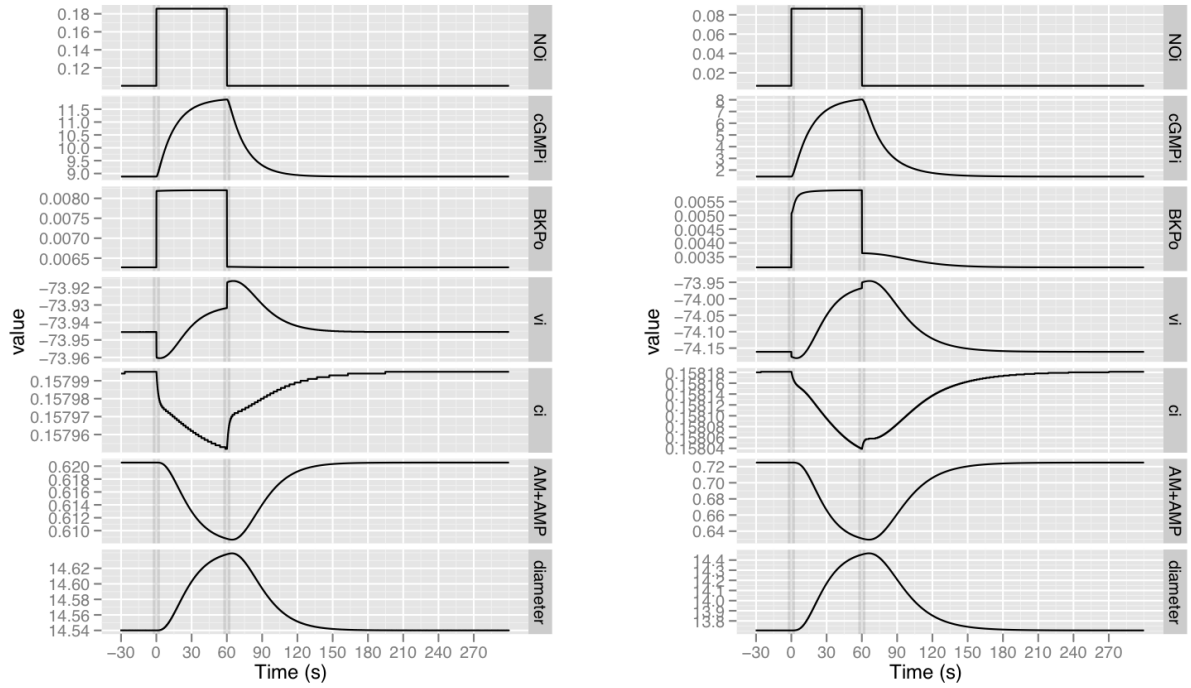

Figure 8.9 SMC response to NO-mediated NVC mechanisms with the contribution from eNOS in endothelial cells included (left hand plot) and omitted (right hand plot). Shown here are SMC NO concentration changes (in μM), SMC cGMP concentration (in μM), voltage (vi, in mV), intracellular Ca^{2+} (also in μM), BK channel open probability (BKPo), AM + AMP, the fraction of attached crossbridges (the states generating a contractile force), and finally, the arteriolar diameter (in μm).

parameter, 2) solving the set of equations again with the new parameter, and 3) plotting the "new" results alongside the results found using the "old" value(s) of the parameter.

A higher baseline O_2 concentration gives a lower baseline NO concentration (Figure 8.10) because O_2 scavenges NO. Higher O_2 concentrations at rest ensures lower levels of resting tone (more relaxed vessels).

Figure 8.11 shows SMC NO concentration and arteriole dilation under different levels of wall shear stress (WSS). Higher levels of WSS result in a more relaxed steady state arteriolar diameter (resting tone). The changes in vessel diameter due to the effects of NO produced during neuronal activation are between 0.5% – 0.8%. Here, as for O_2 , the WSS changes that would result from the diameter change do not feedback into the model; i.e., new diameter-dependent WSS values are not calculated after the diameter changes occur. If we did introduce feedback into the model, we would expect that an increase in shear stress leads to the relaxation of the vessel wall (an increase in the diameter) and thus a decrease in the shear stress; therefore, the entire WSS-arteriole interaction is characterized by the presence of negative feedback.

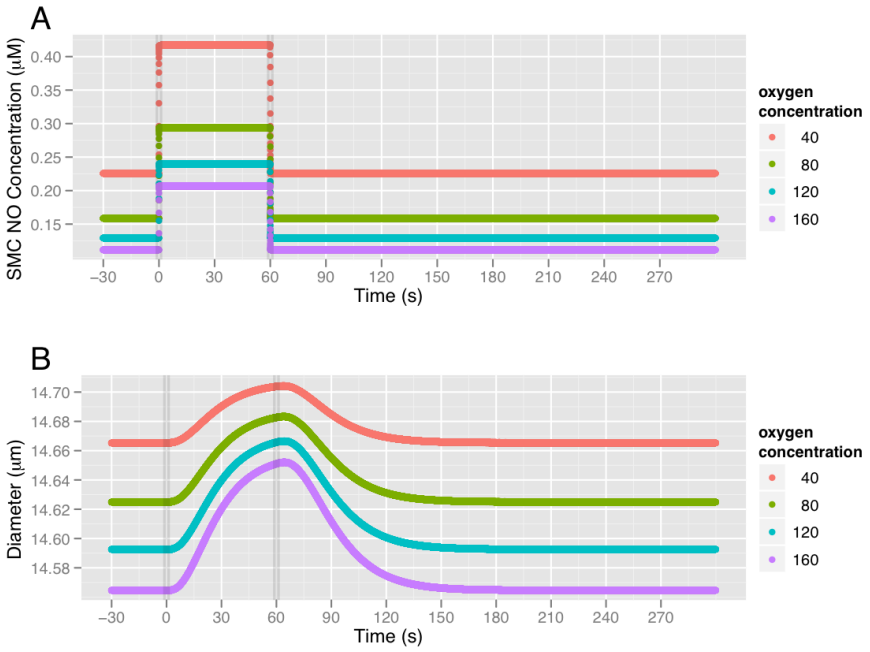

Figure 8.10 NO concentration in the smooth muscle cell under different baseline concentrations of O_2. NO is scavenged by O_2 and a higher O_2 concentration means that NO is scavenged at a faster rate. The changes in vessel diameter due to the effects of NO produced during neuronal activation are between 0.3% and 0.8%. The time taken to achieve maximal dilation is independent of O_2 concentration. Note that the O_2 increases effected by diameter changes are not "fed back" into the model at this stage.

The values of WSS and O_2 concentration, through their exerted effects on vasomodulatory NO, are important determinants of the basal arteriolar tone. The matter of resting tone is not trivial; it is not simply an "initial condition." In fact, resting tone can determine the magnitude and even the polarity (constriction or dilation) of the diameter changes effected by neurovascular coupling signals [23]. In the study of Blanco et al. [23], increases in extracellular K^+ concentration, stimulation of astrocyte Glutamate receptors (mGluR), or application of 11,12-EET all evoked vessel responses that were affected by the resting arteriolar tone. Their data suggests that dilations occur when the resting tone is less than 70% of its initial diameter, i.e., the arteriole is more constricted to begin with. Conversely, constrictions tend to occur when the resting tone is above 70% of the initial arteriolar diameter, i.e., when the arteriole is more relaxed at "rest." Furthermore, larger changes occur when the initial diameter/baseline tone is further from the 70% "setpoint" (for example, larger dilations will occur when the arteriole is relatively more constricted initially). Other studies [101, 106] suggest that NO may have more of a mediating effect than a direct modulating effect. It is possible then that NO serves to establish resting tone, either directly through the pathway modelled here or indirectly through its influence on other agonist pathways.

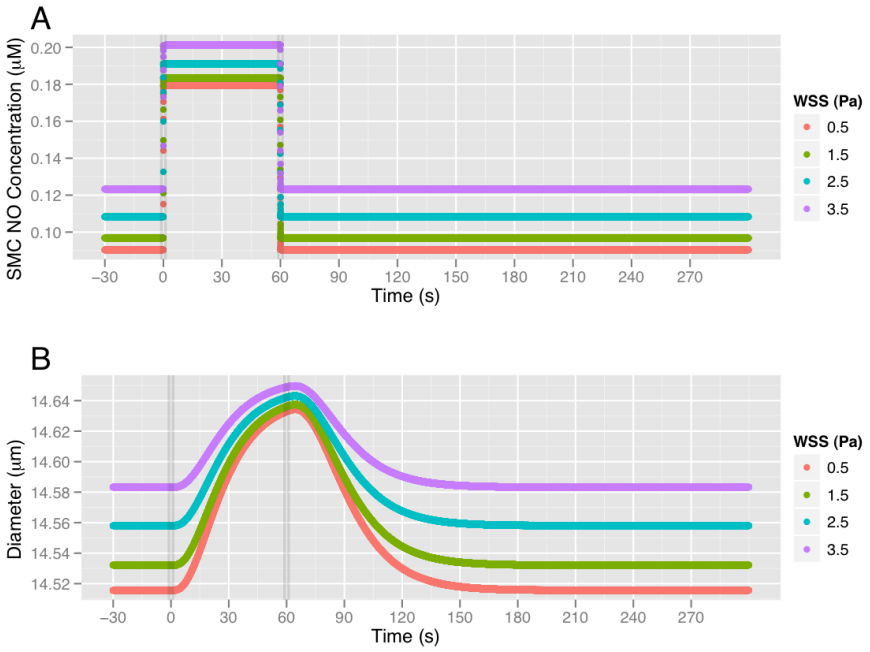

Figure 8.11 Smooth muscle cell NO concentration and arteriolar diameter changes at different baseline levels of wall shear stress (WSS). WSS induces eNOS-dependent NO production in the EC. Higher levels of WSS results in an arteriole that is more relaxed (has a lesser degree of tone). The time taken to achieve maximal dilation is independent of the level of WSS. Note that WSS changes with flow and therefore is influenced by diameter changes; this dependence is not modelled here.

Clearly, there is experimental evidence that tone-dependent vessel behaviour exists [23], and in our model results, we do see larger dilations at more constricted states (Figure 8.9), which could mean that our model also exhibits tone-dependent model behaviour. However, this hypothesis begs the question: how is a tone-dependent relationship actually effected in the model? That is: in this model, how could tone (the value of the diameter) directly lead to cellular changes (of Ca^{2+}, myosin phosphorylation and crossbridge attachment) that would then effect a change in diameter, thus creating a new value of tone?

Answer: the only mathematical formulation in this model that provides a direct link between the level of tone (the diameter of the arteriole) and cellular changes that would effect a new level of diameter is the equation for the flux through the stretch-activated Ca^{2+} (SAC) channel (Equation A.33, Appendix A). In this equation, the radius/diameter of the arteriole determines the activation (or open channel probability) of the SAC channel. Therefore, the diameter of the arteriole can directly affect the value of the Ca^{2+} influx into the SMC, which changes the cytosolic Ca^{2+} concentration. Ca^{2+}-dependent myosin phosphorylation then affects the values of crossbridge attachment, stress development and diameter.

8.3.2 Two Mechanisms of Neurovascular Coupling: NO and K^+/EET

This section focuses on the individual and additive effects that the NO-mediated and K^+/EET-mediated NVC processes have on the NVU (Figure 8.12).

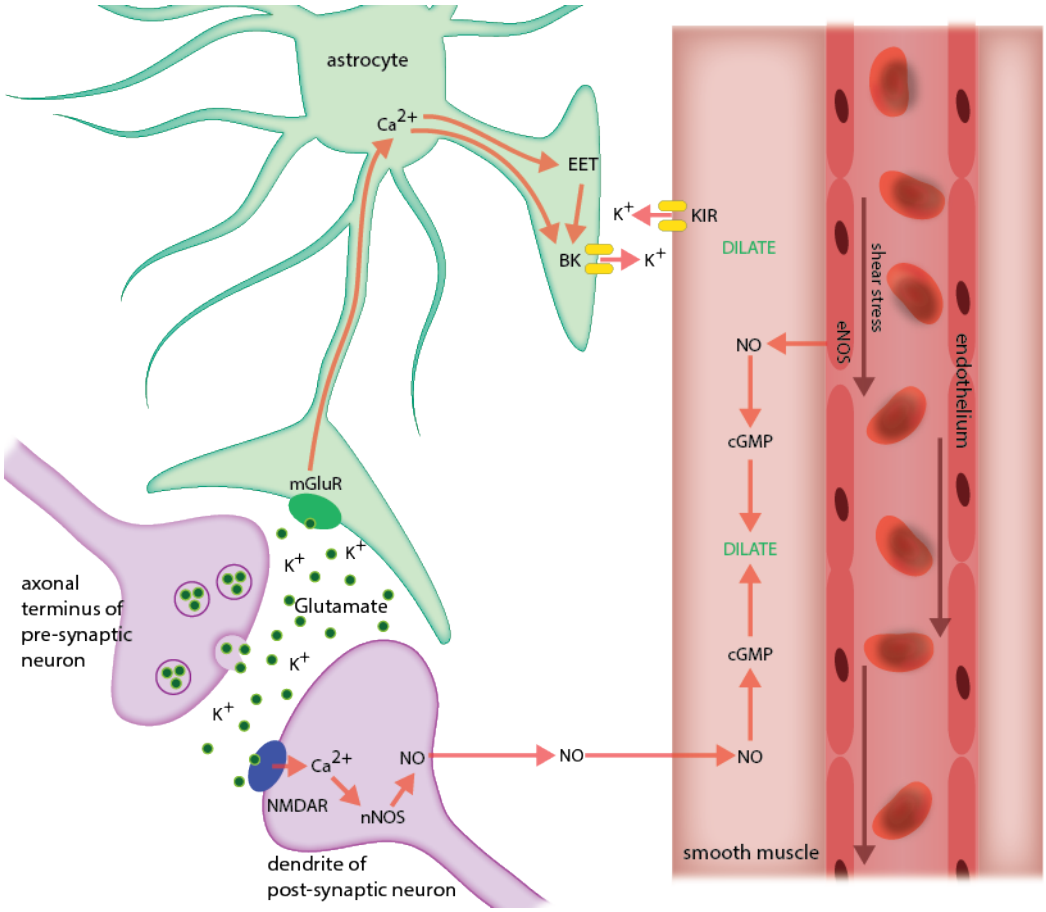

Figure 8.12 Neurovascular coupling: K^+/EET- and NO- mediated processes. Note that this figure is a copy of that shown in Chapter 6 (Figure 6.2).

Figure 8.13 compares the original NVC K^+/EET model results (from the previous chapter) with the NO model results from this chapter. SMC KIR channel open probability (KIRPo) as well as SMC BK channel open probability (BKPo) have been shown for completeness.

In the NO-only case (Figure 8.13 – left plot), very small pvK changes are due to the small changes in KIRPo and BKPo induced by small voltage changes. The basal (resting) diameter of the arteriole is 14.54 μm and the change due to neuronal activation is 1% when simulated using the NO-only model.

When the K^+/EET pathway alone is modelled (Figure 8.13 – right plot), voltage (vi) and calcium (ci) changes in the SMC are much larger than that in the NO-only case (Figure 8.13 –

left plot). This is indicative of the fact that the K^+/EET model provides vasodilation through Ca^{2+}-dependent relaxation, as opposed to the NO model which predominantly relies on calcium desensitization of the contractile apparatus (where relaxation can occur even without changes in SMC Ca^{2+}). The basal arteriolar diameter is larger in the K^+/EET-only model (18.1 μm), meaning that the conditions of the model are such that the arteriole develops less tone at rest – this is potentially due to different definitions of K_2 and K_5 (dephosphorylation rate constants) in the two models (in the K^+/EET model, K_2 and K_5 are constants, and in the NO model, K_2 and K_5 are functions of cGMP (Equation 8.29)). The diameter change due to neuronal activation is 3% for the K^+/EET model. From experiment [127, 145], we would expect that the NO mechanism would effect a similar dilation to that of K^+/EET mechanisms. However, in our results, NO signals only effect a dilation half that of the K^+/EET signal. It is possible that, as discussed in [13], the inhibitory action that NO exerts on the constricting 20-HETE signal (not modelled here) may in fact underlie a considerable fraction of NO's "dilating" effect.

The latency (time till the onset of the arteriolar response) is smaller for the NO-only model ($\approx$ 5 s) than in the K^+/EET-only model ($\approx$ 10 s). Rise times for the arteriolar diameter changes (times to maximal dilation) are similar for the two models (maximum changes occur at 60 s – the end of the activation period). Generally, it would be expected that NO signals would act faster than K^+/EET signals, as NO diffuses rapidly through the extracellular space and acts directly on processes in the SMC, whereas the K^+/EET pathway relies on several ionic transports of K^+ occurring one after another. So although the latency of the response is smaller for the NO results than it is for the K^+/EET results, the rise time is still comparable, and similarly slow. Hillman et al. [74] studies vessel dilation in the rat brain following tactile forepaw stimulation. Their data shows a maximal dilation 5 s after the onset of a 4 s stimuli, considerably quicker than our results. There may be several explanations for the discrepancy in these time scales. Firstly, as previously discussed in Chapter 7, the model (or model parameters) we use to simulate the myosin phosphorylation kinetics may not describe the physiological process of myosin phosphorylation accurately; for example, there is evidence to suggest that there are alternative modes of myosin phosphorylation that we have not attempted to model [149]. Secondly, our model is far from complete; it is possible that other NVC signals could be responsible for the very rapid NVC response, whereas those modelled are responsible for a later, attenuating response. We are yet to develop model equations to describe other known NVC processes, such as those involving 20-HETE. Further, we cannot even begin to develop a clear picture until there has been more experimental investigation that can characterize *unknown* NVC mechanisms (those that still act to effect NVC after all known cellular targets are blocked).

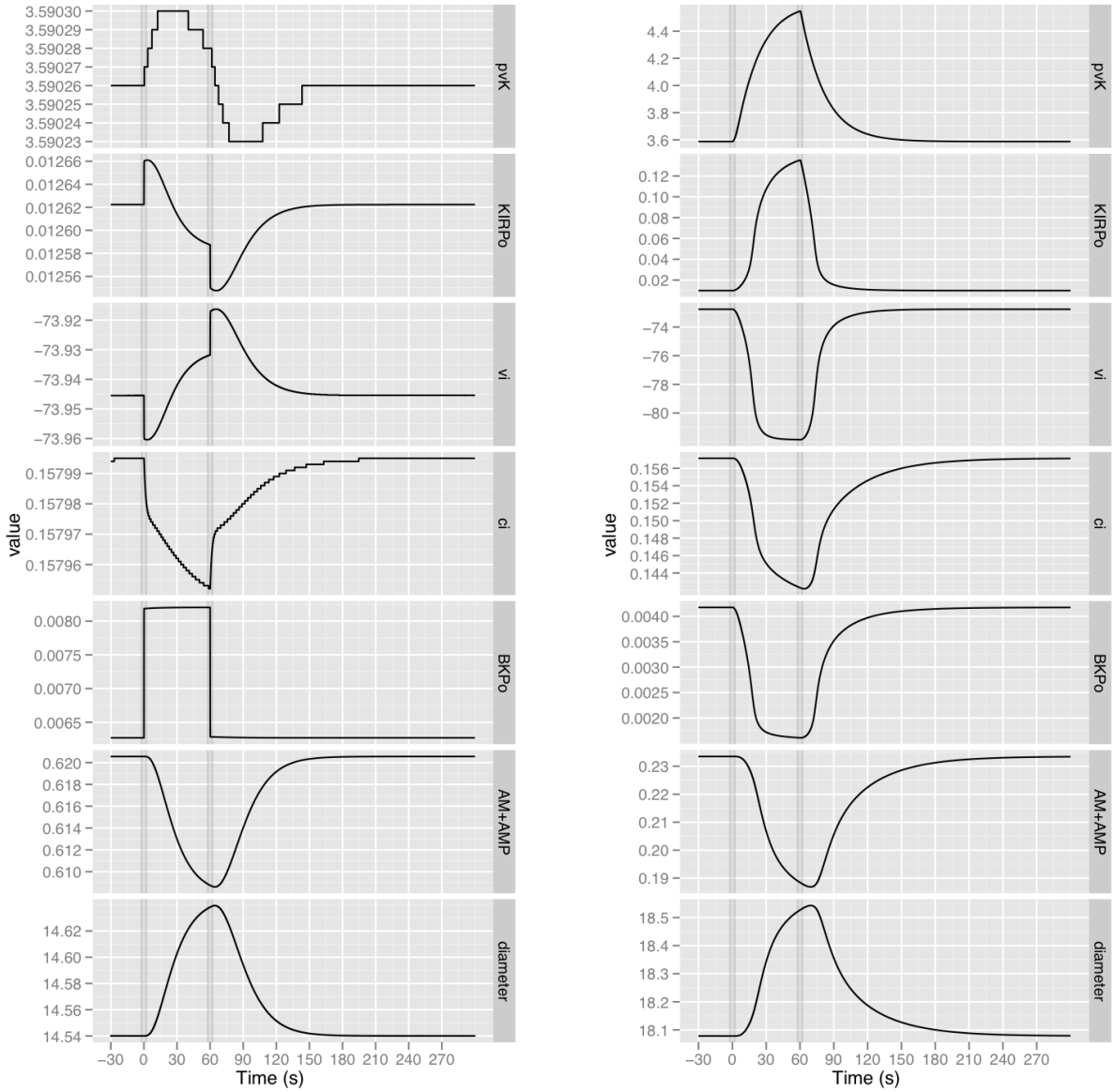

Figure 8.13 Comparing model results when *only* NO-mediated (left side plot) or *only* K^+/EET-mediated (right side plot) processes are considered. Shown are perivascular potassium concentration (pvK, in mM), SMC voltage (vi, in mV), SMC Ca^{2+} concentration (ci, in μM), SMC BK and KIR channel open probabilities, AM + AMP (the fraction of MLC in the attached state) and vessel diameter (in μm). Please note that the "stair-like" appearance of the data in the left hand pvK plot (and also in Figure 8.14) is a consequence of the plotting tool used (where each modelled data point plotted is joined by a straight line rather than a smooth fitted curve) and the large step size used by the RKSUITE solver (a large step size is sufficient for calculating numerical values for pvK in this simulation because the changes in pVK are so small).

In Figure 8.14, NO model results with (right side) and without (left side) the contribution of the K^+/EET model are compared. Note that we are not modelling the inhibitive interactions that potentially exist between these two, just the additive effect of modelling the two neurovascular

coupling pathways at once.

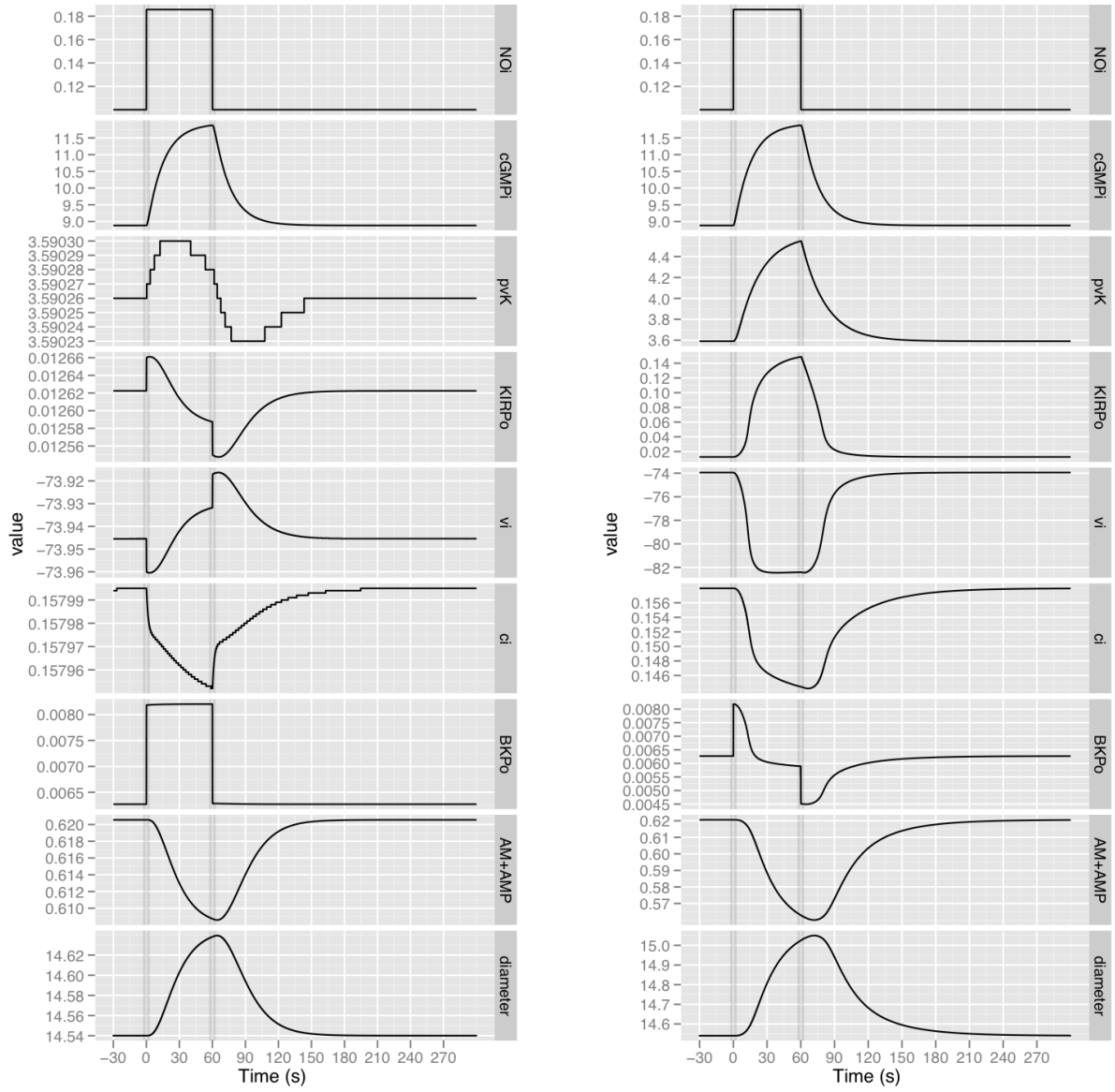

Figure 8.14 The figure on the left shows the model results when *only* NO pathways are modelled. The figure on the right shows the results when *both* NO and K^+/EET mechanisms are simulated together. Shown are SMC NO concentration (in μM), SMC cGMP concentration (in μM), SMC voltage (in mV), SMC Ca^{2+} concentration (ci, in μM), perivascular potassium concentration (pvk, in mM), SMC BK and KIR channel open probabilities, AM + AMP (the fraction of MLC in the attached state) and vessel diameter (in μm). Including K^+/EET in the simulation gives a larger dilation (4% compared to 1%) but the time scale remains the same.

When both pathways are simulated together (Figure 8.14), the magnitude of the change is larger (4%) than when only NO signals are considered (1% change). Rise times and latencies are similar in both simulations. Time to return to baseline after neuronal activation is longer

in the combined NO and K^+/EET model ($\approx$ 270s) than the NO-only model ($\approx$ 180 s); this is potentially due to "lingering" K^+ in the perivascular space – that which has not yet been cleared away via clearance mechanisms – exerting its effects on SMC processes.

SMC NO (and hence cGMP) dynamics are unchanged when K^+/EET are added, as expected (K^+/EET are astrocyte-based signals and therefore do not affect the largely neuronal-based NO pathways). The most striking difference between the two compared simulations in Figure 8.14 is the changes in the SMC BKPo. Small increases in BKPo occur in the NO-only model (as previously discussed) due to the effects of NO/cGMP on BK channels. Therefore, small increases initially occur in the combined model (plot on the right hand side) due to the NO effects, but then decreases are seen due to the influence exerted by the (more delayed) KIR-induced changes in vi and ci (both of which gate the *voltage*- and *calcium*-gated BK channels).

Peng et al. [127] study changes in cerebral blood flow in rats (induced by forepaw stimulation) by blocking the NO and K^+/EET pathways. Blocking either of these vasodilatory routes reduces the increase in cerebral blood flow (CBF) by about 60%. Paradoxically, when *both* pathways are blocked, the decrease is still 60%. They suggest that there exists some interaction between the two mechanisms; such interactions are yet to be accounted for in our model. We also do not model the potential feedback effects that our arteriolar diameter changes may have (on O_2 or WSS or pressure). These potentially important interactions will be added when this NVC model is incorporated with a branching vascular tree model.

8.4 Summary

In this model, NO exerts its vasodilatory effects via neuronal *and* endothelial sources. With both sources included, the model achieves a 1% dilation due to neuronal activation (simulated by synaptic glutamate release). When the endothelial contribution to NO production is omitted, the arteriole is more constricted at baseline (13.7 μm compared to 14.54 μm when both sources are included). Without the EC NO contribution, the arteriolar change in diameter during neuronal activity is 6%. This larger dilation in the more constricted vessel may be due to the fact that the vessel is "pre-constricted" due to the absence of EC NO and therefore has more "room to move", i.e., dilate. The continuous supply of NO from WSS-activated endothelial sources could be responsible for the development of the resting tone, whereas neuronal NO may provide the actual dilating signal after neuronal activation occurs. Perhaps then, NO has a dual purpose in our NVC model: 1) it directly *mediates* NVC through release by neuronal sources, and 2) it *in*directly *modulates* (or *attenuates*) the size of the NVC response by determining the baseline tone. Our findings provide support for two hypotheses put forward by the two experimental groups: Lindauer et al. [101], who postulate that NO acts more as a *modulator* rather than a

direct *mediator* of NVC, and Blanco et al. [23], who show that the magnitude and polarity of NVC responses to certain agonists are tone-dependent.

Arteriolar dilations are smaller (1%) due to NO signals than for K^+/EET signals (3%). When both of these are modelled together, there is a 4% dilation. Although latencies decrease for NO mechanisms as compared to K^+/EET, rise times are similar. Both produce arteriolar dilations slower than that seen in experiment. We postulate that either: 1) the mechanisms modelled are not those responsible for rapid NVC but form part of slower "attenuating" NVC control, or 2) the Ca^{2+}-dependent myosin phosphorylation model that we use is not capable of simulating a fast response (either because SMC Ca^{2+} changes are too small or because important myosin phosphorylation and crossbridge attachment pathways are missing).

Our current NVC model could be improved by the incorporation of: 1) partial differential equations to more accurately describe NO diffusion, 2) a more complete model of myosin phosphorylation and crossbridge attachment, and 3) equations describing other known NVC signals, like that of 20-HETE, including descriptions of the various known interactions between them (such as the inhibition of EET and 20-HETE pathways by NO). Furthermore, we acknowledge that this model has very limited scope in the form of a single neurovascular unit; we must incorporate NVC cellular models into a physiological model of the cerebrovasculature. The process of blood flow autoregulation in the brain does not occur through the solitary efforts of a single cell or a single NVU. Regulation occurs as an integrated multi-scale, multi-level, multi-unit process. Investigations into a particular cellular process *must* involve an investigation into the larger environment in which that cell resides.

Chapter 9

Conclusions and Future Work

9.1 Summary and Key Findings

In this project, we first developed a foundation model of the component cells of the neurovascular unit (NVU), including the astrocyte and both active layers of the arteriole (smooth muscle cells (SMCs) and endothelial cells (ECs)). To accomplish this, we adapted and extended previous models found in the literature. Our foundation model, with the important cells and cell components included, forms a physiologically sound base on which any number of hypothesized or known regulatory pathways can be incorporated and analyzed.

We then created an extension of the foundation model that simulates neurovascular coupling (NVC) using EET and K^+ as the major signalling pathways. We were able to achieve arteriolar dilations similar in magnitude (3%) to those observed experimentally. Using this model, we also investigate the effect where increased perivascular K^+ causes first an arteriolar dilation and then a constriction. We suggest that the interaction of the changing smooth muscle cell membrane potential and the changing K^+-dependent resting potential of the SMC KIR channels are responsible for this effect.

There exist differing views about the exact mechanism and effects of K^+ movement in and out of the space surrounding neurons and glia. In our model of K^+ signalling, both the depolarization of the astrocyte membrane and the produced EETs act on astrocyte endfoot BK channels to cause K^+ efflux into the perivascular space, with the depolarizing effect taking dominance. Furthermore, our simulations demonstrate that the arteriolar behaviour is profoundly affected if the rate of perivascular K^+ clearance, or the volume ratio between the perivascular space and astrocyte, changes. These analyses will further add to the ongoing debate and discussion that surrounds the distinct, but connected, phenomena known as K^+ siphoning, K^+ buffering and K^+-mediated NVC. They may also aid in our understanding of Cortical Spreading Depression (CSD), in which K^+ homeostasis is known to be affected.

In a further extension to the model, NO exerts its vasodilatory effects via sporadic neuronal

and continuous endothelial sources. With both sources included, the model achieves a 1% dilation due to neuronal activation. When the endothelial contribution to NO production is omitted, the arteriole is more constricted at baseline. Without the EC NO contribution, the arteriolar change in diameter during neuronal activity is greater (6%). We hypothesize that NO has a dual purpose in NVC: 1) it directly *mediates* NVC through release by neuronal sources, and 2) it indirectly *modulates* the size of the NVC response by determining the baseline tone via EC sources. Our findings provide support for two existing hypotheses: 1) that NO acts more as a modulator than a mediator of NVC, and 2) that the magnitude of NVC responses is tone-dependent.

Both mechanisms of NVC (K^+/EET-mediated and NO-mediated) produce arteriolar dilations slower than that seen in experiment. We postulate that either: 1) the modelled mechanisms form part of a slower attenuating NVC control mechanism and that we are yet to model the mechanisms responsible for rapid NVC, or 2) the Ca^{2+}-dependent myosin phosphorylation model that we use is simply not capable of simulating a fast response (potentially because SMC Ca^{2+} changes are too small, the SMC resting membrane potential is too negative, or because important myosin phosphorylation and cross-bridge attachment pathways are missing).

Finally, our NVC models have allowed us to replicate and explain some of the phenomena seen in both NVC-oriented and clinically-oriented experimental research. This project highlights the fact that mathematical modelling can be used as a tool to understand biological processes in a way that physical experiment cannot always do, and most importantly, can help to elucidate the cellular processes that induce or accompany our most debilitating diseases.

9.2 Future Work

This model – of NVC working within a single NVU – is incomplete. NVC encompasses a large number of known, unknown and hypothesized pathways, only two of which were investigated in this thesis. In future studies, other NVC mechanisms, such as those involving 20-HETE and pericytes, will be modelled and included. These future models, and the current model, will also benefit from an in-depth validation and a numerical analysis of the dominant mechanisms and parameters (accomplished via the non-dimensionalization of all equations and a sensitivity analysis on the full parameter set).

A common theme found throughout this thesis is that of dimensional consistency in the model equations. One of the largest challenges for any physiological modeller is to develop a model that possesses consistent units and sensible parameters at the same time as building on the work of others who have developed their models (or experimental data) in a variety of different units (or experimental conditions). Building physiological models is a complex

task – developing, documenting, validating, and ensuring consistency in model equations is difficult. In fact, it is rare to find a published model that is completely free of dimensional inconsistencies and misquoted parameters. This need for consistency in the development of physiological models has already been understood by the scientific community and has lead to the development of a group of collaborative "Physiome projects." These projects – including the Human Brain, Cardiome, Lung Physiome and Kidney database – involve the collection of models that have reached certain standards in verification, validation, and documentation [18]. Learning from, and contributing to, these projects and databases may be the best way to ensure model progress and consistency occurs in future extensions to this model.

Our focus in this study was the development of a model for a *single* NVU. However, the complex mechanisms of blood flow regulation and NVC do not occur in isolation in a single unit. They operate as just a tiny part of a larger, integrated, multicellular, and multiplex whole. It is crucial that mathematical investigations into a particular cellular regulation pathway involve the larger environment in which that cell resides. Therefore, a major focus of future work will be the integration of this cellular NVC model into the vascular tree model that has been created by the University of Canterbury's Brain Group [42]. This will create a *physiological* model of blood flow to and within the *entire* cerebrovasculature – a whole "computational brain." Only in creating such a model will we gain an adequate understanding of the true physiological importance of the cellular pathways that we have attempted to model here. However, it is important to understand that the addition of complex cellular models to an already complex representation of the vascular tree will greatly increase the computational expense of the problem. To put the scale of this project into perspective: if our single NVU model requires 15 seconds of CPU time, the solution of an entire brain (which possesses more than 100 billion NVUs) would require a single CPU to be working for 47 millennia. In practice, such a model can only be solved using massively parallel high performance computers such as those belonging to BlueFern, the University of Canterbury's supercomputing facility. Further simplification of the NVU model will also be necessary to reduce computational time – numerical analyses will determine which terms and equations can be safely removed without significantly affecting model behaviour.

Finally, it is not enough to only understand the cellular pathways as they occur normally in a whole brain. It is also essential to understand what effects pathological processes have. We hope that in the future the disease processes involving vascular, neuronal and astrocytic cells, and drugs designed to target these processes, can too be simulated and investigated on our "computational brain."

9.3 Review of Project Objectives

The overall objectives of this project were to build a mathematical model of NVC and investigate the model's response to known physiological (and pathological) changes. In order to achieve these overall objectives, the following key goals were identified:

1. Conduct a review of the current neurovascular (smooth muscle, endothelial and astrocyte cell) models in the literature

2. Construct a working model of the NVU using previous cell models and additional physiological information

3. Analyze the contributions of two known NVC mechanisms to blood flow regulation as a whole; namely, 1) a K^+- and EET- based mechanism, and 2) a NO-based mechanism

4. Ensure that the model and its results are communicated in a format that is accessible to all members of the biological science community (experimentalists, clinicians and mathematicians)

The first goal was achieved by the review of the literature presented in Chapter 5. Goals 2 and 3 were achieved through the model development and analysis performed in Chapters 6, 7 and 8. The final goal, Goal 4, was attempted by providing background chapters (Chapters 2, 3 and 4) that explain many of the mathematical and biological terminology and concepts in simple terms.

I believe the most successful aspect of this work was the part of the model that hinted at how the behaviour of the KIR channel is responsible for the dilation/constriction behaviour seen in real vessels. I expect that further research into this phenomenon and its relationship to cortical spreading depression could yield extremely interesting, and clinically-relevant, findings. The NO-related model equations are the least developed aspect of this work.

Of course, when I began this work four years ago, I was tremendously ambitious and hoped to produce a "perfect" model which would be able to replicate all experimental observations made to date, and would also be capable of answering all of the questions I had about blood flow in the brain. I have answered some of my questions, but I have also created many more. It is tempting to be disappointed that my model results do not more closely fit experimental data. However, as discussed in Chapter 2, "the point of mathematical models is not to fit the data but to sharpen the questions." It is also true that the paradox of the mathematical modeller is this: if we knew how it worked, the model would be perfectly correct (and also very easy to develop), but then, if we already knew how everything worked, the model would be redundant.

The questions I have now are based on a much better understanding of the subject area – they are much "sharper" than they were four years ago. It seems then that one of my objectives should have been "to ask better questions." Better questions are those that steer myself and others away from the dark alleys and instead move us towards the ones that offer elucidation. The asking of better questions is the making of a better scientist. I will therefore continue to work on the science of question-asking. This will be my ongoing objective.

Appendix A

Model Equations

All equations not described in the main text are outlined in this Appendix Chapter.

A.1 Smooth Muscle and Endothelial Cell Model

The smooth muscle cell (SMC) and endothelial cell (EC) model is taken from Koenigsberger et al. [85]. The equations in their model are reproduced in this section for reference. All additions and extensions to this model are described in the main text (Chapters 6, 7, and 8).

A single SMC i is described by five variables:

- the calcium concentration in the cytosol c_i,
- the calcium concentration in the SR s_i,
- the cell membrane potential v_i,
- the open state probability w_i of BK channels, and
- the IP_3 concentration I_i.

A single EC j is modelled using four variables:

- the cytosolic calcium concentration c_j,
- the calcium concentration in the ER s_j,
- the cell membrane potential v_j, and
- the IP_3 concentration I_j.

Cells can be coupled to their neighbour via gap junction connections in three ways: by electrical, calcium, and IP_3 coupling.

A.1.1 Smooth Muscle Cell Differential Equations

The SMC model is as follows:

The change in the cytosolic calcium concentration is the summation of the fluxes moving calcium in and out of the cytosolic space. Each "J" term here represents a different calcium flux in and out of the cytosol (to and from the extracellular space, sarcoplasmic reticulum, or neighbouring cells).

$$\frac{\mathrm{d}c_i}{\mathrm{d}t} = J_{IP3_i} - J_{SRuptake_i} + J_{CICR_i} - J_{extrusion_i} + J_{leak_i} - J_{VOCC_i} + J_{Na/Ca_i} + 0.1J_{stretch_i} \tag{A.1}$$

The change in concentration of calcium ($\frac{\mathrm{d}c_i}{\mathrm{d}t}$) and the fluxes ("J" terms) are all expressed in $\mu\mathrm{Ms}^{-1}$.

The change in the concentration of calcium in the sarcoplasmic reticulum (SR) depends on the fluxes in and out of these calcium "stores" (i.e. fluxes to and from the cytosol).

$$\frac{\mathrm{d}s_i}{\mathrm{d}t} = -J_{SRuptake_i} - J_{CICR_i} - J_{leak_i} \tag{A.2}$$

Again, the change in concentration of calcium in the stores ($\frac{\mathrm{d}s_i}{\mathrm{d}t}$) and the fluxes are all expressed in $\mu\mathrm{Ms}^{-1}$.

Borrowing from electrical theory, we have the relationship $\frac{dv}{dt} = \frac{I}{C}$ (with C=capacitance, v=voltage, and I=current). Therefore, the following differential equation describes the change in membrane potential, where fluxes of ions across the cell membrane (essentially "currents") are related to the change in membrane potential by a scaling factor γ_i (which is related to the inverse of membrane capacitance and carries units of $\mathrm{mV}\mu\mathrm{M}^{-1}$).

$$\frac{\mathrm{d}v_i}{\mathrm{d}t} = \gamma_i \left(J_{Na/K_i} - J_{Cl_i} - 2J_{VOCC_i} - J_{Na/Ca_i} - J_{K_i} - J_{stretch_i} \right) + V^{SMC-EC}_{coupling_i} \tag{A.3}$$

Fluxes coming into the cell are positive (effluxes are negative), and coefficients of these fluxes represent the valency of the ion (2 for Ca^{2+} and 1 for all other fluxes). v_i has units of mV.

The equilibrium distribution of open channel states for the voltage- and calcium-activated potassium channels (BK channels) are described by Koenigsberger et al. [85] as $K_{activation_i}$. The time course of the fraction of K^+ channel open states is described after Morris and Lecar [115] by the first-order kinetics of opening, as shown below:

$$\frac{\mathrm{d}w_i}{\mathrm{d}t} = \lambda_i (K_{activation_i} - w_i) \tag{A.4}$$

where λ_i is the rate constant for opening (in s^{-1}).

Finally, the change in IP_3 concentration is the sum of IP_3 fluxes:

$$\frac{dI_i}{dt} = -J_{degrad_i} + J_{I-coupling_i}^{SMC-EC} \tag{A.5}$$

A.1.2 Endothelial Cell Differential Equations

The EC model is given by equations very similar in formulation to the SMC model described above:

$$\frac{dc_j}{dt} = J_{IP3_j} - J_{ERuptake_j} + J_{CICR_j} - J_{extrusion_j} + J_{leak_j} + J_{cation_j} + J_{0_j} + J_{stretch_j} \tag{A.6}$$

$$\frac{ds_j}{dt} = J_{ERuptake_j} - J_{CICR_j} - J_{leak_j} \tag{A.7}$$

$$\frac{dv_j}{dt} = -\frac{1}{C_{mj}}\left(I_{K_j} + I_{R_j}\right) + V_{coupling_j}^{EC-SMC} \tag{A.8}$$

$$\frac{dI_j}{dt} = -J_{degrad_j} + J_{I-coupling_j}^{EC-SMC} \tag{A.9}$$

Note that in Equation A.8, the electrical capacitance of the EC membrane (C_{mj}, in pF) is used in this equation (as opposed to the scaling factor γ_i used in the SMC voltage DE – Equation A.3.) The fluxes/currents I_{K_j} and I_{R_j} are therefore described as *electrical* fluxes (in fA or pS·mV) instead of *molar* fluxes in μMs^{-1}. A basic description of the relationship between electrical and molar fluxes is given in the subsection **Dimensional Consistency and Unit Conversions** in Chapter 6.

A.1.3 Expressions in the Differential Equations

The various terms that appear in Equations A.1 to A.9 are described by the following expressions given below. (Note the i subscript for the SMC and the j subscript for the EC).

The calcium fluxes

$$J_{IP3_i} = F_i \frac{I_i^2}{K_{ri}^2 + I_i^2} \tag{A.10}$$

and

$$J_{IP3_j} = F_j \frac{I_j^2}{K_{rj}^2 + I_j^2} \tag{A.11}$$

model the release of calcium from IP_3 sensitive stores in the SMC and EC.

$$J_{SRuptake_i} = B_i \frac{c_i^2}{c_i^2 + c_{bi}^2} \tag{A.12}$$

and

$$J_{ERuptake_j} = B_j \frac{c_j^2}{c_j^2 + c_{bj}^2} \tag{A.13}$$

model the uptake of calcium into the SMC sarcoplasmic and EC endoplasmic reticulum, respectively.

$$J_{CICR_i} = C_i \frac{s_i^2}{s_{ci}^2 + s_i^2} \frac{c_i^4}{c_{ci}^4 + c_i^4} \tag{A.14}$$

and

$$J_{CICR_j} = C_j \frac{s_j^2}{s_{cj}^2 + s_j^2} \frac{c_j^4}{c_{cj}^4 + c_j^4} \tag{A.15}$$

describe the calcium-induced calcium release (CICR).

$$J_{extrusion_i} = D_i c_i \left(1 + \frac{v_i - v_d}{R_{di}}\right) \tag{A.16}$$

and

$$J_{extrusion_j} = D_j c_j \tag{A.17}$$

represent the calcium extrusion by Ca^{2+}-ATPase pumps.

Leak currents from the SR/ER are given as

$$J_{leak_i} = L_i s_i \tag{A.18}$$

and

$$J_{leak_j} = L_j s_j \tag{A.19}$$

$$J_{VOCC_i} = G_{Cai} \frac{v_i - v_{Ca_{1i}}}{1 + \exp\left[-\left(v_i - v_{Ca_{2i}}\right)/R_{Cai}\right]} \tag{A.20}$$

is the calcium influx through VOCCs.

$$J_{Na/Ca_i} = G_{Na/Cai} \frac{c_i}{c_i + c_{Na/Cai}} \left(v_i - v_{Na/Cai}\right) \tag{A.21}$$

is the flux of calcium exchanging with sodium in the Na^+/Ca^+ exchange

$$J_{Na/K_i} = F_{Na/Ki} \tag{A.22}$$

is the constant flux due to activation of the Na^+/K^+-ATPase pump

$$J_{Cl_i} = G_{Cli}\left(v_i - v_{Cli}\right) \tag{A.23}$$

models the flux through chlorine channels.

$$J_{K_i} = G_{Ki} w_i \left(v_i - v_{Ki}\right) \tag{A.24}$$

is the flux through voltage- and calcium-gated potassium (BK) channels in the SMC.

$K_{activation_i}$ describes the equilibrium distribution of open channel states for the BK channel in the SMC.

$$K_{activation_i} = \frac{\left(c_i + c_{wi}\right)^2}{\left(c_i + c_{wi}\right)^2 + \beta_i \exp\left[-\left(v_i - v_{Ca_{3i}}\right)/R_{Ki}\right]} \tag{A.25}$$

J_{cation_j} is the flux through two non-selective cation channels in the EC.

$$J_{cation_j} = G_{catj}\left(E_{Caj} - v_j\right)\frac{1}{2}\left(1 + \tanh\left(\frac{\log(c_j) - m_{3_{catj}}}{m_{4_{catj}}}\right)\right) \tag{A.26}$$

J_{0_j} is the constant calcium influx into the cell.

$$I_{K_j} = G_{totj}\left(v_j - v_{Kj}\right)\left(I_{BK_{Caj}} + I_{SK_{Caj}}\right) \tag{A.27}$$

is the potassium efflux through the BK_{Ca} channel (a large-conductance channel activated by calcium and voltage changes in the EC), and the SK_{Ca} channel (a small-conductance channel only activated by calcium), with:

$$I_{BK_{Caj}} = 0.2\left(1 + \tanh\left(\frac{\left(\log(c_j) - c\right)\left(v_j - b_j\right) - a_{1j}}{m_{3bj}\left(v_j + a_{2j}\left(\log(c_j) - c\right) - b_j\right)^2 + m_{4bj}}\right)\right) \tag{A.28}$$

and

$$I_{SK_{Caj}} = 0.3\left(1 + \tanh\left(\frac{\log(c_j) - m_{3sj}}{m_{4sj}}\right)\right) \tag{A.29}$$

Important note about dimensional consistency in Equations A.26, A.28 and A.29: taking the log of a dimensioned quantity – as is done in these equations (e.g., $\log(c_j)$) – makes it difficult to make sense of the physical units used. However, these particular equations were not

developed from descriptions of the underlying physical mechanisms occurring in ion channel opening (see Appendix C). They are instead phenomenological: the sigmoidal (hyperbolic tangent or tanh) relationships in Equations A.26, A.28 and A.29 are simply fitted to experimental data. Koenigsberger et al. [85] publishes these "fitting parameters" ($m_{3_{cat\,j}}$, $m_{4_{cat\,j}}$, c, b_j, a_{1j}, m_{3bj}, a_{2j}, m_{4bj}, m_{3sj} and m_{4sj}) in terms of dimensioned quantities. This is misleading, especially when other model equations are dimensioned correctly. These parameters are therefore listed in this thesis (in Table B.2, Appendix B) with *dimensionless* units to avoid confusion.

The residual current combining Cl^- and Na^+ currents in the EC is written:

$$I_{R_j} = G_{Rj}\left(v_j - v_{rest\,j}\right) \tag{A.30}$$

and the IP_3 fluxes for the SMC

$$J_{degrad_i} = k_i I_i \tag{A.31}$$

and the EC

$$J_{degrad_j} = k_j I_j \tag{A.32}$$

model IP_3 degradation.

A.1.4 Stretch-Activated Calcium Channels

The myogenic (pressure-dependent) response is effected in this model via SACs (stretch-activated channels). These mechano-sensitive channels (present in SMCs and ECs) increase intracellular calcium levels by effecting a direct influx of extracellular calcium, which depolarizes the SMCs and leads to a further calcium influx through VOCCs. J_{stretch_i} and J_{stretch_j} give the SAC-activated calcium fluxes in the SMC and EC, respectively.

$$\begin{aligned} J_{\text{stretch}_i} &= \frac{G_{stretch}}{1+\exp[-\alpha(\sigma-\sigma_0)]}\left(v_i - E_{SAC}\right) \\ &= \frac{G_{stretch}}{1+\exp\left[-\alpha\left(\frac{\Delta pr}{h}-\sigma_0\right)\right]}\left(v_i - E_{SAC}\right) \end{aligned} \tag{A.33}$$

$$\begin{aligned} J_{\text{stretch}_j} &= \frac{G_{stretch}}{1+\exp[-\alpha(\sigma-\sigma_0)]}\left(v_j - E_{SAC}\right) \\ &= \frac{G_{stretch_{EC}}}{1+\exp\left[-\alpha\left(\frac{\Delta pr}{h}-\sigma_0\right)\right]}\left(v_j - E_{SAC}\right) \end{aligned} \tag{A.34}$$

The constants E_{SAC} and $G_{stretch}$ (or $G_{stretch_{EC}}$) are the reversal potential and the whole cell conductance for SACs. $1+\exp\left[-\alpha\left(\frac{\Delta pr}{h}-\sigma_0\right)\right]$ represents the open probability of SACs where σ is the cell membrane tensile stress. This stress can also be rewritten (using Laplace's

Law) as $\frac{\Delta pr}{h}$. Note that the coefficient 0.1 of $J_{stretch_i}$ in Equation A.1 allows for the fact that Ca^{2+} is divalent (has a valency of 2) and constitutes approximately 20% of the total SAC current.

Koenigsberger et al. [85] model a large arteriole (100 μm in diameter), whereas we are interested in modelling a smaller terminal (pre-capillary) arteriole (20 μm in diameter). Therefore, in our model, we "up-regulate" (increase) the conductance of the SAC ($G_{stretch}$) to reflect the increased responsiveness to pressure that smaller arterioles experience (at least in the coronary vasculature [83]).

A.1.5 Coupling between Endothelial Cell and Smooth Muscle Cell

Heterocellular electrical coupling between SMCs and ECs (in each direction) is modelled by the terms:

$$V_{coupling_i}^{SMC-EC} = -G(v_i - v_j) \tag{A.35}$$

$$V_{coupling_j}^{EC-SMC} = -G(v_j - v_i) \tag{A.36}$$

Heterocellular IP_3 coupling between SMCs and ECs (in each direction) is modelled by the terms:

$$J_{I-coupling_i}^{SMC-EC} = -P_{\mathrm{IP}_3}(I_i - I_j) \tag{A.37}$$

$$J_{I-coupling_j}^{EC-SMC} = -P_{\mathrm{IP}_3}(I_j - I_i) \tag{A.38}$$

A.1.6 Corrections to Koenigsberger et al. [85] Model

In [85], J_{stretch_j} is missing from Equation A.8 – we include this term in our model equation. J_{stretch_j} is included in Equation A.6 in [85] but with inconsistent units. We convert J_{stretch_j} from the inconsistent units of $\mu\mathrm{Ms}^{-1}$ to the consistent units of fA (fCs^{-1}) by multiplying by the scaling factor $\left(F \times \mathrm{v}_{EC} \times 10^9\right)$, where F is Faraday's constant (in Cmol^{-1}) and v_{EC} is the volume of the EC (in L). A description of this sort of conversion is given in the subsection **Dimensional Consistency and Unit Conversions** in Chapter 6, but is also given below in Equation A.39.

$$\begin{aligned}
\left[\text{molar flux in } \frac{\mu\text{M}}{\text{s}}\right] \times F \frac{\text{C}}{\text{mol}} \times \text{v}_{EC}\,\text{L} \times \frac{10^9\ \text{fM}}{1\ \mu\text{M}} &= \left[\text{electrical flux in } \frac{\text{fC}}{\text{s}}\right] \\
\left[\text{molar flux in } \frac{\mu\text{M}}{\text{s}}\right] \times (F \times \text{v}_{EC})\ \frac{\text{C}}{\text{M}} \times \frac{10^9\ \text{fM}}{1\ \mu\text{M}} &= \left[\text{electrical flux in } \frac{\text{fC}}{\text{s}}\right] \\
\therefore \quad \left[\text{molar flux in } \frac{\mu\text{M}}{\text{s}}\right] \times \left(F \times \text{v}_{EC} \times 10^9\right) &= \left[\text{electrical flux in } \frac{\text{fC}}{\text{s}}\right] \qquad \text{(A.39)}
\end{aligned}$$

Some of the parameters given in [85] have also been copied incorrectly from their original source; namely, c and m_{3cat}. These parameters are given as $-0.4\ \mu$M and $-0.18\ \mu$M when they should have been $-6.4\ \mu$M and $-6.18\ \mu$M, respectively. We have used the correct values in our model.

A.2 Myosin Phosphorylation and Crossbridge Formation Model

In this NVC model, the cytosolic calcium concentration and the subsequent development of myosin-actin crossbridges in SMCs is related by the crossbridge phosphorylation and latch-state model of Hai and Murphy [65]. In their model:

- An elevation of calcium induces contraction through the formation of crossbridges between myosin and actin
- Myosin can be in four possible states: free non-phosphorylated crossbridges (M), free phosphorylated crossbridges (Mp), attached phosphorylated crossbridges (AMp), and attached dephosphorylated crossbridges (latchbridges) (AM)
- These four states are related by seven rate constants, which were found by Hai and Murphy [65] by fitting their model to experimentally determined time courses of myosin phosphorylation and stress development

The scheme modelled by Hai and Murphy [65] is shown in Figure A.1.

The fraction of myosin in each of the four states is given by the following equations:

$$\frac{\text{d}[M]}{\text{d}t} = -K_{1i}[M] + K_2[Mp] + K_7[Ap] \qquad \text{(A.40)}$$

$$\frac{\text{d}[Mp]}{\text{d}t} = K_4[AMp] + K_{1i}[M] - (K_2 + K_3)[Mp] \qquad \text{(A.41)}$$

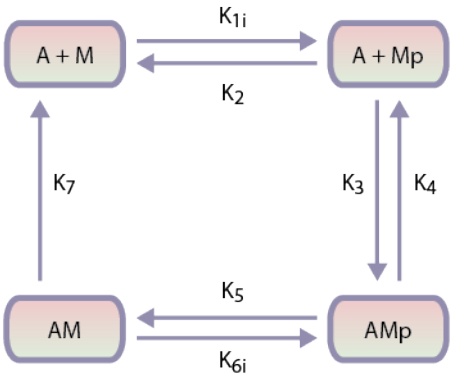

Figure A.1 Crossbridge phosphorylation and latch-state model of Hai and Murphy [65]. Note that this figure also appears in Chapter 5. Adapted from [65].

$$\frac{\mathrm{d}\left[AMp\right]}{\mathrm{d}t} = K_3\left[Mp\right] + K_{6i}\left[AM\right] - \left(K_4 + K_5\right)\left[AMp\right] \tag{A.42}$$

$$\frac{\mathrm{d}\left[AM\right]}{\mathrm{d}t} = K_5\left[AMp\right] - \left(K_7 + K_{6i}\right)\left[AM\right] \tag{A.43}$$

K_{1i} and K_{6i} are the rate constants that represent phosphorylation (of M to Mp and AM to AMp) by the active myosin light chain kinase (MLCK), Ca^{2+}- calmodulin complex. K_2 and K_5 are the rate constants for dephosphorylation (of Mp to M and AMp to AM) by myosin light-chain phosphatase (MLCP). K_3 and K_4 are the rate constants representing the attachment/detachment of fast-cycling phosphorylated crossbridges. Finally, K_7 is the rate constant for latchbridge detachment. K_2 to K_7 are constant and are given in Appendix B.

Their model uses two types of crossbridge interactions: 1) cycling phosphorylated crossbridges and 2) non-cycling dephosphorylated crossbridges ("latchbridges"). The major assumptions of their model are that:

- Ca^{2+} - dependent myosin phosphorylation is the only mechanism for the development of stress in the smooth muscle cell
- Each myosin head acts independently
- Latch bridges are formed by dephosphorylation of an attached crossbridge
- All reactions exhibit first-order kinetics
- Total myosin phosphorylation equals (Mp + AMp) and stress equals (AM + AMp)

- An attachment-to-detachment ratio (K_3/K_4) was chosen as 4:1 for the phosphorylated cycling crossbridges (a ratio of 3:1 is considered reasonable for skeletal muscle, but no estimate was available for smooth muscle). The result of this constraint is that the maximum fraction of crossbridges (AMp + AM) is 0.8 (Figure A.2)

The steady-state dependence of stress (AM + AMp, the fraction of total crossbridges) on myosin phosphorylation in their model approximates that shown in Figure A.2.

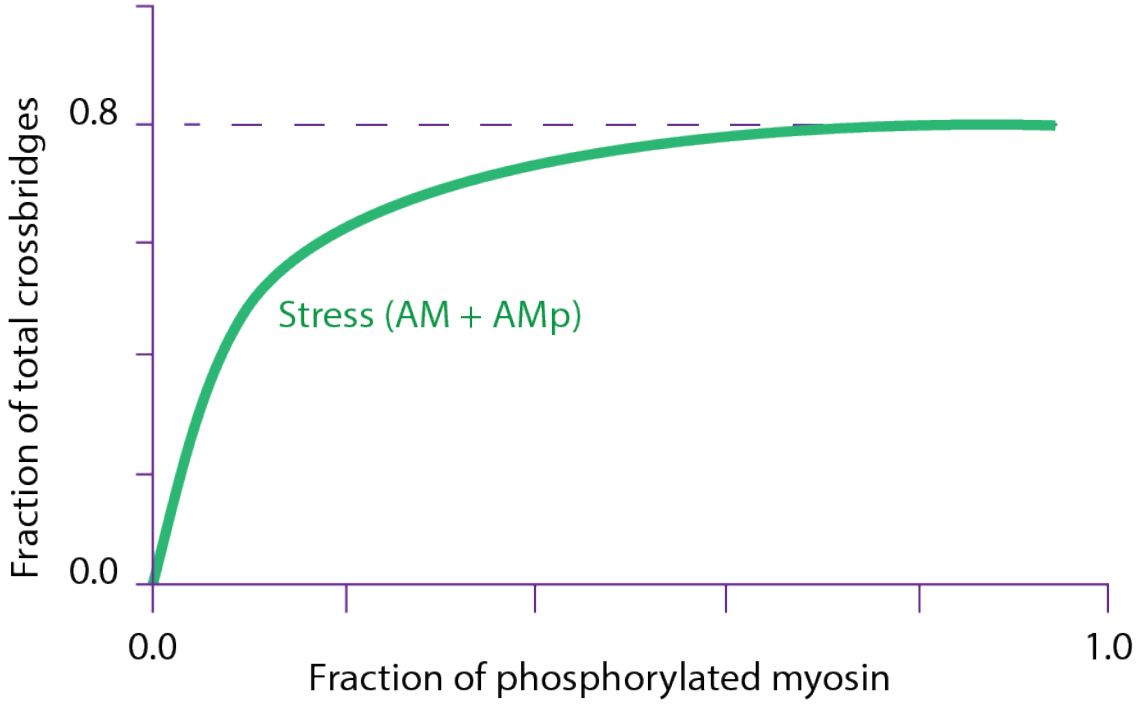

Figure A.2 The steady-state relationship between stress and phosphorylation in the model of Hai and Murphy [65], where the maximum value for (AM + AMp) is 0.8. Adapted from [65].

Appendix B

Model Parameters

B.1 Smooth Muscle Cell Model Parameters

Parameter	Value	Source
F_i	0.23 μM s^{-1}	[85]
K_{ri}	1 μM	[85]
G_{Cai}	0.00129 μM mV^{-1}s^{-1}	[85]
v_{Ca1i}	100.0 mV	[85]
v_{Ca2i}	-24.0 mV	[85]
R_{Cai}	8.5 mV	[85]
$G_{Na/Cai}$	0.00316 μM mV^{-1}s^{-1}	[85]
$c_{Na/Cai}$	0.5 μM	[85]
$v_{Na/Cai}$	-30.0 mV	[85]
B_i	2.025 μM s^{-1}	[85]
c_{bi}	1.0 μM	[85]
C_i	55 μM s^{-1}	[85]
s_{ci}	2.0 μM	[85]
c_{ci}	0.9 μM	[85]
D_i	0.24 s^{-1}	[85]
v_d	-100.0 mV	[85]
R_{di}	250.0 mV	[85]
Li	0.025 s^{-1}	[85]
γ_i	1970 mVμM^{-1}	[85]
$F_{Na/Ki}$	0.2 μM s^{-1}	[85]
G_{Cli}	0.00134 μM mV^{-1}s^{-1}	[85]
v_{Cli}	-25.0 mV	[85]
G_{Ki}	0.0046 μM mV^{-1}s^{-1}	[85]
v_{Ki}	-94 mV	[85]
λ_i	45.0 s^{-1}	[85]
c_{wi}	0.0 μM	[85]
β_i	0.13 μM^2	[85]
v_{Ca3i}	-27.0 μM	[85]
R_{Ki}	12.0 mV	[85]
k_i	0.1 s^{-1}	[85]
K_{KIR_1}	4.5 mV mM^{-1}	[123]
K_{KIR_2}	107.5 mV	[123]

Table B.1 Parameter values for smooth muscle cell model

B.2 Endothelial Cell Model Parameters

Parameter	Value	Source
F_j	0.23 μM s^{-1}	[85]
K_{rj}	1.0 μM	[85]
B_j	0.5 μM s^{-1}	[85]
c_{bj}	1.0 μM	[85]
C_j	5.0 μM s^{-1}	[85]
s_{cj}	2.0 μM	[85]
c_{cj}	0.9 μM	[85]
D_j	0.24 s^{-1}	[85]
L_j	0.025 s^{-1}	[85]
k_j	0.1 s^{-1}	[85]
G_{catj}	0.00066 μM mV^{-1}s^{-1}	[85]
E_{Caj}	50.00 mV	[85]
m_{3catj}	-6.18	[85] – Corrected
m_{4catj}	0.37	[85]
J_{0j}	0.029 μM s^{-1}	[85]
C_{mj}	25.8 pF	[85]
G_{totj}	6927 pS	[85]
v_{Kj}	-80.0 mV	[85]
a_{1j}	53.3	[85]
a_{2j}	53.3	[85]
b_j	-80.8	[85]
c	-6.4	[85] – Corrected
m_{3bj}	0.00132	[85]
m_{4bj}	0.30	[85]
m_{3sj}	-0.28	[85]
m_{4sj}	0.389	[85]
G_{Rj}	955 pS	[85]
v_{restj}	-31.10 mV	[85]
v_{EC}	1.173×10^{-12} L	[142]

Table B.2 Parameters for EC equations

B.3 Other SMC and EC Model Parameters

Parameter	Value	Source
$G_{stretch}$	0.0061 μM mV^{-1}s^{-1}	[86]
Δp	30 mmHg (3990 Pa)	[96]
α	0.0074 mmHg^{-1}	[86]
E_{SAC}	-18 mV	[86]
σ_0	500 mmHg	[86]
G	50 s^{-1}	Estimation
P_{IP_3}	0.05 s^{-1}	[86]

Table B.3 Parameters for stretch-activated calcium channels and heterocellular coupling equations

B.4 Myosin Phosphorylation and Crossbridge Formation Model Parameters

Parameter	Value	Source
γ	$17\ \mu\mathrm{M}^{-3}\mathrm{s}^{-1}$	[86]
K_2	$0.5\ \mathrm{s}^{-1}$	[86]
K_3	$0.4\ \mathrm{s}^{-1}$	[86]
K_4	$0.1\ \mathrm{s}^{-1}$	[86]
K_5	$0.5\ \mathrm{s}^{-1}$	[86]
K_7	$0.1\ \mathrm{s}^{-1}$	[86]

Table B.4 Parameters for model of myosin-actin crossbridge formation

B.5 Smooth Muscle Mechanics Model Parameters

Parameter	Value	Source
R_0	10×10^{-6} m	[96]
h_0	4×10^{-6} m	[96]
Δp	3990 Pa (30 mmHg)	[96]
ρ_w	1100 kg m^{-3}	[92]
ν	0.5	[92]
c_1	0.015	[92]
ϕ	2.8×10^7 Pa s m^{-1}	[22]
c_2	2.25×10^5 Pa	Estimation – based on [62]
E_0	3×10^5 Pa	Estimation – based on [92]
ε	0.1	Estimation
F_{max}	0.8	[65]

Table B.5 Parameters used in muscle mechanics equations

B.6 Astrocyte Model Parameters

Parameter	Value	Source
F	96500 C mol^{-1}	Faraday's Constant
B_{cyt}	0.0244	[20]
VR_{ERcyt}	0.185	[158]
J_{max}	2880 μM s^{-1}	[20]
K_I	0.03 μM	[20]
K_{act}	0.17 μM	[20]
P_L	5.2 μM s^{-1}	[99]
V_{max}	20 μM s^{-1}	[20]
k_{pump}	0.24 μM	[20]
k_{on}	2 μM^{-1}s^{-1}	[20]
K_{inh}	0.1 μM	[20]
r_h	4.8 μM s^{-1}	Estimation
k_{deg}	1.25 s^{-1}	Estimation
δ	1.235×10^{-3}	[99]
K_G	8.82	[20]
V_{eet}	72 s^{-1}	Estimation
k_{eet}	7.2 s^{-1}	Estimation
$c_{k,min}$	0.1 μM	[20]
C_{ast}	40 pF	[124]

Table B.6 Parameters for the astrocyte equations

Parameter	Value	Source
g_{leak_k}	78.54 pS	[61]
v_{leak_k}	-70 mV	[61]
g_{BK_k}	13854 pS	Estimation
v_{BK_k}	-95 mV	[61]
eet_{shift}	2 mVμM^{-1}	Estimation – based on [104]
ψ_n	2.664 s^{-1}	[61]
v_4	14.5 mV	[61]
v_5	8 mV	[61]
v_6	-15 mV	[61]
Ca_3	0.4 μM	[61]
Ca_4	0.15 μM	[61]

Table B.7 Parameters for the astrocyte ion channel equations

B.7 K^+/EET Model Extension Parameters

Parameter	Value	Source
$J_{NaK_{max}}$	10^10 mM s^{-1}	Estimation
KKo_a	1.5 mM	[124]
Nai_a	15 mM	[124]
$KNai_a$	10 mM	[124]
v_{cleft}	8×10^{-21} L	[140]

Table B.8 Parameters for synaptic cleft equations

Parameter	Value	Source
VR_{pa}	0.0009	Estimation – based on [110]
VR_{ps}	0.1	Estimation – based on [150]
R_{decay}	0.05 s^{-1}	Estimation
$K_{p_{min}}$	3 mM	[87]
v_{ast}	3.8×10^{-11} L	[124]

Table B.9 Parameters for perivascular space equations

B.8 NO Model Extension Parameters

Parameter	Value	Source
β_A	0.41 nM	[137]
β_B	1.02 nM	[137]
G_M	46 pS	[137]
P_{Ca}/P_M	3.6	[137]
Ca_{ex}	2 mM	[137]
M	130 mM	[137]
R	8.314 J mol^{-1}K^{-1}	[137]
T	306.15 K	Assumed
V	-40 mV	[137]
κ_{ex}	1600 s^{-1}	[137]
Ca_{rest}	0.0001 mM	[137]
Λ	20	[137]
v_{spine}	8×10^{-17} L	[137]

Table B.10 Parameters for calcium influx into the neuron

Parameter	Value	Source
Q_1	1.9×10^5 mM^{-1}	[40]
Q_2	2.1×10^5 mM^{-1}	[40]
Q_3	0.4×10^5 mM^{-1}	[40]
Q_4	0.26×10^5 mM^{-1}	[40]
$V_{max_{NOS}}$	25 μM s^{-1}	Estimation
$K_{act_{NOS}}$	92.7 $\times 10^{-6}$ mM	[35]
$[CaM]_{thresh}$	25×10^{-6} mM	Estimation
k_{O_2}	9.6×10^{-6} μM^{-2}s^{-1}	[35]
D_{NO}	3.33×10^{-9} m^{2}s^{-1}	[35]
h_1	6×10^{-6} m	Estimation
K_{dis}	0.09 μM s^{-1}	[38]
μ_2	0.0167 s^{-1}	[38]
K_{enos}	0.45 μM	[38]
g_{max}	17.6 μM s^{-1}	[38]
W_0	1.4 Pa^{-1}	[164]
δ_{WSS}	2.86 Pa	[164]
h_2	6×10^{-6} m	Estimation
k_{dno}	0.01 s^{-1}	[35]

Table B.11 Parameters for nNOS and eNOS activation and NO diffusion

Parameter	Value	Source
k_1	2000 μM^{-1}s^{-1}	[169]
k_{-1}	100 s^{-1}	[169]
k_2	0.1 s^{-1}	[169]
k_3	3 μM^{-1}s^{-1}	[169]
m	0	[169]
$V_{max,sGC}$	1.26 μM s^{-1}	[169]
k_{pde}	0.0695 s^{-1}	[169]
C_4	0.4 s^{-1}	[169]
$K_{m,pde}$	2.0 μM	[169]
$n_{H,cGMP}$	2	[169]
$K_{m,cGMP}$	0.55 μM	[169]
V_{cGMP}	68 mV	Fitted to [151]
$n_{H,NO}$	1	[169]
$K_{m,NO}$	0.2 μM	[169]
V_{NO}	100 mV	[169]
V_b	215 mV	Fitted to [151]
$R_{K_{fit}}$	55 mV	Fitted to [151]
k^b_{mlcp}	0.0086 s^{-1}	[169]
k^c_{mlcp}	0.0327 s^{-1}	[169]
$K_{m,mlcp}$	5.5 μM	[169]
$n_{H,mlcp}$	2	[169]

Table B.12 Parameters for NO interactions in the SMC

Appendix C

Ion Channels and Sigmoidal Behaviour

There are many ways to mathematically represent a sigmoidal function; some use the exponential function ($\exp(x)$) and some use the hyperbolic tan function (tanh), as shown in Figures C.1 and C.2, respectively.

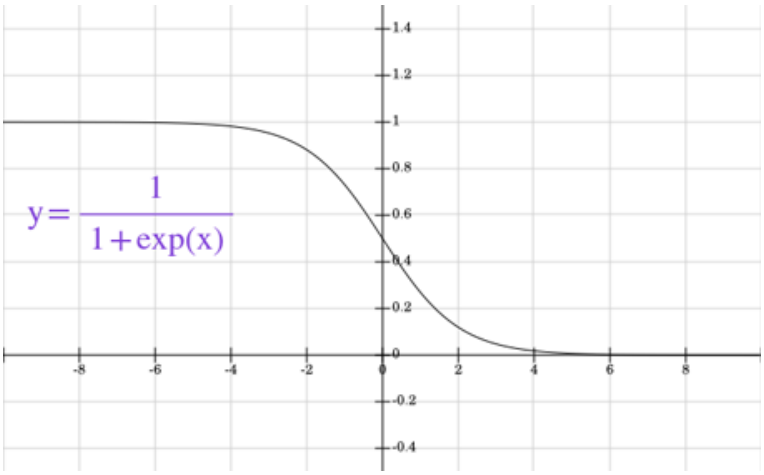

Figure C.1 Sigmoidal behaviour modelled using an exponential term. Note that the function decreases in value from left to right.

We can mathematically show how the differential equation for ion channel opening is formulated by considering the following argument:

Suppose we have an ion channel that has two states:

1. open (O)

2. closed (C)

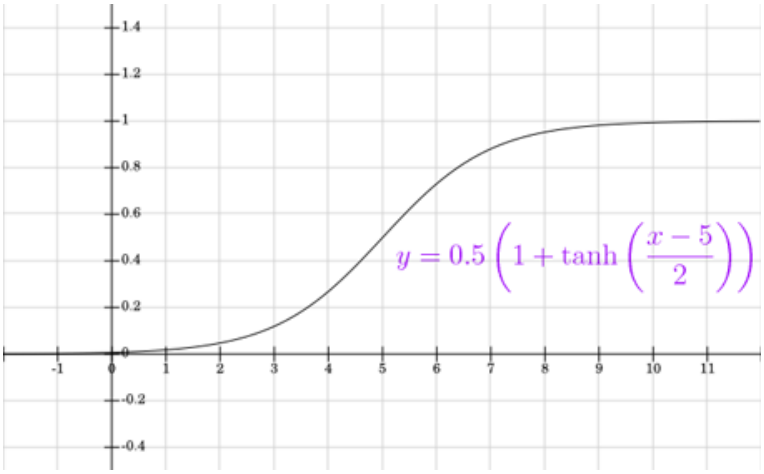

Figure C.2 Sigmoidal behaviour modelled using a hyperbolic tangent term. This function is similar to that in Figure C.1 except that it has been reflected about the y-axis (due to the lack of a negative sign in front of the variable x) and now increases in value from left to right. It has also been translated (shifted along to the right in the y-axis by the value -5) and transformed (compressed by a factor of 0.5 in the y-direction and the slope reduced by the factor 2 in the denominator).

$$C \underset{\beta}{\overset{\alpha}{\rightleftharpoons}} O \tag{C.1}$$

with reaction rates α and β, respectively.

The "flux" of channels moving from an open to a closed state (the number of channels changing state per unit time) is proportional to the number of open channels, and is therefore represented by:

$$flux\, O \rightarrow C = j_{-} = \beta f_O \tag{C.2}$$

where f_O is the fraction of ion channels in the open state. Similarly, the "flux" of ions moving from closed to open states is proportional to the number of closed channels (Equation C.3). As there are only two states, open and closed, the proportions in each state must add up to 1, so the proportion of channels in the closed state must be $(1 - f_O)$.

$$flux\, C \rightarrow O = j_{+} = \alpha (1 - f_O) \tag{C.3}$$

The differential equation for the rate of change in the fraction of open ion channel states is

given by the difference between the two fluxes, j_+ and j_-:

$$\begin{aligned}\frac{\mathrm{d}f_O}{\mathrm{d}t} &= \text{rate of opening} - \text{rate of closing} \\ &= j_+ - j_- \\ &= -\beta f_O + \alpha(1 - f_O) \\ &= -(\beta + \alpha)\left(f_O - \frac{\alpha}{\beta + \alpha}\right)\end{aligned} \tag{C.4}$$

Now let:

$$\frac{1}{\beta + \alpha} = \tau \tag{C.5}$$

where τ is a characteristic time scale, and

$$f_\infty = \frac{\alpha}{\beta + \alpha} \tag{C.6}$$

where f_∞ is the fraction of open channel states at equilibrium.

Equation C.4 can then be written as:

$$\frac{\mathrm{d}f_O}{\mathrm{d}t} = -\frac{(f_O - f_\infty)}{\tau} \tag{C.7}$$

This is an example of what is known as a "reverting" differential equation; when $f_O < f_\infty$, $\frac{\mathrm{d}f_O}{\mathrm{d}t} > 0$ and f_O will revert to f_∞, but when $f_\infty < f_O$, $\frac{\mathrm{d}f_O}{\mathrm{d}t} < 0$ and f_O will still revert to f_∞.

The potential difference (voltage, V) across the membrane can influence the rate of transition from O to C and C to O states, and so α and β, and hence f_∞ and τ, can be rewritten in terms of voltage. We see an example of this in Chapter 6 (in Equations 6.23 and 6.24).

f_∞, when expressed as a function of voltage, tends to have a sigmoidal shape. f_∞ can be determined by fitting experimental data to a sigmoidal function. Equations A.26, A.28 and A.29 in Appendix B are examples of fitted sigmoidal functions.

Appendix D

Analysis of EET Increase With Respect to a Calcium Input Function

We show below an argument to support the hypothesis that [EET] does increase "after" Ca^{2+} The differential equation for [EET] (denoted by $\phi(t)$) is given by

$$\frac{d\phi}{dt} = V(c(t) - c_{min}) - k\phi \tag{D.1}$$

We assume that $c(t) - c_{min} = C(t)$ with $C(0) = 0$. then

$$\frac{d\phi}{dt} + k\phi = VC(t) \tag{D.2}$$

A solution to this is easily formed

$$e^{kt}\phi(t)|_0^t = V\int_0^t C(\tau)e^{kt}d\tau \tag{D.3}$$

However, we do not know the exact formulation of $C(t)$. For small values of time t we assume that $C(t) \simeq \alpha t$ then:

$$\phi(t) = [\phi(0) + \gamma(t)]e^{-kt} \tag{D.4}$$

with

$$\gamma(t) = V\int_0^t \alpha t e^{kt}d\tau \tag{D.5}$$

Integrating $\gamma(t)$ by parts we have that

$$\gamma(t) = \alpha V[\frac{\tau}{k}e^{k\tau} - \int_0^t e^{k\tau}d\tau] \tag{D.6}$$

$$= \frac{\alpha V}{k}[e^{kt}(t-1)+1] \tag{D.7}$$

so

$$\phi(t) = \frac{\alpha V}{k}(t-1) + \frac{\alpha V}{k}e^{-kt} \tag{D.8}$$

Using a Taylor expansion for e^{-kt} we have that

$$\phi(t) = \alpha V t[\frac{1}{k} - 1] + \bigcirc(kt^2) \tag{D.9}$$

Clearly $\phi(t)$ increases; hence $(\frac{1}{k} - 1) > 0$ since all α, V and k are > 0. If $\phi(t)$ is to increase at a slower rate than Ca^{2+} then

$$V[\frac{1}{k} - 1] < 1 \tag{D.10}$$

$$\frac{1}{k} < \frac{1}{V} + 1 \tag{D.11}$$

So, by choosing either V or k the other is completely defined for [EET] to lag [Ca^{2+}]. If we choose $C(t) = \widetilde{c}H(t)$ then

$$\phi(t) = \frac{V}{k}[1 - e^{-kt}] \Rightarrow \phi(t) \simeq Vt \tag{D.12}$$

for small t and therefore always lags [Ca^{2+}].

Appendix E

Source Code

All code used for the simulations presented in this thesis were developed in C++ using the Open Source software Code::Blocks[1]. The attached folders are Code::Blocks "projects" and include:

- nvc_keet_code – code used to simulate K^+/EET-mediated neurovascular coupling (Chapter 7)
- nvc_no_code – code used to simulate NO-mediated neurovascular coupling (Chapter 8)

Both Code::Blocks projects include:

- main.cpp – file that includes all model parameters and ODEs, calls the RKSUITE solver and defines the methods and tolerances it must use, and manages the files in which the results will be placed
- rksuite.cpp – file containing RKSUITE, the numerical ODE solver[2]
- rksuite.h – the header file for RKSUITE

[1] A free copy of this software can be downloaded from http://www.codeblocks.org/downloads

[2] To obtain a copy of the RKSUITE documentation, see http://www.phy.ornl.gov/csep/ode/node9.html

References

[1] Butcher tableau images. http://en.wikipedia.org/wiki/Runge-Kutta_methods.

[2] Elsevier author rights and responsibilities. http://http://www.elsevier.com/authors/author-rights-and-responsibilities.

[3] Image for Poisson's ratio. http://en.wikipedia.org/wiki/File:PoissonRatio.svg.

[4] Image of animal cell. http://www.enchantedlearning.com/subjects/animals/cell/.

[5] Image of cartesian stresses. http://www.efunda.com/formulae/solid_mechanics/mat_mechanics/stress.cfm.

[6] Image of Circle of Willis. http://www.proprofs.com/flashcards/tableview.php?title=cns-contrast-agents-blood-flow--bbb-wk-7.

[7] Image of cylindrical stresses. http://www.tf.uni-kiel.de/matwis/amat/def_en/kap_5/backbone/r5_2_1.html.

[8] Image of Michaelis-Menten kinetics. http://depts.washington.edu/wmatkins/kinetics/michaelis-menten.html.

[9] Image of neuron. http://commons.wikimedia.org/wiki/File:Derived_Neuron_schema_with_no_labels.svg.

[10] Image of stress-strain curve. http://forum.wordreference.com/showthread.php?t=1822364.

[11] Images of fibrous and protoplasmic astrocytes. http://www.studyblue.com/notes/note/n/neuro-histology-lecture/deck/1827872.

[12] Images of the brain. http://www.webmd.com/brain/picture-of-the-brain.

[13] Attwell, D., A. M. Buchan, S. Charpak, M. Lauritzen, B. A. Macvicar, and E. A. Newman (2010, Nov). Glial and neuronal control of brain blood flow. *Nature 468*(7321), 232–43.

[14] Ayata, C. (2009, Oct). Spreading depression: from serendipity to targeted therapy in migraine prophylaxis. *Cephalalgia 29*(10), 1095–114.

[15] Ayata, C., H. K. Shin, S. Salomone, Y. Ozdemir-Gursoy, D. A. Boas, A. K. Dunn, and M. A. Moskowitz (2004, Oct). Pronounced hypoperfusion during spreading depression in mouse cortex. *J Cereb Blood Flow Metab 24*(10), 1172–82.

[16] Bailey, J. E. (1998). Mathematical modeling and analysis in biochemical engineering: past accomplishments and future opportunities. *Biotechnol Prog 14*(1), 8–20.

[17] Barnett, M. W. and P. M. Larkman (2007, Jun). The action potential. *Pract Neurol 7*(3), 192–7.

[18] Bassingthwaighte, J. B. (2008, Nov). Microcirculation and the Physiome projects. *Microcirculation 15*(8), 835–9.

[19] Beard, D. A., J. B. Bassingthwaighte, and A. S. Greene (2005, Sep). Computational modeling of physiological systems. *Physiol Genomics 23*(1), 1–3; discussion 4.

[20] Bennett, M. R., L. Farnell, and W. G. Gibson (2008, Jan). Origins of blood volume change due to glutamatergic synaptic activity at astrocytes abutting on arteriolar smooth muscle cells. *J Theor Biol 250*(1), 172–185.

[21] Bezanilla, F. The Nerve Impulse. `http://nerve.bsd.uchicago.edu/med98a.htm`.

[22] Bia, D., L. Gamero, J. C. Grignola, M. Rodríguez, L. Núñez, R. L. Armentano, and F. Ginés (2001). Pulmonary artery viscoelastic properties: Buffering function characterization. In *2nd Virtual Congress of Cardiology*.

[23] Blanco, V. M., J. E. Stern, and J. A. Filosa (2008, Jun). Tone-dependent vascular responses to astrocyte-derived signals. *Am J Physiol Heart Circ Physiol 294*(6), H2855–63.

[24] Bogacki, P. and L. F. Shampine (1996). An efficient Runge-Kutta (4,5) pair. *Computers and Mathematics with Applications 32*(6), 15–28.

[25] Borisova, L., S. Wray, D. A. Eisner, and T. Burdyga (2009, Oct). How structure, Ca signals, and cellular communications underlie function in precapillary arterioles. *Circ Res 105*(8), 803–10.

[26] Brankin, R. W., I. Gladwell, and L. F. Shampine (1991). RKSUITE Release 1.0. Technical report.

[27] Bray, J. J., P. A. Cragg, A. D. Macknight, and R. G. Mills (2000). *Lecture notes on human physiology* (4 ed.). Blackwell Science.

[28] Brennan, K. C., L. Beltrán-Parrazal, H. E. López-Valdés, J. Theriot, A. W. Toga, and A. C. Charles (2007, Jun). Distinct vascular conduction with cortical spreading depression. *J Neurophysiol 97*(6), 4143–51.

[29] Buerk, D. G. (2001). Can we model nitric oxide biotransport? A survey of mathematical models for a simple diatomic molecule with surprisingly complex biological activities. *Annu Rev Biomed Eng 3*, 109–43.

[30] Bushong, E. A., M. E. Martone, Y. Z. Jones, and M. H. Ellisman (2002, Jan). Protoplasmic astrocytes in CA1 stratum radiatum occupy separate anatomical domains. *J Neurosci 22*(1), 183–92.

[31] Cameron, I. R. and J. Caronna (1976, Nov). The effect of local changes in potassium and bicarbonate concentration on hypothalamic blood flow in the rabbit. *J Physiol 262*(2), 415–30.

[32] Campbell, N. A., J. B. Reece, and L. G. Mitchell (1999). *Biology* (5 ed.). Benjamin/Cummings.

[33] Carmignoto, G., L. Pasti, and T. Pozzan (1998, Jun). On the role of voltage-dependent calcium channels in calcium signaling of astrocytes in situ. *J Neurosci 18*(12), 4637–45.

[34] Charles, A. and K. Brennan (2009, Oct). Cortical spreading depression-new insights and persistent questions. *Cephalalgia 29*(10), 1115–24.

[35] Chen, K. and A. S. Popel (2007, Mar). Vascular and perivascular nitric oxide release and transport: biochemical pathways of neuronal nitric oxide synthase (NOS1) and endothelial nitric oxide synthase (NOS3). *Free Radic Biol Med 42*(6), 811–22.

[36] Chen, K. C. and C. Nicholson (2000, Jun). Spatial buffering of potassium ions in brain extracellular space. *Biophys J 78*(6), 2776–97.

[37] Chrissobolis, S., J. Ziogas, Y. Chu, F. M. Faraci, and C. G. Sobey (2000, Dec). Role of inwardly rectifying K(+) channels in K(+)-induced cerebral vasodilatation in vivo. *Am J Physiol Heart Circ Physiol 279*(6), H2704–12.

[38] Comerford, A., M. J. Plank, and T. David (2008, Feb). Endothelial nitric oxide synthase and calcium production in arterial geometries: an integrated fluid mechanics/cell model. *J Biomech Eng 130*(1), 011010.

[39] Creager, M. A., T. F. Lüscher, F. Cosentino, and J. A. Beckman (2003, Sep). Diabetes and vascular disease: pathophysiology, clinical consequences, and medical therapy: Part I. *Circulation 108*(12), 1527–32.

[40] Crouch, T. H. and C. B. Klee (1980, Aug). Positive cooperative binding of calcium to bovine brain calmodulin. *Biochemistry 19*(16), 3692–8.

[41] D'Ambrosio, R., J. Wenzel, P. A. Schwartzkroin, G. M. McKhann, 2nd, and D. Janigro (1998, Jun). Functional specialization and topographic segregation of hippocampal astrocytes. *J Neurosci 18*(12), 4425–38.

[42] David, T., S. Alzaidi, and H. Farr (2009, 08). Coupled autoregulation models in the cerebro-vasculature. *Journal of Engineering Mathematics 64*(4), 403–415.

[43] de la Torre, J. C. (2002, Apr). Alzheimer disease as a vascular disorder: nosological evidence. *Stroke 33*(4), 1152–62.

[44] De Young, G. W. and J. Keizer (1992, Oct). A single-pool inositol 1,4,5-trisphosphate-receptor-based model for agonist-stimulated oscillations in ca2+ concentration. *Proc Natl Acad Sci U S A 89*(20), 9895–9.

[45] Dickinson, C. J. (2001, Sep). Why are strokes related to hypertension? Classic studies and hypotheses revisited. *J Hypertens 19*(9), 1515–21.

[46] Edvinsson, L. and E. Hamel (2002). *Cerebral Blood Flow and Metabolism*. Lippincott, Williams and Wilkins, Philadelphia.

[47] Edvinsson, L., E. T. Mackenzie, and J. Mcculloch (1992). *Cerebral Blood Flow and Metabolism*. Raven Pr.

[48] Edwards, F. R., G. D. Hirst, and G. D. Silverberg (1988, Oct). Inward rectification in rat cerebral arterioles; involvement of potassium ions in autoregulation. *J Physiol 404*, 455–66.

[49] Ehrenstein, G. and H. Lecar (1977, Feb). Electrically gated ionic channels in lipid bilayers. *Q Rev Biophys 10*(1), 1–34.

[50] Ellsworth, M. L., C. G. Ellis, D. Goldman, A. H. Stephenson, H. H. Dietrich, and R. S. Sprague (2009, Apr). Erythrocytes: oxygen sensors and modulators of vascular tone. *Physiology (Bethesda) 24*, 107–16.

[51] Fabricius, M., N. Akgoren, and M. Lauritzen (1995, Jul). Arginine-nitric oxide pathway and cerebrovascular regulation in cortical spreading depression. *Am J Physiol 269*(1 Pt 2), H23–9.

[52] Faraci, F. M., G. L. Baumbach, and D. D. Heistad (1990, Jul). Cerebral circulation: humoral regulation and effects of chronic hypertension. *J Am Soc Nephrol 1*(1), 53–7.

[53] Farkas, E. and P. G. Luiten (2001, Aug). Cerebral microvascular pathology in aging and Alzheimer's disease. *Prog Neurobiol 64*(6), 575–611.

[54] Farr, H. and T. David (2011, Oct). Models of neurovascular coupling via potassium and EET signalling. *J Theor Biol 286*(1), 13–23.

[55] Filosa, J. A. and V. M. Blanco (2007, Jul). Neurovascular coupling in the mammalian brain. *Exp Physiol 92*(4), 641–646.

[56] Filosa, J. A., A. D. Bonev, S. V. Straub, A. L. Meredith, M. K. Wilkerson, R. W. Aldrich, and M. T. Nelson (2006, Nov). Local potassium signaling couples neuronal activity to vasodilation in the brain. *Nat Neurosci 9*(11), 1397–1403.

[57] Fleming, I. (2004, Jun). Cytochrome P450 epoxygenases as EDHF synthase(s). *Pharmacol Res 49*(6), 525–33.

[58] Girouard, H., A. D. Bonev, R. M. Hannah, A. Meredith, R. W. Aldrich, and M. T. Nelson (2010, Feb). Astrocytic endfoot Ca(2+) and BK channels determine both arteriolar dilation and constriction. *Proc Natl Acad Sci U S A 107*(8), 3811–6.

[59] Girouard, H. and C. Iadecola (2006, Jan). Neurovascular coupling in the normal brain and in hypertension, stroke, and Alzheimer disease. *J Appl Physiol 100*(1), 328–335.

[60] Golding, E. M., M. L. Steenberg, T. D. Johnson, and R. M. Bryan, Jr (2000, Oct). The effects of potassium on the rat middle cerebral artery. *Brain Res 880*(1-2), 159–66.

[61] Gonzalez-Fernandez, J. M. and B. Ermentrout (1994, Feb). On the origin and dynamics of the vasomotion of small arteries. *Math Biosci 119*(2), 127–167.

[62] Gore, R. W. and M. J. Davis (1984). Mechanics of smooth muscle in isolated single microvessels. *Ann Biomed Eng 12*(5), 511–20.

[63] Grosche, J., V. Matyash, T. Möller, A. Verkhratsky, A. Reichenbach, and H. Kettenmann (1999, Feb). Microdomains for neuron-glia interaction: parallel fiber signaling to bergmann glial cells. *Nat Neurosci 2*(2), 139–43.

[64] Hai, C.-M. and H. R. Kim (2005, Apr). An expanded latch-bridge model of protein kinase C-mediated smooth muscle contraction. *J Appl Physiol 98*(4), 1356–65.

[65] Hai, C. M. and R. A. Murphy (1988, Jan). Cross-bridge phosphorylation and regulation of latch state in smooth muscle. *Am J Physiol 254*(1 Pt 1), C99–106.

[66] Hajdu, M. A., D. D. Heistad, J. E. Siems, and G. L. Baumbach (1990, Jun). Effects of aging on mechanics and composition of cerebral arterioles in rats. *Circ Res 66*(6), 1747–54.

[67] Halassa, M. M., T. Fellin, H. Takano, J.-H. Dong, and P. G. Haydon (2007, Jun). Synaptic islands defined by the territory of a single astrocyte. *J Neurosci 27*(24), 6473–7.

[68] Hama, K., T. Arii, E. Katayama, M. Marton, and M. H. Ellisman (2004, May). Tri-dimensional morphometric analysis of astrocytic processes with high voltage electron microscopy of thick Golgi preparations. *J Neurocytol 33*(3), 277–85.

[69] Hamilton, N. B., D. Attwell, and C. N. Hall (2010). Pericyte-mediated regulation of capillary diameter: a component of neurovascular coupling in health and disease. *Front Neuroenergetics 2*.

[70] Harder, D. R., J. Narayanan, E. K. Birks, J. F. Liard, J. D. Imig, J. H. Lombard, A. R. Lange, and R. J. Roman (1996, Jul). Identification of a putative microvascular oxygen sensor. *Circ Res 79*(1), 54–61.

[71] Hayashi, Y., M. Nishio, Y. Naito, H. Yokokura, Y. Nimura, H. Hidaka, and Y. Watanabe (1999, Jul). Regulation of neuronal nitric-oxide synthase by calmodulin kinases. *J Biol Chem 274*(29), 20597–602.

[72] Higashi, K., A. Fujita, A. Inanobe, M. Tanemoto, K. Doi, T. Kubo, and Y. Kurachi (2001, Sep). An inwardly rectifying K(+) channel, Kir4.1, expressed in astrocytes surrounds synapses and blood vessels in brain. *Am J Physiol Cell Physiol 281*(3), C922–31.

[73] Higashimori, H., V. M. Blanco, V. R. Tuniki, J. R. Falck, and J. A. Filosa (2010, Nov). Role of epoxyeicosatrienoic acids as autocrine metabolites in glutamate-mediated K(+) signaling in perivascular astrocytes. *Am J Physiol Cell Physiol 299*(5), C1068–78.

[74] Hillman, E. M. C., A. Devor, M. B. Bouchard, A. K. Dunn, G. W. Krauss, J. Skoch, B. J. Bacskai, A. M. Dale, and D. A. Boas (2007, Mar). Depth-resolved optical imaging and microscopy of vascular compartment dynamics during somatosensory stimulation. *Neuroimage 35*(1), 89–104.

[75] Hires, S. A., Y. Zhu, and R. Y. Tsien (2008, Mar). Optical measurement of synaptic glutamate spillover and reuptake by linker optimized glutamate-sensitive fluorescent reporters. *Proc Natl Acad Sci U S A 105*(11), 4411–6.

[76] Holthoff, K. and O. W. Witte (2000, Feb). Directed spatial potassium redistribution in rat neocortex. *Glia 29*(3), 288–92.

[77] Horiuchi, T., H. H. Dietrich, K. Hongo, and R. G. Dacey, Jr (2002, Nov). Mechanism of extracellular K(+)-induced local and conducted responses in cerebral penetrating arterioles. *Stroke 33*(11), 2692–9.

[78] Iadecola, C. (2004, May). Neurovascular regulation in the normal brain and in Alzheimer's disease. *Nat Rev Neurosci 5*(5), 347–60.

[79] Iadecola, C., F. Zhang, K. Niwa, C. Eckman, S. K. Turner, E. Fischer, S. Younkin, D. R. Borchelt, K. K. Hsiao, and G. A. Carlson (1999, Feb). SOD1 rescues cerebral endothelial dysfunction in mice overexpressing amyloid precursor protein. *Nat Neurosci 2*(2), 157–61.

[80] Jiang, Z. G., J. Q. Si, M. R. Lasarev, and A. L. Nuttall (2001, Dec). Two resting potential levels regulated by the inward-rectifier potassium channel in the guinea-pig spiral modiolar artery. *J Physiol 537*(Pt 3), 829–42.

[81] Johnson, T. D., S. P. Marrelli, M. L. Steenberg, W. F. Childres, and R. M. Bryan, Jr (1998, Feb). Inward rectifier potassium channels in the rat middle cerebral artery. *Am J Physiol 274*(2 Pt 2), R541–7.

[82] Johnston, J. M., P. Burnett, A. P. Thomas, and N. Tezapsidis (2006, Mar). Calcium oscillations in type-1 astrocytes, the effect of a presenilin 1 (PS1) mutation. *Neurosci Lett 395*(2), 159–64.

[83] Jones, C. J., L. Kuo, M. J. Davis, and W. M. Chilian (1995, May). Regulation of coronary blood flow: coordination of heterogeneous control mechanisms in vascular microdomains. *Cardiovasc Res 29*(5), 585–96.

[84] Knot, H. J., P. A. Zimmermann, and M. T. Nelson (1996, Apr). Extracellular K(+)-induced hyperpolarizations and dilatations of rat coronary and cerebral arteries involve inward rectifier K(+) channels. *J Physiol 492 (Pt 2)*, 419–30.

[85] Koenigsberger, M., R. Sauser, J.-L. Bény, and J.-J. Meister (2005, Jun). Role of the endothelium on arterial vasomotion. *Biophys J 88*(6), 3845–54.

[86] Koenigsberger, M., R. Sauser, J.-L. Beny, and J.-J. Meister (2006, Sep). Effects of arterial wall stress on vasomotion. *Biophys J 91*(5), 1663–1674.

[87] Kofuji, P. and E. A. Newman (2004). Potassium buffering in the central nervous system. *Neuroscience 129*(4), 1045–56.

[88] Koide, M., M. A. Nystoriak, G. Krishnamoorthy, K. P. O'Connor, A. D. Bonev, M. T. Nelson, and G. C. Wellman (2011, Jan). Reduced Ca(2+) spark activity after subarachnoid hemorrhage disables BK channel control of cerebral artery tone. *J Cereb Blood Flow Metab 31*(1), 3–16.

[89] Krabbe-Hartkamp, M. J., J. van der Grond, F. E. de Leeuw, J. C. de Groot, A. Algra, B. Hillen, M. M. Breteler, and W. P. Mali (1998, Apr). Circle of Willis: morphologic variation on three-dimensional time-of-flight MR angiograms. *Radiology 207*(1), 103–11.

[90] Kraus, H. (1967). *Thin Elastic Shells*. John Wiley and Sons.

[91] Kuchibhotla, K. V., C. R. Lattarulo, B. T. Hyman, and B. J. Bacskai (2009, Feb). Synchronous hyperactivity and intercellular calcium waves in astrocytes in Alzheimer mice. *Science 323*(5918), 1211–1215.

[92] Kudryashov, N. and I. Chernyavskii (2008, 02). Numerical simulation of the process of autoregulation of the arterial blood flow. *Fluid Dynamics 43*(1), 32–48.

[93] Kurachi, Y. (1985, Sep). Voltage-dependent activation of the inward-rectifier potassium channel in the ventricular cell membrane of guinea-pig heart. *J Physiol 366*, 365–85.

[94] Kuschinsky, W., M. Wahl, O. Bosse, and K. Thurau (1972, Aug). Perivascular potassium and pH as determinants of local pial arterial diameter in cats. A microapplication study. *Circ Res 31*(2), 240–7.

[95] Lamarck, J. B. P. A. d. M. d. (1820). *Système analytique des connaissances positives de l'homme: restreintes à celles qui proviennent directement ou indirectement de l'observation*. Paris: L'auteur.

[96] Lauwers, F., F. Cassot, V. Lauwers-Cances, P. Puwanarajah, and H. Duvernoy (2008, Feb). Morphometry of the human cerebral cortex microcirculation: general characteristics and space-related profiles. *Neuroimage 39*(3), 936–48.

[97] Leao, A. A. P. (1944, November). Pial circulation and spreading depression of activity in the cerebral cortex. *J Neurophysiol 7*(6), 391–396.

[98] Leao, A. A. P. and R. S. Morison (1945, Jan). Propagation of spreading cortical depression. *J Neurophysiol 8*(1), 33–45.

[99] Lemon, G., W. G. Gibson, and M. R. Bennett (2003, Jul). Metabotropic receptor activation, desensitization and sequestration-I: modelling calcium and inositol 1,4,5-trisphosphate dynamics following receptor activation. *J Theor Biol 223*(1), 93–111.

[100] Li, Y. X. and J. Rinzel (1994, Feb). Equations for InsP3 receptor-mediated [Ca(2+)]i oscillations derived from a detailed kinetic model: a hodgkin-huxley like formalism. *J Theor Biol 166*(4), 461–73.

[101] Lindauer, U., D. Megow, H. Matsuda, and U. Dirnagl (1999, Aug). Nitric oxide: a modulator, but not a mediator, of neurovascular coupling in rat somatosensory cortex. *Am J Physiol 277*(2 Pt 2), H799–811.

[102] Lovick, T. A., L. A. Brown, and B. J. Key (1999). Neurovascular relationships in hippocampal slices: physiological and anatomical studies of mechanisms underlying flow-metabolism coupling in intraparenchymal microvessels. *Neuroscience 92*(1), 47–60.

[103] Lu, K., J. W. Clark, Jr, F. H. Ghorbel, C. S. Robertson, D. L. Ware, J. B. Zwischenberger, and A. Bidani (2004, Feb). Cerebral autoregulation and gas exchange studied using a human cardiopulmonary model. *Am J Physiol Heart Circ Physiol 286*(2), H584–601.

[104] Lu, T., P. V. Katakam, M. VanRollins, N. L. Weintraub, A. A. Spector, and H. C. Lee (2001, Aug). Dihydroxyeicosatrienoic acids are potent activators of Ca(2+)-activated K(+) channels in isolated rat coronary arterial myocytes. *J Physiol 534*(Pt 3), 651–67.

[105] Luchsinger, J. A., M. X. Tang, Y. Stern, S. Shea, and R. Mayeux (2001, Oct). Diabetes mellitus and risk of Alzheimer's disease and dementia with stroke in a multiethnic cohort. *Am J Epidemiol 154*(7), 635–41.

[106] Ma, J., C. Ayata, P. L. Huang, M. C. Fishman, and M. A. Moskowitz (1996, Mar). Regional cerebral blood flow response to vibrissal stimulation in mice lacking type I NOS gene expression. *Am J Physiol 270*(3 Pt 2), H1085–90.

[107] Maragakis, N. J. and J. D. Rothstein (2006, Dec). Mechanisms of Disease: astrocytes in neurodegenerative disease. *Nat Clin Pract Neurol 2*(12), 679–689.

[108] Marrelli, S. P., T. D. Johnson, A. Khorovets, W. F. Childres, and R. M. J. Bryan (1998, Jul). Altered function of inward rectifier potassium channels in cerebrovascular smooth muscle after ischemia/reperfusion. *Stroke 29*(7), 1469–1474.

[109] Mashour, G. A. and R. J. Boock (1999, Sep). Effects of shear stress on nitric oxide levels of human cerebral endothelial cells cultured in an artificial capillary system. *Brain Res 842*(1), 233–8.

[110] Matyash, V. and H. Kettenmann (2010, May). Heterogeneity in astrocyte morphology and physiology. *Brain Res Rev 63*(1-2), 2–10.

[111] McCarron, J. G. and W. Halpern (1990, Sep). Potassium dilates rat cerebral arteries by two independent mechanisms. *Am J Physiol 259*(3 Pt 2), H902–8.

[112] Merriam-Webster (2013). Merriam-webster.com. `http://www.merriam-webster.com`.

[113] Metea, M. R., P. Kofuji, and E. A. Newman (2007, Mar). Neurovascular coupling is not mediated by potassium siphoning from glial cells. *J Neurosci 27*(10), 2468–71.

[114] Miller, R. H. and M. C. Raff (1984, Feb). Fibrous and protoplasmic astrocytes are biochemically and developmentally distinct. *J Neurosci 4*(2), 585–92.

[115] Morris, C. and H. Lecar (1981, Jul). Voltage oscillations in the barnacle giant muscle fiber. *Biophys J 35*(1), 193–213.

[116] Nagele, R. G., J. Wegiel, V. Venkataraman, H. Imaki, K.-C. Wang, and J. Wegiel (2004, May-Jun). Contribution of glial cells to the development of amyloid plaques in Alzheimer's disease. *Neurobiol Aging 25*(5), 663–674.

[117] Nakahata, K., H. Kinoshita, Y. Tokinaga, Y. Ishida, Y. Kimoto, M. Dojo, K. Mizumoto, K. Ogawa, and Y. Hatano (2006, Feb). Vasodilation mediated by inward rectifier K(+) channels in cerebral microvessels of hypertensive and normotensive rats. *Anesth Analg 102*(2), 571–6.

[118] Nielsen, A. N., M. Fabricius, and M. Lauritzen (2000). Scanning laser-Doppler flowmetry of rat cerebral circulation during cortical spreading depression. *J Vasc Res 37*(6), 513–22.

[119] Niwa, K., K. Kazama, L. Younkin, S. G. Younkin, G. A. Carlson, and C. Iadecola (2002, Jul). Cerebrovascular autoregulation is profoundly impaired in mice overexpressing amyloid precursor protein. *Am J Physiol Heart Circ Physiol 283*(1), H315–23.

[120] Niwa, K., K. Kazama, S. G. Younkin, G. A. Carlson, and C. Iadecola (2002, Feb). Alterations in cerebral blood flow and glucose utilization in mice overexpressing the amyloid precursor protein. *Neurobiol Dis 9*(1), 61–68.

[121] Niwa, K., V. A. Porter, K. Kazama, D. Cornfield, G. A. Carlson, and C. Iadecola (2001, Dec). A beta-peptides enhance vasoconstriction in cerebral circulation. *Am J Physiol Heart Circ Physiol 281*(6), H2417–24.

[122] Niwa, K., L. Younkin, C. Ebeling, S. K. Turner, D. Westaway, S. Younkin, K. H. Ashe, G. A. Carlson, and C. Iadecola (2000, Aug). Abeta 1-40-related reduction in functional hyperemia in mouse neocortex during somatosensory activation. *Proc Natl Acad Sci U S A 97*(17), 9735–9740.

[123] Oonuma, H., K. Iwasawa, H. Iida, T. Nagata, H. Imuta, Y. Morita, K. Yamamoto, R. Nagai, M. Omata, and T. Nakajima (2002, Mar). Inward rectifier K(+) current in human bronchial smooth muscle cells: inhibition with antisense oligonucleotides targeted to Kir2.1 mRNA. *Am J Respir Cell Mol Biol 26*(3), 371–9.

[124] Østby, I., L. Øyehaug, G. T. Einevoll, E. A. Nagelhus, E. Plahte, T. Zeuthen, C. M. Lloyd, O. P. Ottersen, and S. W. Omholt (2009, Jan). Astrocytic mechanisms explaining neural-activity-induced shrinkage of extraneuronal space. *PLoS Comput Biol 5*(1), e1000272.

[125] Park, L., J. Anrather, C. Forster, K. Kazama, G. A. Carlson, and C. Iadecola (2004, Mar). Abeta-induced vascular oxidative stress and attenuation of functional hyperemia in mouse somatosensory cortex. *J Cereb Blood Flow Metab 24*(3), 334–42.

[126] Paulson, O. B. and E. A. Newman (1987, Aug). Does the release of potassium from astrocyte endfeet regulate cerebral blood flow? *Science 237*(4817), 896–898.

[127] Peng, X., C. Zhang, N. J. Alkayed, D. R. Harder, and R. C. Koehler (2004, May). Dependency of cortical functional hyperemia to forepaw stimulation on epoxygenase and nitric oxide synthase activities in rats. *J Cereb Blood Flow Metab 24*(5), 509–17.

[128] Plank, M. J., D. J. N. Wall, and T. David (2006, Jul). Atherosclerosis and calcium signalling in endothelial cells. *Prog Biophys Mol Biol 91*(3), 287–313.

[129] Price, D. L., J. W. Ludwig, H. Mi, T. L. Schwarz, and M. H. Ellisman (2002, Nov). Distribution of rSlo Ca(2+)-activated K(+) channels in rat astrocyte perivascular endfeet. *Brain Res 956*(2), 183–93.

[130] Quayle, J. M., C. Dart, and N. B. Standen (1996, Aug). The properties and distribution of inward rectifier potassium currents in pig coronary arterial smooth muscle. *J Physiol 494 (Pt 3)*, 715–26.

[131] Quinn, K., C. Guibert, and D. J. Beech (2000, Jul). Sodium-potassium-ATPase electrogenicity in cerebral precapillary arterioles. *Am J Physiol Heart Circ Physiol 279*(1), H351–60.

[132] Retzius, G. (1894). *Biologische Untersuchungen. Die Neuroglia des Gehirns beim Menschen und bei Saeugethieren*, Volume 6. Verlag von Gustav Fischer, Jena.

[133] Rhodin, J. A. and T. Thomas (2001, Aug). A vascular connection to Alzheimer's disease. *Microcirculation 8*(4), 207–220.

[134] Roher, A. E., C. Esh, T. A. Kokjohn, W. Kalback, D. C. Luehrs, J. D. Seward, L. I. Sue, and T. G. Beach (2003, Nov). Circle of Willis atherosclerosis is a risk factor for sporadic Alzheimer's disease. *Arterioscler Thromb Vasc Biol 23*(11), 2055–2062.

[135] Roman, R. J. (2002, Jan). P-450 metabolites of arachidonic acid in the control of cardiovascular function. *Physiol Rev 82*(1), 131–85.

[136] Roy, C. S. and C. S. Sherrington (1890, Jan). On the regulation of the blood-supply of the brain. *J Physiol 11*(1-2), 85–158.

[137] Santucci, D. M. and S. Raghavachari (2008, Oct). The effects of NR2 subunit-dependent NMDA receptor kinetics on synaptic transmission and CaMKII activation. *PLoS Comput Biol 4*(10), e1000208.

[138] Sasaki, H., F. Sato, and H. Mannen (1989, Nov). Morphological analysis of single astrocytes of the adult cat central nervous system visualized by HRP microinjection. *Brain Res 501*(2), 339–54.

[139] Sasaki, N., R. Fukatsu, K. Tsuzuki, Y. Hayashi, T. Yoshida, N. Fujii, T. Koike, I. Wakayama, R. Yanagihara, R. Garruto, N. Amano, and Z. Makita (1998, Oct). Advanced glycation end products in Alzheimer's disease and other neurodegenerative diseases. *Am J Pathol 153*(4), 1149–55.

[140] Savtchenko, L. P. and D. A. Rusakov (2007, Feb). The optimal height of the synaptic cleft. *Proc Natl Acad Sci U S A 104*(6), 1823–8.

[141] Scheckenbach, K. E. L., J. P. Dreier, U. Dirnagl, and U. Lindauer (2006, Dec). Impaired cerebrovascular reactivity after cortical spreading depression in rats: Restoration by nitric oxide or cGMP. *Exp Neurol 202*(2), 449–55.

[142] Schuster, A., J.-L. Bény, and J.-J. Meister (2003, Jul). Modelling the electrophysiological endothelial cell response to bradykinin. *Eur Biophys J 32*(4), 370–80.

[143] Secomb, T. W. (2008, Nov). Theoretical models for regulation of blood flow. *Microcirculation 15*(8), 765–75.

[144] Secomb, T. W., D. A. Beard, J. C. Frisbee, N. P. Smith, and A. R. Pries (2008, Nov). The role of theoretical modeling in microcirculation research. *Microcirculation 15*(8), 693–8.

[145] Shi, Y., X. Liu, D. Gebremedhin, J. R. Falck, D. R. Harder, and R. C. Koehler (2008, Jan). Interaction of mechanisms involving epoxyeicosatrienoic acids, adenosine receptors, and metabotropic glutamate receptors in neurovascular coupling in rat whisker barrel cortex. *J Cereb Blood Flow Metab 28*(1), 111–25.

[146] Siegl, D., M. Koeppen, S. E. Wölfle, U. Pohl, and C. de Wit (2005, Oct). Myoendothelial coupling is not prominent in arterioles within the mouse cremaster microcirculation in vivo. *Circ Res 97*(8), 781–8.

[147] Smith, M. A., L. M. Sayre, and G. Perry (1996, Feb). Diabetes mellitus and Alzheimer's disease: glycation as a biochemical link. *Diabetologia 39*(2), 247.

[148] Solomon, A., M. Kivipelto, B. Wolozin, J. Zhou, and R. Whitmer (2009, Aug). Midlife serum cholesterol and increased risk of Alzheimer's and vascular dementia three decades later. *Dement Geriatr Cogn Disord 28*(1), 75–80.

[149] Somlyo, A. V., Y. E. Goldman, T. Fujimori, M. Bond, D. R. Trentham, and A. P. Somlyo (1988, Feb). Cross-bridge kinetics, cooperativity, and negatively strained cross-bridges in vertebrate smooth muscle. A laser-flash photolysis study. *J Gen Physiol 91*(2), 165–92.

[150] Stensaas, L. J. (1975, May). Pericytes and perivascular microglial cells in the basal forebrain of the neonatal rabbit. *Cell Tissue Res 158*(4), 517–41.

[151] Stockand, J. D. and S. C. Sansom (1996, Nov). Mechanism of activation by cGMP-dependent protein kinase of large Ca(2+)-activated K(+) channels in mesangial cells. *Am J Physiol 271*(5 Pt 1), C1669–77.

[152] Strandgaard, S. (1976, Apr). Autoregulation of cerebral blood flow in hypertensive patients. The modifying influence of prolonged antihypertensive treatment on the tolerance to acute, drug-induced hypotension. *Circulation 53*(4), 720–7.

[153] Sun, H., H. Zhao, G. M. Sharpe, D. M. Arrick, and W. G. Mayhan (2008, Apr). Influence of chronic alcohol consumption on inward rectifier potassium channels in cerebral arterioles. *Microvasc Res 75*(3), 367–372.

[154] Sun, J., L. J. Druhan, and J. L. Zweier (2008, Mar). Dose dependent effects of reactive oxygen and nitrogen species on the function of neuronal nitric oxide synthase. *Arch Biochem Biophys 471*(2), 126–33.

[155] Tomlin, C. J. and J. D. Axelrod (2007, May). Biology by numbers: mathematical modelling in developmental biology. *Nat Rev Genet 8*(5), 331–40.

[156] Traub, O. and R. Van Bibber (1995, May). Role of nitric oxide in insulin-dependent diabetes mellitus-related vascular complications. *West J Med 162*(5), 439–45.

[157] Tyml, K., D. Anderson, D. Lidington, and H. M. Ladak (2003, May). A new method for assessing arteriolar diameter and hemodynamic resistance using image analysis of vessel lumen. *Am J Physiol Heart Circ Physiol 284*(5), H1721–8.

[158] Ullah, G., P. Jung, and A. H. Cornell-Bell (2006, Mar). Anti-phase calcium oscillations in astrocytes via inositol (1, 4, 5)-trisphosphate regeneration. *Cell Calcium 39*(3), 197–208.

[159] Vogel, S. (2001). *Prime Mover: A Natural History of Muscle*. W. W. Norton and Company.

[160] Wang, D. D. and A. Bordey (2008, Dec). The astrocyte odyssey. *Prog Neurobiol 86*(4), 342–67.

[161] Webb, R. C. (2003, Dec). Smooth muscle contraction and relaxation. *Adv Physiol Educ 27*(1-4), 201–6.

[162] Weiss, J. N. (1997, Sep). The Hill equation revisited: uses and misuses. *FASEB J 11*(11), 835–41.

[163] Westerman, M. A., D. Cooper-Blacketer, A. Mariash, L. Kotilinek, T. Kawarabayashi, L. H. Younkin, G. A. Carlson, S. G. Younkin, and K. H. Ashe (2002, Mar). The relationship between Abeta and memory in the Tg2576 mouse model of Alzheimer's disease. *J Neurosci 22*(5), 1858–67.

[164] Wiesner, T. F., B. C. Berk, and R. M. Nerem (1997, Apr). A mathematical model of the cytosolic-free calcium response in endothelial cells to fluid shear stress. *Proc Natl Acad Sci U S A 94*(8), 3726–31.

[165] Wilcock, D. M., M. P. Vitek, and C. A. Colton (2009, Mar). Vascular amyloid alters astrocytic water and potassium channels in mouse models and humans with Alzheimer's disease. *Neuroscience 159*(3), 1055–1069.

[166] Wild, S., G. Roglic, A. Green, R. Sicree, and H. King (2004, May). Global prevalence of diabetes: estimates for the year 2000 and projections for 2030. *Diabetes Care 27*(5), 1047–53.

[167] Wisniewski, H. M. and J. Wegiel (1991). Spatial relationships between astrocytes and classical plaque components. *Neurobiol Aging 12*(5), 593–600.

[168] Yaksh, T. L. and R. E. Anderson (1987, Jun). In vivo studies on intracellular pH, focal flow, and vessel diameter in the cat cerebral cortex: effects of altered CO2 and electrical stimulation. *J Cereb Blood Flow Metab 7*(3), 332–41.

[169] Yang, J., J. W. Clark, R. M. Bryan, and C. S. Robertson (2005, Aug). Mathematical modeling of the nitric oxide/cGMP pathway in the vascular smooth muscle cell. *Am J Physiol Heart Circ Physiol 289*(2), H886–97.

[170] Yang, J., J. W. Clark, Jr, R. M. Bryan, and C. Robertson (2003a, Oct). The myogenic response in isolated rat cerebrovascular arteries: smooth muscle cell model. *Med Eng Phys 25*(8), 691–709.

[171] Yang, J., J. W. Clark, Jr, R. M. Bryan, and C. S. Robertson (2003b, Oct). The myogenic response in isolated rat cerebrovascular arteries: vessel model. *Med Eng Phys 25*(8), 711–7.

[172] Yemisci, M., Y. Gursoy-Ozdemir, A. Vural, A. Can, K. Topalkara, and T. Dalkara (2009, Sep). Pericyte contraction induced by oxidative-nitrative stress impairs capillary reflow despite successful opening of an occluded cerebral artery. *Nat Med 15*(9), 1031–7.

[173] Zhou, M. and H. K. Kimelberg (2000, Dec). Freshly isolated astrocytes from rat hippocampus show two distinct current patterns and different [K(+)](o) uptake capabilities. *J Neurophysiol 84*(6), 2746–57.

[174] Zlokovic, B. V. (2005, Apr). Neurovascular mechanisms of Alzheimer's neurodegeneration. *Trends Neurosci 28*(4), 202–8.